JULY 2017 Ph.D in Civil Engineering ALI KADHIM AL-KARAGHOLI

UNIVERSITY OF GAZIANTEP

GRADUATE SCHOOL OF

NATURAL AND APPLIED SCIENCES

MECHANICAL CHARACTERISTIC OF CONVENTIONAL AND GEOPOLYMER MODIFIED UHPC AND DESIGN CODE ASSESSMENT OF AXIALLY LOADED COMPOSITE MEMBERS WITH SUCH CONCRETE

Ph.D THESIS

IN

CIVIL ENGINEERING

BY

ALI KADHIM AL-KARAGHOLI

JULY 2017

Mechanical Characteristic of Conventional and Geopolymer Modified UHPC and Design code Assessment of Axially Loaded Composite Members with Such Concrete

Ph.D Thesis

in

Civil Engineering

University of Gaziantep

Supervisor

Assoc. Prof. Dr. Esra METE GÜNEYİSİ

by

Ali Kadhim AL-KARAGHOLI

July 2017

REPUBLIC OF TURKEY
UNIVERSITY OF GAZİANTEP
GRADUATE SCHOOL OF NATURAL AND APPLIED SCIENCES
CIVIL ENGINEERING DEPARTMENT

Name of the thesis: Mechanical Characteristic of Conventional and Geopolymer Modified UHPC and Design code Assessment of Axially Loaded Composite Members with Such Concrete

Name of the student: Ali Kadhim AL-KARAGHOLI
Exam date: July 10, 2017

Approval of the Graduate School of Natural and Applied Sciences.

Prof. Dr. A. Necmeddin YAZICI
Director

I certify that this thesis satisfies all the requirements as a thesis for the degree of Doctor of Philosophy.

Prof. Dr. Abdulkadir ÇEVİK
Head of Department

This is to certify that we have read this thesis and that in our consensus opinion it is fully adequate, in scope and quality, as a thesis for the degree of Doctor of Philosophy.

Assoc. Prof. Dr. Esra METE GÜNEYİSİ
Supervisor

Examining Committee Members:	Signature
Prof. Dr. Hanifi ÇANAKCI	....
Assoc. Prof. Dr. Esra METE GÜNEYİSİ	....
Assoc. Prof. Dr. Kasım MERMERDAŞ	....
Asst. Prof. Dr. Hatice Öznur ÖZ	....
Asst. Prof. Dr. Ayşe Y. GÜNAL	....

I hereby declare that all information in this document has been obtained and presented in accordance with academic rules and ethical conduct. I also declare that, as required by these rules and conduct, I have fully cited and referenced all material and results that are not original to this work.

Ali Kadhim AL-KARAGHOLI

ABSTRACT

MECHANICAL CHARACTERISTIC OF CONVENTIONAL AND GEOPOLYMER MODIFIED UHPC AND DESIGN CODE ASSESSMENT OF AXIALLY LOADED COMPOSITE MEMBERS WITH SUCH CONCRETE

AL-KARAGHOLI, Ali Kadhim
Ph. D. in Civil Engineering
Supervisor: Assoc. Prof. Dr. Esra METE GÜNEYİSİ
July 2017
183 pages

The need for developing new structural members having high performance has gained significant attention in the construction industry all over the world. This thesis covers the material aspects of ultra-high performance conventional and geopolymer concrete (UHPC/UHPGC) and the structural aspects of the composite columns in the case of UHPC/UHPGC used as an infill. For this, the experimental and numerical works were carried out. The experimental work included two phases aim to investigate the possibility of producing and developing UHPC/UHPGC. In the first, a total of 11 conventional UHPC mixes were designed with different binder type and content at fixed micro steel fiber volume fraction. Whereas in the second, a total of 10 UHPGC mixtures were produced with the same parameters used in the first, but with a constant material/alkaline solution ratio. Three curing methods were adopted for the specimens and then they were tested for identifying the material characterization. On the other hand, the numerical work included the structural behavior of the steel tubular columns infilled with conventional and geopolymer modified UHPC. For the composite columns, circular cross-section with fixed slenderness ratio and wall thickness were taken account. However, the diameter to wall thickness ratio and yield strength of the steel tubes varied. Furthermore, a special theoretical procedure was adopted to take the benefit of compressive strength results on the axial behavior of CFST column. Three international design codes of ACI-318R, Eurocode 4 and Chinese code DL/T were used to evaluate and discuss the performance of the composite compression members.

Keywords: Composite column, Concrete filled steel tubular member, Geopolymer concrete, Mechanical performance, Ultra high performance concrete.

ÖZET

GELENEKSEL VE JEOPOLİMER MODİFİYELİ UYPB’UN MEKANİK ÖZELLİKLERİ VE BU BETONLARLA ÜRETİLEN EKSENEL YÜKLÜ KOMPOZİT ELEMANLARIN TASARIM KODLARINA GÖRE DEĞERLENDİRİLMESİ

AL-KARAGHOLI, Ali Kadhim
Doktora Tezi, İnşaat Mühendisliği Bölümü
Tez Yöneticisi: Doç. Dr. Esra METE GÜNEYİSİ
Temmuz 2017
183 sayfa

Yüksek performansa sahip yeni yapı elemanlarının geliştirilmesi ihtiyacı, dünya genelinde yapı endüstrisinde büyük önem kazanmaktadır. Bu tez kapsamında, malzeme açısından ultra yüksek performansa sahip geleneksel ve jeopolimer betonlar (UYPB/UYPJB) ve yapısal açıdan da bunların dolgu olarak kullanıldığı kompozit kolonların özellikleri incelenmiştir. Bu bağlamda, deneysel ve nümerik çalışmalar yürütülmüştür. Deneysel kısım, UYPB/UYPJB’nun üretim ve geliştirme olanaklarını araştırmayı amaçlayan iki bölümden oluşmaktadır. Birincisinde, toplam 11 geleneksel UYPB karışımı, farklı bağlayıcı tipi ve miktarı ile sabit mikro çelik lif hacim oranında hazırlanmıştır; ikincisinde ise toplam 10 UYPJB karışımı birinci grupla aynı parametrelere sahip, ancak sabit malzeme/alkalin oranında hazırlanmıştır. Üç kürleme metodu numunelere adapte edilmiş ve sonrasında malzeme özellikleri belirlenmek üzere testler yapılmıştır. Diğer yandan, nümerik kısımda geleneksel ve modifiye edilmiş UYPB dolgulu çelik boru şeklindeki kolonların yapısal davranışı araştırılmıştır. Kompozit kolonlar için, sabit narinlik oranı ve cidar kalınlığına sahip dairesel kesitler dikkate alınmıştır. Fakat, çap - cidar kalınlığı oranı ve çelik tüplerin akma dayanımı değiştirilmiştir. Bunun da ötesinde, basınç dayanımı sonuçlarının beton dolgulu çelik tüp kolonların eksenel davranışı üzerindeki etkisini görmek için teorik bir prosedür uygulanmıştır. Kompozit basınç elemanlarının performans değerlendirmelerinin yapılması için, Amerikan, Avrupa ve Çin gibi üç farklı uluslararası tasarım kodu kullanılmıştır.

Anahtar Kelimeler: Kompozit kolon, Beton dolgulu çelik tüp eleman, Jeopolimer beton, Mekanik performans, Ultra yüksek performanslı beton.

To my family

ACKNOWLEDGEMENTS

I am using this opportunity to express my gratitude and deepest appreciation to Assoc. Prof. Dr. Mehmet GESOĞLU, who is the main supervisor of the first six semesters of this thesis and Assoc. Prof. Dr. Esra METE GÜNEYİSİ, who is the primary supervisor of the following two semesters. In this regard, I am thankful for their aspiring guidance, invaluably constructive criticism, and friendly advice during the scientific work. I am honestly grateful to them for sharing their truthful and illuminating views on a number of matters related to my thesis.

I express my warm thanks to Assoc. Prof. Dr. Erhan GÜNEYİSİ, Prof. Dr. Hanifi ÇANAKÇI, Assist. Prof. Dr. Hatice Öznur ÖZ, Assoc. Prof. Dr. Kasım MERMERDAŞ and Assist. Prof. Dr. Ayşe Y. GÜNAL, for their support, guidance, and suggestions to improve thesis quality.

I would like to extend my thanks to my colleague especially Dr. Oday Ali AZEZ for his precious helps in experimental phase of the study.

I would also like to express my very profound gratitude to my parents and to my brothers and sisters for providing me with unfailing support and continuous encouragement throughout my years of study and through the process of researching and writing this thesis. This accomplishment would not have been possible without them.

Finally, I am greatly indebted to my devoted wife Hiba and my sweet daughters Tuqa, Sama and Raya. They form the backbone and origin of my happiness. Their love and support without any complaint or regret has enabled me to complete this Ph.D project.

TABLE OF CONTENTS

Page

LIST OF TABLES

Page

LIST OF FIGURES

Page

LIST OF SYMBOLS/ABREVIATIONS

A_c Cross-sectional area of the concrete specimen core,

A_s Cross sectional area of steel

A_{sc} Area of composite section

ASTM American Society for Testing and Materials

CFFT Concrete filled fiber-reinforced tube

CFSST Concrete filled stainless steel tube

CFST Concrete filled steel tube

CH Calcium hydroxide

CHS Circular hollow section

D Diameter

E_{c2} Eelastic modulus of concrete

EHS Elliptical hollow section

$(EI)_{eff^2}$ Effective flexural stiffness of CFST

E_s Elastic modulus of steel

f_c' Compressive strength of concrete cylinders (150×300 mm),

f_{ck} Characteristic concrete strength

f_{cu} Compressive strength of 150 mm cube,

f_{scy} Nominal yielding strength of the composite section

f_y Yield stress of steel

FA Fly ash

FRP	Fiber-reinforced polymer
GF	Fracture energy
GPC	Geopolymer concrete
GRC	Geopolymer recycled concrete
GRCFST	Geopolymer recycled concrete filled steel tube
HC	Heat curing
HSC	High strength concrete
ITZ	Interfacial transition zone
l_{ch}	Characteristic Length
LVDT	Linear Variable Displacement Transducer
MK	Metakaolin
N_{cr}	Euler buckling load of the pin-ended CFST column
N_{pIR}	Cross-section plastic resistance of the CFST column
NS	Nano silica
NSC	Normal strength concrete
OPC	Ordinary Portland cement
OPCC	Ordinary Portland cement concrete
RA	Recycled aggregate
RAC	Recycled aggregate concrete
RHA	Rise husk ash
SC	Steam curing
SCMs	Supplementary cementing materials
SF	Silica fume
SHS	Square hollow section
SL	Slag

SP Superplasticizer

t Thickness

UHPC Ultra high performance concrete

UHPFRC Ultra high performance fiber reinforced concrete

UHPGC Ultra high performance geopolymer concrete

UHSCFST Ultra high strength concrete filled steel tube

w/b Water to binder ratio

WC Water curing

WG Water glass

λ Relative slenderness of the CFST column

ξ Confinement factor

CHAPTER 1
INTRODUCTION

1.1 General

In the recent years, there are considerable interests for the utilization of ultra-high-performance concrete (UHPC) in a wide assortment of structural implementations such as constructing the bridges, large span shell structures and field-cast or pre-cast elements. As well, it is utilized for repairing and strengthening purposes in different structures. Moreover, the implementation of UHPC filled steel tubes in building and bridges is very new (Schmidt et al., 2004). It is known that is a relatively new generation of construction products and for this reason, has aroused the interest of researchers and industrial communities since its first introduction in the mid of 1990s (Wille et al., 2011), but until now it is not completely understood because there is no worldwide harmonization of the existing of acceptable unique definition, codes and standards. The CEB/FIP model code (Fib, 2009) calls it the concrete with a compressive strength exceeds 120 MPa and with a highly durability, accomplished by an optimized packing density of all granular ingredients. According to JSCE Guide Line (2010), UHPC is a concrete with the features of a minimum 150 MPa compressive strength and more than 5 MPa tensile strength. According to AFGC / SETRA working group (2002), UHPC defined as a material with a compressive strength that must be above 150 MPa, and taking the maximum size for aggregates and a maximum water-binder ratio (w/b) into consideration. Kazemi and Lubell (2012) considered UHPC as a cement-based composite with compressive strength above150 MPa and manifesting a pseudo-strain hardening response in tension after cracking due to use fibers. While Naaman and Wille (2012) defined UHPC as a cement-based concrete with more or equal to 150 MPa of compressive strength. This very dense and durable concrete is accomplished by using amorphous silica and minimizing the w/b ratio to less than 0.3 by weight. The most widely amorphous silica used in cementitious systems is silica fume (Oertel et al., 2014).

Traditional concrete is a standout amongst the most important and widely used construction materials, owing to their excellent properties, accessibility, cost effectiveness and overall performance. The major problems connected with the cement are its production, which has an energy consuming includes very high temperatures, destruction of natural resources due to the extraction of crude materials and emissions of greenhouse gases. The production of cement contributed to 5-7% of the worldwide emissions of CO_2 (Chen et al., 2010; Meyer, 2009) and production of each tonne resulted in 0.6 -1 tonne of CO_2 (JX et al., 2012; Li et al., 2011).

Applying large amounts of cement in UHPC not only have adversely affected the environment but also affected the production costs, heat of hydration and can cause shrinkage problems. This has increased the interest of researchers to reduce the exhaustion of cement by using alternative cementitious materials like fly ash, slag and silica fume, or finding an environmentally eco-friendly cementitious material gives competitor performance to the cement concrete and can be produced with an acceptable level of energy consumption (Hardjito et al., 2004).

Davidovits (1999) demonstrated that the possibility of producing a binder by a polymeric reaction between alkaline activator solutions and source materials of silicon and the aluminium comes from a geological radix or industrial waste materials like fly ash and he characterize this binder as geopolymer. Palomo et al. (1999) proposed that it could be completely replaced the cement in structural concrete by activating pozzolanic material such as slag by using alkaline liquids to made a binding material.

The “geopolymer” expression depicts a group of mineral binders that have a polymeric Si-O-Al system structure, like zeolites, but without the crystal structure. The polymerisation process comprises a quick chemical reaction as a result of the greatly alkaline status on Si-Al minerals that created in a polymeric chain of three-dimension and ring structure involving of Si-O-Al-O bonds (Naidu et al., 2012). Geopolymers are mainly comprising of source ingredients and the alkaline activators. The source ingredients ought to rich in silicon and aluminium. These materials might be natural minerals like clays, kaolinite, or industrial waste materials like silica fume, fly ash, slag, etc. Many aspects that affected the selecting of the source materials like accessibility, cost, kind of enforcement and particular request of the end users (Motorwala et al., 2013). While the alkaline activation of materials can be characterized as a chemical process that provides a rapid change of specific structures partially or completely amorphous into compact cemented structure (Fernández-Jiménez and Palomo, 2003). The most used alkaline activators are a combination of sodium silicate ($nSiO_2Na_2O$) or potassium silicate solution ($nSiO_2K_2O$) with sodium or potassium hydroxide (NaOH or KOH) (Davidovits, 1994; Torgal et al., 2008; Palomo et al., 1999; Rangan, 2008).

Many researchers studied the chemistry of geopolymer binders (Bijen, 1996; Davidovits, 1991; Duxson et al., 2007; Palomo et al., 1999; Xu and Van Deventer, 2000) and it has been confirmed that it is conceivable to utilize geopolymers as an alternative binder to cement in concrete production, not only for the environmental benefits but also in terms of their performance and durability, where such properties are not only equivalent but often better than those obtained with cement.

The geopolymerisation reactions can be summarized in three basic steps: Dissolution of the alumino silicate solids, gel formation and polycondensation (Duxson et al., 2007). Many factors can be affected on the polymerisation reaction like the chemical composition of the alkaline solution and the source material, water content and curing condition. Curing temperature has a considerable affected the microstructural and development of the mechanical strength of geopolymer system. In general, the polymerisation is accelerated with rising the temperature comparing with ambient (Vijai et al., 2010). The properties of geopolymer concrete (GPC) also affecting by Na_2SiO_3/NaOH ratio. Hardjito et al. (2004) find out that when the ratio equal to 2.5 gives the highest compressive strength for GPC, whereas the ratio of 0.4 gives a lower strength. The molarity of sodium or potassium hydroxide solution also affect the properties of geopolymer products. Palomo et al. (1999) found that a 12 M gives better results than an 18 M concentration.

Nevertheless, numerous mechanistic parts of geopolymerisation are not even well recognized. Former investigations have found that the adding of calcium mineral positively affect the mechanical properties of the geopolymeric binder (Weil et al., 2007; Yip and Van Deventer, 2003) but the precise function of calcium mineral through the geopolymerisation operation stays unclear. Phase separation between geopolymer and partly Al-replaced calcium silicate hydrate gels has been noticed in a several of Ca-comprising geopolymer systems (Alonso and Palomo, 2001; Nicholson et al., 2005; Yip and Van Deventer, 2003; Yip et al., 2005). It has likewise been proposed, but never proved conclusively, the ability of Ca^{2+} to perform a charge-balancing cation within the structure of geopolymeric binder (Davidovits, 1991).

1.2 Concrete filled steel tubular columns

Steel and concrete are the most commonly utilized constructional materials in civil engineering structures. The former is characterized by its high tensile strength, excellent ductility and greater modulus of elasticity, resulting in smaller cross section and slender member of which the buckling behavior predominantly regarded in design. Whereas, the latter is characterized by high compressive a low tensile strength, relatively lower material cost per unit weight and lower thermal conductivity when compared with steel. This is can be affected the long term structural performance of huge members where brittle tensile cracking, creep and shrinkage may be occurs (Liew and Xiong, 2015).

Steel-concrete composite structures incorporate the benefits of steel and concrete materials to accomplish overall improvement in strength and stiffness. Concrete filled steel tubular (CFST) column, including a hollow steel tube filled with concrete with or without additional steel section or reinforcements, has been generally utilized in the construction of high-rise constructions. The local buckling of the outer steel tube is delayed or even prohibited by the concrete core while the inner concrete core is restricted by the steel tube providing promoting in strength and ductility when undergoes to high compressive load. The steel tube can serve as perpetual formwork for concrete casting and thus it eliminates the need of additional work and leads to speed up the construction (Liew and Xiong, 2015). In Figure 1.1, two ways of concrete filling operation into the structural steel tubes are illustrated, one is the pump filling method from the bottom level of the column and the other is the gravity filling method from the top level of the column (Han et al., 2014).

CFST columns have different composite cross sections such as circular, square and rectangular sections which are commonly adopted, whereas polygonal or elliptical sections also may be used for architectural and functional requirements as shown in Figure 1.2. Traditionally, the hollow steel sections only filled by plain concrete. Nowadays, the concrete core may be reinforced by steel bars or fibers to improve ductility and fire resistance of the column. For convenience, the reinforcements can be substituted by an internal steel tube which can gives higher confinement to the concrete core. Other steel sections, such as solid steel section or H-section, can be inserted into the concrete core to further promote the compression resistance and thus reduce the column size. Concrete filled double tube sections can be used for columns subjected to high flexural loading to raise the flexural stiffness using less material (Liew and Xiong, 2015). The use of CFST in real constructions can be illustrated in Figures 1.3 and 1.4. The first figure shows CFST pile groups for supporting the main span of Nooksack River Bridge and completed view of the bridge (WSDOT, 2016) while the second figure demonstrates a composite frame building with circular CFST columns and steel I-beams joined by exterior diaphragms in China (Lin-Hai et al., 2011).

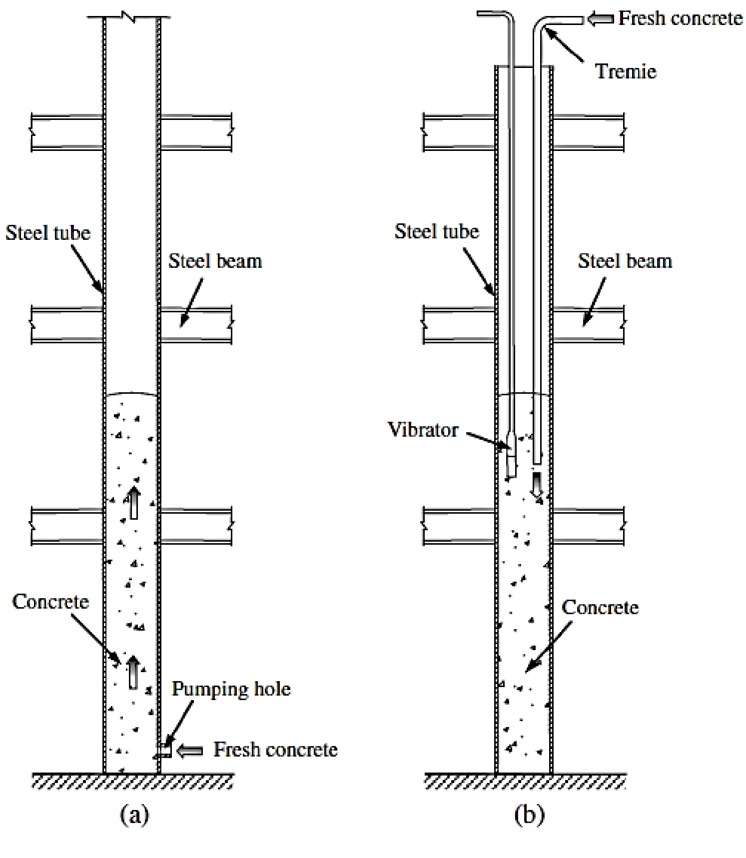

Figure 1.1 Schematic view of concrete placement into steel tubular column (Han et al., 2014)

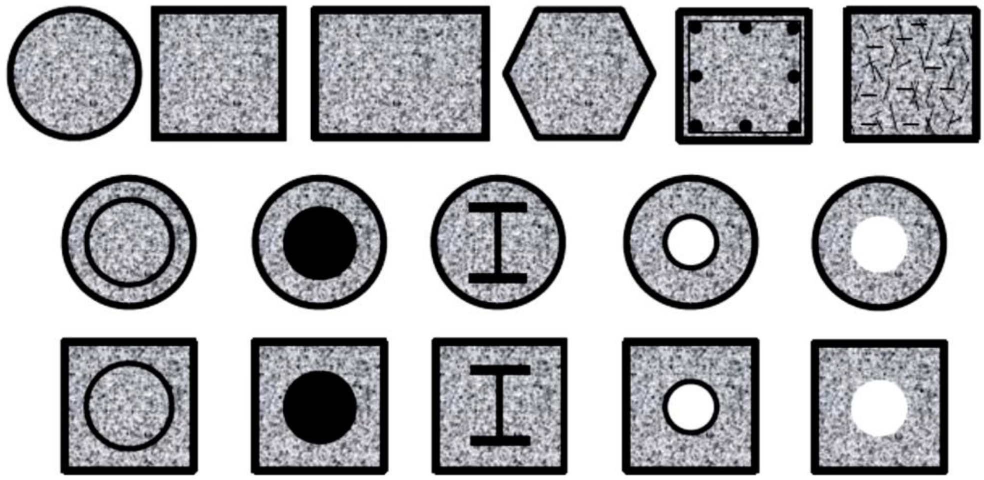

Figure 1.2 Types of concrete filled steel tubular cross sections (Liew and Xiong, 2015)

Nowadays, high strength construction materials aroused the interest of researchers owing to their economic and architectural advantages. The higher the material strength leads to use smaller member size. Cost can be significantly reduced and floor space can be saved in high-rise construction. Brittleness of material is one of the problems for ultra-high strength concrete and local buckling may be a problem for structural members with high tensile steel. Using composite structural members, especially concrete filled steel tubes as columns, is the solution to conquer these problems, where the ductility and strength of the concrete core maybe advanced by the confinement effect supplied by the steel tubes whereas the local buckling of the steel tube can be delayed or even prohibited by the concrete core. In addition, the steel tube can be considered as sustained formwork for concrete casting and thus it eliminates the need for formwork and leads to speed up construction and economical design (Liew and Xiong, 2012; Liew et al., 2014). In Table 1.1, a comparison of a conventional composite column with steel core and another column made with high strength filling materials (i.e., UHPC filling) is performed. As seen from the table, UHPC filled steel tubes offers a good alternative to the steel composite columns in terms of dimensions and cost of the columns. By means of the very high load-carrying capacity, the realization of more transparent structure would be possible (Tue et al., 2004).

(a)

(b)

Figure 1.3 CFST pile groups during construction and completed Nooksack River Bridge (WSDOT, 2016)

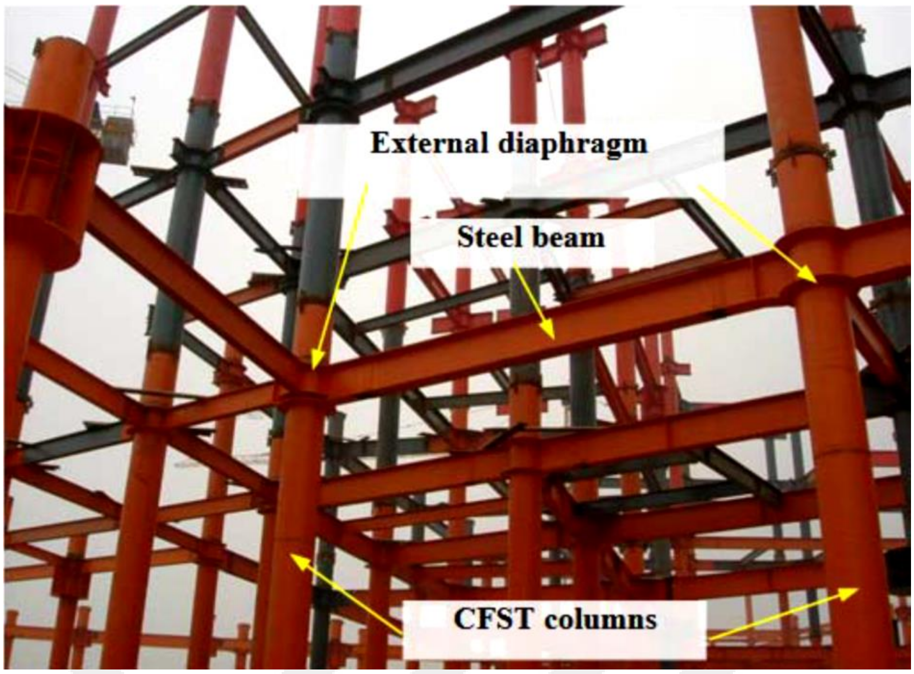

Figure 1.4 A CFST composite frame under construction (Lin-Hai et al., 2011)

Table 1.1 Comparison of a conventional composite column with steel core and a column with UHPC filling (Tue et al., 2004)

			Column 1 	Column 2 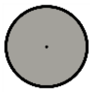
Concrete strength	f_{ck} $f_{cd} = 0.85\ f_{ck}/(\gamma_c\gamma)$	MPa MPa	60 34	180 81.6
Tube strength	$f_{ak,t}$ $f_{ad,t} = f_{ak,t}/\gamma_a$	MPa MPa	360 327.3	360 327.3
Steel core strength	$f_{ak,c}$ $f_{ad,c} = f_{ak,c}/\gamma_a$	MPa MPa	320 290.9	--- ---
Tube steel core diameter	$D_t \times t$ D_c	Mm Mm	406.4×8.8 167.4	406.4×8.8 ---
Bearing capacity Quantity of steel Price of steel	$N_{pl,d}$	MN Kg/m Euro/kg	13.29 259.1 1.00	13.29 86.3 0.90
Quantity of concrete Price of concrete		m^3/m $Euro/m^3$	0.0967 500	0.1187 500
Material costs		Euro/m	259	137

1.3 Research Significance

Many researches have been performed in order to produce and improve the performance of structural UHPC, but unfortunately most of these researches used high amounts of cement to reach to the target ultra-high strength and excellent durability during the service life. As previously discussed, using high amounts of cement adversely affects on the environment due to emission of high amounts of CO_2 during the production of cement and exhaustion of raw materials. This has prompted researchers to reduce the consumption of cement by utilizing additives or by using alternative eco- friendly cementitious products like geopolymer concrete. Thus in the one side of the study, the engineering properties of traditional UHPC with low cement content and geopolymer modified UHPC (UHPGC) have been investigated.

However, in the second side of the study, due to the structural benefit of CFST columns such as the confinement effect of encompassing steel besides contributing in load carrying capacity. Furthermore, the construction time is shortened by abolishing the perpetual formwork. Further important property is restraint or postponement the buckling of the steel tube due to the existence the concrete core. Due to the lack of knowledge with respect to the behavior of ultra-high performance conventional and geopolymer concrete filled steel tube columns exposed to compressive load, an analysis of such composite columns was carried out to examine its structural response.

As a summary, this thesis covers the material aspects of UHPC/UHPGC and the structural aspects of the composite columns in the case of the UHPC/UHPGC used as an infill. For this aim, the experimental and numerical works were carried out. The experimental work included two stages aim to investigate the possibility of producing and developing the UHPC/UHPGC. In the first, the cement was substituted with silica fume, fly ash and/or slag at different proportions up to 75% by weight, whereas in the second, geopolymer concrete was produced by using different proportions of the same additives utilized in the first and activating it using a mixture of sodium silicate and sodium hydroxide as alkaline activator. The following curing methods were used as, water at 20 °C and steam at 90 °C in the first stage, whilst heat and steam curing at 90 °C in the second stage. On the other hand, the numerical work included the structural behavior of the steel tubular columns infilled with conventional and geopolymer modified UHPC. For the composite columns, circular cross-section with fixed slenderness ratio and wall thickness were taken account. However, the diameter to wall thickness ratio and yield strength of the steel tubes varied. Furthermore, a special theoretical procedure was considered to take the benefit of compressive strength results on the axial behavior of CFST column. Three different international design codes were used to evaluate and discuss the performance of the composite compression members.

1.4 Outline of the thesis

The work presented in this PhD thesis is given through six chapters.

Chapter one represents a general introduction on ultra-high performance concrete and concrete filled steel tubular column and the significance of the thesis.

Chapter two deals with review of the literatures and a background on ultra-high performance concrete and ultra-high performance geopolymer concrete as well as the literatures on the structural behavior of the concrete filled steel tubular composite columns.

Chapter three includes the experimental program and numerical analysis accomplished in this study. The properties of the materials used, mixture design, mixing procedures, the preparation of test specimens, curing types, and testing procedures are mentioned. Moreover, this chapter containing the overview of the international design codes and the design model formulas for the ultimate capacity of the composite columns as well as summary of main computation steps used in numerical study.

Chapter four provides mainly the test results and discussion of the compressive strength, splitting tensile strength, static modulus of elasticity, flexural strengths, load–displacement behavior and fracture energy of UHPC and UHPGC. The results on the fresh states of UHPC/UHPGC are also discussed.

Chapter five comprises the results and discussion of the numerical study obtained from ultra-high performance conventional/ geopolymer concrete filled steel tubular short circular columns undergoes to compressive load. As well as the comparison between the results obtained from the design codes of ACI 318, Eurocode 4 and DL/T is also provided.

Chapter six contains the summary of the conclusions obtained from the comprehensive study presented in this thesis.

CHAPTER 2
LITERATURE REVIEW AND BACKGROUND

2.1 General

Many different kinds of structures (i.e., low to high rise buildings, bridges, tunnels, etc.) and the components of the structures (i.e., columns, beams, slabs, etc.) are built by using the structural concretes. For this reasons, concrete is a standout amongst the most widely construction product used in the world, with a current consumption about 1 m^3 per person per year (Gartner, 2004). The traditional binder used in concrete is ordinary Portland cement (OPC), however it has high embodied energy, with high emissions about 0.66 to 0.82 kg of CO_2 released for each kg of cement manufactured (Huntzinger and Eatmon, 2009; Li et al., 2011; Peng et al., 2013). This is approximately contributed between 5–7% of the global emissions of CO_2 (Huntzinger and Eatmon, 2009). Deja et al. (2010) detailed that the industry of cement participate about 7% of the overall worldwide emissions of CO_2. It is assessed that, based on the type of fuels used, about 0.9–1.0 tons of CO_2 are emitted during the production of one ton of clinker (Anand et al., 2006; Dejaa et al., 2010). Hoenig et al. (2007) announced that 0.65–0.92 kg of CO_2 is yielded for each kg of cement produced depended on the equipment and technology used in plant. The main reasons of high CO_2 emissions emerging from OPC manufacture have been assigned to formation and release of CO_2 during the calcination of limestone and to consumption of high energy during heating the crude materials at a high temperature (Gartner, 2004). At the present rate of increment of production, worldwide situation is expected to ascend from about 2.5 to 5 billion ton from the period between 2006 and 2020, which means that the emission of CO_2 caused by production of cement ascending to 100% from the present level by 2020 (Naik, 2008). This obviously mirrors the impact of global warming in not so distant future.

Recently the construction industry has inserted various methods to minimize emissions of CO_2 in concrete manufacturing. The main methods comprise the capture and storage of CO_2 emissions (Yang et al., 2013) and decreasing the quantity of clinker by substituting it with blended cements, comprising partly substituted of OPC by supplementary cementing materials (SCMs). Flower and Sanjayan (2007) demonstrated that about 13–22% of CO_2 emissions can be reduced by using blended cements, although this assessment can change depending on the source of crude materials, amount of binder and OPC substitution, manufacturing facilities type, climate, source of energy, and transportation distances.

Davidovits (1991) found out an alternative binder has been considered as a substitute for OPC involving of an alkali-activated fly ash (FA), named ‘‘geopolymer’’, and he described it as inorganic materials mainly consist of silicon and aluminium that react with alkaline solutions to become a binding material. The CO_2 emission values for geopolymer concrete is estimated about 80% less than OPC (Van Deventer et al., 2010; Duxson et al., 2007) to 26–45% lower than OPC concrete (Habert et al., 2010; Habert et al., 2011; Mclellan et al., 2011; Witherspoon et al., 2009). Weil et al. (2009) concluded that the alkali activated FA concrete can reduce approximately 70% of the global warming compared with OPC concrete.

This distinction in CO_2 emission values emerges from whether the mining, treatment, and transmission of crude materials have been deemed and whether the considerable energy exhausted through industrialization of the alkaline liquids is comprised into the assessment. Another fundamental ingredient in regards to appreciation of CO_2 emission is the observance of energy exhausted throughout the curing of geopolymers with elevated temperature, which is necessary for developing the strength of geopolymer that has not been deemed in previous investigations (Turner and Collins, 2013).

2.2 Ultra high performance concrete

Ultra-high-performance concrete (UHPC) is standout amongst the most recent developments in concrete technology. It has attracted the attention of researchers and practitioners since its introduction in the mid- 1990s. UHPC, also called as reactive powder concrete (RPC), which is exhibits superior mechanical and durability properties. The high compressive strength (generally exceeding 150 MPa), tensile strength, toughness, and ductility along with negligible water and chloride permeability, and therefore high durability, of this new concrete material make it UHPC (Ahmad et al., 2014).

UHPC is established to attain a cement matrix as dense as conceivable (by decreasing capillary pores and microcracks in the matrix) and enhancing interfacial transition zone (ITZ) between cement paste and aggregate (Ahmad et al., 2014). These requirements of UHPC can be accomplished by utilizing high amounts of cement and silica fume (SF) as a binder, using crushed quartz of about 10 µm sizes, and promoting the homogeneity by replacing the coarse aggregate by fine sand of 150–600 µm sizes. Typically a very low water/binder (w/b) ratio is also utilized in UHPC mixes occasioning in decreased workability that may be compensated by addition an efficient type of superplasticizer (Graybeal, 2005; Tue et al., 2008). In order to achieve excellent mechanical properties of UHPC, it is vital to promote the strength and stiffness of the ITZ to be equivalent to that of bulk paste-aggregate. This can be accomplished by utilizing an amorphous siliceous materials such as SF (Smith et al., 2014). The large amounts of binder in UHPC leads to brittle behavior and a tendency toward microcracking due to high autogenous shrinkage. This is the reason of adding steel or organic fibers in the concrete composition (Magureanu et al., 2012). Adding an adequate amount of steel fibers in UHPC gives many advantages such as: enhancing compressive, tensile and bending strength, reduce the crack width, reduce requirements for independent reinforcement bars, improve ductility, recover efforts of contractions and improve resistance to freezing and thawing. There are some disadvantages in using steel fibers; sometimes it can be observed on the concrete surface and it might rust in corrosive environments (Popa et al., 2013).

Decreasing the w/b leads to reduce the porosity of concrete and straiten the space obtainable for the development the crystals of calcium hydroxide (CH). Using high curing temperature quickens the hydration of cement, and enhances the reaction between mineral admixtures and CH (Reda et al., 1999). Increasing curing temperature to 90 ºC which not only affect the pozzolanic activity but also improved the chain length of C–S–H (Masse et al., 1993). Steam curing at 90 ºC for 12 days enhanced the compressive strengths of all mixes compared with standard water curing at ambient temperature. The similar trend of influence can be seen on flexural strength, but in a greater degree of influence (Yazıcı, 2007).

2.2.1 Engineering properties of UHPC

Many researchers studied the properties of UHPC. Ahmad et al. (2014) utilized different natural and byproduct materials like natural pozzolana (NP), FA, cement kiln dust (CKD), powdered steel slag (PSS) and limestone powder (LSP) to develop various mixtures of UHPC. A reference mix of UHPC without replacement was chosen and a total of twenty four trial mixes of UHPC were intended with partially replacing the SF and sand by NP, FA, LSP, CKD, and PSS. Flow and compressive strength at 28 day of each mix were tested to lastly select those mixes, which gives the required flow and strength conditions of UHPC. The outcomes revealed that it can be produce UHPC with acceptable flow and strength by utilizing of NP, FA, LSP, CKD, and PSS.

Tuan et al. (2011) investigated the development of the hydration and microstructure of UHPC by using rice husk ash (RHA) and compared it with reference and SF samples. The results indicated that RHA can improved the hydration of cement at later ages and it can also cultivate the pore structure of UHPC and decrease the $Ca(OH)_2$ content, but considerably lower than SF. The thickness of the ITZ between cement matrix and sand particles of all specimens is too small at 28 days. The results also showed that the mix containing RHA gave higher compressive strength than the reference and SF mix after 7 days.

Tue et al. (2008) investigated the influence of direct and stepwise addition of superplasticizer (SP) on the fresh properties of UHPC. The results indicated that the gradual adding considerably improved the diffusing influence of the SP and improved the flowability of UHPC and the flowability can be improved with delayed addition of SP. The improvement obtained from stepwise and postponed addition is associated to the interaction of the cement/SP in the primary period of cement hydration and influenced by the activity of cement in addition to the adsorption behavior of SP.

Oertel et al. (2014) explored the influence of different kinds of silica by calorimetric analysis, scanning electron microscopy, in situ X-ray deviation and appreciation of compressive strength. The silica ingredient was SF, pyrogenic silica or silica produced by a wet-chemical way. Water/cement ratio was 0.23. Results showed that SF and pyrogenic silica promote the hydration of alite by growing the surface for nucleation of C–S–H phases whilst no accelerating effect was showed.

Kazemi and Lubell (2012) investigated the effect of fiber content and specimen size on the properties of ultra-high-performance fiber-reinforced concrete (UHPFRC) by using short steel fibers with up to 5% of volume fraction. Test specimens were used to characterize the mechanical properties in compression. The flexural tests of unnotched prism using four-point method and direct shear tests of notched specimens were performed. The ultimate strengths and post-peak ductility in compression, direct shear and flexure were all initiate considerably raise with increasing the fiber content. They state that the increasing of specimen size leads to decrease normalized strengths. The mixes containing higher fiber content significant improved the toughness of UHPFRC.

Gesoglu et al. (2016) utilized mixtures of microsilica and nanosilica (NS) to investigate the properties of UHPC with low binder. Two groups of concrete with a constant binder content and w/b ratio were designed with and without SF. NS was replaced up to 3% by weight of cement. The results revealed that the mix incorporating 2% NS gives the superior outcomes of compressive strength, splitting tensile strength, flexural strengths, modulus of elasticity, fracture energy and load–displacement behavior at 90 days. The specimens of UHPC comprising binary cementing products provided superior results than concrete comprising just NS. On the other hand, the results indicated that the influence of 1% NS is practically equivalent to that 10% of SF.

Kadri et al. (2009) discovered the effect of SF on the compressive strength and heat of hydration on UHPC. SF was replaced cement in amounts ranging from 10 to 30% by mass. The strength improvement tends to reduce in the long term. SF has a positive part up to 20% of replacing level and has the most important effect when replaced from 10 to 15%. The calorimetric study revealed that the hydration is modified by the presence of SF. The fine particles of SF provided nucleation sites for hydrates development, this leads to improve the pozzolanic activity and increased both strength and the heat of hydration. Replacing of cement by 10% with SF yielded greater strength and cumulative heat of hydration as compared with that of the control.

Wille et al. (2011) characterize the progression of UHPC with a compressive strength above 200 MPa, which was achieved by utilizing commercially accessible materials in the U.S. and without utilize of any heat processing, pressure, or special mixer. The effect of various variables like cement type, SF, sand, and SP on strength is estimated. The outcomes indicated that the spread value, measured during a slump cone test on a flow table, is a good and rapid index to improve the mix packing density and thus its strength.

Yu et al. (2014) addresses the mix design and assessment the properties of UHPFRC. A modified particle packing model was used to obtain a densely compacted cementitious matrix. Workability, porosity, air content, flexural and compressive strengths of the intended UHPFRC are analyzed. The results showed that it is possible to design UHPFRC with a comparatively low binder content by employing the modified packing model. The results also indicated that after 28 day there is a big quantities of cement still unhydrated in the matrix. This amount can be substituted by fillers to enhance the workability and cost effectiveness of UHPFRC.

Yazıcı et al. (2008) aimed to reduce the cement and SF content of UHPC by utilizing FA and/or slag (SL) and studied the influence of these mineral admixtures on compressive strength using autoclave curing. In the initial step determined the influence of autoclave period and SF content on strength, whereas in the second step, cement was replaced with FA and/or SL at different levels and SF was decreased gradually. The microstructure was inspected by scanning electron microscope (SEM). Results presented that the using of FA and/or SL is conceivable without considerable loss in mechanical performance. SEM micrographs detected that the tobermorite having various morphology.

Alsalman et al. (2017) investigated the development of UHPC with locally available materials, the influence of sand gradation, binder type and content, and curing regimes on compressive strength was measured. The outcomes showed that the 90- day strength of 155 MPa can be accomplished with a SF content of 5% and without heat curing. A curing regime for 2 days at 60 °C followed by 3 days at 90 °C gives the highest strength.

Kim et al. (2016) studied improving the flowability and sustainability of UHPC containing high substitution levels of industrial slag particle. Packing analysis was performed for mixture proportioning. The cement and natural fine aggregates were efficiently substituted by using of SL and rapid-cooling oxidizing slag, respectively. Flow test and V-funnel apparatus were applied to measure the flowability. The sustainability of the proposed UHPC mixes embracing several low energy concentrated products is distinguished by relating decisive environmental effect denominations. Synergistic influences the flowability and ecological features could be accomplished when two forms of industrialized slags utilized simultaneously.

Pyo and Kim (2017) studied the physical properties of eco-friendly UHPC containing by-product materials such as coal bottom ash, FA and two types of SL powder. The results revealed that coal bottom ash and FA are effectively replacing silica powder in UHPC without considerable losses in workability and strength development. It is detected that normal-sized and finer-sized SL can also be used without additional activator to partially replaced cement and SF, respectively. Moreover, it is found that using different forms of industrial by-products in UHPC does not significantly affect the autogenous shrinkage, porosity and water absorption of UHPC.

Sobuz et al. (2016) showed that UHPC can be produced with compressive strength in the range of 130–160 MPa by utilizing commonly available fine and coarse graded aggregates without needing to use complicated mixing or curing conditions. It has been revealed that the strength significantly affected by the fineness modulus of aggregates and SP content. The relationship of the axial and lateral stress–strain show that they own a fundamental residual stress plateau post softening.

2.2.2 Curing of UHPC

Steam curing is beneficial when early strength development in concrete is important or where additional heat is wanted to improve the hydration. Yazıcı (2007) state that the steam curing at 90 °C for 12 day enhanced the compressive strength compared with standard curing. Flexural strength results demonstrated a comparable trend of compressive strength, but with the greater degree of influence. It was vital to extend the period of heat curing when the curing temperature increased to 90 °C, which is not only affected the pozzolanic activity of both SF and crushed quartz, but also improved the chain length of C–S–H (Masse et al., 1993).

Yazıcı et al. (2009) explored the mechanical properties of UHPC comprising class-C FA and SL with three curing conditions. The results revealed that the steam and autoclaving curing enhanced the compressive strength compared to the ambient curing. Furthermore, applying of autoclave and steam curing leads to decrease the flexural strength and toughness. The results also showed that under all curing regimes, toughness of UHPC improved with increasing the replacement of SL and/or FA.

Yazıcı et al. (2010) experienced the mechanical properties of steel microfiber reinforced UHPC under different curing conditions. Cement was substituted with SL at 20, 40 and 60%. The autoclave cured high volume SL mix gives compressive strength over 250 MPa. The compressive strength amounted to 400 MPa when applying an external pressure during setting and hardening stages. The results also showed that the quantity of SF can be reduced with increasing quantity of SL.

Graybeal (2007) studied the uniaxial compressive behavior of UHPFRC. In steam curing regime, the cylinders were subjected to 90 °C and 95% relative humidity for two days. The results indicated that UHPFRC gives higher compressive strength and improved stiffness. The linearity of the stress-strain response of this concrete is argued and the equation for the rising part of the compressive stress-strain behavior was determined.

Ahlborn et al. (2008) explored the effect of curing age and regimes of specimen on the strength and durability of UHPC. Thermally steam cured samples were exposed to a 90°C and 100 % relative humidity steam bath for two days immediately after demolding. UHPC gives compressive strength, elastic modulus and a Poisson's ratio of 207 MPa, 55 GPa, and 0.21 respectively. UHPC also revealed a considerable resistance to the cycling of freezing and thawing with a durability factor exceed 100.

Yiğiter et al. (2012) studied the mechanical properties of UHPC with low cement content and high replacement level of class-C FA reached to 60%. Three curing regimes were applied autoclave, steam and water curing. Two groups of the composites were intended with granite and bauxite aggregates. The results revealed that compressive strength of 200 MPa can be achieved using low cement content and high replacement level of FA. A compressive strength higher than 250 MPa was obtained by thermally treated specimen with high volume FA. Moreover, with applying external pressure, strength value reached up to 400 MPa.

Magureanu et al. (2012) discovered the effect of curing age and regimes on mechanical and durability properties of UHPC. The steam treatment was done inside a specially designed treatment room with digital control. The results demonstrated that the samples acquired a compressive strength of approximately 150 MPa and elastic modulus greater than 50 GPa. The results also showed that the flexural strength depend on the specimen's size and the fiber addition, the flexural tensile strength values ranged between 14 and 34 MPa.

Yunsheng et al. (2008) applied three types of curing conditions (standard curing at 20 °C for 28 days, steam curing at 90 °C for 24 h and autoclave curing at 200 °C for 8 h) to produce a new type of UHPC with compressive strength, flexural strength, fracture energy and fiber–matrix bonding strength are higher than 200 MPa, 60 MPa, 30,000 J/m^2 and 14 MPa, respectively. The dynamic results revealed that the rate of strain has a significant affected the behavior of dynamic tensile of UHPC. The highest stress in the curves of dynamic tensile stress–time, increases rapidly with an increment of strain rate. They shows a distinct strain rate stiffening effect at high strain rate.

Kamen et al. (2007) discovered the effect of curing conditions on the physico-mechanical properties and the time dependent behavior of UHPFRC. Increasing curing temperature leads to accelerate the hydration process at early age and therefore enhanced the material's compressive strength and the carrying capacity tests; but, a higher curing temperature had adverse effects on the mechanical properties at later ages. Furthermore, the UHPFRC gives comparable autogenous shrinkage at long term with normal concrete.

Prem et al. (2013) performed an experimental investigation to determine an efficient curing regimes for UHPC to obtain compressive strength exceeded 150 MPa. The thermal condition shows a fundamental role owing to the limited fineness of components and low w/b ratio. Three curing regimes, ambient air, water and hot air curing were used. The samples were subjected to thermal condition at 90, 150 and 200°C for period of 1, 2 or 3 days at the age of third and seventh day followed with air curing or water curing till 28 days. The results revealed a remarkable variation in compressive strength ranging from 142 to 217 MPa with alteration in curing conditions.

2.3 Geopolymer concrete

Geopolymer is considered as the third generation cement after lime and ordinary cement. The expression ''geopolymer'' is generally applied to depict an amorphous alkali aluminosilicate which is most widely applied for inorganic polymers, alkali-activated cements, geocements, alkali-bonded ceramics, hydroceramics, etc.

Regardless of this variation in naming, these expressions all depict products manufactured using the similar chemistry (Duxson et al., 2007).

Geopolymer is a kind of amorphous alumino-hydroxide product that shows the typical properties of rock-forming elements, i.e., hardness, chemical stability and longevity. Geopolymer binders are utilized with aggregates to yield geopolymer concrete (GPC) which are typical for construction and renovating infrastructures and for precasting units, since they have highly early strength gain, their setting times can be organized and they continue undamaged for long time without needing for conservation. The properties of geopolymer comprise high early strength gain, low shrinkage, resistance to freezing and thawing, resistance to sulphate and corrosion and not produce any alkali-aggregate reaction. The geopolymer binder not depend on the calcination of limestone that generates CO_2. This leads to be low-CO_2 cementious product. This technology can conserve about 80% of CO_2 emissions resulted from the industries of cement and aggregate (Raijiwala and Patil, 2011).

Geopolymer binder comprising of source material which is mainly consist of silicon and aluminium that react with alkaline activator solution. The most alkaline solutions utilized in geopolymers are a conjunction of sodium hydroxide or potassium hydroxide with a glassy silicate comprising of sodium silicate or potassium silicate (Barbosa and MacKenzie, 2003; Duxson et al., 2007; Hardjito et al., 2004; Palomo et al., 1999; Turner and Collins, 2013), sodium hydroxide and sodium silicate being the most widely recognized alkaline activator because of lower cost and availability. It is necessary to cure GPC with raised temperature between 40 and 80 °C for at least 6 h to provide comparable strength to OPC concrete (Duxson et al., 2007; Hardjito et al., 2004; Palomo et al., 1999).

2.3.1 Engineering properties of GPC

There are several studies on GPC in the literature. For example, Gunasekara et al. (2015) explored the microstructure and durability characteristics of GPC produced from class F FA obtained in different power plants in Australia. Each FA based GPC were activated by utilizing different ratios of sodium hydroxide and sodium silicate to determine the optimum mix design. Compressive strength, workability, ultrasonic pulse velocity, rebound hammer and resistivity were investigated in this work. The 28-day compressive strength for the five FA geopolymers ranged between 24.1 and 48.7

MPa. To find the optimum mix for each FA, various fundamental durability parameters were then analyzed. The difference in strength, durability and microstructure among the five GPCs are ascribed to the different reactivity of the source materials and the amount of nonreactive fillers.

Duan et al. (2015) studied the durability and microstructure of FA and metakaolin (MK) based geopolymer subjected to acid attack and high temperatures. A combination of FA and MK activated by sodium hydroxide and sodium silicate solutions were used to prepare geopolymer specimens. Microwave radiation plus a heat curing time were applied for the specimens. A denser microstructure was indicated compared with OPC. Experimental results also revealed that the geopolymer with FA and MK exhibited superior resistance to the acidic solution and raised temperatures compared with OPC as pointed out by the comparatively lower strength loss and mass variation.

Albitar et al. (2014) accomplished an experimental work on the behavior of fresh and hardened states of GPC utilizing class F FA. The study comprises 15 mix to find the effect of w/b and SP/b ratios on the strength and workability of FA based GPC. The outcomes showed that the addition of SP based on naphthalene sulphonate polymer has a slight to no effect on workability and a deleterious influence on strength. Moreover, indirect tensile strength, modulus of elasticity and flexural strength of FA based GPC were tested in this work. The comparison assumptions that existing OPC models supply impartially precise prophecies of the modulus of elasticity and stress-strain relationships, whilst they a little underestimate flexural and splitting tensile strengths.

Ramujee and Potharaju (2014) presented experimental study to improve the mix design for medium grade GPC and compared it with amounting to mix proportions of grade of OPC concrete in both ambient and heat cured regimes. Many parameters were suggested to improve the GPC of standard grade like alkaline solution to FA ratio and water to geopolymer solids ratio. They concluded that the w/b ratio and alkaline liquid/FA ratio are the main factors affecting the geopolymer mix design.

Lavanya and Jegan (2015) performed an experimental study to assess the durability of high calcium FA based GPC when exposed to 2% solution of sulfuric acid and 5% magnesium sulphate for up to 45 days and compared it with OPC concrete. The alkaline activator used was a mixture of sodium silicate and sodium hydroxide solution with the ratio of 2.50 and the sodium hydroxide molarity was 12. The results revealed that, after 45 days of exposure in the magnesium sulfate solution, the strength reduced by 12% and 25% for GPC and OPC concrete, respectively, and the corresponding reduction when exposure to the sulphuric acid solution were 20% and 28% for GPC and OPC concrete, respectively.

Nath et al. (2015) performed experimental work on low calcium FA based GPC with a small quantity of additives and cured in room temperature. The results showed that utilizing of FA considerably improved the early age properties and reduced the setting time to reasonable values and improved compressive strength to enable early demoulding of specimens. Based on workability results, the optimum binder content for the FA geopolymer was obtained. The results demonstrated that with replacement of FA, it can be designed geopolymer mixtures with ambient curing temperature.

Adak et al. (2014) presents experimental study on low calcium FA geopolymer mortar having three different molarity concentrations of activator solution along with different percentage addition of nano silica. Geopolymer mortar with adding 6% of nano silica gives obvious upgrading in compressive, flexural and tensile strength at 28 days under ambient curing temperature. The improvement geopolymer mortar containing nano silica is related to transformation of amorphous compound to crystalline compound.

Padmaroja and Chandana (2015) presented an experimental program on geopolymer mortar and testing it at different ages for compressive strength and sorptivity. Different parameters are considered as the molarity of alkaline activator solution and curing age. The results showed that the geopolymer mortar progresses the strength even in sunlight curing without any conventional curing. Strength results showed an increase with an increase in the molarity of sodium hydroxide and minimum sorptivity of geopolymer mortar was obtained in 12 molar.

Sarker et al. (2013) investigated the effect of the geopolymer binder on fracture features of concrete based on three point bending test of RILEM TC 50 – FMC type notched beam samples. The results showed that for the similar compressive strength, GPC specimens gives higher peak load than the OPC specimens, and GPC specimens manifested more brittle failure modes with comparatively smooth fracture planes compared to the OPC samples. GPC specimens showed steeper post-peak parts of the load vs. deflection curves than that of OPC samples. Moreover, the critical stress intensity parameter of GPC was greater than that of OPC ones.

Komljenović et al. (2010) investigated the effect of characteristics of class F FA from Serbia and the concentration of different alkaline liquids on mechanical and microstructural properties of geopolymers. It was specified that the most prevalent factor in the alkali activation process is the nature and concentration of alkaline activator. The fineness of FA is the main parameter in regard of physical features. The maximum compressive strength was achieved applying sodium silicate and increment of sodium silicate mass ratio leads to increase the reaction outcomes of Si/Al ratio. Under this experimental conditions, high strength was specifically identified to the high Si/Al ratio.

Jun and Oh (2015) studied the mechanical strength of GPC for six different class F FA under various parameters like activator/binder ratios, activator concentrations and curing temperature. The results indicated that the activator/binder ratio is the most affecting factor on the strengths of the alkali-activated FA than the other variables. The existence of these crystalline products affected the strength gain of the alkali-activated FA samples and in addition offer some value-added properties for the geopolymer binder.

Hardjito et al. (2008) discussed the role of different parameters on the properties of class F FA geopolymer mortar. The test results indicated that, increasing the concentration of alkaline solutions leads to improve the compressive strength of geopolymer mortar. The samples cured at 65°C for 1 day gives the maximum compressive strength at 28 days. The compressive strength was ranged from of 1.6 to 20 MPa.

De Vargas et al. (2011) performed an experimental investigation to produce alkali-activated FA geopolymers with a dense matrix. The results of compressive strength test were analyzed using ANOVA. The highest compressive strength was achieved from the mix prepared with a Na_2O/SiO_2 0.40 molar ratio. The analysis of paste morphology revealed that this pastes had a denser appearance, which is in consent with compressive strength test results.

Assi et al. (2016) investigated the effects of many parameters like the ratio of sodium hydroxide, amount of exterior heat, and substitution percent of cement on FA GPC.

The early compressive strength, absorption, permeable voids and density were tested, and the microstructure of the FA geopolymer paste was monitored and considered. The alkaline activator of a mixture of SF, sodium hydroxide, and water was employed. The results demonstrated that implementation of external heat have a main effect on compressive strength.

Nath and Sarker (2014) investigated the improvement of fresh and hardened properties of FA-based geopolymers using SL without using elevated temperature at curing. The results demonstrate that using SL as a small part of the binder exhibited desirable workability, setting time, and compressive strength of FA based GPC cured at standard room condition. Adding SL with class F FA helped to give setting time and compressive strength equivalent to those of OPC concrete.

Ng and Foster (2013) investigated the improvement of a mix design process for geopolymer mortar depending on the assumption that the total strength of geopolymer mortar based on the strength of the geopolymer binder constituents, the aggregates packing density in the mortar and the quantity of geopolymer binder. Firstly, the binder strength was specified. The main components of the geopolymer binder used were FA obtained from two different sources and SL. After that, a relationship between aggregates packing density in the mortar and their effect on the binder required and compressive strength were discovered. Finally, proposed a theoretical framework for a geopolymer mortar mix design procedure.

Ambily et al. (2014) presents an experimental study to produce ultra-high-performance geopolymer concrete (UHPGC) by utilizing industrial byproduct materials such as SF and SL and curing it at ambient temperature. Steel fibers of 0.16 mm diameter and 6 and 13 mm length were used. Fresh properties such as density and flowability and compressive strength of the UHPGC were tested. Five mixes were tested, four mixes with fibers and one mix without fiber. The highest compressive strengths achieved were 175 MPa for UHPGC with 1% 6 mm and 2% 13 mm steel fibers and 124 MPa for the mix without fibers. The flexural strength achieved was 10.3–13.5 MPa for the mixes containing steel fibers and 9.1 MPa without steel fibers. They found that the production of UHPGC with byproducts materials and without the conventional curing regimes used for UHPC will improved sustainability and lead to cast-in-situ employment of UHPC.

Singh et al. (2016) studied the geopolymerization of geopolymer containing FA and slag at ambient curing condition with different activator concentrations. Mechanical properties, hardening with age and drying shrinkage was tested. The optimal compressive strength was achieved by using 14 M activator concentration. The results revealed that the compressive strength, impact strength and elastic modulus improved and the Poisson's ratio reduced with increment the alkali solution concentration. GPC acquired an early strength compared with the OPC concrete as prophesy by the formula particular in ACI 209R-92. The drying shrinkage of specimens was about 0.1% only at the age of 6 months. It is found that FA/SL GPC can be formed at ambient temperature with a comparable compressive strength comparable to that of OPC concrete.

Albitar et al. (2015) performed an investigational work on the production and behavior of GPC produced with a blend of granulated lead smelter SL and FA. A overall of 32 mix were designs to study the influence of: FA substituted with SL as a binder, sand substitution with SL as a filler, SL particle size to reactivity, alkaline solution/binder ratio and curing time. It was establish that the mix comprising 75% of SL as FA substitution and 100% of SL as fine aggregate yields concrete gives compressive strength of 31 MPa. The results also revealed substantial improvement in the compressive strength of the hardened concrete could be acquired by fine crushing of the SL to a fineness comparable to OPC and FA (<20 µm).

Yip et al. (2008) study the role of calcium in geopolymerisation using 7 various calcium silicate products. The compressive strength of matrices arranged with prevalently amorphous calcium silicates or comprising crystalline phases precisely produced for reactivity is substantially greater than when the calcium is provided as crystalline silicate minerals at low alkalinity. At high alkalinity, the distinction in compressive strength between matrices synthesized utilizing various calcium silicate sources is considerably decreased. A deficient quantity of calcium is dissolved from crystalline calcium silicates at comparatively low alkalinity to facilitate formation of calcium silicate hydrate in existence with the aluminosilicate geopolymeric gel, and this contributes to the indigent mechanical properties of these matrices.

Soutsos et al. (2016) investigated the factors influencing the reactivity of FA for GPC such as physical and chemical properties of various sources of FA, implying of SL, alkali activator dosages and curing temperature. The alkaline solution used was a combination of sodium hydroxide and sodium silicate. The existence of silicates in alkaline solution was found to be a considerable parameter affecting the strength. The physical and chemical characterization of 13 FA sources from the UK were performed. The partial substitution of FA with SL was found to be useful in increasing compressive strengths and avoiding the need for elevated curing temperatures.

Krishnan et al. (2014) proposed to promote the setting time and strength of FA based GPC at ambient temperature by adding SL. The alkaline liquid used was a mixture of sodium silicate and sodium hydroxide with 12 molarity solution. The result showed that the strength gains of GPC can be achieved within 24 hours without water curing at ambient temperature. The results also demonstrated that increasing the percentage of SL leads to increase the strength of GPC. It was noticed that the mix comprising 60% FA + 40% SL gave maximum compressive strength of 80.5 MPa. Thus, GPC is deemed to be an environmentally free contamination construction product.

Lee et al. (2016) performed an experimental work to investigate the reactivity improvement of a combination of FA and SL based geopolymer on by the adding SF. The geopolymer was produced by activating a blend of FA, SL and three kinds of SF with alkaline solution. X-ray diffraction (XRD) and inductively coupled plasma-optical emission spectroscopy (ICP-OES) were applied to characterize the reaction. The silicate structure was investigated by nuclear magnetic resonance (NMR) spectrometry. The ratio of Si/Al in the aluminosilicate gel was relatively constant, ranging from 2.0 to 2.6, whereas the addition of SF leads to increase the Si/Al ratio of the C-S-H gel.

Partha et al. (2013) presented a study on the ambient cured FA based GPC. The alkaline activator used was a mixture of sodium hydroxide and sodium silicate solutions. The setting and hardening of 10% or 20 % of blending SL from the total binder with FA GPC were achieved without using heat curing. The 28 days compressive strength of GPC ranged from 27 to 47 MPa. Results revealed that the increase of the slag content in the GPC leads to increase the strength and decrease the water absorption. Generally, strength and permeation properties of geopolymer concrete improved by mixing of SL with FA when cured at ambient temperature.

Gokulram and Anuradha (2013) presents an experimental work on the mechanical properties of different binder composition of GPC. The mechanical properties of GPC tested in this work were tested for compressive, split tensile and flexural strengths prior of 28 days of ambient curing and one day of heat curing. Mixtures with two alkaline solution to binder ratios by mass value of 0.45 and 0.55 were prepared. The volume fraction of polypropylene fibers used in the mixture were 0.25% volume of concrete. Two types of methods were consider in this study utilizing 100% substitution of cement by class F FA and SL and 100% substitution of natural sand by manufactured sand.

Madhava et al. (2016) presents an experimental investigation to produce the GPC using SL and MK with alkaline solutions of sodium silicate and sodium hydroxide with 10 molar. Sodium hydroxide is taken for the preparation of different mixes by changing the percentages of SL and MK. The curing was executed by exposing the specimens directly to sunlight. The result revealed that the strength of GPC is increased with an increasing SL content up to 40% then it is decreasing. Therefore it is preferable to use 40% SL with MK to give high strength. MK and SL can be utilized as a replacement material for cement gives an excellent result.

Gautam et al. (2015) present an experimental work of developing FA based and FA + SL based GPC having a compressive strength of 50 MPa and 70 MPa at 28 days with ambient curing temperature. A total of 20 mixes using different molarity of sodium hydroxide solutions were casted. The results showed that the 7 day compressive strength improvement by GPC is about 83% of the 28 days strength compared with 60% of the corresponding conventional concrete at the same age. The results at 7 days of flexural strength of GPC improved by 68% of the 28 days strength comparing with 42% of the corresponding conventional concrete at the same age.

Deb et al. (2014) explored the influence of various proportions of SL and alkaline solution content on the fresh and hardened properties of FA GPC. SL was used with 10 and 20% of the total binder with alkali solution contents of 35 and 40% and the sodium silicate to sodium hydroxide ratio of (1.5–2.5). The mixes containing higher SL and lower ratio of sodium silicate to sodium hydroxide improved the strength and reduced the workability. The results also demonstrated that the tensile strength of geopolymer cured at ambient temperature is well correlated with the compressive strength comparable to conventional concrete. The AS 3600 and ACI 318 codes were used to estimate the tensile strength from compressive strength of ambient cured GPC tend to be identical to that for conventional concrete. The estimation for heat cured is more conservative than for ambient cured GPC.

Memon et al. (2013) discovered the influence of SF on the fresh and mechanical properties of self-compacted FA-based GPC. The work was done with 400 kg/m^3 binder content and 0.33 water-to-geopolymer solid ratio. SF replaced by FA up to 15% by weight. The results demonstrated that the partial replacement of FA by SF leads to decrease the workability and obvious improvement in the mechanical properties of GPC up to 10%. At this replacement level of SF the slump flow reduced by 4.3% and the increment of the compressive, tensile and flexural strengths by 6.9, 12.8 and 11.5%, respectively.

Assi et al. (2016) investigates the influence of the type of alkali activated solution, curing condition, and source of FA in relevance to the occasioning compressive strength of FA GPC. The microstructure of FA geopolymer paste was monitored and absorption, density and voids were tested. A combination of sodium hydroxide, SF, and water; and a combination of sodium hydroxide, sodium silicate and water were used as alkali activated solutions. The results disclosed that the compressive strength is directly affected by FA source.

2.3.2 Curing of GPC

Several researches have been prepared to investigate the influence of various curing regimes on the properties of geopolymer pastes and concrete. Palomo et al. (1999) explored curing of alkali activated FA with liquid/ solid ratio of 0.25 and 0.30 at 65 °C and 85 °C. They argued that the compressive strength of geopolymers with 8–12 M of alkaline solution cured at 85 °C for 24 h was greater than the corresponding geopolymers cured at 65 °C, and when extended curing time after 24 h show much smaller rise in strength.

Al Bakri et al. (2012) investigated the processing of geopolymers using FA and alkaline solutions. The geopolymer paste specimens were cured at 70°C for 1 day and kept at ambient temperature till the age of testing. The compressive strength was tested after 7 days. The results disclosed that the geopolymer paste with a mixture of sodium silicate to sodium hydroxide ratio of 2.5 and a 12 M of NaOH concentration produces the maximum compressive strength. The density achieved for geopolymer is in the range of 1760 to 1855 kg/m^3. The porosity of the geopolymer was ranged between 12.2 to 26.2%, and the water absorption was ranged between 5.0 to 8.1%.

Vijai et al. (2010) presents of an experimental work on the compressive strength and density of GPC. The experiments were implemented on FA GPC by using two kinds of curing regimes heat and ambient curing. The ratio of FA to alkaline solution was 2.5. The compressive strength test was taken for each specimen and the outcomes revealed that, for ambient cured specimens there is an increment in compressive strength with age, while for hot cured samples the strength development was much lower than that of samples undergoes to ambient curing. The density of GPC was about 2400 kg/m^3, which is identical to that of OPC concrete.

Görhan and Kürklü (2014) presents an experimental investigation to produce geopolymer mortar utilizing class F FA from the thermal power plant in Kütahya Seyitömer in Turkey. They applied different curing temperatures and various curing times on geopolymer mortars with different NaOH concentrations to explore the effect of geopolymerization on the properties of the final product. Two different temperatures 65 and 85 °C were applied for curing the samples. The outcomes of this survey found that curing time and temperature had an influence on the physical features of the geopolymer mortars.

Noushini and Castel (2016) aimed to assess the transport properties of type F FA GPC cured with 12 various heat curing conditions comprising 3 temperatures of 60, 75 and 90 ^{o}C and 4 curing periods of 8, 12, 18 and 24 h, and in addition ambient curing, were enforced to the samples. Results demonstrated that appropriate curing regime like curing at 75 ^{o}C for 18-24 h produced a GPC with low volume of porous voids and sorptivity coefficient. Reducing the volume of porous voids and fewer continuous capillaries gained by utilizing the appropriate curing condition, prompts to increase the compressive strength and electrical resistivity of the type F FA GPC.

Demie et al. (2011) presents an investigational work on the influence of SP and curing temperature on the workability and compressive strength of self-compacted GPC. They were produced from type F FA activated by a mixture of sodium hydroxide and sodium silicate solutions. The dosages of SP were 3, 4, 5, 6 and 7% and the various curing temperatures were 60, 70, 80 and 90°C. Results demonstrated that increasing the SP dosage improved the workability and compressive strength. An increment in strength was observed with rising in temperature up to 70°C.

Srinivasan et al. (2015) discovered the effect of various types of curing regimes like ambient temperature, hot air oven at 50°C, 100°C and steam curing at 75°C on the performance of the concrete in the compressive strength. The steel fiber was added in 0.5, 1 and 1.5% of mass of the concrete to improve the strength of GPC. The strength up to 90 days was predict from the one day strength by applying a polynomial regression equation, which is developed for all the mixtures from the test results.

Andini et al. (2008) introduced a study on coal FA used to produce geopolymers. The alkali hydroxide needful to begin polycondensation has been appended in proper quantity as concentrated solution for each of the two systems. The concentration of each alkali liquid has been set to ensure constant workability. The systems subjected to four curing temperatures for various times depending on the temperature were considered. The results demonstrated that the systems were appropriate for the production of building blocks at ambient temperature.

2.4 Concrete filled steel tubular columns

The steel and concrete are the two key constructional materials utilized in building, bridge and civil engineering structures. The former is featured by its very high tensile strength, ductility and elastic modulus, leading to smaller section and slender member. However, the buckling problems are required to be considered in the structural design. In the case of the latter, it is featured by very high compressive strength whereas low tensile strength. This results in brittle tensile crack, leading to negative effect on long term structural performance. From the structural points of view, the steel- concrete composite structures combine the benefits of the steel and concrete products to gain whole improvement in strength and stiffness (Liew and Xiong, 2015).

Composite structures are a common and economical form of construction utilized in a broad assortment of structural types. Composite construction is known as a construction with structural members with composite sections consisting two materials, reinforced concrete and steel section are bound to work together. Steel reinforcement is normally considered as part of reinforced concrete construction (Peng, 2014). With the development of this new material, the strength of steel and concrete for building structures have turned out to be higher, the cross section with these materials become smaller and this significantly affected on the load carrying capacity of the column. The structural feature of concrete filled steel tubular (CFST) columns is due to the stipulation of the confinement influence of embracing steel in addition to contributing in load carrying capacity. Furthermore, the construction period is likewise shortened by disregarding the enduring formwork. A further important property is suppression or delay the buckling of the steel tube owing to concrete core (Lu and Zhao, 2010; Zeghiche and Chaoui, 2005). Thus, the utilization of concrete-filled steel tubes has become predominant in various parts of construction and turning an attractive result. Furthermore, as a consequence of the increment in the load carrying capacity, ductility and stiffness in addition to economy and quick construction (Zeghiche and Chaoui, 2005).

In Figure 2.1, six CFST column sections, namely, circular, square, rectangular, polygon, round-ended rectangular and elliptical sections, are illustrated. Among them, the better confinement is observed for the circular section while the square and rectangular sections suffers more from the local buckling problems. However, the beam-column connections are relatively simple for the latter. They also have very high sectional flexural stiffness. The other sections of polygon, round-ended rectangular and elliptical are applied particularly for the aesthetical reasons. More complicated cross-sections for constructing CFST members are also given in Figure 2.2. In practice, they can be undergoes to various loading situations such as compression, tension, bending and torsion. In Figure 2.3, the behavior of hollow steel tube, concrete alone, and CFST member under tension, bending and torsion are shown comparatively (Han et al., 2014).

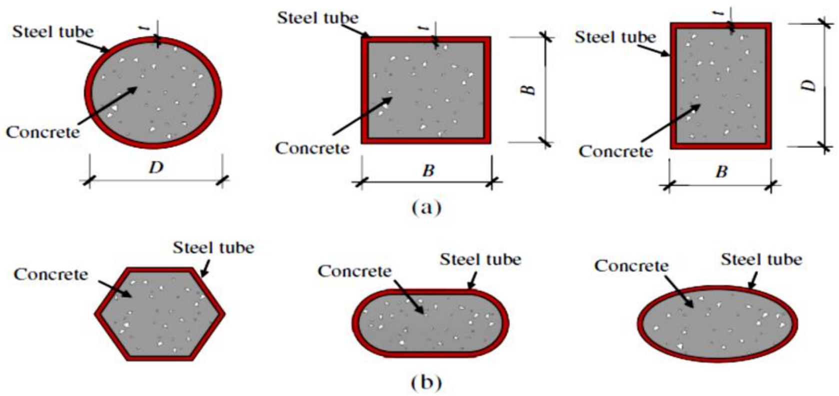

Figure 2.1 Typical concrete-filled steel tubular sections (Han et al., 2014)

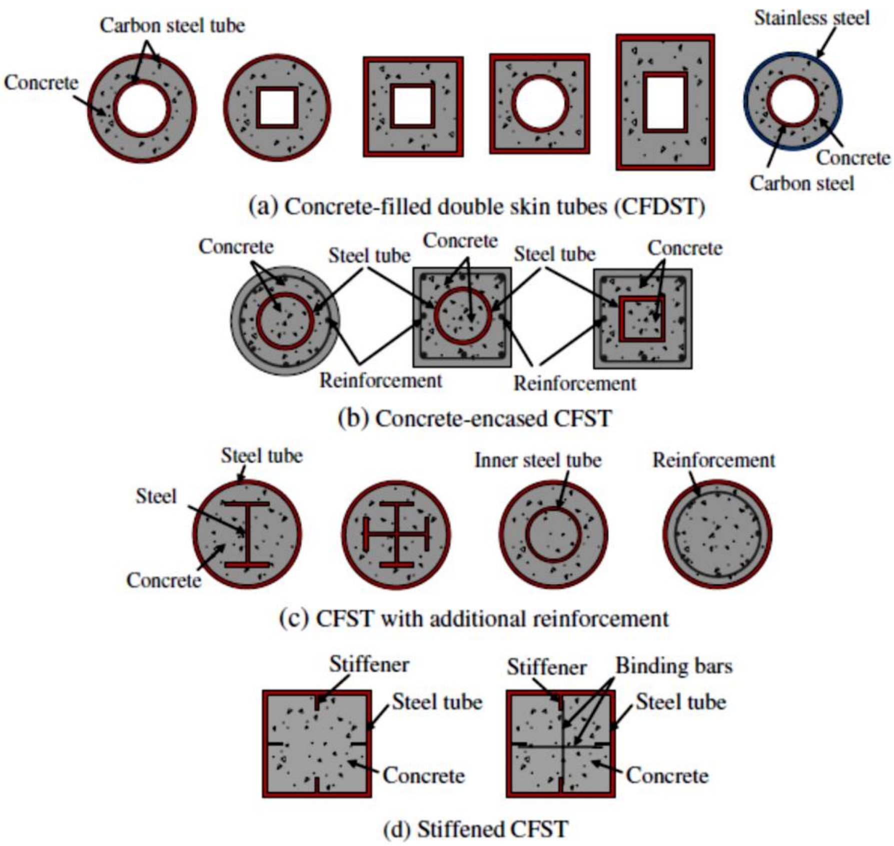

Figure 2.2 General CFST cross sections (Han et al., 2014)

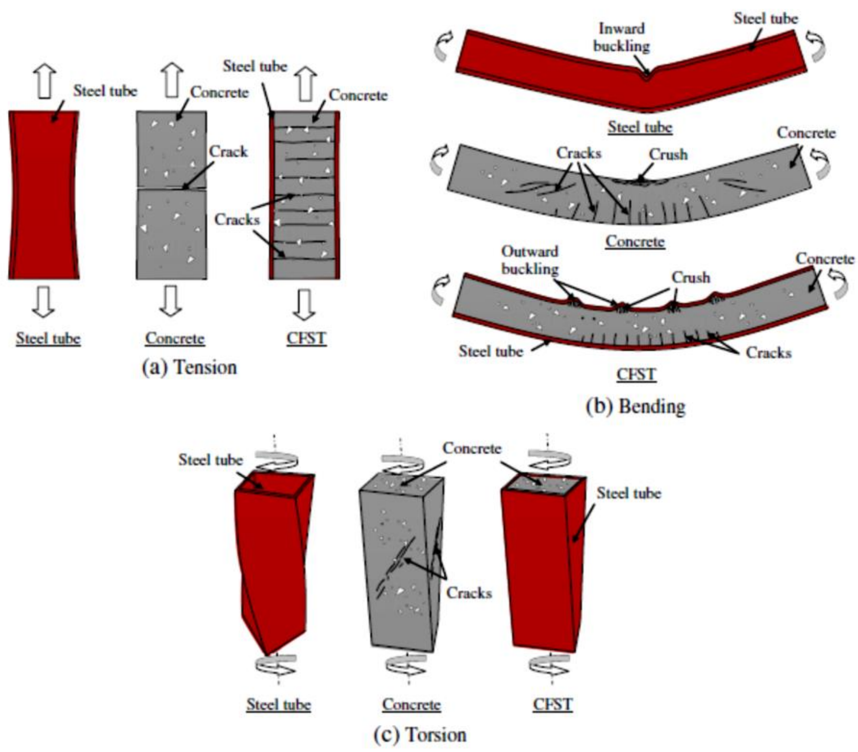

Figure 2.3 Schematic failure modes of steel tube, concrete and CFST under tension, bending and torsion (Han et al., 2014)

The structural response of CFST members is very complicated resulting from the interaction between the concrete core and steel tube shell. As reportedly, unexpected increment in the capacity of CFST is developed by the restricting influence of tube on the concrete core. The distinction between Poisson’s ratios of steel and concrete significantly affects the behavior of CFST members. In Figure 2.4, the stress circumstance in steel tube and concrete core is shown. As seen from the figure, the longitudinal, compressive hoop, tension hoop, confining stresses as well as the lateral tension forces are developed at different stage of loading (Kuranovas and Kvedaras, 2007).

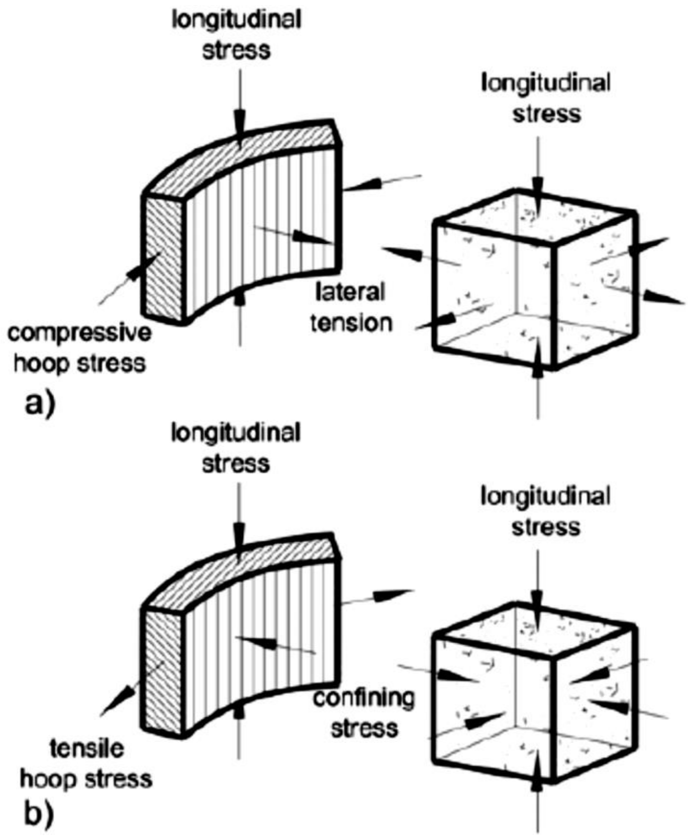

Figure 2.4 Stress situation in steel tube and concrete core at various stages of loading (Kuranovas and Kvedaras, 2007)

As explained above, the confinement considerably alters the stress-strain behavior of the composite section. The difference between the stress-strain curves of unconfined and confined concrete core in each type of steel sections (i.e., circular hollow section (CHS), square hollow section (SHS) and elliptical hollow section (EHS) are show in Figure 2.5. the elastic and inelastic behavior of tubular section filled with concrete improve and shift to higher stiffness, strength and ductility (Santos, 2012).

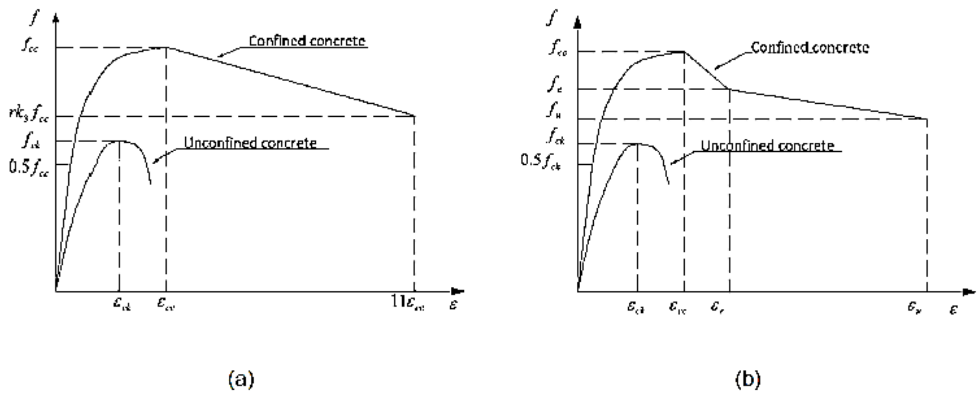

Figure 2.5 Stress- strain curves of non-confined and confined concrete in: (a) CHS and SHS, (b) EHS (Santos, 2012)

2.4.1 Behavior of CFST columns under axial compression

Gardner and Jacobson (1967) performed investigational studies on CFST short columns subjected to axial compression with concrete strength from 25.0 to 43.4 MPa, yield stress of steel between 363 to 650 MPa and diameter-to-thickness ratio (D/t) ranged from 25.9 to 49.7. They found out that the dilation properties of steel tube and concrete have considerable effects on the behavior of CFST columns loaded on entire section. Steel tube does not supply any restricting stress to the concrete core in the primary loading stage owing to the expansion of concrete in this stage is lesser than that of steel tube. With increasing axial strain, the micro-cracking of concrete beginning to form and the extension of concrete overrides that of steel tube. Subsequently, the steel tube has to further extend to follow the fast expansion of concrete and thus the confining stress is initiated. Afterward, the concrete core is exposed to tri-axial state, which considerably encourages its strength and ductility. The mechanical behavior of CFST columns also investigated by Johansson (2002) and Teng et al. (2013) and they provided similar practically presumptions.

O'Shea and Bridge (1998) implemented experiments on thin-walled circular CFST columns with a D/t > 100 and reached to 220 for some specimens. They found out that the local buckling significantly influence on the strength of hollow steel tubular columns. Nevertheless, the in-filled concrete could be enhanced the buckling resistance of square or rectangular tubes, this was unclear in the circular CFST columns because of that the in-filled concrete could not prohibit the outer local buckling of circular samples. Aside from, O'Shea and Bridge (2000) as well monitored a critical information of local buckling and in the thin steel tube of the bond between the steel and concrete core, the deficiency of interface bonding would conduct in tube buckling in the initial elastic phase for CFST columns in-filled with high strength concrete (HSC). Otherwise, a clarification for the local buckling resistance of thin-walled circular CFST columns was derivative by Bradford et al. (2002). They found that the hypothetical elastic buckling stress for the CFST columns was 1.73 times more than that of hollow steel tubular columns. The variations between theoretical and experimental results might be because of the de-bonding between steel tube and concrete core in the thin-walled samples or due to the differences in material properties like the remaining stresses and the geometric deficiency.

In the study of Chu (2014), five different types of the failure modes for the CFST columns exposed to axial compression were observed from the experiment. They are given in Figure 2.6. It was reported that the failure by radial expansion, local buckling failure, formation of plastic hinge, shear failure and global buckling were clearly detected for the columns. In the case of the radial expansion failure, the concrete pushed outwards on the steel tube till it bulges into a barrel like shape. The local buckling failure case was occurred at the multiple location along the length of the column. In the case of the failure mode of plastic hinge, several local buckling were formed at one location in the column. However, for the case of the global buckling, it was occurred where the CFST column bended at one location, usually near mid-height.

Schneider (1998) performed an analytical and experimental investigation on the conductance of concentrically loaded CFST columns. A total of 14 samples, comprising 3 circular, 5 square and 6 rectangular sections were examined to find the influence of wall thickness and the shapes of cross-sectional on the conductance of CFST columns. Test outcomes revealed that circular CFST column had higher strength, ductility and stiffness than the square or rectangular column. Identical supposition was drawn by Ren et al. (2014). They considered 44 special-shaped cross-sections axially loaded CFST short columns: 0.25 circular, semi-circular, fan-shaped, D-shaped, triangular and circular section as references. As a final point, they established that the strength was decreased by 16.0%, 32.1%, 28.4%, 25.1% and 40.0% when changing the cross-sectional from circular to the sections stated above, respectively. The confinement influence afforded by the circular section is higher and more uniform and this leads to outstanding behavior of circular CFST column, which is membrane-type hoop stress rather than plate bending in the steel plates of further sections. In another study forwarded by Dong et al. (2013), the tube configurations, circular or square, solid or hollow were examined. Figure 2.7 displays the section of the test samples. The steel tubes were prepared by cutting a selected size of long cold form tubes. The analysis of the results revealed that under the action of axial compression, the structural behavior of the composite columns having circular section with solid or hollow performed better than those having square cross section (either solid or hollow configuration).

Figure 2.6 Classification of CFST column failure modes (Chu, 2014)

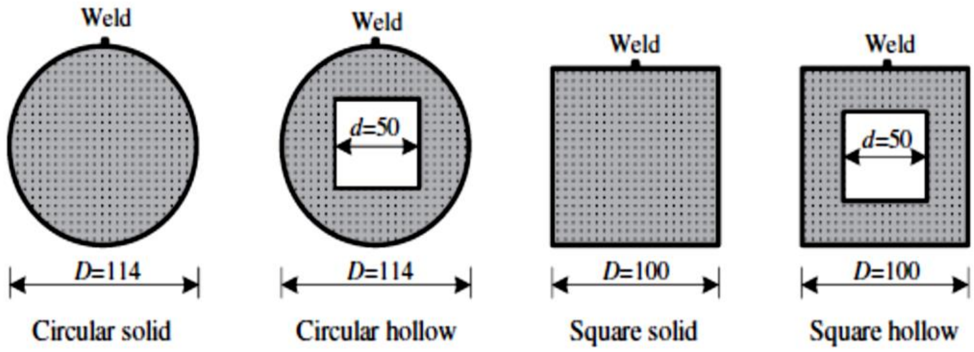

Figure 2.7 The tube configurations of the specimens tested by Dong et al. (2013)

The strength of concrete is a standout amongst the greatest essential factors that affect the behavior of CFST columns. A lot of experimental investigations have been performed to explore the influence of concrete strength (Elremaily and Azizinamini, 2002; Gupta et al., 2007; Han et al., 2001; O'Shea and Bridge, 1998 and Sakino et al., 2004). The concrete strength of these experiments ranged from 20 to 100 MPa. They specified that the ductility and improvement ratio of the strength of the samples decreased with increasing the concrete strength. In another meaning, higher strength concrete needs larger confining stress to afford the similar level of confinement, i.e. thicker steel tube or higher steel yield stress. The HSCFST columns could present strain hardening behavior by restraining HSC with this type of steel tube, which was related to most of the NSCFST columns. Furthermore, investigation on CFST columns in-filled with UHSC of compressive strength ≥120 MPa is quiet limited (Sakino and Hayashi, 1991). As the fast progress of concrete technique, the manufacture of UHSC is simply attainable without addition special types of fibers. This type of concrete can spare additional floor space and the embodied carbon. Nevertheless, the brittleness of UHSC is more than HSC. By restraining UHSC with a steel tube, persistent confinement can be supplied to progress the strength and ductility. Thereafter, it is predictable that UHSCFST can have satisfactory deformability for practical design and construction if sufficient restraining stress is supplied.

Investigations on the concrete-filled carbon steel tubular columns offered that the larger the yield stress leads to higher the confining stress (Han, 2002; Han et al., 2005; O'Shea and Bridge, 2000; Schneider, 1998). In contrast, Sakino et al. (2004) described the prolonged investigation on the conductance of CFST columns in Japan by using cold-form steel tube with yield stress ranged from 262 to 835 MPa, encasement the ranges of mild steel to high yield steel. They indicated that the confining stress provided to the concrete at extreme circumstance increased with increasing the yield stress of steel tube. The variance between the maximum strength and the nominal smash load of circular CFST columns also increased. Then, utilizing high-strength steel considerably promote the behavior of CFST columns. Uy et al. (2011) discovered the behavior of concrete-filled stainless steel tubular (CFSST) columns, with the yield stress of stainless steel tube ranged from 259 to 435 MPa. This type of steel has higher corrosion resistance, easier repairs and more durable than carbon steel. They noticed that with a nearby confinement factor, the CFSST column exhibited more progressive yielding behavior on the load-strain curves compared with the concrete-filled carbon steel tubular column, this might be because of the "roundhouse" form of the stress-strain curve of stainless steel compared with "linearly-elastic-perfectly-plastic" form of carbon steel. They also detected that the load-carrying capacity of these two types of columns was identical. However, the CFSST column had higher enduring strength.

Furthermore, the D/t is an important factor that influence the behavior of CFST columns and it may be the most significant one affecting the provision of restricting stress and thus the ductility and strength of CFST columns. As revealed before, the steel tube would buckle firstly before yielding if the D/t ratio transcended a specified limit. Sakino et al. (2004) presented that as the D/t increment, the restricting stress reduced and this leads to reduce the strength and ductility of CFST columns. Additionally, the D/t ratio also influenced the strain relating to peak load. Smaller D/t ratio provides larger peak strain, and thus the samples had a higher strain in mobilizing the strength (Han et al., 2005). In the study of Güneyisi et al. (2016), the effect and interaction of several parameters of CFST member (i.e., strength of concrete core, yield strength of steel tube, diameter of column, wall thickness of column, length of column, length to diameter ratio (L/D) and (D/t) ratio of columns) on the experimental and prognosticated axial capacity of the CFST composite columns were discussed by using 314 test results. The variations are given in Figure 2.8. They reported that those factors were very effective on both experimental and numerical results.

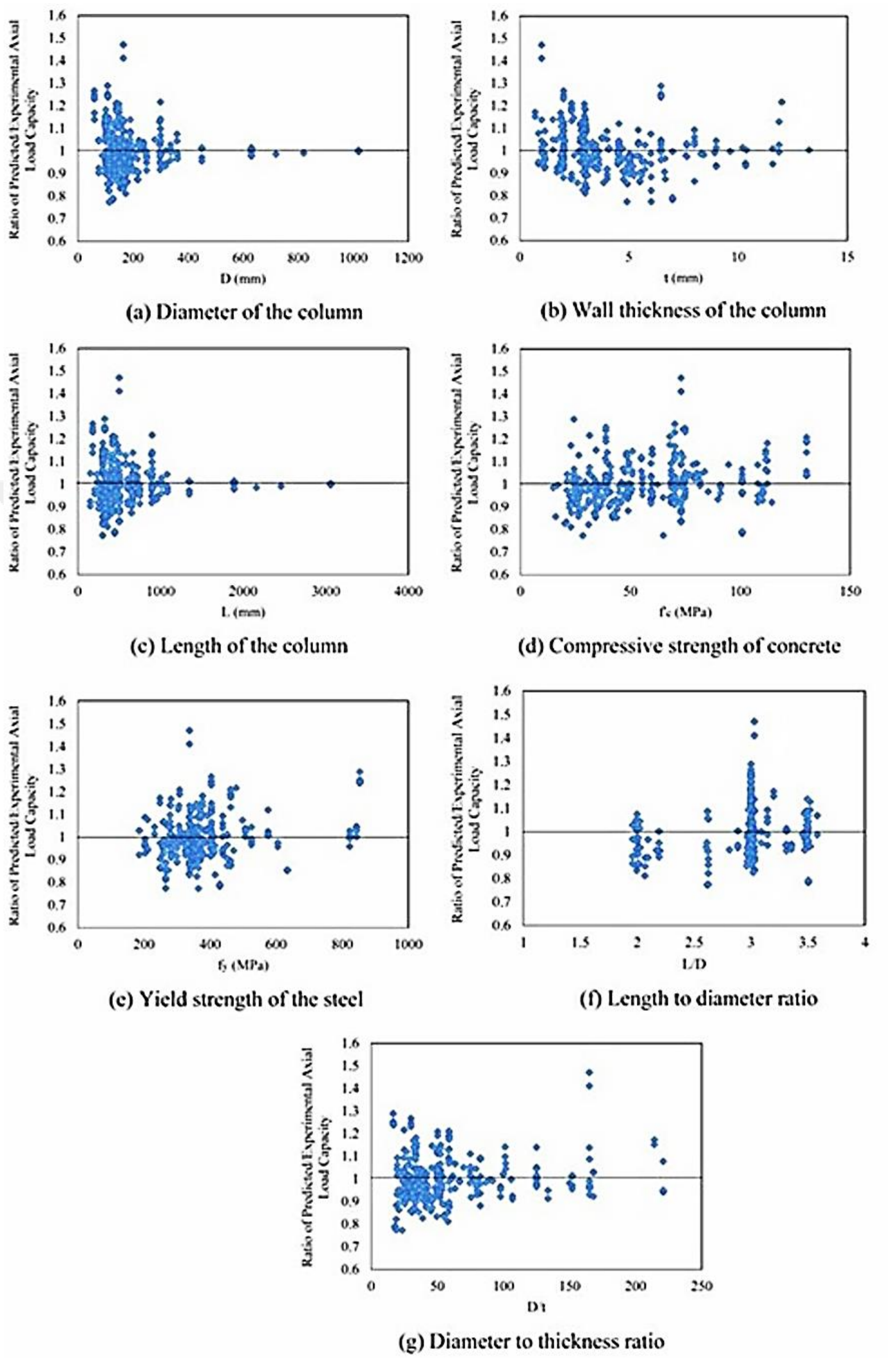

Figure 2.8 Effect and interaction of several parameters on CFST columns (Güneyisi et al., 2016)

It is also reported that the slenderness ratio of the composite CFST columns influences the structural behavior in the case of the axial compression. The length to diameter ratio (L/D) is less than 3.5, indicating that the column is stub. A relatively small slenderness influence could be occurred and the column could not fail under the buckling (Lu and Zhao, 2010). However, the large slenderness ratio resulted in overall flexural buckling for the composite columns as mentioned in the study of Dundu (2012). He studied the behavior of 24 CFST columns having L/D ratios of 5.16 to 21.77, loaded under compression. Typical experimental test configuration is given in Figure 2.9. The behavior of different CFST columns is shown in Figure 2.10. It is noted that the slenderness columns revealed inadequate radial strain in steel tube section to confined concrete core. In addition to these Figures 2.11 and 2.12 show clearly the influence of slenderness ratio on the axial capacity of the columns. Irrespective of the diameter used, the load carrying capacity of the columns had tendency to drop.

Figure 2.9 Typical experimental test configuration (Dundu, 2012)

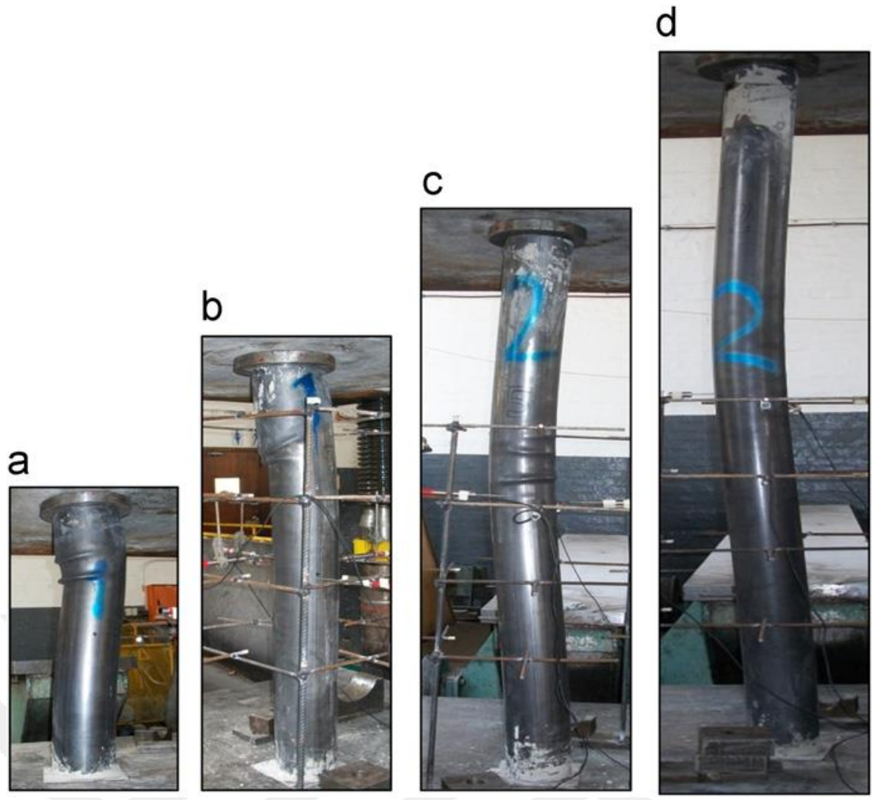

Figure 2.10 Failure behavior of different CFST columns. (a)1.0 m, (b)1.5 m, (c) 2.0 m and (d) 2.5 m (Dundu, 2012)

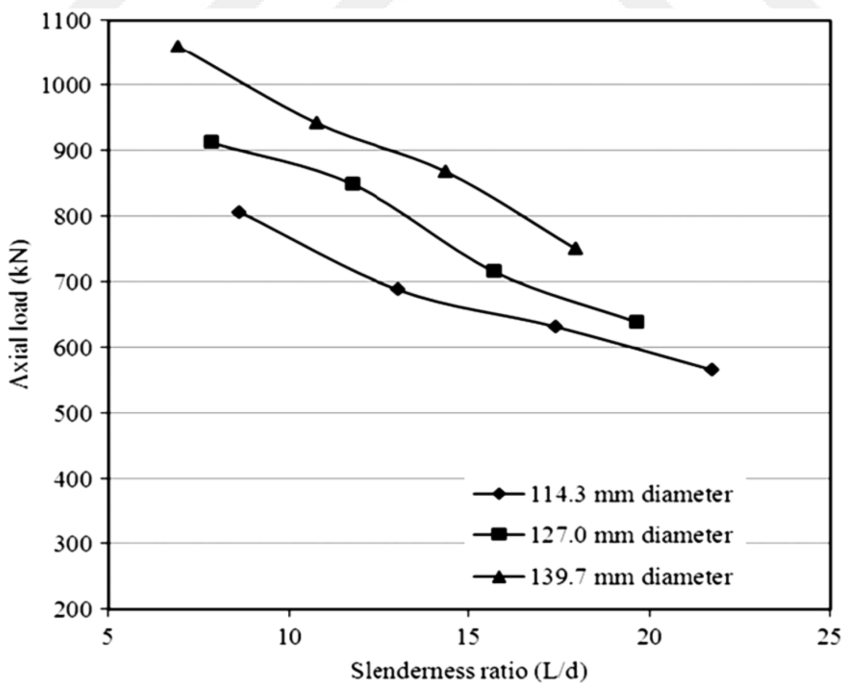

Figure 2.11 Influence of slenderness ratio on the axial capacity (Dundu, 2012)

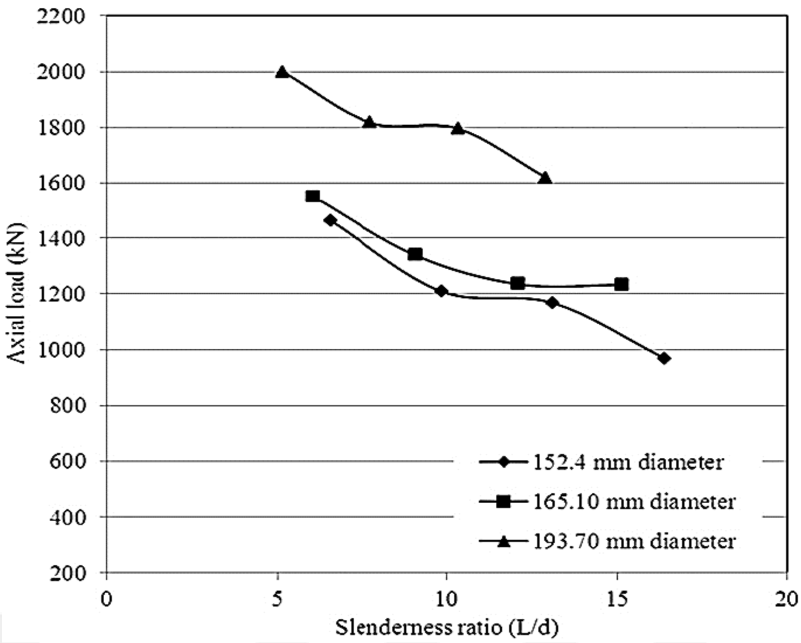

Figure 2.12 Influence of slenderness ratio on the axial load capacity (Dundu, 2012)

Aside from the concrete strength, steel yield stress, D/t and L/D ratios, the confinement influence of CFST columns can also be affected by the loading mode (Fam et al., 2004; Johansson and Gylltoft, 2002; de Oliveira et al., 2010; Yu et al., 2007), i.e. Three modes of applying load were considered. Case (1) applied load to the concrete core only. In this case, the steel tube was acted fundamentally as lateral restricting devices whereas the axial stress of steel tube was progressed by the friction of steel-concrete interface. Case (2) applied load to the steel section only. In this case, the in-filled concrete performed as a rigid medium to prohibit the steel tube from interior buckling at the primary stage. Nevertheless, the steel-concrete interface bond would break with increasing the axial strain and no axial stress progressed for the core concrete. Without the interface bond stress, the steel tube separately acted as the HST column and the strength was not improved at all. Whereas in the case (3) Steel tube and concrete were loaded together. In this case the ordinary loading manner supposed in the design and construction. The progress of confinement influence was reliant on the stretching properties of steel tube and concrete. The steel tube would act as both longitudinal and transverse reinforcement, which supplied both axial resistance and restricting stress together. Since the axial stress in a steel tube would have an adverse influence on the hoop stress as in the Von Mises' failure criterion of steel tube, the restricting stress supplied in case three was commonly lesser than that in case one. Furthermore, in case three, there would be negative confining stress at the initial loading stage (compressive hoop stress), the improvement of confining stress need large hoop strain. Consequently, it is found out that applying load to core concrete, the confinement influence is the paramount and thus the improvement in strength and ductility.

Owing to the limitation of the laboratory, most of the experimental investigations were performed in view of steel tube with a comparatively small diameter less than 300 mm this deals that the conclusions may or may not be veracious when scaling up the samples to the real structural sizes. Subsequently, it may be vital to deem the scale influence on the design of uni-axially loaded CFST short columns. Sakino et al. (2004) deemed the scale influence on the compressive strength of concrete by inserting the strength reduction factor for concrete reliant on other's test results. The reduction factor reduced with increment the diameter of the cylinder. On the contrary, CFST columns with steel tube diameter greater than 1000 mm were fabricated and tested (Kilpatrick and Rangan, 1999; Luksha and Nesterovich, 1991; Ren et al., 2013), results pointed that the behavior of large and small diameters CFST column was comparable each other's.

As looked before, the adverse confining stress that happens between concrete and steel tube throughout preliminary elastic stage under uni-axial load would have negative influence on the composite action, occasioning to smaller elastic strength and also initial stiffness. For instance, Giakoumelis and Lam (2004) studied the bond strength of steel tube with core concrete in CFST columns. In their investigation, a total of thirteen CFST columns with concrete strength up to 100 MPa were examined. Amongst these samples, five CFST columns were lubricated and thus there would not be any interface bond stress. They found out that when the concrete strength lesser than 50 MPa there was a slight difference in the axial capacity between lubricated and unlubricated samples but the elastic strength of unlubricated column was greater than that of lubricated column. For samples with concrete strength of 100 MPa, the variance between the load-carrying capacity of the bonded and un-bonded samples was 14%, denoted that the interface bonding was more crucial with higher strength concrete samples. Liao et al. (2011) discovered the impact of circumferential and spherical-cap gap experimentally through fourteen short column tests. They established that the circumferential gap could cause a considerable impact on the behavior of CFST columns. With circumferential gap ratio 2.2%, maximum strength of CFST columns could reduce by 29%. In the opposite way, with the spherical-cap, the behavior of

CFST columns was identical to the undamaged columns and with the gap ratio of 2.2%, the maximum strength diminished by only 2%. The variation between these two gaps might be because of the fact that with a circumferential gap, there would be no interface bond stress. Whilst for samples with a spherical-cap gap, there occurred interface bond stress, however it might be lesser than that of the undamaged samples. Hu et al. (2011) established that thin-walled CFST columns without any confinement might suffer de-bonding and buckle at very small axial strain through compression, occasioning in reduced axial load-carrying capacity and less ductile behavior. Consequently, the interface bonding between the steel tube and core concrete should be enhanced with a view to completely use the composite action. Xue et al. (2012) premeditated the effect of de-bonding on circular CFST columns numerically and experimentally. To be more particular, a total of twelve CFST short columns separated into three sets were experienced under uni-axial compression. They indicated that the de-bonding would take contrary impacts on the maximum load and ductility of CFST short columns and the maximum load could reduce by 16.9% when changing the de-bonding arc-length ratio and the tube diameter-to-thickness ratio.

2.4.2 Use of UHPC and GPC in CFST columns

In the technical literature and construction practice, the CFST columns made with UHPC and GPC are rarely utilized since such infill materials are relatively new generation products in the concrete technology. For this reason, they also have the opportunity to create new structural elements. For example, in the study of Tue et al. (2004), it was stated that UHPC filled tubes attained very high ultimate loads. They also proposed a new joint for tall buildings and truss bridges. It was found that using UHPC in fabricated or prefabricated steel tube structures could be a good substitute for cast iron joints and avoid great wall thickness at the joint are as it could often needed for normal steel tube structures. Figure 2.13 shows the experimental testing conditions of UHPC filled steel tube joint. The core concrete compressive strength was reported as 150 MPa. It was found that the filled tubes had high bearing capacity and sufficient ductility.

In the study of Scholle and Lohaus (2012), a filigree steel wrapped UHPC tube was tested under a centrically loading condition. Figure 2.14 illustrations the test set-up and the test sample. The UHPC material properties were reported as 181.5 MPa compressive strength, 6.8 MPa tensile strength and 36300 MPa elastic modulus. The experimental results on the force-deformation curve was also compared with the results of the numerical simulation as shown in Figure 2.15. They used a finite element program of ABAQUS to model the behavior. They discussed the potential application of such hybrid tube for large-scale truss composite structures. It was reported that the extremely high compressive strength of UHPC accompanied by explosive brittle failure could turn into the ductile failure behavior as structural elements by means of surrounding thin steel tube.

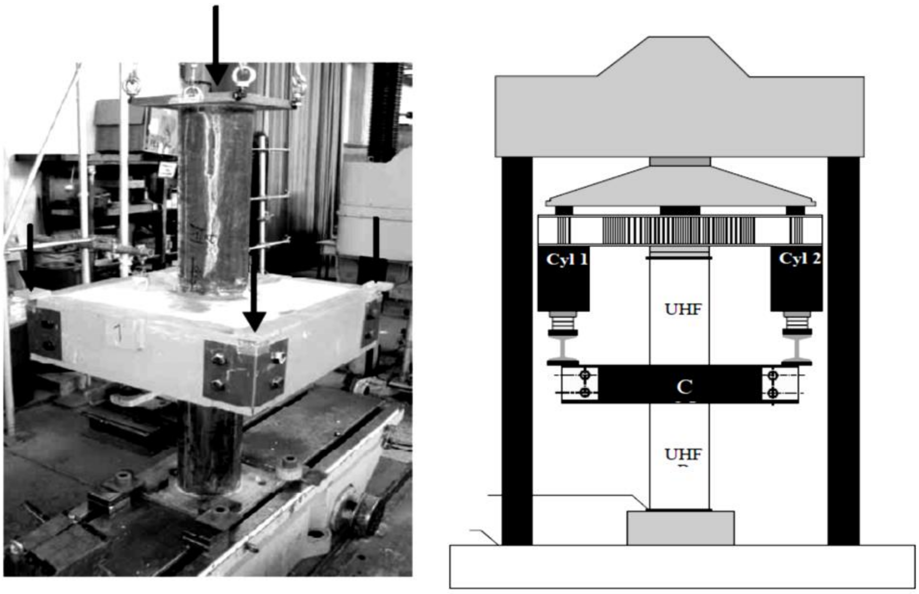

Figure 2.13 The experimental testing conditions of UHPC filled steel tube joint (Tue et al., 2004)

Figure 2.14 Steel-wrapped UHPC tube: test set-up (left) and cut open specimen (right) (Scholle and Lohaus, 2012)

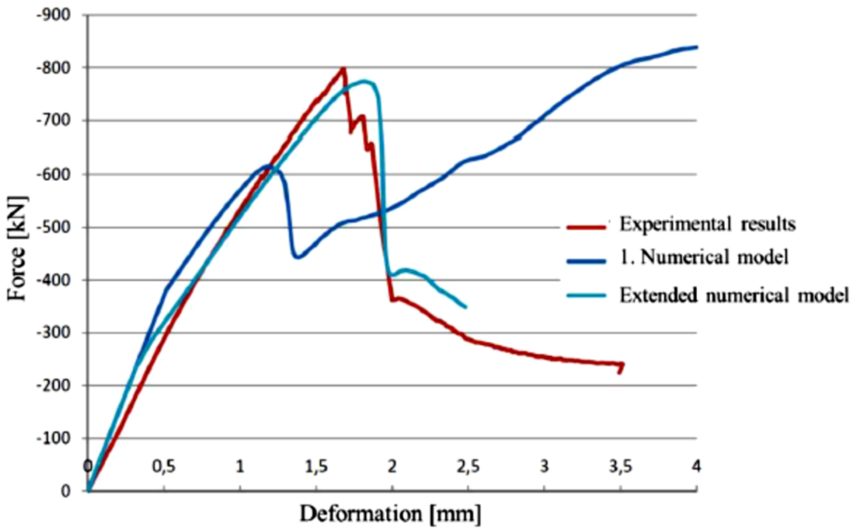

Figure 2.15 Force-deformation-process (Scholle and Lohaus, 2012)

In another study forwarded by Zhang and Wu (2015), the numerical modeling of UHPC filled tube columns under the action of blast loads was investigated. They considered the double skin tubes. The numerical simulation was developed by 8-node solid elements with single point integration algorithm in LS-DYNA. They used the steel tubes with outside diameter of 210 mm, internal diameter of 100 mm and wall thickness of 5 mm. The infill UHPC core compressive strength was about 170 MPa. The consequences exhibited that the experimental peak load and numerical one had similar tendency, producing up to 9.1 % error.

In a recent study of Markowski and Lohaus (2017), the possibility of production UHPC sandwich structures with composite coating subjected to compressive loading were investigated. The hollow section concrete core was covered by two steel tube as double skin CFST section. The outer steel tube was also wrapped with and without carbon fiber reinforced plastic composites. Figure 2.16 reveals UHPC filled double skin steel tube member cross-section. The yield strength of the steel tubes was 235 MPa while the compressive strength of concrete core was 220 MPa. It was observed that the destroyed concrete core of the test sample caused a buckling formation on the outside steel tube. The internal tube was not influenced. The positive effect of composite layer at the outer side of UHPC filled tube in reducing the local buckling was also detected.

Ozbakkaloglu and Xie (2016) performed an investigational work on the behavior of concrete filled fiber-reinforced polymer (FRP) tubes (CFFTs) subjected to axial compressive, arranged utilizing either ordinary Portland cement concrete (OPCC) or

FA-based GPC. 36 CFFTs subjected to axial compression were examined. The influence of the kind of the concrete and FRP tube material, number of FRP layers utilized in the FRP tube and the cross sectional shape of specimen were investigated. The consequences proposed that the behavior of CFFTs under axial stress-strain of is influenced by the concrete type. The CFFTs with GPC developed a same strength development ratio but with minimize axial strain development ratio than the CFFTs with OPCC. Because of the higher shrinkage of the OPCC, the CFFTs with OPCC indicate a plateau at the transition area of their stress-strain curves, which is not observed in the CFFTs with GPC. At a same confinement ratio, CFFT-OPCC restricted with various fibers gives similar strength and strain development ratios, whilst slight variances are observed among CFFT-GPC produced with various fibers. The strength and strain improvement coefficients of both types of the columns reduction with an increment in the thickness of FRP tube. A precise model that was initially suggested to prophesy the eventual situations of FRP confined OPCC was improved to enable the implementation of the model to circular and square CFFTs with GPC.

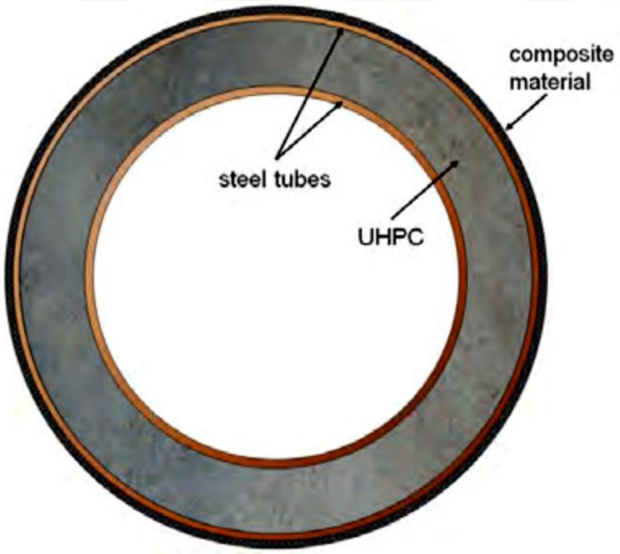

Figure 2.16 UHPC sandwich structure with composite coating, cross-section (Markowski and Lohaus, 2017)

Shi et al. (2015) performed an investigational work on twelve concrete filled steel tubular columns under axial loading. Two section sizes of square hollow sections filled with geopolymeric recycled concrete (GRC) and recycled aggregate concrete (RAC) respectively, with various recycled aggregate (RA) substitution ratios up to 100% were utilized in the tests. The results revealed that when addition more RAs in the columns, the peak strain was improved, while the ultimate strength reduced. The ductility of the columns was enhanced by increasing the RA substitution ratio. Generally, the effect of RA on the strength and ductility of GRC filled steel tubular columns is higher than that of RAC filled steel tubular columns. The supposed analytical model for prophesying the relation of load vs. deformation of GRCFST columns subjected to axial loading was tested, and a reviewed analytical model suggested. The new model exhibited good correspondence with the investigational results.

CHAPTER 3
METHODOLOGY

This chapter containing two parts, in the first part, experimental investigation was implemented to study the properties of ultra-high performance conventional and geopolymer concretes. Two types of curing were used, water and steam curing for conventional UHPC and heat and steam curing for geopolymer modified UHPC (UHPGC). Whereas the second part of this chapter dealt with the overview of the international design codes and the design model formulas for the ultimate capacity of the UHPC and UHPGC composite columns used in numerical study.

3.1 Experimental study

3.1.1 Materials

The cement utilized in this investigation is ordinary Portland cement (OPC) CEM I 42.5 R, conforming to the TS EN 197 (2002). Silica fume (SF), fly ash (FA) and slag (SL) are also used in UHPC and as source materials in UHPGC mixes. The chemical compositions and some physical properties of these materials are presented in Table 3.1, and their particle size distributions are given in Figure 3.1.

Quartz fine aggregate with a specific gravity of 2.65 was used in 3 fractions, namely 0-0.4, 0.6-1.2, and 1.2-2.5 mm. The particle size distribution of 0-0.4 mm quartz fine aggregate is also presented in Figure 3.1. Micro steel brass glazed fibers with a length of 6 mm and a diameter of 0.16 mm were used to give fiber reinforcement for all mixes. The properties of micro steel fibers are presented in Table 3.2 which is given by the industrialist. Whereas the required workability of the mixes was attained by applying a new generation type F polycarboxylate-based superplasticizer (SP) conforming to ASTM C494 (2013). The properties of SP presented in Table 3.3.

The alkaline solution utilized in this investigation was a conjunction of sodium silicate (water glass) (Na_2SiO_3) with a (SiO_2/Na_2O ratio by mass of equal to 2, Na_2O = 14.7%,

SiO_2 = 29.4%, and water = 55.9%) and sodium hydroxide (NaOH) solutions. Firstly sodium hydroxide with a 99% purity in a flake form were thawed in distilled water to obtain alkali solutions of 12 M, which is recommended to give highest compressive strength (Al Bakri et al., 2012). Thereafter, the NaOH and Na_2SiO_3 solutions mixed together and allowing the mixture for at least of 24 h to the reaction of polymerization before casting, which is recommended by Rangan (2008). All geopolymer concrete mixes were made with an alkaline solution ratio of 2.5 by mass which is gives the maximum strength (Hardjito et al., 2004; Al Bakri et al., 2012; Sanni and Khadiranaikar, 2012).

Table 3.1 Properties of OPC, SF, FA and SL

Item	OPC	SF	FA	SL
CaO (%)	57.87	0.45	4.24	34.19
SiO_2 (%)	17.99	90.36	57.2	40.42
Al_2O_3 (%)	3.88	0.71	24.2	10.6
Fe_2O_3 (%)	3.36	1.31	7.1	1.28
MgO (%)	1.49	-	2.4	7.63
SO_3 (%)	2.47	0.41	0.29	0.68
K_2O (%)	-	1.52	3.37	-
Na_2O (%)	-	0.45	0.38	-
Cl (%)	0.005	-	-	0.0128
Loss of Ignition (%)	3.37	3.11	1.58	2.74
Insoluble Residue (%)	0.34	-	-	-
Free CaO (%)	2.18	-	-	-
Specific surface (m^2/kg)	394	21080	379	575
Specific gravity	3.15	2.2	2.25	2.79

Table 3.2 Physical, mechanical properties and aspect ratios of micro steel fibers

Fiber name	Length (L) (mm)	Diameter (d) (mm)	Aspect ratio (L/d)	Density (g/cm^3)	Tensile strength (MPa)
Micro steel fiber	6	0.16	37.5	7.17	2250

Table 3.3 Properties of the SP

Properties	Results
Appearance	Light brown to yellow liquid
Specific gravity at 20°C gm/cm^3	1.08 ± 0.02
PH- value	7 ± 1
Alkali content (%)	≤ 1
Chloride content (%)	≤ 0.1

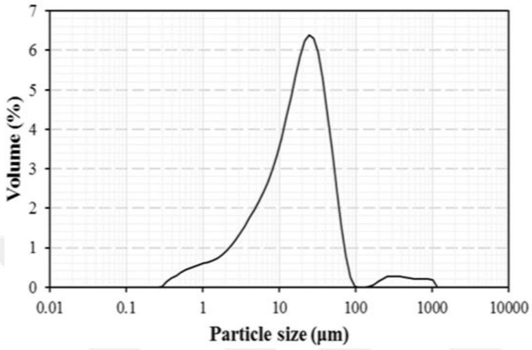

(a)

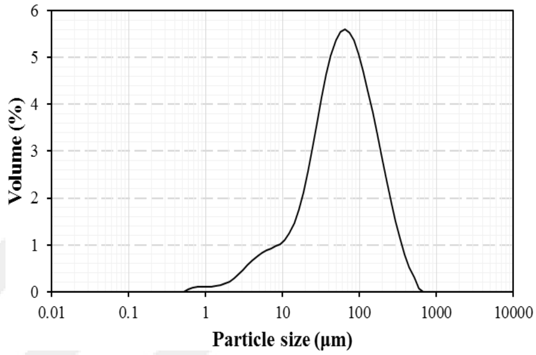

(b)

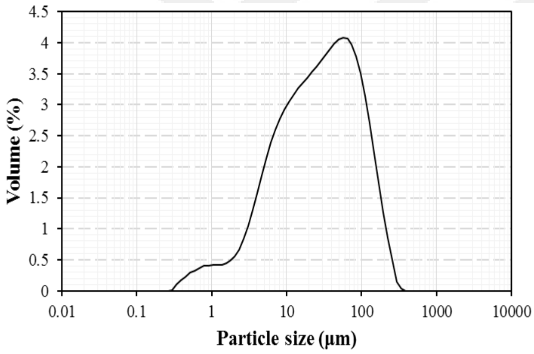

(c)

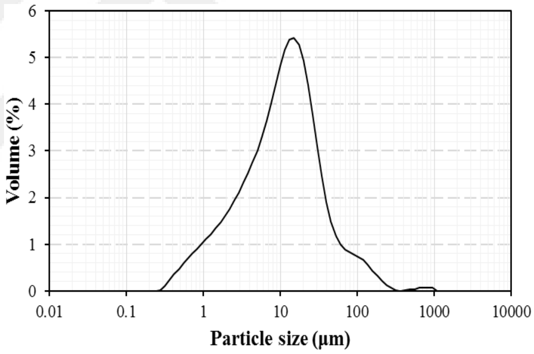

(d)

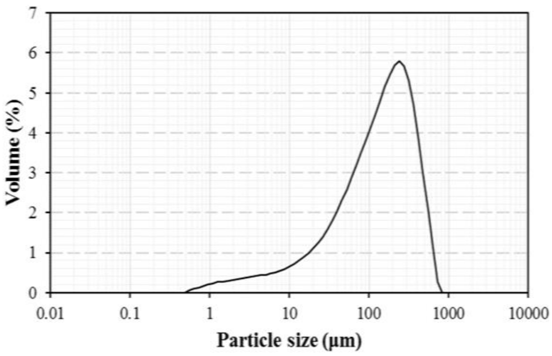

(e)

Figure 3.1 Particle size distribution of: a) OPC, b) SF, c) FA, d) SL and e) 0-0.4 mm quartz

Figure 3.2 Materials to cast UHPC/UHPGC

3.1.2 Proportioning, casting and curing conditions

The mixture proportioning of UHPC is demonstrated in Table 3.4. A total of 11 concrete mixtures were produced with binder content of 1150 kg/m^3 and a w/b ratio of 0.17. The control mix contained only OPC as a binder whereas the other mixtures had binary (OPC + SF), ternary (OPC + SF + FA and OPC + SF + SL), and quaternary (OPC + SF + FA + SL). A constant replacement level for SF was 15% of the binder, while for FA or/and SL were 25, 50 and 75% of cement by mass. All UHPC mixtures comprised a constant percentage of micro steel fibers as 2% of volume fraction.

UHPC were mixed using a high speed mixer that could mix with a speed up to 470 rpm. At first, aggregates and dry powders were mixed with low speed of 100 rpm for about 3 min. Then, a half of water was applied to the dry powders and the mix was remixed for another 3 min. with the low speed. The residual water and SP were mixed with each other and added to the mixture and the mixing was persistent at 470 rpm for about 3 min. Finally, adding the micro steel fibers to the mix and mixed for another 2 min at 470 rpm. Thereafter, the fresh concretes were filled in the molds and compacted by means of vibrating table. Then, the samples were wrapped with polyethylene sheets and retained in the molds for 24 h at ambient temperature of 22 ± 2 ºC. UHPC samples were demoulded after 24 h from casting and cured. Two different methods of curing were used in this research water curing (WC) and steam curing (SC). In WC, the samples retained in water at 20 ± 2 ºC until the date of testing. While in SC the specimens placed in the steam chamber for 48 h including 3 h of heating until reaching the maximum temperature, which was selected as 90 ºC and keeping the temperature constant on this temperature for 42 h and finally cooling of the chamber which took 3 h. The humidity in SC chamber's was about 95 ± 2%. The specimens were brought out from curing and placed in water at 20 ± 2 ºC until the time of testing.

The mixture proportioning of UHPGC is demonstrated in Table 3.5. A total of 10 mixtures were produced with a source material/alkaline solution ratio equal to 2.5, a w/b ratio of 0.17 and a total binder content of 1150 kg/m^3. For the half of mixtures, SF was added to the geopolymer concrete with 15%, while in the other it included. Each group containing (FA, SL, 25%FA + 75% SL, 50%FA + 50% SL, 75%FA + 25% SL). All mixtures comprised a constant percent of micro steel fibers is 2% of volume fraction.

UHPGC were mixed in the same mixer used for UHPC. At first, aggregates and dry powders were mixed together with low speed of 100 rpm for about 3 min. Thereafter, water and alkali activated solution were applied to the dry powders and the mixture was remixed for another 3 min with the speed of 100 rpm. Finally, the micro steel fibers were added and mixed for another 2 min with a speed of 470 rpm. Then, the fresh geopolymer concretes were filled in the molds and compacted by means of vibrating table. The samples were then wrapped with polyethylene sheets and retained in the molds for 24 h at ambient temperature of 22 ± 2 ºC. After 24 h from casting, the UHPGC samples were demoulded and cured. Two different methods of curing were applied in this research heat curing (HC) and steam curing (SC). In HC, the samples kept in an oven at 90 ºC for 48 h. While in SC, applying the same procedure used with UHPC specimens. For the two curing methods, the specimens were taken out and placed in air at 20 ± 2 ºC till the age of testing. Moreover, it is noted that in Tables 3.4 and 3.5, in abbreviation, the letter C and G indicate conventional UHPC and geopolymer modified UHPC (UHPGC), respectively.

Figure 3.3 Hobart mixer used for mixing UHPC and UHPGC

Table 3.4 Mixture proportions of UHPC

Abbreviation	w/b	OPC (kg/m^3)	SF (kg/m^3)	FA (kg/m^3)	SL (kg/m^3)	Water (kg/m^3)	SP (kg/m^3)	Micro steel fiber (kg/m^3)	Quartz aggregate size (kg/m^3)		
									1.2-2.5 mm	0.6-1.2 mm	0-0.4 mm
C	0.17	1150.0	0.0	0	0	195.5	43.7	143.4	243.7	341.1	389.9
CSF	0.17	977.5	172.5	0	0	195.5	20.1	143.4	242.6	339.6	388.1
CSF25FA	0.17	733.1	172.5	244.4	0	195.5	16.1	143.4	224.6	314.5	359.4
CSF50FA	0.17	488.8	172.5	488.8	0	195.5	11.5	143.4	207.1	289.9	331.3
CSF75FA	0.17	244.4	172.5	733.1	0	195.5	8.1	143.4	188.8	264.3	302.1
CSF25SL	0.17	733.1	172.5	0	244.4	195.5	17.3	143.4	237.9	333.0	380.6
CSF50SL	0.17	488.8	172.5	0	488.8	195.5	13.2	143.4	233.9	327.4	374.2
CSF75SL	0.17	244.4	172.5	0	733.1	195.5	9.8	143.4	229.5	321.3	367.2
CSF12.5FA12.5SL	0.17	733.1	172.5	122.2	122.2	195.5	16.1	143.4	231.6	324.3	370.6
CSF25FA25SL	0.17	488.8	172.5	244.4	244.4	195.5	12.7	143.4	220.3	308.4	352.5
CSF37.5FA37.5SL	0.17	244.4	172.5	366.6	366.6	195.5	8.6	143.4	209.3	293.1	334.9

Table 3.5 Mixture proportions of UHPGC

Abbreviation	w/b	SF (kg/m³)	Geopolymer ingredients					Actual water (kg/m³)	Micro steel fiber (kg/m³)	Quartz aggregate size (kg/m³)		
			FA (kg/m³)	SL (kg/m³)	SF (kg/m³)	WG (kg/m³)	NaOH (kg/m³)			1.2-2.5 mm	0.6-1.2 mm	0-0.4 mm
SF-GFA	0.17	172.5	698.2	0.0	0.0	199.5	79.8	32.8	143.4	235.5	329.7	376.8
SF-GSL	0.17	172.5	0.000	698.2	0.0	199.5	79.8	32.8	143.4	275.3	385.4	440.4
SF-G25FA75SL	0.17	172.5	174.55	523.7	0.0	199.5	79.8	32.8	143.4	265.3	371.5	424.5
SF-G50FA50SL	0.17	172.5	349.1	349.1	0.00	199.5	79.8	32.8	143.4	255.4	357.5	408.6
SF-G75FA25SL	0.17	172.5	523.7	174.6	0.0	199.5	79.8	32.8	143.4	245.4	343.6	392.7
GSFFA	0.17	0.0	698.2	0.0	123.2	234.7	93.9	4.1	143.4	246.8	345.5	394.9
GSFSL	0.17	0.0	0.07	698.2	123.2	234.7	93.9	4.1	143.4	286.6	401.2	458.5
GSF25FA75SL	0.17	0.0	174.6	523.7	123.2	234.7	93.9	4.1	143.4	276.6	387.3	442.6
GSF50FA50SL	0.17	0.0	349.1	349.1	123.2	234.7	93.9	4.1	143.4	266.7	373.3	426.7
GSF75FA25SL	0.17	0.0	523.7	174.6	123.2	234.7	93.9	4.1	143.4	256.7	359.4	410.8

3.1.3 Testing Procedures

3.1.3.1 Evaluating of fresh property

The flow of UHPC/UHPGC was measured utilizing the workability test recommended by ASTM C1437 (2015) as presented in Figure 3.4. After pouring fresh mixture to the mini cone, the cone was raised straight upwards to permit free flow for the fresh UHPCs on the plate. The flow value of the designed UHPC /UHPGC was estimated as the average of two measured diameters.

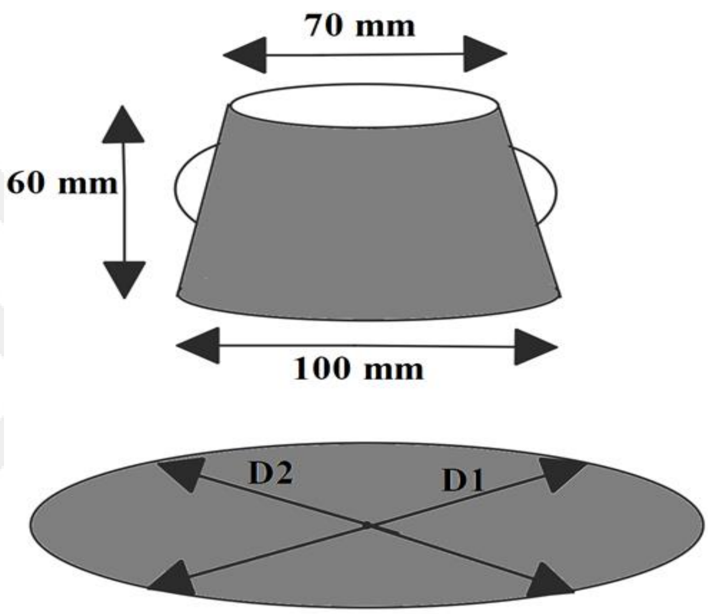

Figure 3.4 Mini slump flow test

3.1.3.2 Evaluating of mechanical property

The mechanical properties tested in this work were compressive strength, splitting tensile strength and static modulus of elasticity. The compressive strength test was performed on 50 mm cubes with a rating load of 0.9 kN/s according to ASTM C109/C109M (2016) as shown in Figure 3.5. This test was conducted by taking the average of three samples at the ages of 7, 28, and 90 days. Whereas the splitting tensile strength test was evaluated according to BS 1881-117 (1983) by taking the average of three of 70 mm cube samples for each mix at 90 days, with rating load of 0.2 kN/s.

The static modulus of elasticity is estimated from the stress-strain curve specified according to ASTM C469 (2014) as presented in Figure 3.6. Where the slope of the inclined line drawn between two points on stress-strain curves that characterize the modulus of elasticity. The first point specified at strain value equal to 0.00005, whilst the second point specified at the point where stress is equivalent to 40% of the maximum stress. The average results gained from three individual 150 mm cubic specimens for each concrete mix at 90 days.

Figure 3.5 Compressive strength test

Figure 3.6 Modulus of elasticity test

3.1.3.3 Evaluating of fracture property

Fracture energy (GF) is a significant parameter to depict the resistance to cracking and deforming. A simple three-point bending test was performed with respect to the recommendation of RILEM 50-FMC (1985). The displacement was quantified instantaneously by means of linear variable displacement transducer (LVDT) at middle span.

A test beam was used with cross-section of 70 × 70 × 280 mm. The distance between supports was 200 mm. The beams were notched with 28 mm depth and the notch opening was accomplished through decreasing the effective cross section to 42×70 mm by sawing in order to conciliate large aggregates in more abundance. Load vs. deflection at the mid-span (δ) curve was achieved for each sample and the area below the load vs. displacement at mid span (W_o) was applied in the determination of the GF. The GF was calculated by applying the equation specified by RILEM 50-FMC.

$$G_F = \frac{W_0 + mg\frac{S}{U}\delta_o}{B(W-a)} \tag{3.1}$$

Where B: width of the specimen, W: depth of the specimen, a: the notch depth, S: the span of the specimen (the distance between supports), U: length of the specimen, m: mass of the specimen, δ_o: maximum deflection at final fracture and g: gravitational acceleration.

The flexural strength, f_{flex}, was calculated via equ. 3.2 by supposing no notch sensitivity (Akcay et al., 2012; Ravindra and Henderson, 1999).

$$f_{flex} = \frac{3P_{max}\,S}{2B(W-a)^2} \tag{3.2}$$

Where P_{max}, S, W, B and a are ultimate load, span length, depth, width and notch depth of the beam, respectively.

Characteristic length (l_{ch}) is a ductility measurement parameter was calculated using equ. (3.3) as a function of elastic modulus (E), splitting tensile strength (f_{st}) and fracture energy (G_f) (Hillerborg, 1985).

$$l_{ch} = \frac{E\,G_f}{f_{st}^2} \tag{3.3}$$

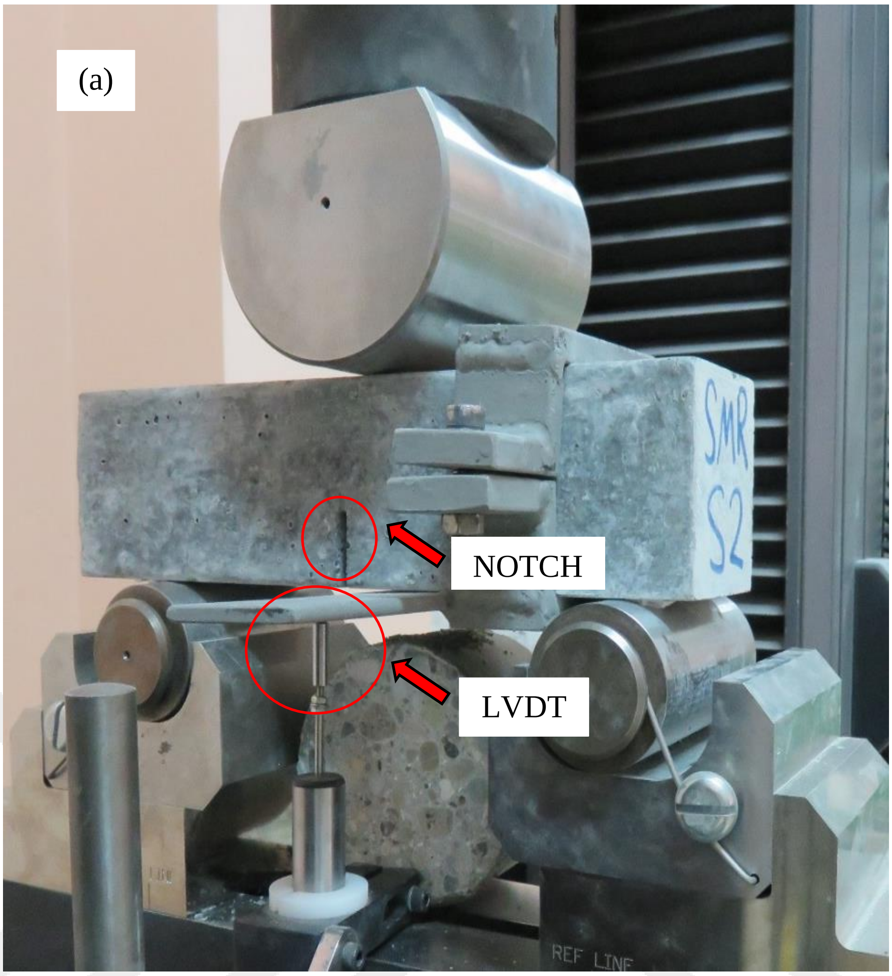

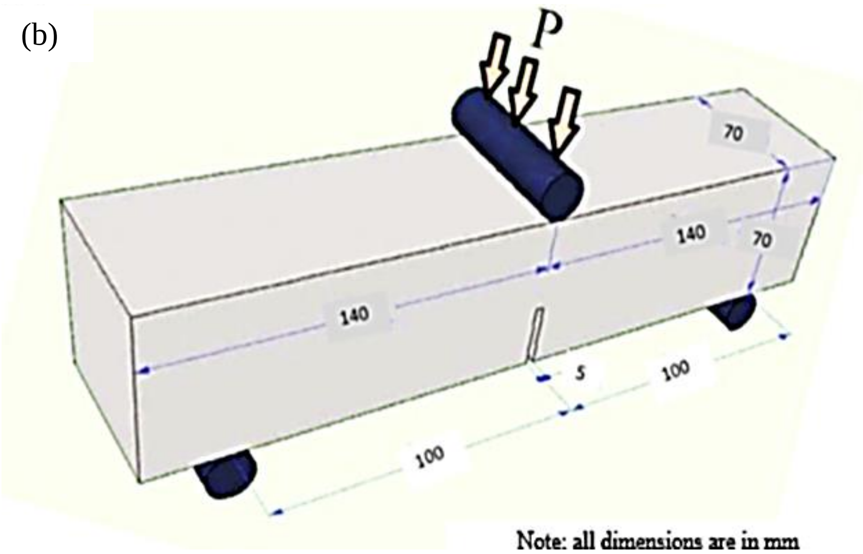

Figure 3.7 Three point bending test on the beam

3.2 Numerical study

3.2.1 Introduction to CFST column

CFST structure offers considerable structural advantages, comprising high strength and fire resistances, adequate ductility and large energy absorption capacities. The utilizing of shuttering during concrete construction is not required. This leads to reduce the construction cost and time. These benefits have led to the extensive utilize of CFST structures in civil engineering structures (Han et al., 2014).

CFST columns enhanced bearing capacity, as well as a very large deformability due to the hooped compression, which is generated by the steel holder for the concrete core. It gives the quasi-plastic nature of their destruction, even when the HSC is utilized. Using CFST columns in the building frames considerably increases the survivability of buildings during earthquakes (Krishan et al., 2016).

3.2.2 Details of study

The fundamental purpose of analytical investigation is to evaluate the behavior of ultra-high performance conventional and geopolymer CFST short circular columns subjected to axial compressive load. Three different international design models for computing the axial load carrying capacity of circular CFST short columns were used. They are ACI 318 (2005), Eurocode 4 (2004) and Chinese (DL/T) (1999) codes. Four ratios of diameter to thickness (D/t) of 25, 50, 75 and 100 and three yield stress of steel values of 150, 325 and 500 MPa were specified for the tested CFST columns. The results of compressive strength obtained from experimental program in this thesis were used for analytical study. Furthermore, the study comprises the representation of the effect of curing type, age of specimen and replacement level of pozzolanic byproduct materials on the axial load carrying capacity of each type of concrete produced in this thesis as well as the comparison between the studied codes. The test arrangement considered into account is uniaxial compression test which is schematically described in Figure 3.8.

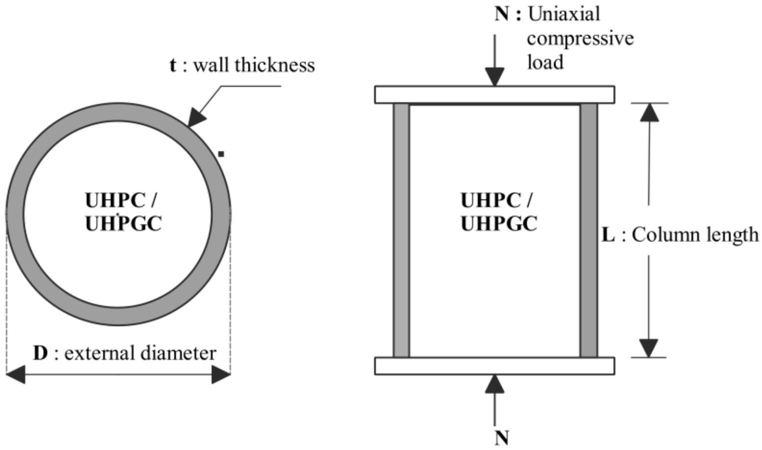

Figure 3.8 Presentation of load applied to the section of circular CFST column infilled with UHPC/UHPGC

3.2.3 Design code formulas

3.2.3.1 ACI 318R code

The ACI-318R (2005) suggests a simple equation for computing the axial load-carrying capacity of CFST considering the reinforced-concrete theory. It may be too preventative because of ignoring the confinement effect consideration. The anticipated formula for axial capacity of a circular CFT column by ACI, $N_{u,ACI}$ is given by:

$$N_{u,ACI} = 0.85\, f_c'\, A_c + f_y\, A_s \qquad (3.4)$$

Where f_c' is the compressive strength of concrete cylinders (150×300 mm), A_c is the cross-sectional area of the concrete specimen core, f_y is the yield stress of steel and A_s is the cross sectional area of steel.

3.2.3.2 Eurocode 4

The Eurocode 4 (2004) designate the resistant capacity of a circular CFT column by counting the involvement of the steel tube and the concrete core and the confinement influence is taken into account. The strength of the concrete is increment by the coefficient η_c because the concrete has a higher strength when a triaxial state of stress take place. The steel tube strength is reduced by η_a because the reduction in effective yield stress of the steel by the hoop stresses. The ultimate strength equations by EC4 are summarised below:

$$N_{u,EC4} = \left(1 + \eta_c\, \frac{t}{D}\frac{f_y}{f_c'}\right) f_c'\, A_c + \eta_a\, f_y\, A_s \qquad (3.5)$$

where

$$\eta_a = 0.25(3 + 2\lambda) \qquad (\eta_a \leq 1.0) \tag{3.6}$$

$$\eta_c = 4.9 - 18.52\lambda + 17\,\lambda^2 \qquad (\eta_c \geq 0) \tag{3.7}$$

In which the relative slenderness (λ) of CFST column can be estimated from the following equation:

$$\lambda = \sqrt{\frac{N_{pIR}}{N_{cr}}} \tag{3.8}$$

Where:

N_{pIR} is the cross-section plastic resistance of the CFST column, given as

$$N_{pIR} = f_y\, A_s + f_c'\, A_c \tag{3.9}$$

N_{cr} is the Euler buckling load of the pin-ended CFST column, represented by:

$$N_{cr} = \frac{\pi^2 (EI)_{eff^2}}{l^2} \tag{3.10}$$

Where:

$(EI)_{eff^2}$ is the effective flexural stiffness of CFST and can be computed as:

$$(EI)_{eff^2} = E_s\, I_s + K_e\, E_{c2}\, I_c \tag{3.11}$$

Where: E_s and E_{c2} is the elastic modulus of steel and concrete, respectively.

The elastic modulus of concrete $= 22000[(f_c' + 8)/10]^{0.3}$ (3.12)

Typically, when λ=0, the sectional capacity (the zero length strength), $P_{0,EC4}$ can be simplified as

$$P_{0,EC4} = \left(1 + 4.9\,\frac{t}{D}\frac{f_y}{f_c'}\right) f_c'\, A_c + 0.75\, f_y\, A_s \tag{3.13}$$

3.2.3.3 Chinese code DL/T (1999)

The equations specified in the Chinese code DL/T (1999) are related to the unified theory, in which the composite CFST column is considered as an equivalent section comprising of one material with a total cross-sectional area A_{sc} and corresponding yield strength f_{scy}. The confinement effect is deemed by introducing the confinement factor. The design equations are listed as follows:

$$N_{u,DL/T} = f_{scy} A_{sc} = f_{scy}(A_s + A_c) \tag{3.14}$$

In which:

$$f_{scy} = (1.212 + B\xi + C\xi^2) f_{ck} \tag{3.15}$$

$$B = 0.1759 \frac{f_y}{235} + 0.974 \tag{3.16}$$

$$C = -0.1038 \frac{f_{ck}}{20} + 0.0309 \tag{3.17}$$

$$\xi = \frac{A_s f_y}{A_c f_{ck}} \tag{3.18}$$

$$f_{ck} = 0.67\, f_{cu} \tag{3.19}$$

Where: ξ the confinement factor; A_{sc} and f_{scy} the area of composite section and the nominal yielding strength of the composite section respectively, f_{cu} the compressive strength of 150 mm cube, and f_{ck} the characteristic concrete strength.

3.2.4 Summary of main computation steps

The calculation of ultimate axial load carrying capacities of the circular ultra-high performance conventional and geopolymer filled steel tubular by using ACI 318 (2005), Eurocode 4 (2004) and Chinese (DL/T) (1999) codes as follows:

1. The experimental results of compressive strength of conventional and geopolymer modified ultra-high performance have been used.
2. Four different diameter-to-thickness D/t ratios of the specimens were specified, those are: 25, 50, 75, and 100.
3. Three different yield strength of the steel tube (f_y) of 150, 325 and 500 MPa were selected to comprise different specification regarded steel material characteristics.
4. The wall thickness of the steel tube (t) was 2 mm and the length to diameter ratio of short composite columns (L/D) was 2.5 to ensure that they would be with a small slenderness influence and would not fail in overall buckling.

It ought be noted that the conversion of compressive strength of 50 mm cubes to 100×200 mm cylinder taken 1.14 and multiplied by 0.9 to convert it to standard compressive strength cylinders 150×300 mm (f_c'), and using the ratio of the compressive strength of 50 mm cube to 100 mm cube is 1.09 (Abbas et al., 2016). The conversion of compressive strength of 100 mm cube to 150 mm cube taken as 0.96 (Rashid et al., 2002).

CHAPTER 4
RESULTS OF EXPERIMENTS AND DISCUSSION

4.1. Fresh properties of UHPC/UHPGC

Utilization of superplasticizer (SP) is crucial in order to get the required workability of UHPC. The desired flowability for all mixtures was attained as fixed as 20±1 cm by using various amount of SP as presented in Figure 4.1. From the figure, it can be noticed that the replacing of cement by 15% silica fume (SF) improved the flowability of UHPC, and also it can be detected that the mixes containing fly ash (FA) required less amount of SP than the corresponding the mixes containing slag (SL) and FA + SL at all replacement levels. Whereas in UHPGC mixes the flow diameter ranged between 19 to 22 cm without using SP. The UHPGC mixes containing 15%SF with 85% geopolymer gives higher flowability than the corresponding mixes of 100% geopolymer this is may be because that the actual water added to the former mixes higher than that for the latter mixes. The flow results showed that the mixes containing FA gives higher flow diameter than the corresponding mixes containing SL and the diameter were reduced with increasing the SL replacement level as shown in Figure 4.2.

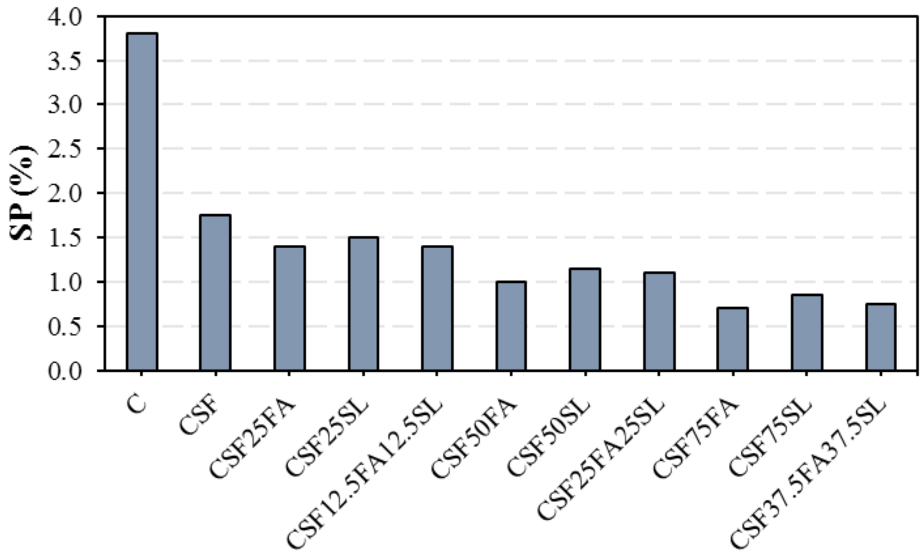

Figure 4.1 SP percent of UHPC

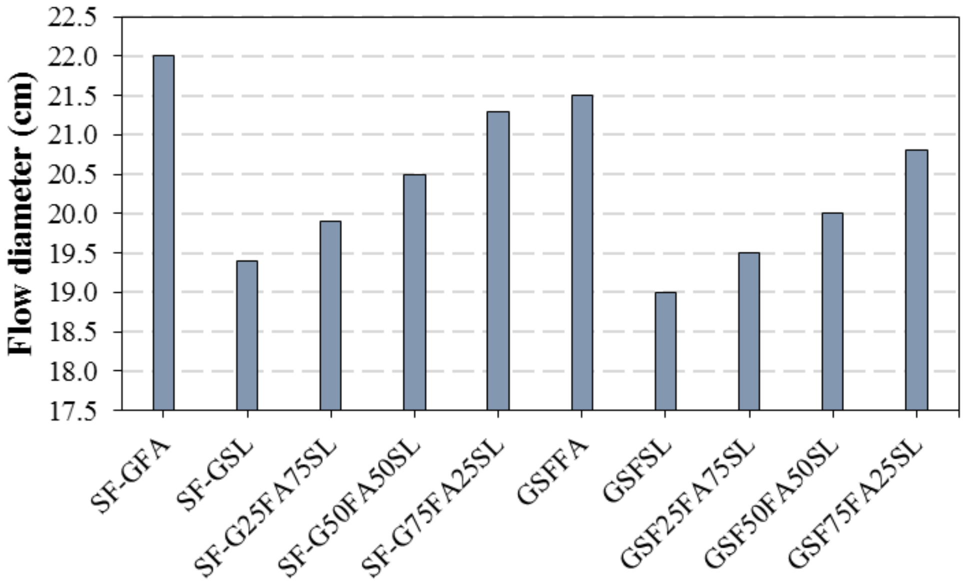

Figure 4.2 Flow diameter of UHPGC

4.2. Mechanical and fracture properties of UHPC

4.2.1. Compressive strength

The compressive strength test results of indicated that for the same mix proportions the steam cured (SC) specimens had higher compressive strength compared to standard water cured (WC) samples at all ages up to 90 days as shown in Figures 4.3, 4.4 and 4.5. For example, the increasing was 16.1, 13.3and 11.6% for control mix and 33.6, 9.4 and 5.5% for the mix containing 15% SF at 7, 28 and 90 days, respectively. This is because of increasing the curing temperature leads to quickens the hydration of cement and enhances the reaction between mineral admixtures and $Ca(OH)_2$ (Reda et al., 1999). From the results it can be perceived that, for the same mix, the strength progress due to SC at 7 days higher than at 28 and 90 days.

The results also revealed that the replacing of cement by 15% SF lead to improve the compressive strength compared with control mix for all ages up to 90 days Figure 4.6. The increasing was 14.7, 29.5 and 28.7% for WC compared with 31.9, 25.1 and 21.7% for SC at 7, 28 and 90 days, respectively. This is can be attributed to the pozzolanic reaction between SF and $Ca(OH)_2$ and producing additional C–S–H gel at final stages (Greenberg, 1961; Korpa et al., 2008; Qing et al., 2007) as well as the addition of SF quickens the hydration of cement (Korpa et al., 2008; Lothenbach et al., 2011; Senff et al., 2010).The acceleration is generally due to the seeding effect because of the hydration proceeds faster in the existence of nucleation sites for C–S–H phases (Thomas et al., 2009) and increase of particle packing density of concrete (Oertel et al., 2014).

For WC regime the mix containing 15% SF gives higher compressive strength (119.4 MPa) compared to the other mixes at 7 days, while the mix containing (15% SF+ 25% SL) gives highest compressive strength (160.7 MPa) in SC condition at the same age. This is because that the SC promotes the pozzolanic reaction of mineral admixtures with $Ca(OH)_2$ (Reda et al., 1999), while the mix containing (15% SF+ 25% SL) gives higher compressive strength compared to other mixes in WC and SC at 28 and 90 days. This mix gives 163.3 and 166.3 MPa for WC at 28 and 90 days with corresponding 168 and 173.2 MPa for SC at the same ages, respectively. This is can be ascribed to increase of particle packing density with 25% SL. The results also indicated that the compressive strength decreased with increasing the replacement of FA and/or SL beyond 25% for all ages, but the decreasing in the compressive strength of the mixes containing FA was higher than the corresponding mixes containing SL and (SL+FA). The decreasing at 28 days were 10.9, 8.7 and 10.5% at 50% replacement level for WC for the mixes containing FA, SL and FA+SL and 12.2, 9.97 and 11.1% for the corresponding SC mixes, respectively. The corresponding decreasing at the same age for 75% replacement level were 31.8, 14.6 and 28.0 % for WC and 31.2, 18.7 and 25.8% for SC for the mixes comprising FA, SL and FA+SL, respectively.

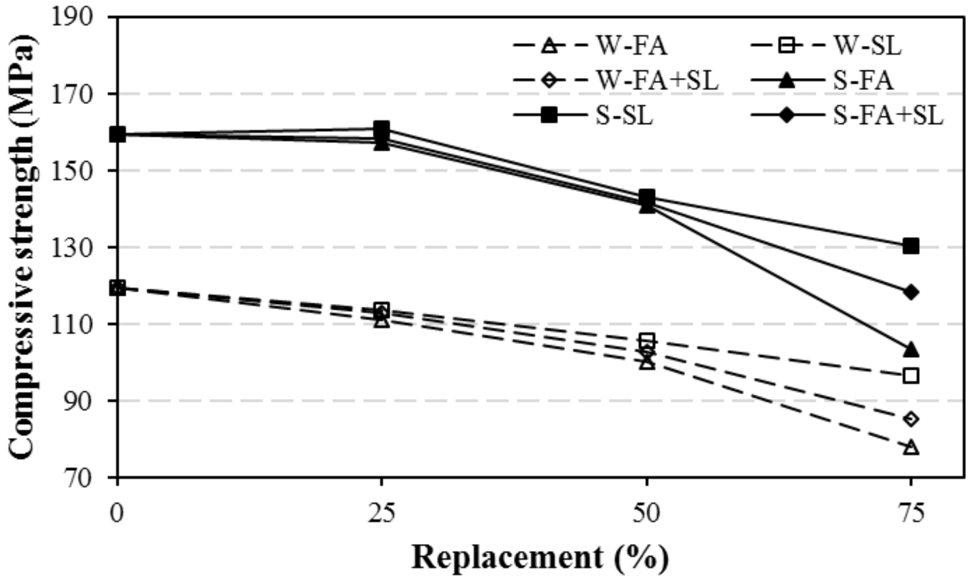

Figure 4.3 Compressive strength of WC and SC UHPC at 7 days

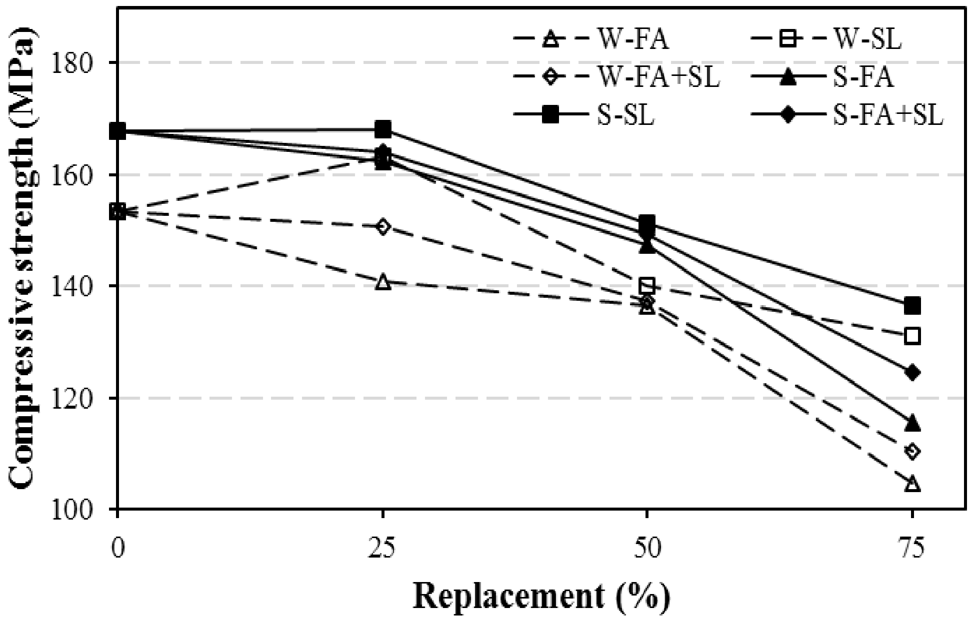

Figure 4.4 Compressive strength of WC and SC UHPC at 28 days

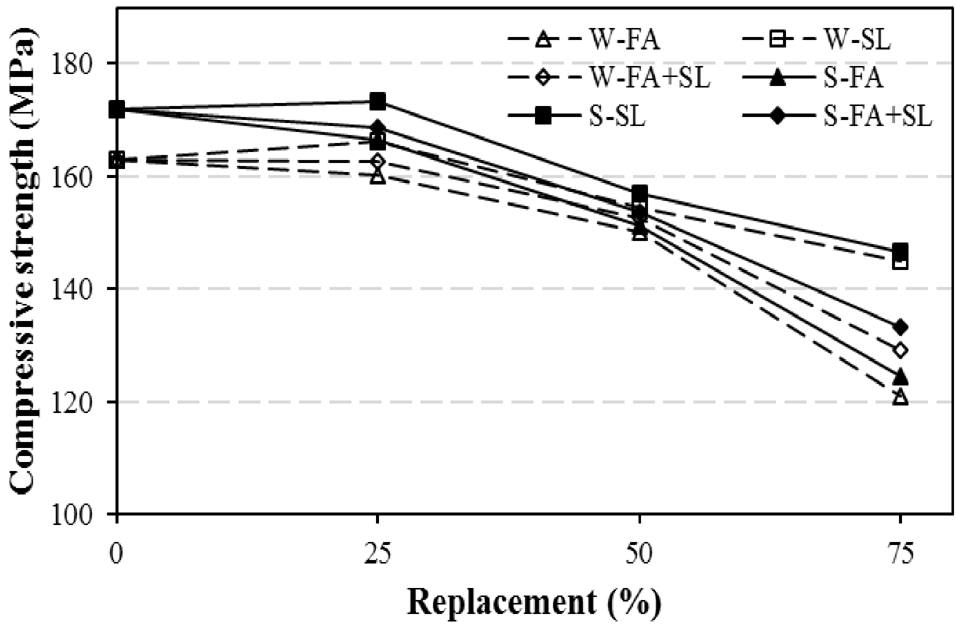

Figure 4.5 Compressive strength of WC and SC UHPC at 90 days

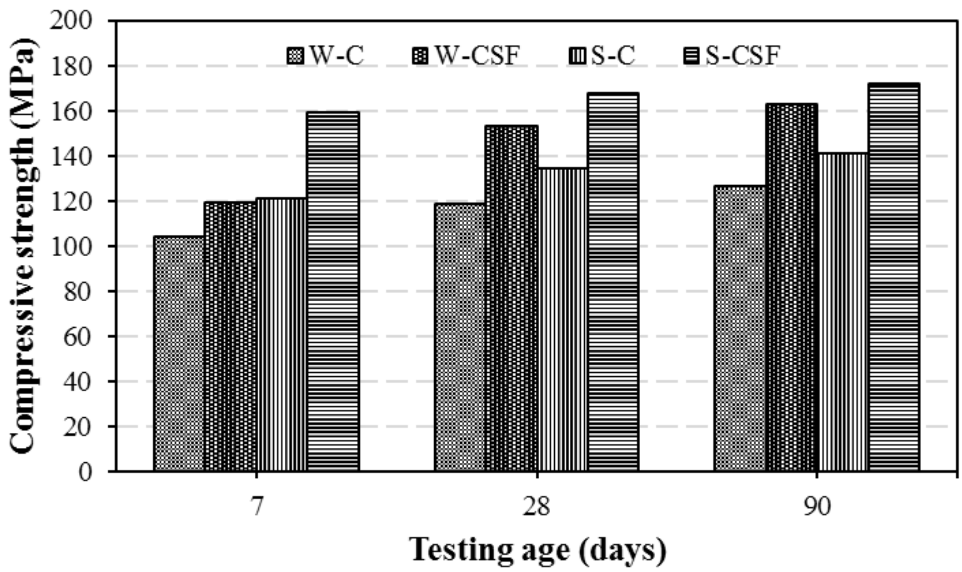

Figure 4.6 Effect of SF on compressive strength of UHPC

4.2.2. Splitting tensile strength

Splitting tensile strength is the most easily method used to determine the tensile strength of concrete, which is crucial to provide the knowledge for the ultimate tensile load that concrete can resist before cracking (Gesoglu et al., 2016). When a concrete specimen subjected to tensile stress, micro-cracks firstly occurred thereafter macro cracks forms. Increasing the load promotes progressing the critical crack at the tip of macro-cracks, which eventually cause failure of concrete (Banthia, 1994). The results of splitting tensile strength at 90 days of both WC and SC UHPCs are revealed in Figure 4.7. The results demonstrated that the SC specimens gives higher splitting tensile strength compared with corresponding WC specimens. For instance the increasing were 9.39 and 6.62% for control mixture and the mixture comprising 15%SF respectively. This is due to that the pozzolanic reaction was activated and pore size was reduced through the application of SC. The results also indicated that for the same curing regime, the mix containing 15% SF gives higher splitting tensile strength compared with control mix at 90 days (Figure 4.8). The improvement was 28.5 and 25.3% for WC and SC, respectively.

Regardless of the curing regime, the results demonstrated that the splitting tensile strength decreased with increasing the replacement of FA and/or SL beyond 25%, but the mixes comprising SL gives the lowest decreasing in splitting tensile strength compared with corresponding FA and FA+SL mixes. The decreasing for 50%

replacement level were (7.2, 4.3 and 5.7%) and (12.7, 10.7 and 11.7%) for WC and SC of the mixes containing FA, SL and FA+SL, respectively, whereas the corresponding decreasing with 75% replacement level were (43.6, 11.8 and 22.4%) and (43.7, 15.4 and 29.2%) for WC and SC of the mixes containing FA, SL and FA+SL, respectively. In both curing regime, the highest splitting tensile strength at 90 days showed in the mix containing (15% SF+ 25% SL), which gives 11.7 and 12.7 MPa for WC and SC, respectively.

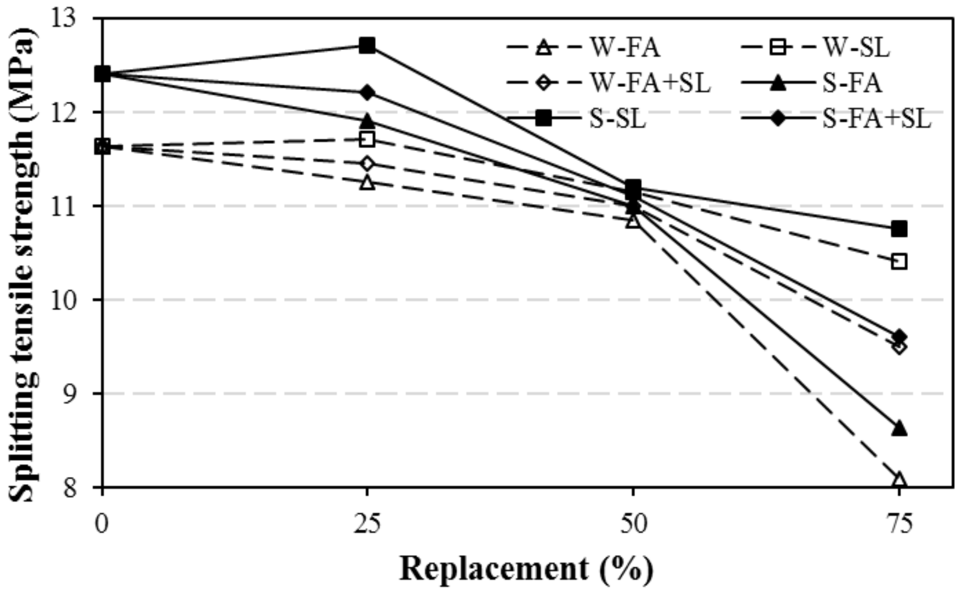

Figure 4.7 Splitting tensile strength of WC and SC UHPC

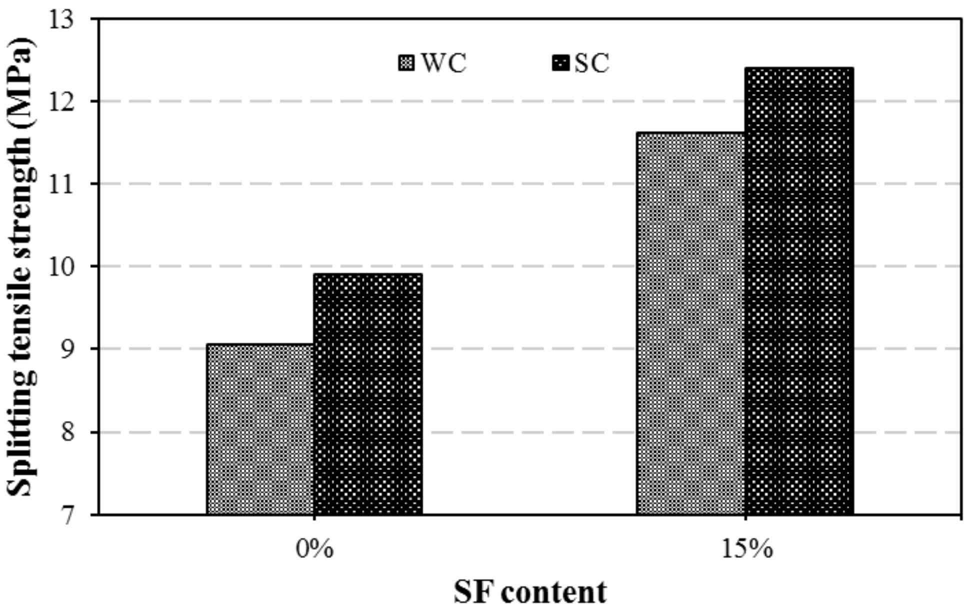

Figure 4.8 Effect of SF on splitting tensile strength of UHPC

4.2.3. Static modulus of elasticity

Static modulus of elasticity is standout amongst the most significant material properties used in design of concrete structures because it gives valuable knowledge about the aptitude of the concrete to elastic deformation. The results of modulus of elasticity demonstrated in Figure 4.9. The results revealed that the SC mixes gives higher modulus of elasticity at 90 days compared with the corresponding WC mixes. The increasing for example were 5.5 and 4.6% for control mix and the mix comprising 15%SF, respectively. The results also indicated that for the same curing method the mix containing 15% SF gives higher modulus of elasticity compared with control mix (Figure 4.10). The increasing in the modulus of elasticity were 15.2 and 14.2% for WC and SC, respectively. This can be ascribed to the increasing in the compressive strength level owing to the pozzolanic reaction of SF.

The results of elastic modulus also showed that for the same curing regime the modulus of elasticity decreased with increasing the replacement of FA and/or SL above 25%, but the mixtures comprising SL gives the lowest decreasing in modulus of elasticity compared with corresponding FA and FA+SL mixes. The decreasing for 50% replacement level were (6.6, 4.3 and 5.8%) and (11.3, 8.3 and 9.7%) for WC and SC of the mixes containing FA, SL and FA+SL, respectively, whereas the corresponding decreasing with 75% replacement level were (18.3, 7.9 and 14.3%) and (22.1, 12.2 and 16.8%) for WC and SC of the mixes containing FA, SL and FA+SL, respectively. In both curing regime, the highest modulus of elasticity at 90 days showed in the mix containing (15% SF+ 25% SL) were 44.4 and 46 GPa for WC and SC, respectively. This behavior is identical with the results of compressive strength test.

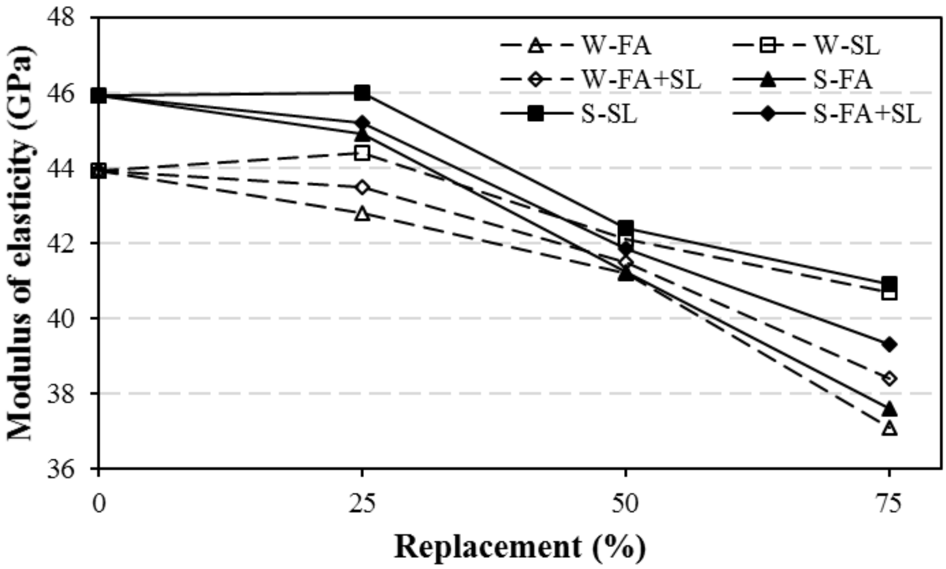

Figure 4.9 Modulus of elasticity of WC and SC UHPC

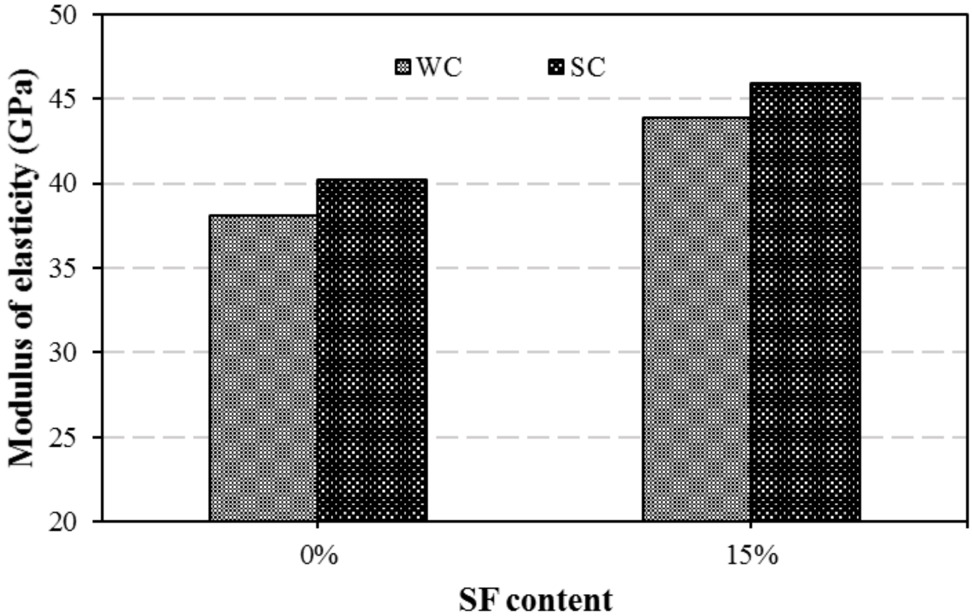

Figure 4.10 Effect of SF on modulus of elasticity of UHPC

4.2.4. Fracture energy

Fracture energy is a material distinguishing value used to characterize the resistance of concrete undergoes to tensile stresses. The fracture energy is definite as the energy wanted to propagate a tensile crack of unit area. It has the dimension Nm/m^2 or N/m (CEB/FIP, 2009). In calculating the overall energy, the area under the load vs.

displacement curve in addition to the weight of the prism were anticipated as the energy supplied by the specific weight of the beam. The displacement up to 5 mm was selected as the cut-off point to be utilized in the computation. The fracture energy test results at 90 days revealed that for the same mix proportions the SC samples gives higher fracture energy compared to corresponding standard WC samples as shown in Figure 4.11. The fracture energy ranged between 765.8 to 1992.5 N/m for WC samples and from 914.4 to 2431 N/m in corresponding SC samples. The results also indicated that for the same curing regime, replacing of cement by 15% SF gives higher fracture energy compared with control mix Figure 4.12. The increasing was 75.1 and 67.9 % for WC and SC, respectively. This increasing may be because of reducing the porosity in the cement paste and enhancing the ITZ zone because of using SF.

For the same curing regime, the results indicated that the fracture energy decreased with increasing the replacement of FA and/or SL beyond 25%, but the mixes containing SL gives higher fracture energy compared with corresponding FA and FA+SL mixes at all replacement levels as shown in Figure 4.11. This is because the fracture energy is directly related to the area under load- displacement curve. The mix containing (15% SF+ 25% SL) showed highest fracture energy at 90 days, which is gives 1992.5 and 2431 N/m for WC and SC, respectively. This is due to the improvement in bond strength by using SL (Yazıcı et al., 2010).

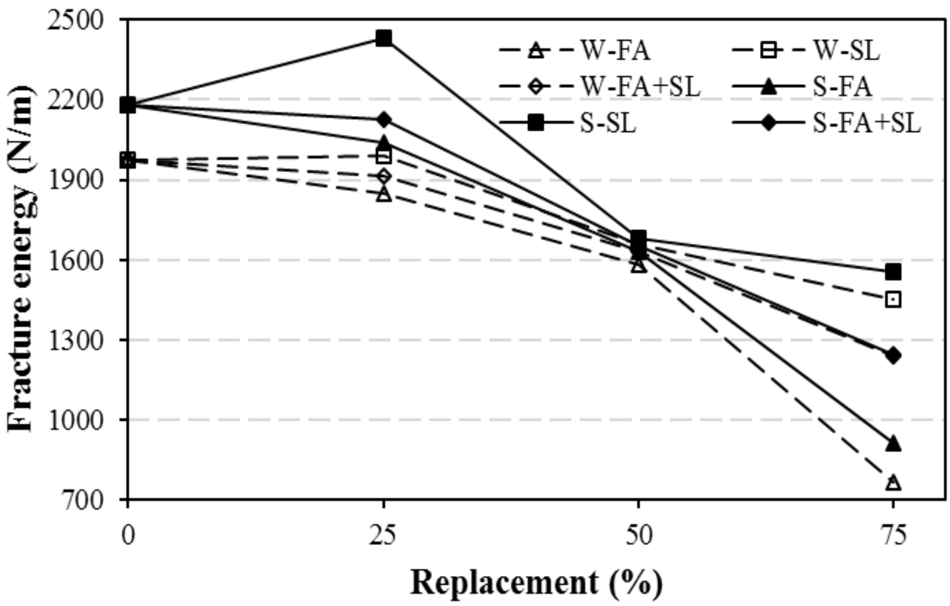

Figure 4.11 Fracture energy of WC and SC UHPC

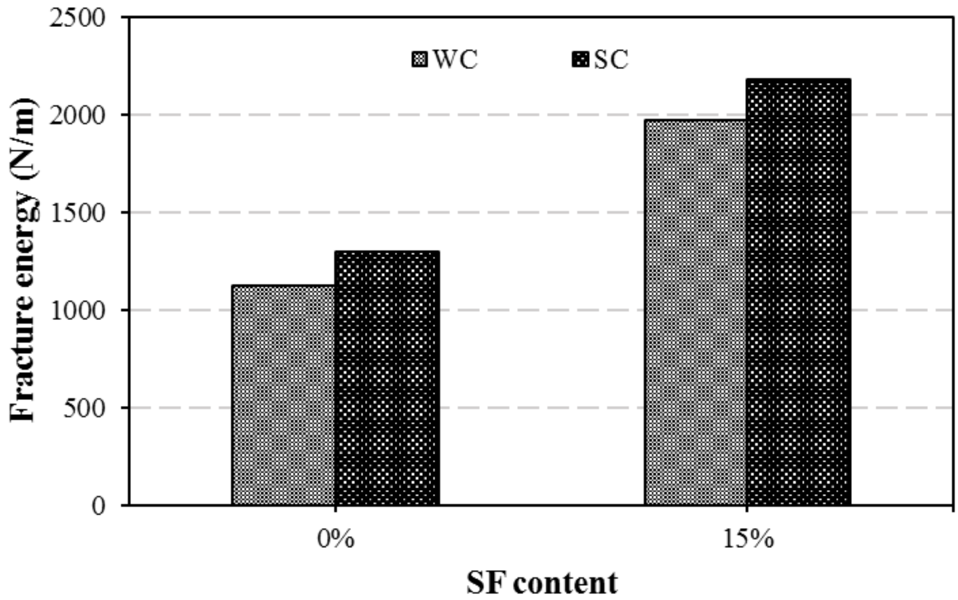

Figure 4.12 Effect of SF on fracture energy of UHPC

4.2.5. Modulus of rupture

The flexural strength results of the UHPCs reinforced with 2% of micro steel fiber at 90 days indicated that for the same mix proportions the SC samples gives higher fracture energy compared to corresponding standard WC samples (Figure 4.13). The increasing in flexural strength ranged between 1.0 and 10.7%. This is probably because of high steam have motivated the pozzolanic reaction of the calcium hydroxide formed during the hydration of cement. In addition, the reaction may take place between unwanted $Ca(OH)_2$ and very fine quartz aggregates as well as the pozzolanic materials due to hot SC conditions (Alaee, 2002). The results also revealed that for the same curing regime and like to compressive and splitting tensile strengths, replacing of cement by 15% SF also improved the flexural strength of UHPCs mixes compared with control mix (Figure 4.14). The improvement was 43.7 and 41.2 % for WC and SC, respectively. This was attributed to the promoting of the interfacial bond between paste and aggregates (Memon et al., 2013). And for the same curing regime, the results indicated that the flexural strength diminished with increasing the replacement of FA and/or SL above 25%, but the mixes containing SL gives higher flexural strength compared with corresponding FA and FA+SL mixes at all replacement levels as presented in Figure 4.13. The mix containing (15% SF+ 25% SL) showed highest flexural strength at 90 days in both curing regime, which gives 12.6 and 14 MPa for WC and SC, respectively.

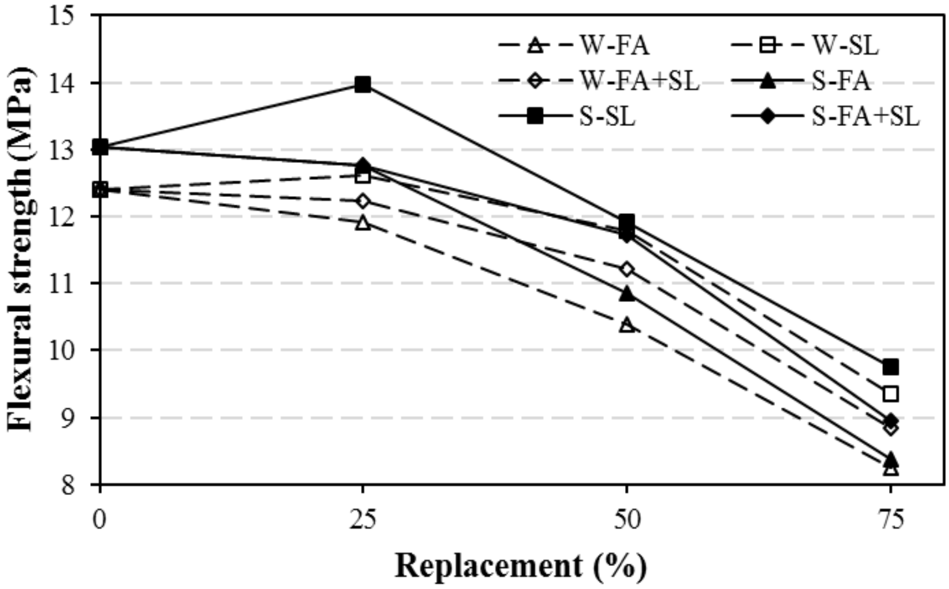

Figure 4.13 Flexural strength of WC and SC UHPC

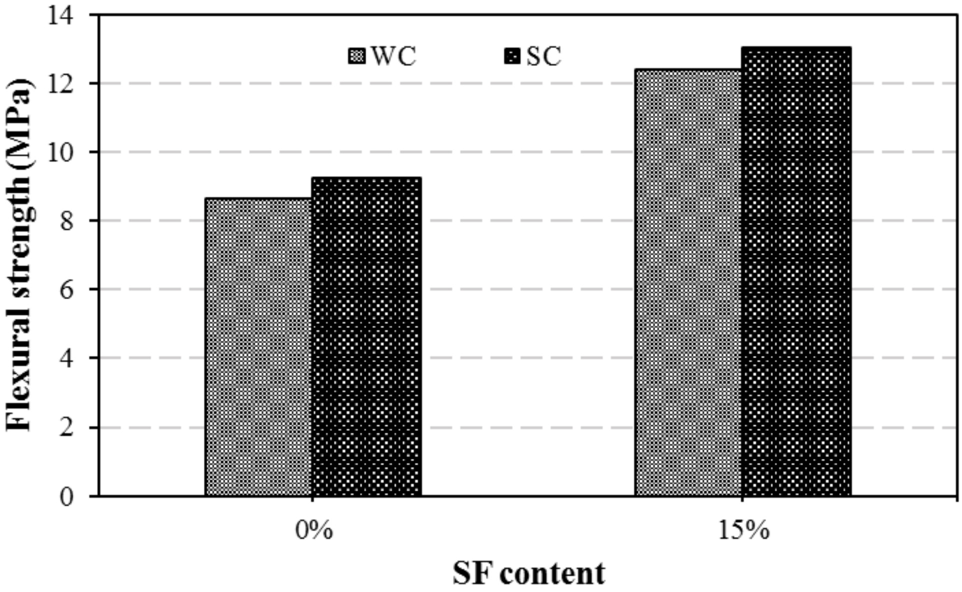

Figure 4.14 Effect of SF on flexural strength of UHPC

4.2.6. Characteristic length

Characteristic length, l_{ch}, is a convenient parameter to estimate the brittleness of concrete so that smaller l_{ch}, deals that the material is more brittle. From equ. 3.3, it can be perceived that the characteristic length of concrete is fundamentally directly affected by fracture energy and modulus of elasticity, and inversely affected by the tensile strength (Gesoglu et al., 2016). The variation in the characteristic length at 90 days of UHPC comprising 2% of micro steel fibers with different replacement levels of FA and/or SL that divided into two curing regimes, WC and SC shown in Figure 4.15. The effects of increasing replacement level from 25% up to 75% seemed to be significant on decreasing ductility 'increasing brittleness' of UHPC. The characteristic length for all mixes ranging between 433.0 and 693.3 mm. On the other hand, it can be seen that ductility of SC specimen was higher than that the corresponding WC specimen. These occurred due to that the hydration process probably activated and continued for a long time in the SC condition.

The results in Figure 4.16 also showed that irrespective to the curing regime, the mix containing 15% SF gives higher l_{ch} value comparing with corresponding control mix containing only cement as a binder. This increasing in l_{ch} were 22.2 and 22.2% for WC and SC, respectively. This is can be due to the improving the interfacial bond between paste and aggregates due to pozzolanic reaction of SF.

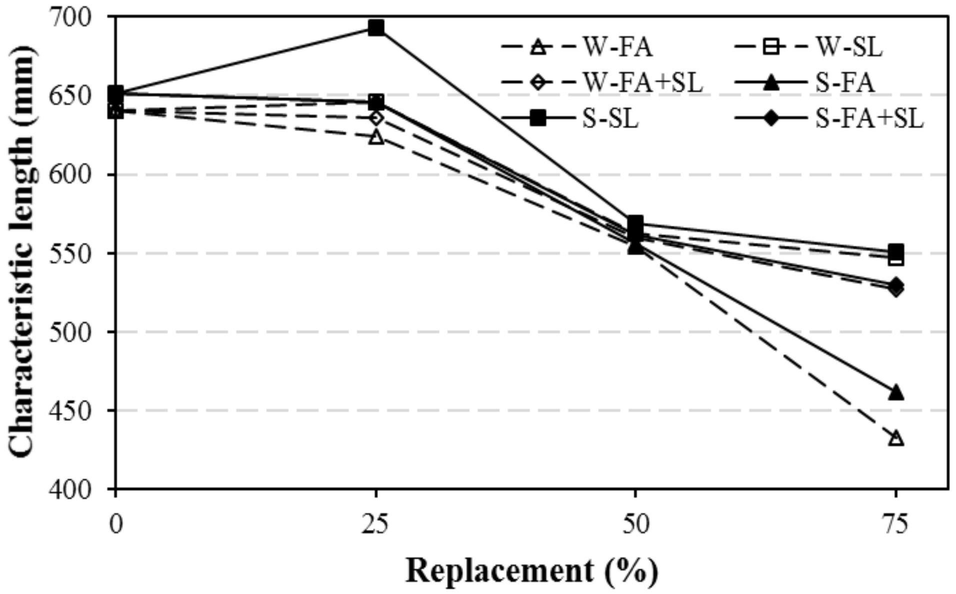

Figure 4.15 Characteristic length of WC and SC UHPC

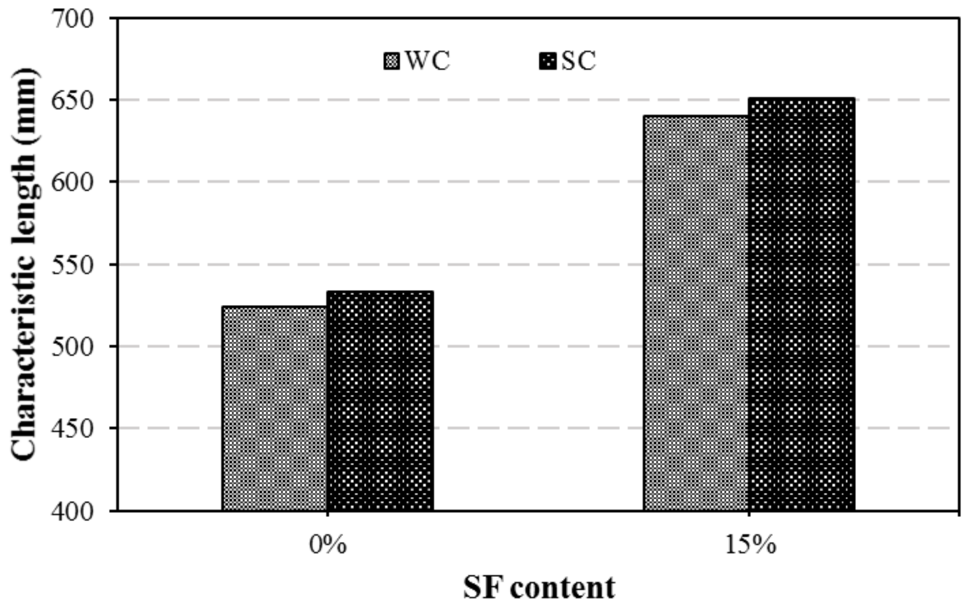

Figure 4.16 Effect of SF on characteristic length of UHPC

4.2.7. Load-displacement curves

When the fibers and UHPC matrix could not afford the maximum applied load, the first crack appeared and simultaneously reduced in applied load. This is due to the load associated with potential energy transported in fracturing the beam (Gopalaratnam et al., 1984). Thereafter, related to fiber content, the slope of the pre-peak section as well as the post-peak of the curve exposed to some extent due to pulled out of the fibers. The load versus displacement curves of UHPCs at the mid-span of notched beams under two curing regimes of WC and SC are presented in Figures 4.17 and 4.18, respectively. The results indicated that for the same mix proportions the SC samples gives higher load carrying capacity compared to corresponding standard WC samples. The increasing in load ranged between 1.0 and 10.7%. The results also revealed that for the same curing regime, replacing of cement by 15% SF gives higher load carrying capacity compared with control mix as shown in Figure 4.19. The increasing was 43.7 and 41.2 % for WC and SC, respectively. For the same curing regime, the results indicated that the maximum load decreased with increasing the replacement of FA and/or SL beyond 25%, but the mixes containing SL gives higher maximum load compared with corresponding FA and FA+SL mixes at all replacement levels. The mix containing (15% SF+ 25% SL) showed highest carrying load at 90 days, which yields 5.2 and 5.8 kN for WC and SC, respectively.

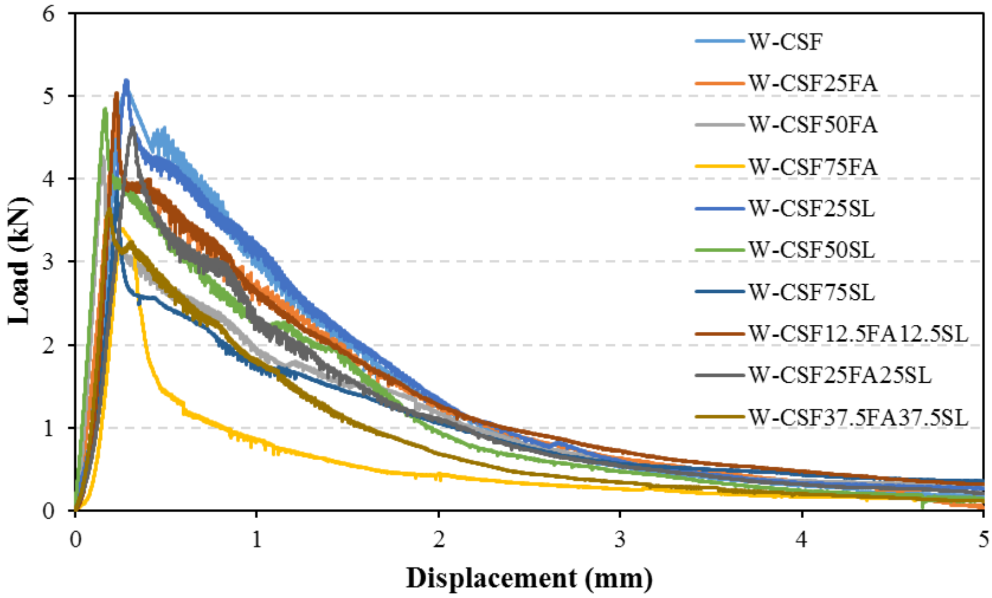

Figure 4.17 Load displacement curve for WC UHPC

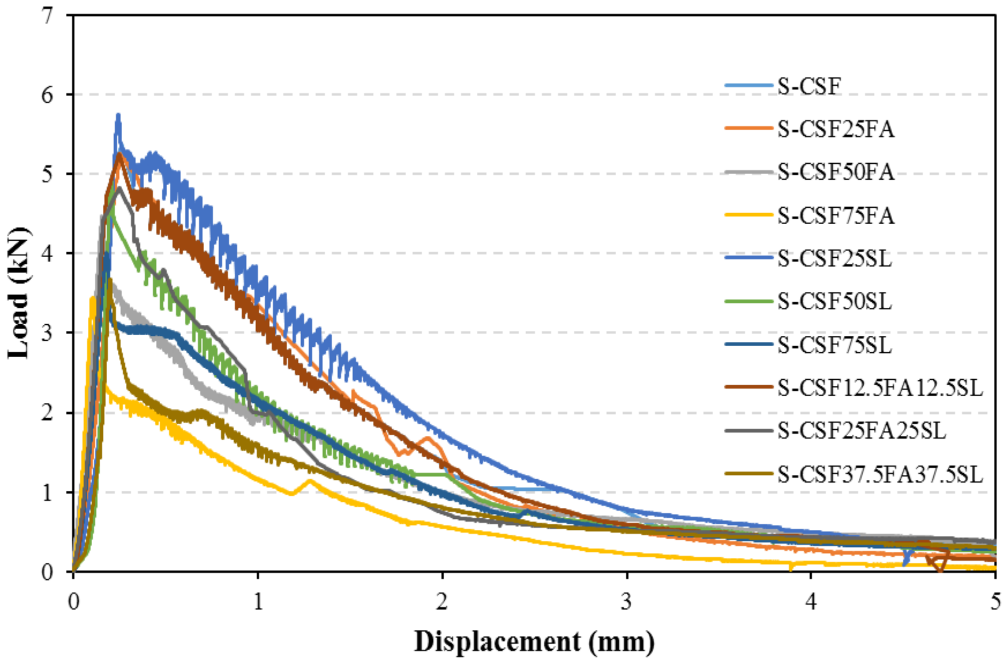

Figure 4.18 Load displacement curve for SC UHPC

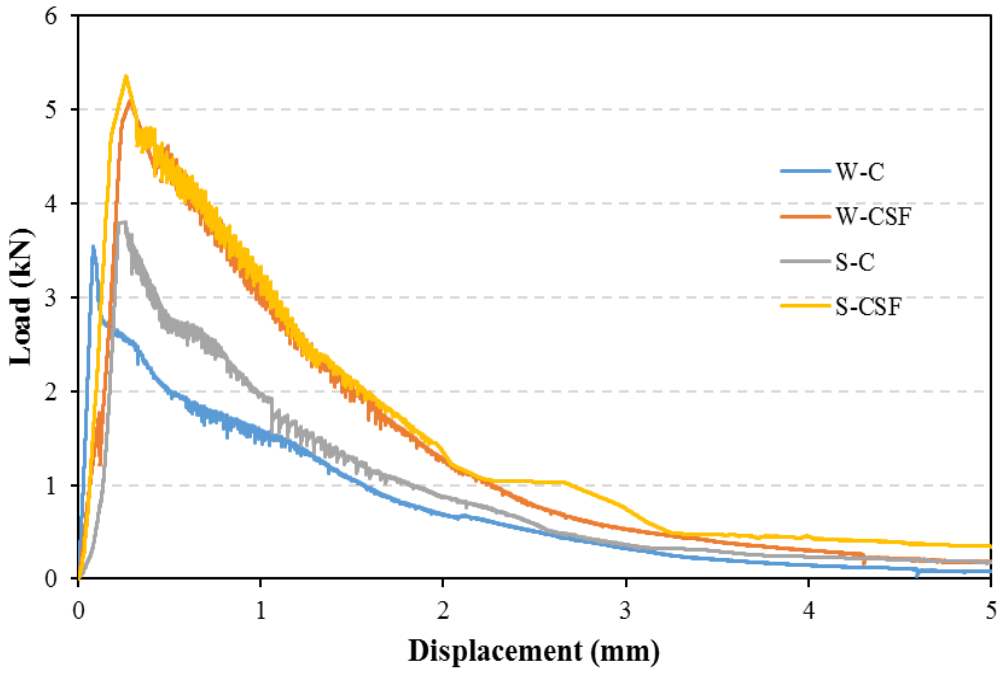

Figure 4.19 Effect of SF on load displacement curve of UHPC

4.3. Mechanical and fracture properties of UHPGC

4.3.1. Compressive strength

The compressive strength of the two curing regimes of ultra-high performance geopolymer concrete are presented in Figures 4.20, 4.21 and 4.22. The results indicated that, in the mixes containing (FA + SF), the heat curing (HC) gives higher compressive strength than the corresponding SC. This is agreed with Rangan (2008), the increasing when the SF added to the geopolymer were 14.7, 11.2 and 11.2% at 7, 28 and 90 days, respectively, and the corresponding increasing when the SF inclusion in the geopolymer concrete were 12.2, 10.4 and 9.4% at the 7, 28 and 90 days, respectively, while the mixes containing (SL + SF) and (SL + FA + SF) gives higher compressive strength in SC comparing with corresponding HC mixes at all ages. For instance the increasing in compressive strength of S-SF-GSL mix compared with corresponding HC mix (H-SF-GSL) was 17.1, 18.5 and 18.3% at 7, 28 and 90 days, respectively. The results demonstrated that irrespective to the curing regime the compressive strength increased with increasing SL percent. This is because of the existence of calcium oxide (CaO) (Albitar et al., 2015), because increasing the CaO content leads to decrease the microstructure porosity and increased the compressive strength (Sumajouw et al., 2007) and the addition of SL contributed to increase the rate of hardening and the calcium that dissolves from SL considerably affected the properties at early and late ages, and the accessibility of free calcium ions appears to extend FA dissolution and improved the formation of gel in geopolymer (Puligilla and Mondal, 2013). The increasing in compressive strength due to use SL reached to 108.8, 106.8 and 105.4% in HC regime at 7, 28 and 90 days, respectively, whereas the corresponding increasing in SC regime reached to 215.4, 205.3 and 197.9% at 7, 28 and 90 days, respectively.

The results also showed that when adding SF to the geopolymer concrete gives higher compressive strength than when it is included in the geopolymer concrete in HC mixes and in S-SF-GFA mix, while it is gives higher compressive strength when it is included in the geopolymer concrete in other SC mixes. The S-GSFSL mix gives the highest compressive strength of 153.4, 155.2 and 156.6 MPa at 7, 28 and 90 days, respectively. Regardless to the curing condition, the results of ultra-high performance geopolymer concrete showed very low strength gain with age. This is conforms with Hardjito and Rangan (Hardjito and Rangan, 2005). This is resulting from higher curing temperature which is attributed to substantially fast polymerisation process through the chemical reaction of the geopolymer gel (Hardjito et al., 2004). The strength gain at 28 day compared with 7 days ranged between 0.55 to 5.3% and the strength gain at 90 days was ranged between 1.9 to 8.1% when compared with the strength at 7 days.

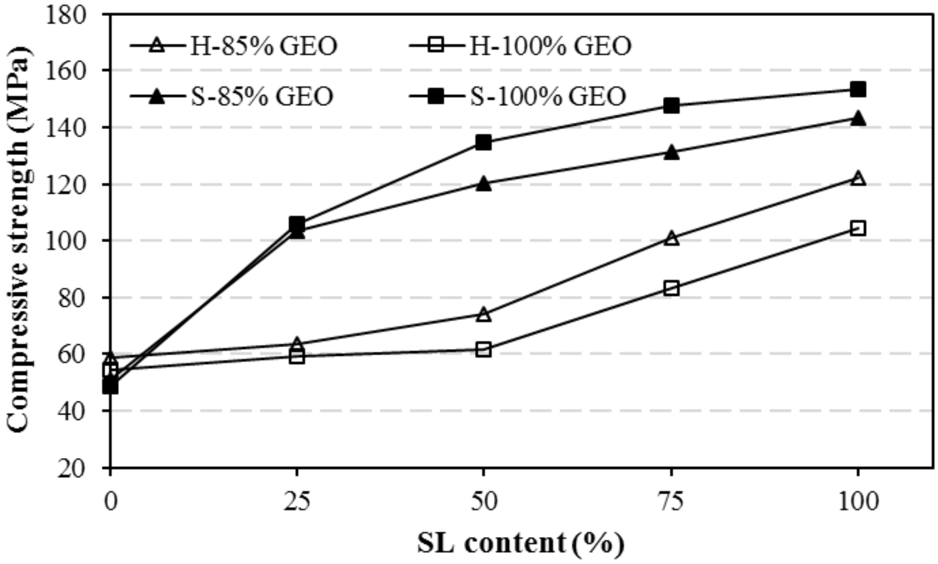

Figure 4.20 Compressive strength of HC and SC UHPGC at 7 days

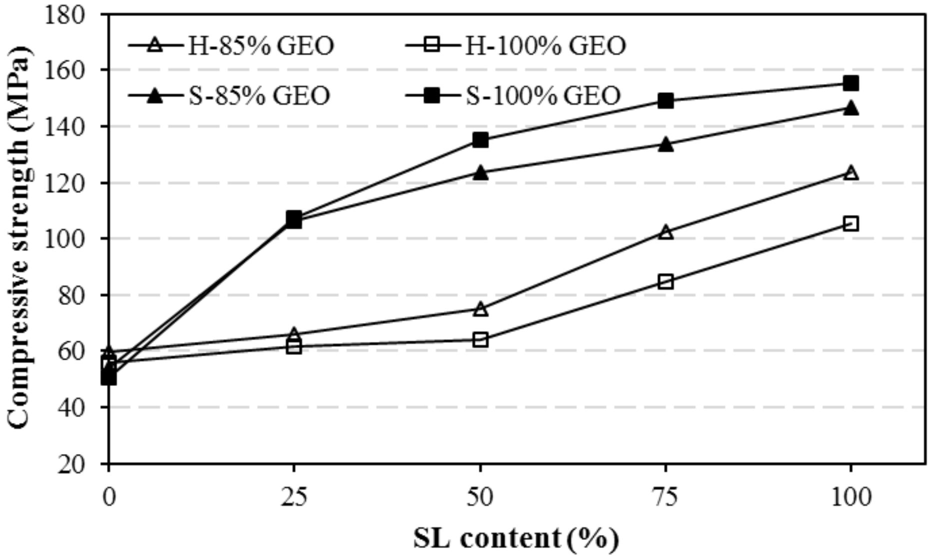

Figure 4.21 Compressive strength of HC and SC UHPGC at 28 days

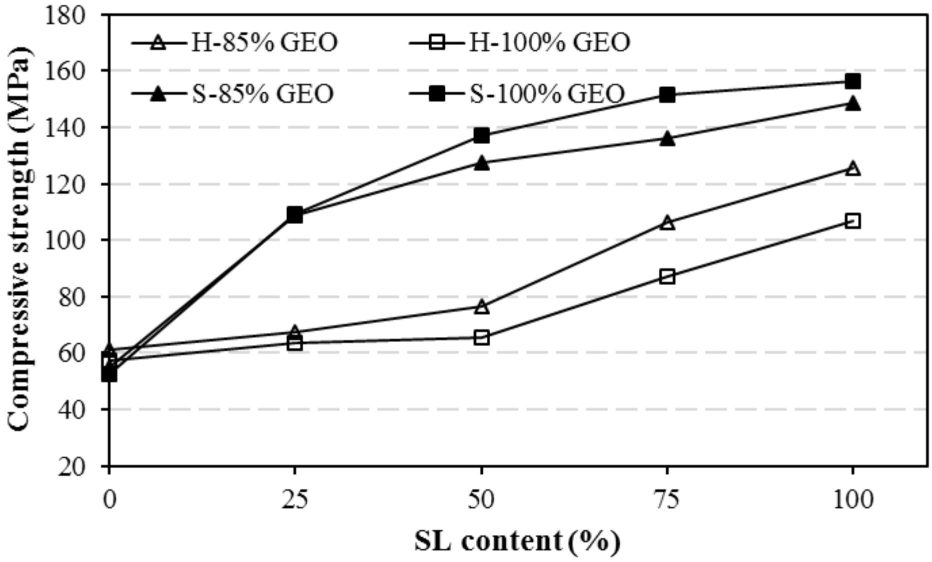

Figure 4.22 Compressive strength of HC and SC UHPGC at 90 days

4.3.2. Splitting tensile strength

The splitting tensile of the HC and SC regimes of UHPGC at 90 days displayed in Figure 4.23. The results point out that, the HC mixes containing (FA + SF) gives higher splitting tensile strength than corresponding SC mixes. The splitting tensile strength were 6.1 and 5.8 MPa for HC SF-GFA and GSFFA mixes compared with 5.5 and 5.4 MPa for the corresponding SC mixes, respectively. Whereas, the mixes containing (SL + SF) and (SL + FA + SF) gives higher splitting tensile strength in SC comparing with corresponding HC mixes as shown in Figure 4.23. The results of UHPGC revealed that the splitting tensile strength increased with increasing SL percent. This is attributed to decrease the microstructure porosity of geopolymer concrete. The increasing in splitting tensile strength due to use SL ranged between 11.5 to 64.5% in HC regime and the corresponding increasing range in SC regime were between 65.5 to 122.2%.

The results also showed that when adding SF to the geopolymer concrete gives higher splitting tensile strength than when it is included in the geopolymer concrete in HC mixes and in S-SF-GFA mix, while it is gives higher splitting tensile strength when it is included in the geopolymer concrete in other SC mixes. This is similar trend that detected in the results of compressive strength. The S-GSFSL mix gives the highest tensile strength in UHPGC mixes of 12 MPa at 90 days.

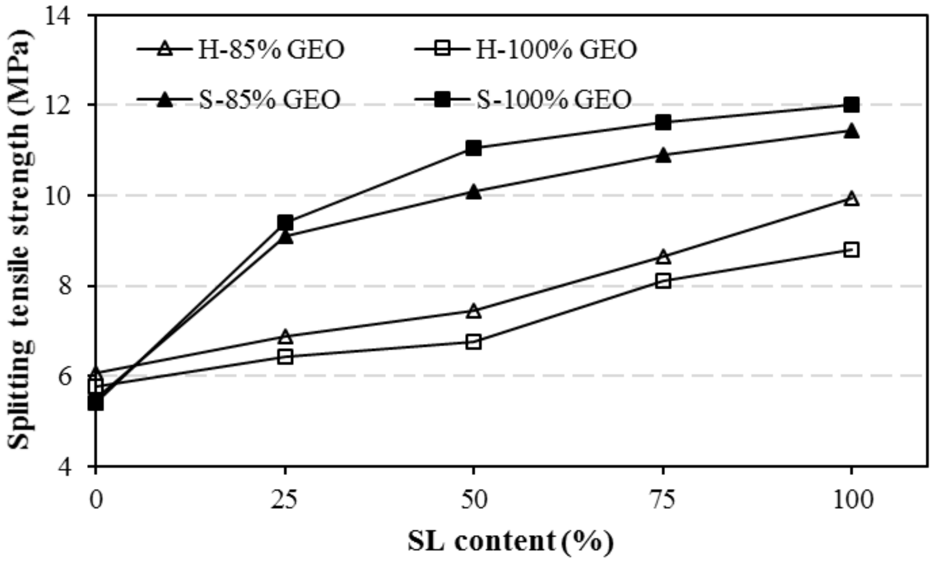

Figure 4.23 Splitting tensile strength of HC and SC UHPGC

4.3.3. Static modulus of elasticity

The modulus of elasticity of the two curing regimes of ultra-high performance geopolymer concrete summarized in Figure 4.24. The results showed that, in the mixes containing (FA+ SF), the HC mix gives higher modulus of elasticity than the corresponding SC mix. The increasing in the modulus of elasticity of the H-SF-GFA and H-GSFFA mixes were 9.2 and 6.9% when comparing with the corresponding SC mixes (S-SF-GFA and S-GSFFA), respectively. While, the mixes containing (SL + SF) and (SL + FA + SF) gives higher modulus of elasticity in SC comparing with corresponding HC mixes. From the results of UHPGC it was established that the modulus of elasticity increased with increasing the percentage of SL. This behavior was consistent with the compressive strength test results. The increment due to the use of SL reached to 76.4 and 147.2% in HC and SC, respectively.

The results also indicated that the modulus of elasticity obtained when adding SF to the geopolymer concrete higher than when it is included in the geopolymer concrete in HC mixes and in S-SF-GFA mix, while it is gives higher modulus of elasticity when it is included in the geopolymer concrete in other SC mixes as shown in Figure 4.24. This is similar trend that observed for the compressive strength results. The S-GSFSL mix gives the highest modulus of elasticity in UHPGC mixes of 44.5 GPa at 90 days.

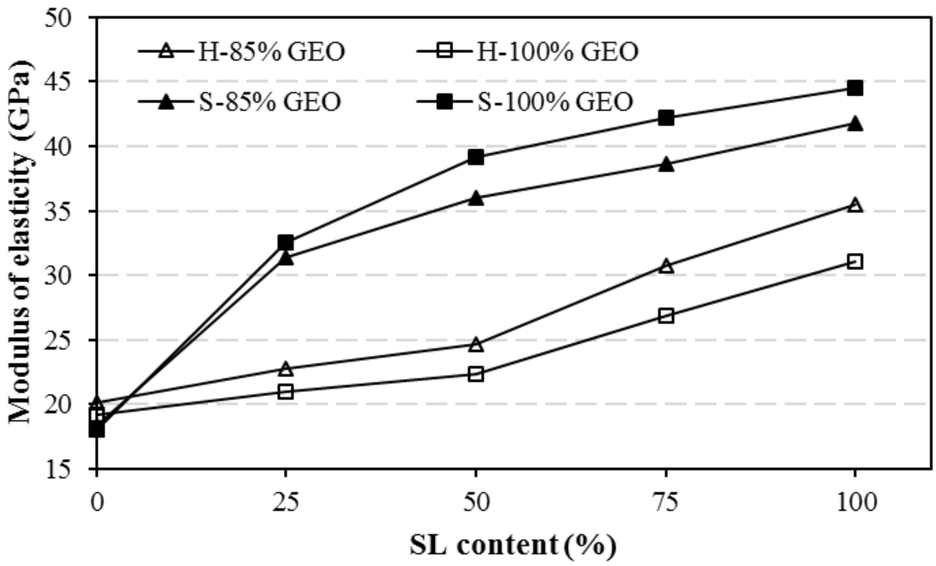

Figure 4.24 Modulus of elasticity of HC and SC UHPGC

4.3.4. Fracture energy

Fracture energy is an important parameter in the exploration of cracks in concrete structures. Indeed the fracture energy is considered as a material parameter and can be considered as a measurement for the ductility of concrete (Yuvaraj et al., 2014). The Fracture energy at 90 days of the two curing regimes of UHPGC presented in Figure 4.25. The results specified that the HC mixes containing (FA + SF) gives higher fracture energy than the corresponding SC. The increasing in the fracture energy of the H-SF-GFA and H-GSFFA mixes were 18.7 and 24% when comparing with the corresponding SC mixes (S-SF-GFA and S-GSFFA), respectively, while the mixes containing (SL+ SF) and (SL + FA + SF) gives higher fracture energy in SC comparing with corresponding HC mixes. The results of UHPGC showed that the fracture energy related to SL percent and increased with it. This is attributed to decrease the microstructure porosity of geopolymer concrete. The increasing in fracture energy due to use SL reached to 65.8 and 215.7% in HC and SC mixes, respectively. The results also indicated that when adding SF to the geopolymer concrete gives higher fracture energy than when it is included in the geopolymer concrete in HC mixes and in S-SF-GFA mix, while it is gives higher fracture energy when it is included in the geopolymer concrete in other SC mixes as illustrated in Figure 4.25. This is similar trend that observed for the compressive strength and splitting tensile strength results. The S-GSFSL mix gives the highest fracture energy in UHPGC mixes of 2236.3 N/m at 90 days.

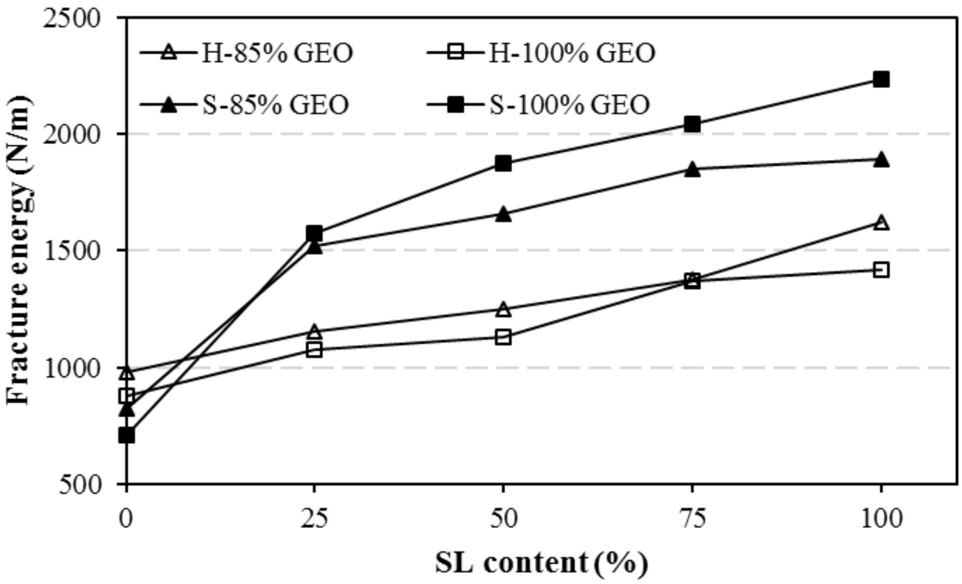

Figure 4.25 Fracture energy of HC and SC UHPGC

4.3.5. Modulus of rupture

The flexural strength results of the UHPGC containing 2% micro steel fiber at 90 days as shown in Figure 4.26 showed that the HC mixes containing (FA + SF) gives higher flexural strength than the corresponding SC. The increasing in the flexural strength of the H-SF-GFA and H-GSFFA mixes were 5.15 and 11.37% when comparing with the corresponding SC mixes (S-SF-GFA and S-GSFFA), respectively. Whilst, the mixes containing (SL + SF) and (SL+ FA + SF) gives higher flexural strength in SC comparing with corresponding HC mixes. The results of UHPGC revealed that the flexural strength increased with increasing SL percent. The increasing in flexural strength due to use SL reached to 110.0 and 191.1% in HC and SC mixes, respectively.

The results also revealed that when adding SF to the geopolymer concrete gives higher flexural strength than when it is inclusion in the geopolymer concrete in HC mixes and in S-SF-GFA mix, while it is gives higher flexural strength when it is included in the geopolymer concrete in other SC mixes. This is similar trend that observed for the compressive strength and splitting tensile strength results. The maximum flexural strength in UHPGC mixes at 90 days was 14.0 MPa obtained from S-GSFSL mix.

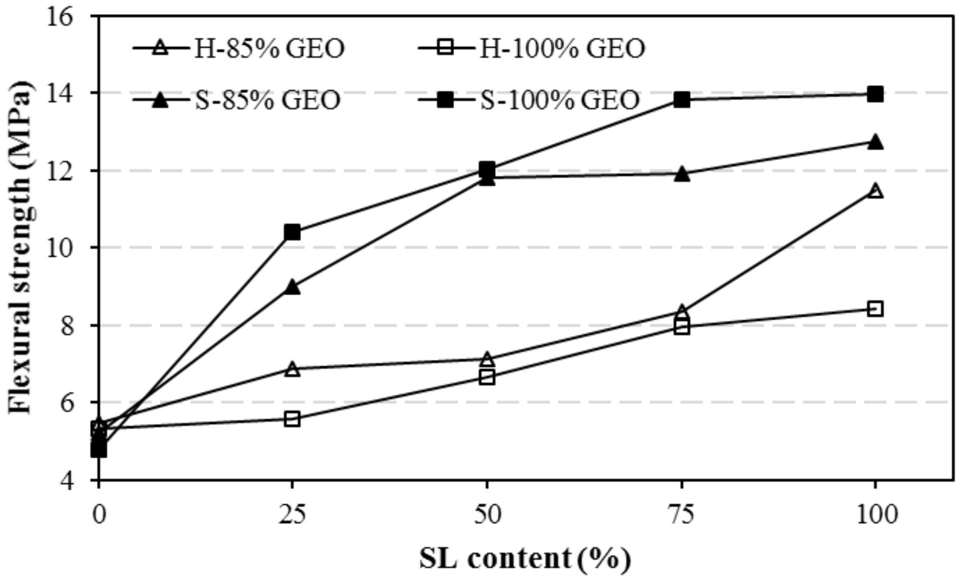

Figure 4.26 Flexural strength of HC and SC UHPGC

4.3.6. Characteristic length

Brittleness is generally comprehended to be the tendency of a material to fracture suddenly earlier occurring of considerable irreversible deformation (Zhang et al., 2000). Hillerborg et al. (1976) defined the characteristic length as a brittleness parameter in the fictitious crack model for concrete. The lower the degree of brittleness, the higher the value of l_{ch}. The l_{ch} results of the UHPGC containing 2% micro steel fiber at 90 days ranged between 437.2 and 691.1 mm as shown in Figure 4.27. The results showed that the HC mixes containing (FA + SF) gives higher l_{ch} than the corresponding SC. The increasing in the characteristic length of the H-SF-GFA and H-GSFFA mixes were 7.2 and 16.9% when comparing with the corresponding SC mixes (S-SF-GFA and S-GSFFA), respectively. While, the mixes containing (SL + SF) and (SL + FA + SF) gives higher l_{ch} in SC comparing with corresponding HC mixes as illustrated in Figure 4.27. The results of UHPGC revealed that the characteristic length increased with increasing the SL percent. The increasing in characteristic length due to use SL reached to 11.3 and 58.1% in HC and SC mixes, respectively. The results also indicated that when adding SF to the geopolymer concrete gives higher l_{ch} than when it is inclusion in the geopolymer concrete in HC mixes and in S-SF-GFA mix, while it is gives higher l_{ch} when it is included in the geopolymer concrete in other SC mixes. This is similar trend that observed for the flexural strength results. The S-GSFSL mix gives the highest l_{ch} in UHPGC mixes of 691.1 mm at 90 days.

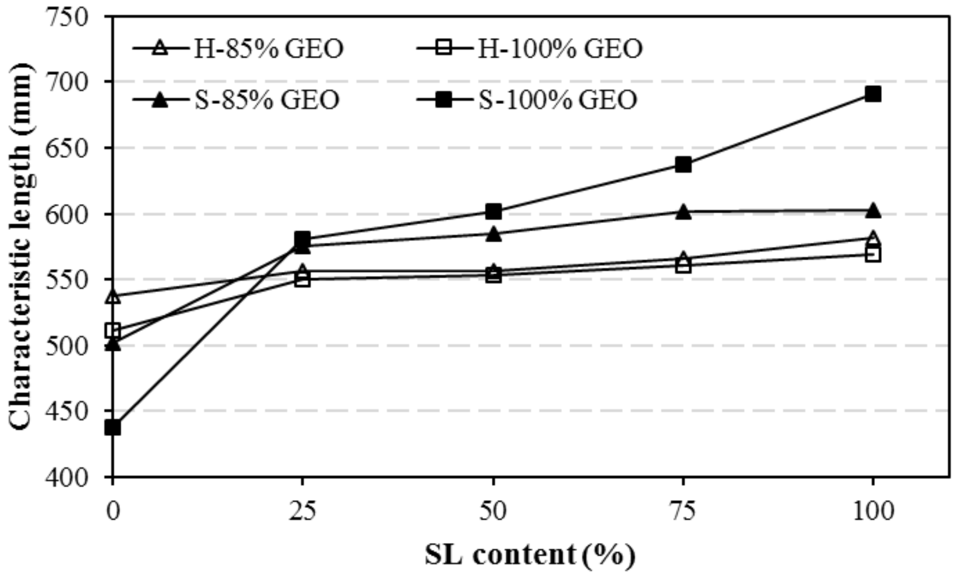

Figure 4.27 Characteristic length of HC and SC UHPGC

4.3.7. Load-displacement curves

The load–displacement curves of UHPGC specimens at middle span of notched beams under two curing regimes of HC and SC are presented in Figures 4.28 and 4.29, respectively.

The results showed that the HC mixes containing (FA + SF) carrying higher maximum load than the corresponding SC mixes. The increasing in carrying load of the H-SF-GFA and H-GSFFA mixes were 5.2 and 11.4% when comparing with the corresponding SC mixes (S-SF-GFA and S-GSFFA), respectively. While, the mixes containing (SL + SF) and (SL + FA + SF) carrying higher load in SC comparing with corresponding HC mixes. The results also revealed that when adding SF to the geopolymer concrete carrying higher load than when it is included in the geopolymer concrete in HC mixes and in S-SF-GFA mix, while it is carrying higher load when it is inclusion in the geopolymer concrete in other SC mixes. This is similar trend that observed for the flexural strength results. The results of UHPGC indicated that, regardless to curing type, the maximum load increased with increasing SL percent. The increasing in maximum load due to use SL reached to 110.0 and 191.1% in HC and SC mixes, respectively. The S-GSFSL mix yields the highest maximum load in UHPGC mixes of 5.8 kN at 90 days.

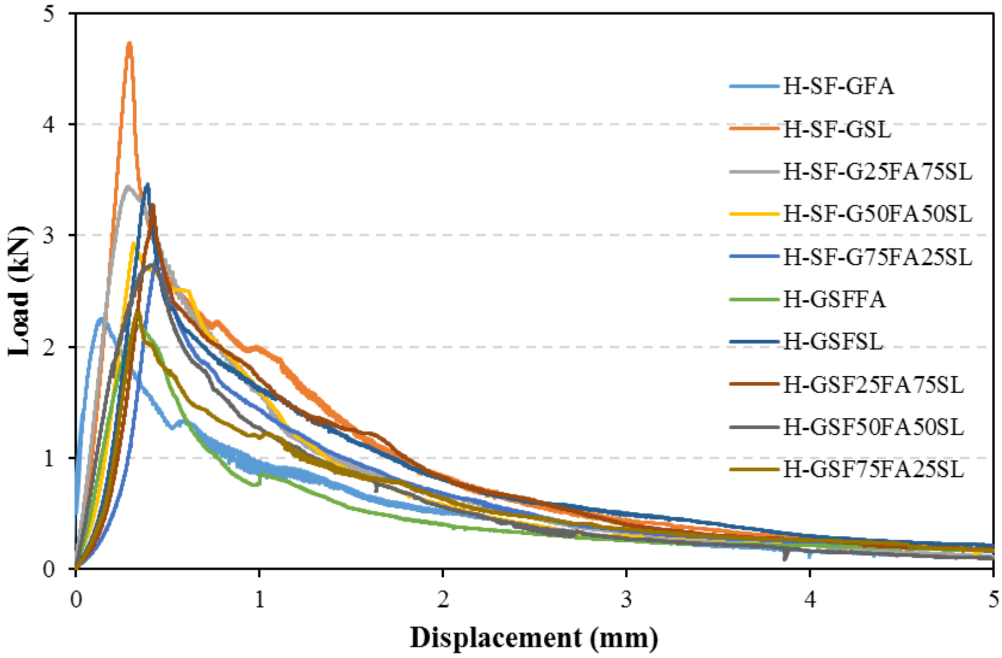

Figure 4.28 Load displacement curve for HC UHPGC

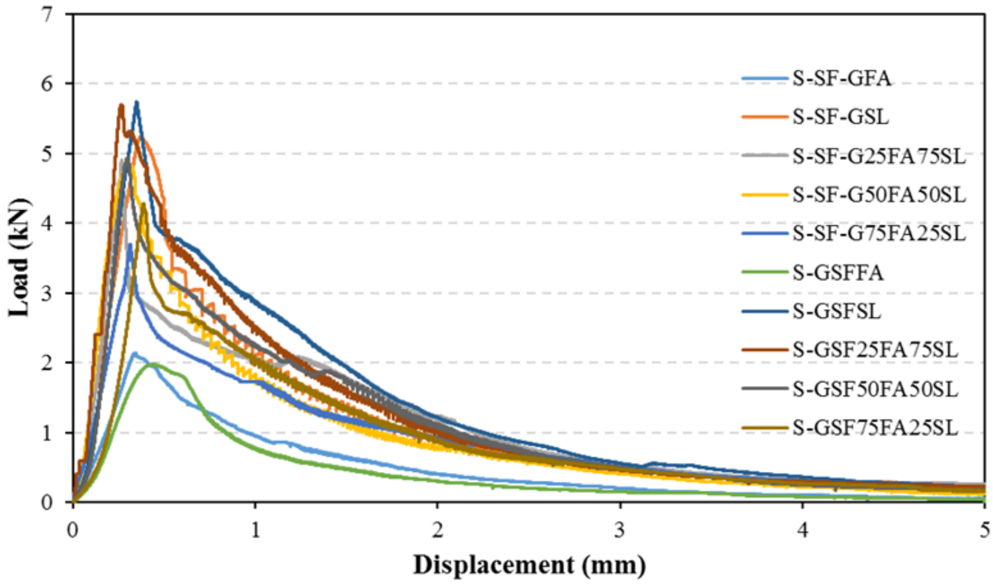

Figure 4.29 Load displacement curve for SC UHPGC

4.4. Comparison between UHPC and UHPGC

The results of ultra-high performance conventional and geopolymer concrete showed that, for the same binder content of 1150 kg/m^3 and w/b ratio (0.17), the ultra-high performance conventional concrete gives higher compressive strength than geopolymer concrete. The compressive strength reached to 160.7, 168.0 and 173.2 MPa for conventional concrete compared with 153.4, 155.2 and 156.6 MPa for geopolymer concrete at 7, 28 and 90 days, respectively. The conventional concrete also gives higher splitting tensile strength, modulus of elasticity and fracture energy than the geopolymer concrete.

The results also revealed that the strength gain of geopolymer concrete lower than conventional concrete even in the SC regime of conventional concrete. The strength development at 28 days compared with 7 days in ultra-high performance conventional concrete reached to 43.77 and 11.82% for WC and SC, respectively, while the corresponding development in geopolymer concrete reached to 4.33 and 5.3% for HC and SC, respectively. The results presented that for the same compressive strength the ultra-high performance geopolymer concrete gives higher splitting tensile strength than the ultra-high performance conventional concrete as presented in Figure 4.30. This is related to the higher bond strength with reinforcing steel and comparatively higher splitting tensile strength than OPC concrete (Fernández-jiménez et al., 2006; Sarker, 2011; Sofi et al., 2007). The results of peak load of geopolymer concrete sample was in general higher than that of the conventional concrete sample of the identical compressive strength as shown in Figure 4.31. This is conforming with the results achieved by Sarker et al. (2013). Similar trend was observed with the fracture energy, flexural strength and characteristic length as shown in Figures 4.32, 4.33 and 4.34, respectively. Whereas the results of modulus of elasticity was comparable between the two types of concrete as illustrated in Figure 4.35.

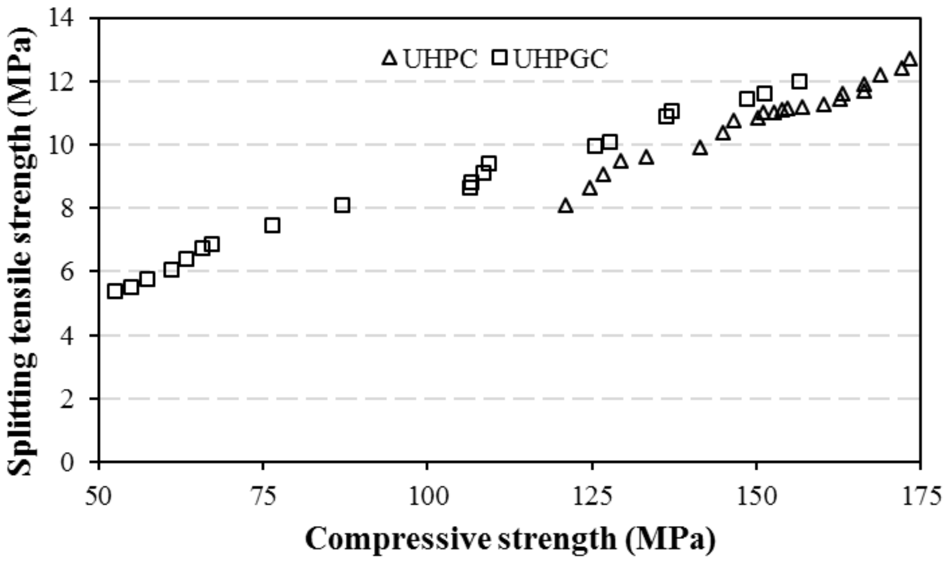

Figure 4.30 Relation between splitting tensile strength and compressive strength of UHPC and UHPGC

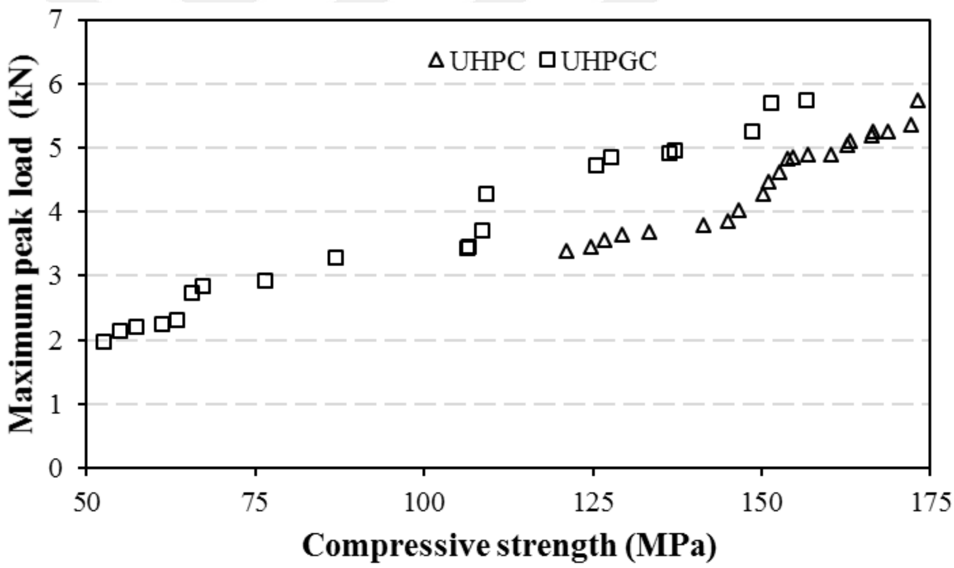

Figure 4.31 Relation between maximum peak load and compressive strength of UHPC and UHPGC

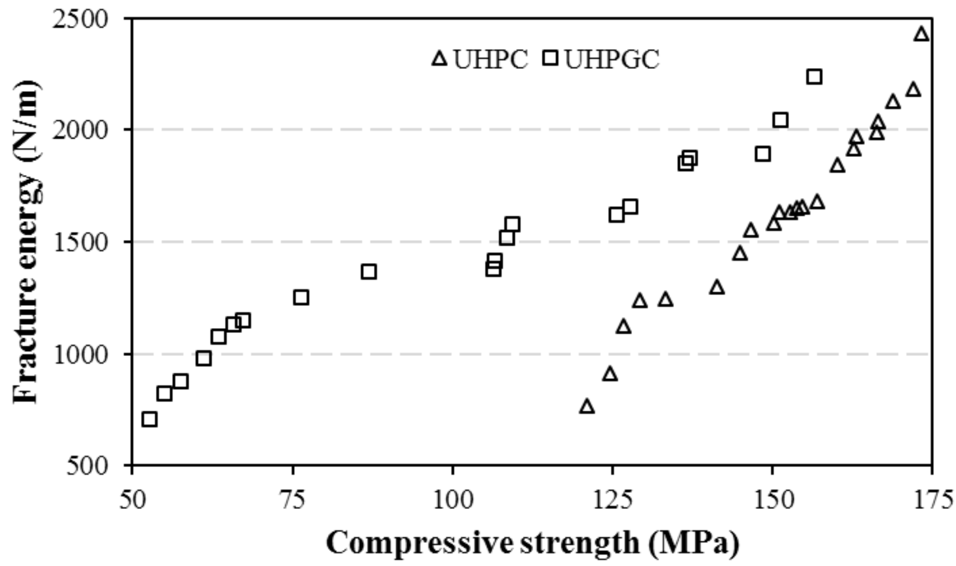

Figure 4.32 Relation between fracture energy and compressive strength of UHPC and UHPGC

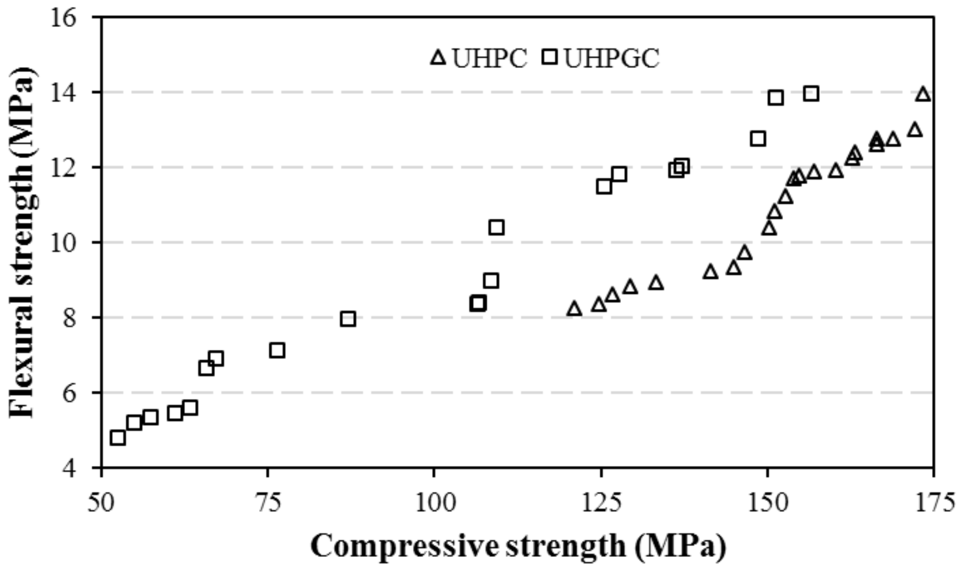

Figure 4.33 Relation between flexural strength and compressive strength of UHPC and UHPGC

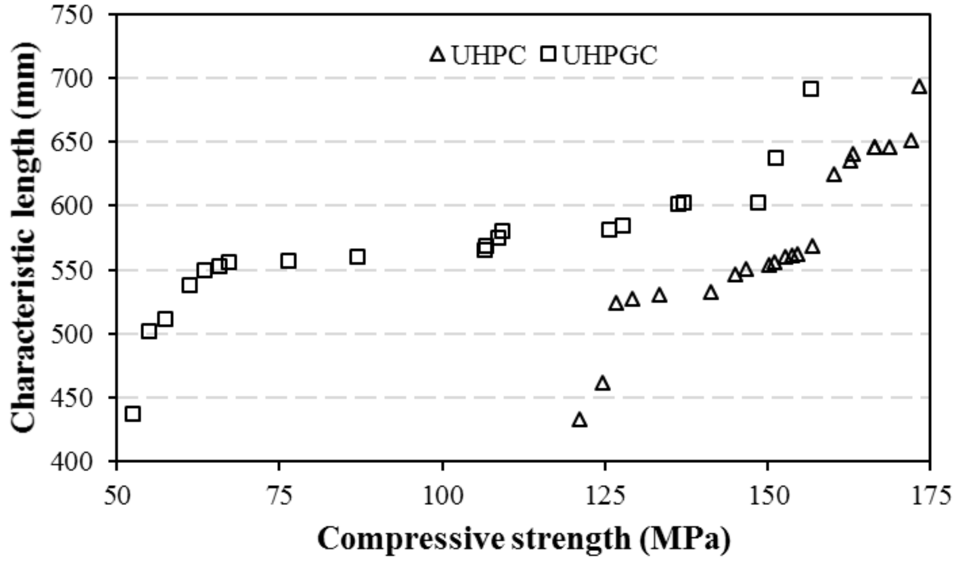

Figure 4.34 Relation between characteristic length and compressive strength of UHPC and UHPGC

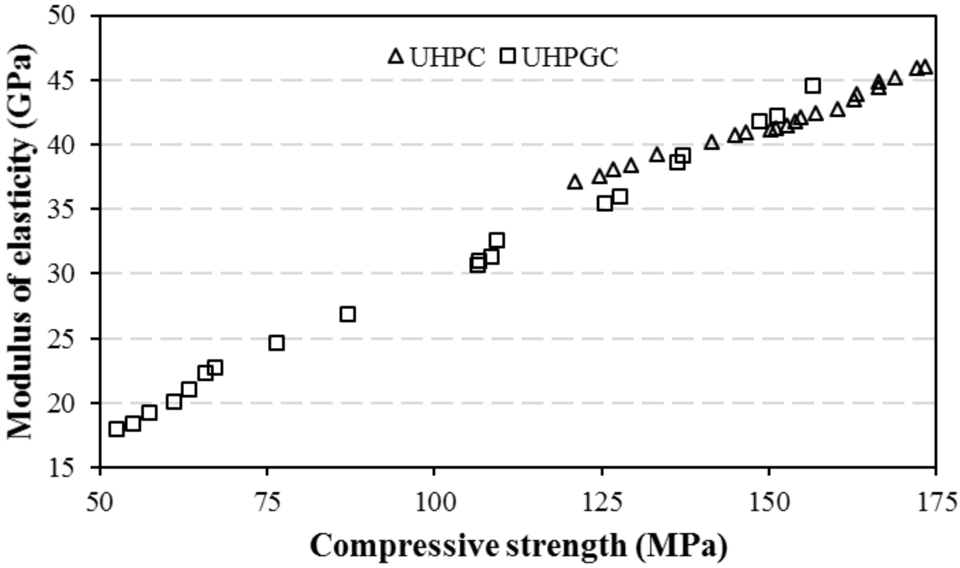

Figure 4.35 Relation between modulus of elasticity and compressive strength of UHPC and UHPGC

CHAPTER 5
RESULTS OF NUMERICAL STUDY AND DISCUSSION

5.1 General

Concrete-filled steel tubular (CFST) column is a kind of the composite steel-concrete structures currently applied in civil engineering and commonly applied in the high-rise buildings, barriers, subway platforms, and bridges. Using CFST gives superior static and earthquake-resistant properties, like high strength, stiffness and ductility, and considerable energy-absorption capacity (Lu and Zhao, 2010). CFST columns merge the features of ductility of the steel structures with the stiffness of a concrete. Comparing with other composite systems, the concrete-filled steel tube column have many benefits such as the steel tube supplies persistent formwork for the concrete, the local buckling of the steel tube wall concrete was prolonged by concrete, excessive concrete spalling was prevented by the steel tube, and a significant stiffness can be added to the frame by using composite columns compared to more conventional steel frame construction. Utilizing of CFSTs in construction has been limited in spite of several benefits be existent. This is may be due, partly, to a deficiency of construction expertise, a lack of comprehension of the design necessities and the complication of the connection description. Then, a joint was required that could apply the favourable strength and stiffness features of the concrete-filled tube column yet be constructible (Schneider et al., 2004).

In spite of the above benefits, CFST columns have some drawbacks such as the incomplete interface bonding occurring between concrete and steel tube under compression through the primary elastic stage will have an inappropriate influence on the composite action. Fundamentally, there are two conceivable conditions of de-bonding in CFST structures: (1) Owing to poor placing of concrete or shrinkage and difference the temperature in the core concrete (Liao et al., 2011); (2) Because of the differences in Poisson’s ratios between concrete and steel (0.2 for concrete and 0.3 for steel) leads to larger expansion of steel than concrete at the primary stage under compression (Ferretti, 2004; Lu and Hsu, 2007; Persson, 1999). The insufficient interface bonding will reduce the restricting stress that is supplied by the steel tube to the in-filled concrete, which in turn decreases the elastic strength and stiffness. One of the outcomes is the increment in the inter-story and/or whole drift ratio of high rise buildings, which may disrupt the serviceability of the limit state demand. As well, decreasing the interface bonding would rise the opportunity of having tube buckling at elastic phase if the thin wall is associated with its diameter (O'Shea and Bridge, 2000). When the micro-cracking begin to form in concrete and the expansion of concrete go beyond that of steel tube this leads to initiate the effectiveness of the composite. Otherwise, degeneration of restricting stress, strength and ductility would happen in the post-elastic phase because of the inelastic exterior buckling of steel tube.

The main parameters which predominate the conductance and capacity of CFST columns are geometry and material properties. The crucial geometrical factors are the diameter to thickness (D/t) ratio, slenderness ratio and preliminary geometry of columns (Ghasemian and Schmidt, 1999; O'Shea and Bridge, 2000). Furthermore, the main mechanical properties for composite columns are the strength of concrete and steel, the level of concrete confinement and the loading and the boundary conditions. The load carrying capacity is also reliant on the column length and the eccentricity. In short columns, the failure is noticed by compressive yielding of steel and crushing of concrete while for longer columns the overall instability failure mode occurs by partial compressive yielding of steel and cracking of concrete. Local buckling is the failure mode happens in columns having high D/t ratio (Zeghiche, 1988; Zeghiche and Chaoui, 2005).

5.2 UHPC filled steel tubular columns

5.2.1 Axial capacity variarions

The computed axial load carrying capacity of UHPC at 7, 28 and 90 days shown in Figures 5.1 (a-d), 5.2 (a-d) and 5.3 (a-d) for Eurocode 4 (2004), ACI-318R (2005) and Chinese code DL/T (1999), respectively. The axial compressive load capacities of CFST columns were sensitive to D/t ratio and steel yield strength of steel. It clearly appears that the axial capacity increased with increasing the D/t ratio and f_y. The higher the concrete diameter used, the higher the concrete cross section area, consequently, the ultimate axial capacity value enhanced with increasing of D/t ratio as the increase of cross section area of concrete core in all the three codes contribute to the ultimate axial capacity. CFST columns with high strength steel caused higher axial capacity for the column with UHPC. The figures also indicated that, irrespective to the variation in D/t and yield strength of steel tube, the axial load carrying capacity increased with age.

Regardless to D/t, f_y and age the axial load capacity decreased with increasing the replacement of FA and/or SL beyond 25% for all ages, but the decreasing in axial load capacity of the mixes containing FA was higher than the corresponding mixes containing SL and (SL+FA). The decreasing in for D/t=25 and f_y =150 MPa in ACI-318R (2005) at 28 days were 9.4, 7.4 and 9.1% at 50% replacement level for water curing for the mixes containing FA, SL and FA+SL and 10.9, 8.7 and 9.8% for the corresponding steam curing mixes, respectively. The corresponding decreasing at the same age for 75% replacement level were 33.7, 13.0 and 28.5% for water curing and 33.5, 17.7 and 26.2% for steam curing for the mixes comprising FA, SL and FA+SL, respectively. Similar trend were observed in Eurocode 4 (2004), and Chinese code DL/T (1999).

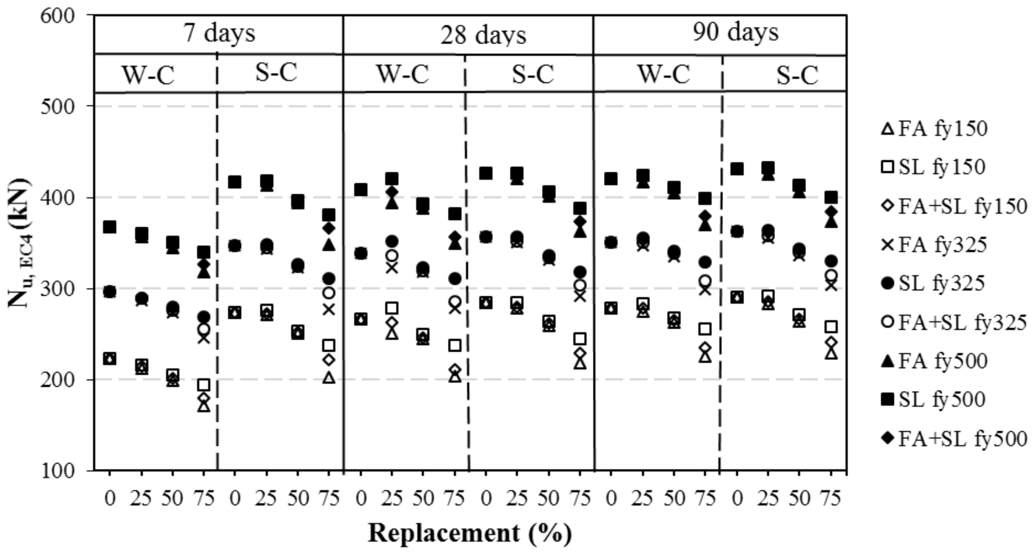

(a)

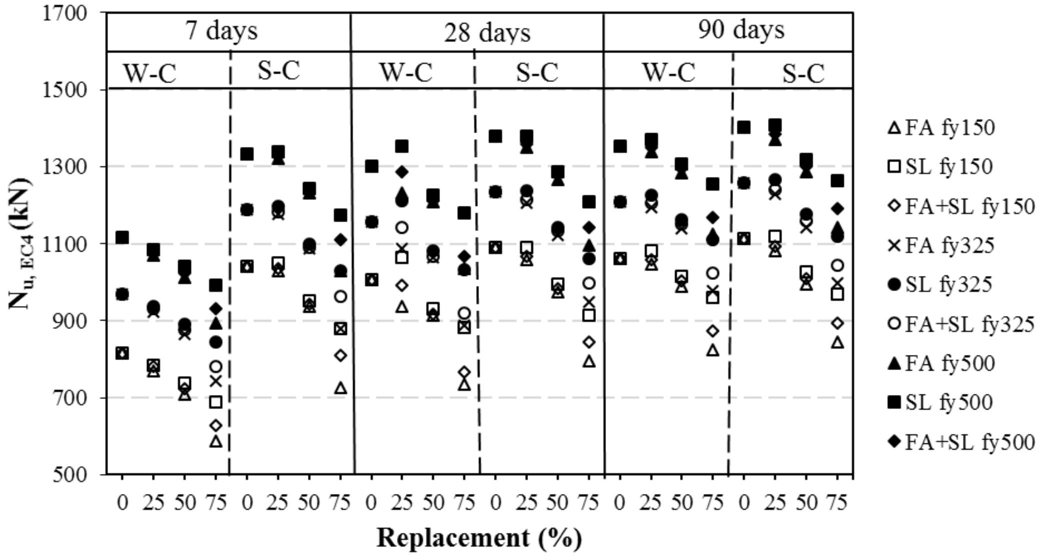
7 days
28 days
90 days
W-C
S-C
Nu, EC4 (kN)
Replacement (%)
FA fy150
SL fy150
FA+SL fy150
FA fy325
SL fy325
FA+SL fy325
FA fy500
SL fy500
FA+SL fy500

(b)

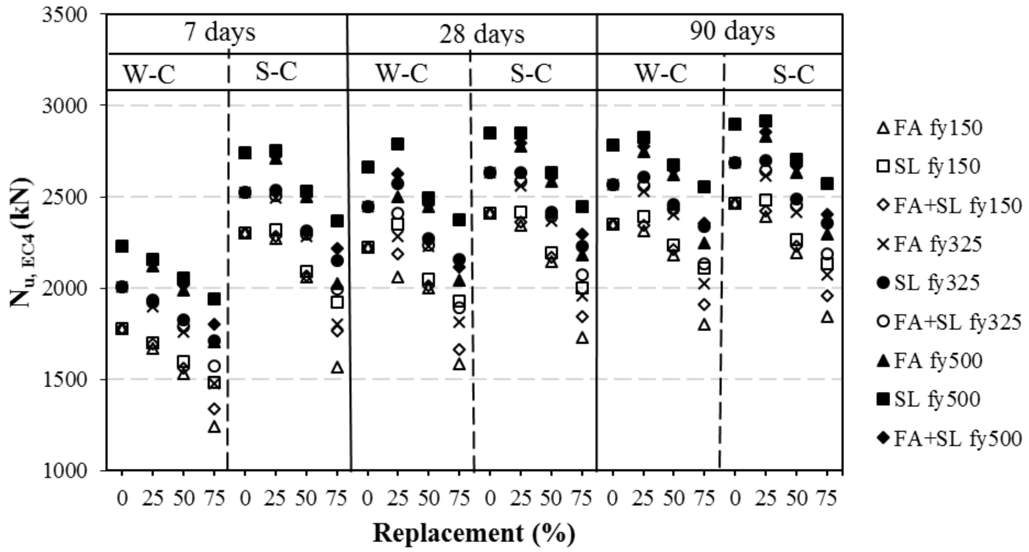
7 days
28 days
90 days
W-C
S-C
Nu, EC4 (kN)
Replacement (%)
FA fy150
SL fy150
FA+SL fy150
FA fy325
SL fy325
FA+SL fy325
FA fy500
SL fy500
FA+SL fy500

(c)

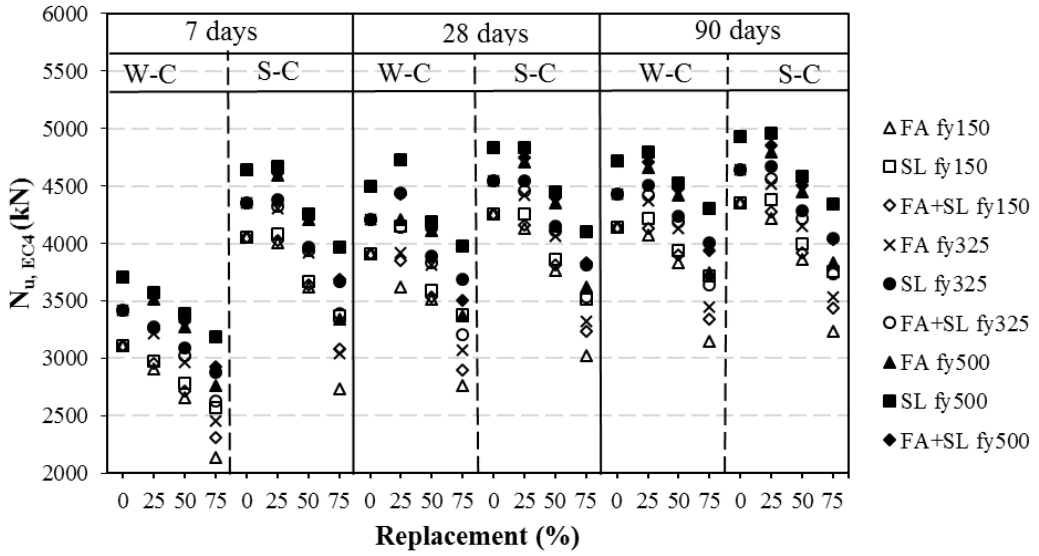

(d)

Figure 5.1 Axial capacity of UHPC filled steel tubular columns based on Eurocode 4 for D/t ratios of a) 25, b) 50, c) 75 and d) 100

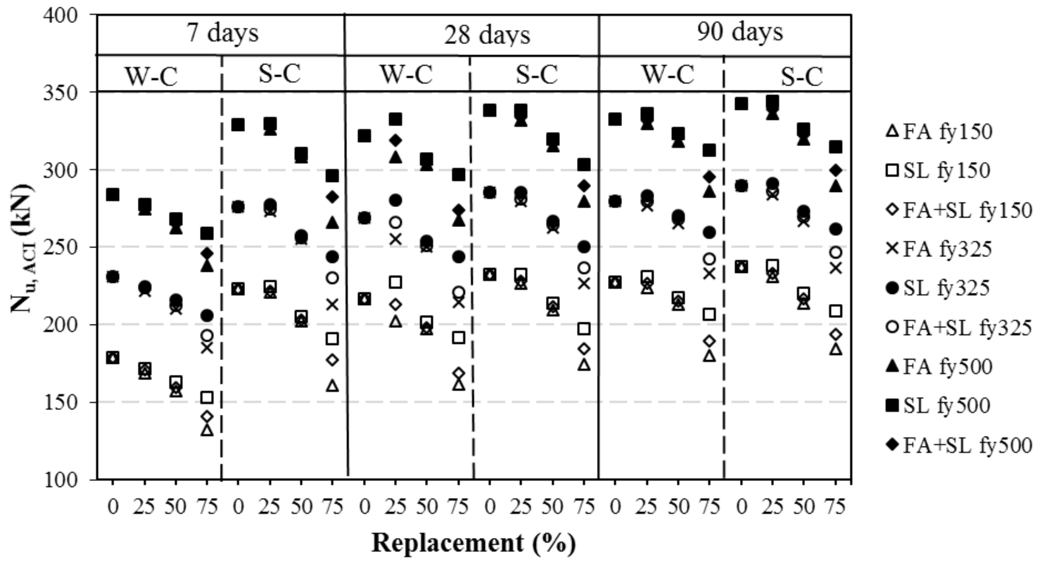

(a)

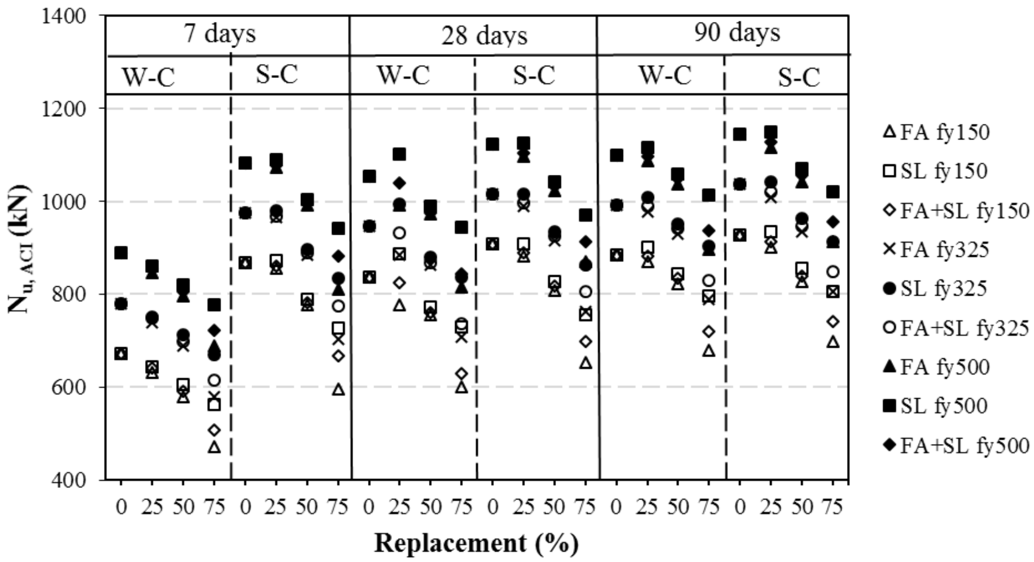
7 days
28 days
90 days
W-C
S-C
Nu, ACI (kN)
Replacement (%)
FA fy150
SL fy150
FA+SL fy150
FA fy325
SL fy325
FA+SL fy325
FA fy500
SL fy500
FA+SL fy500

(b)

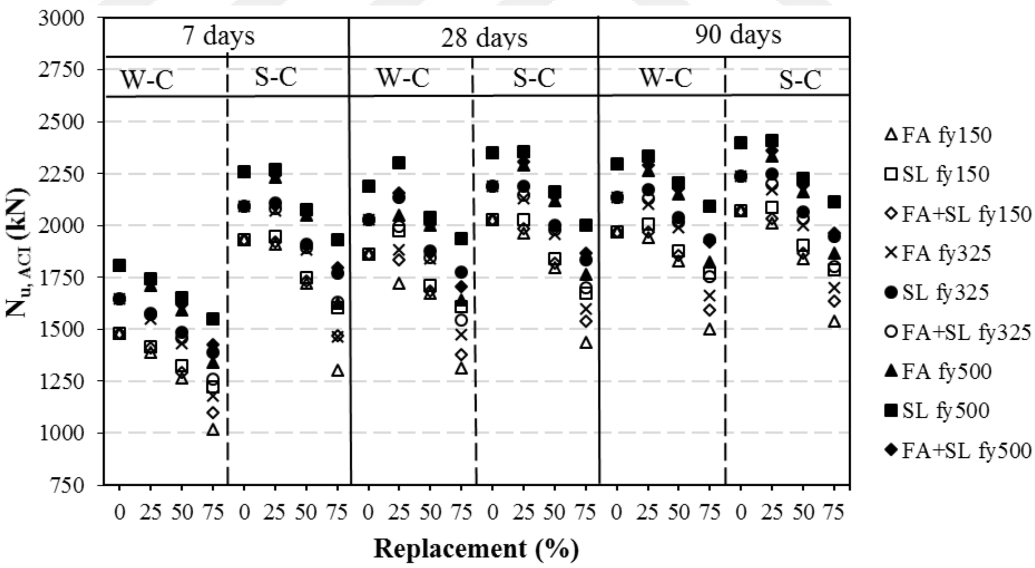
7 days
28 days
90 days
W-C
S-C
Nu, ACI (kN)
Replacement (%)
FA fy150
SL fy150
FA+SL fy150
FA fy325
SL fy325
FA+SL fy325
FA fy500
SL fy500
FA+SL fy500

(c)

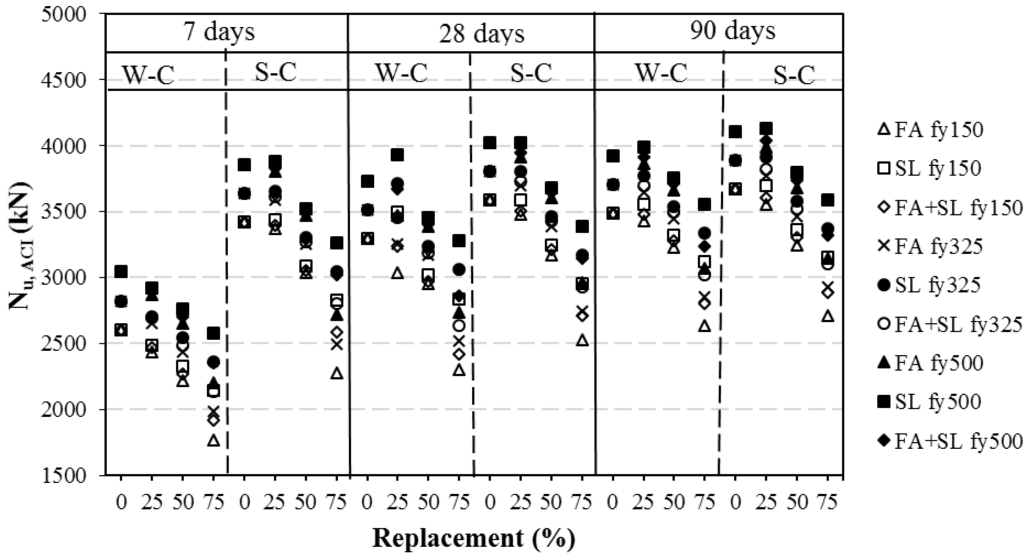

(d)

Figure 5.2 Axial capacity of UHPC filled steel tubular columns based on ACI 318 code for D/t ratios of a) 25, b) 50, c) 75 and d) 100

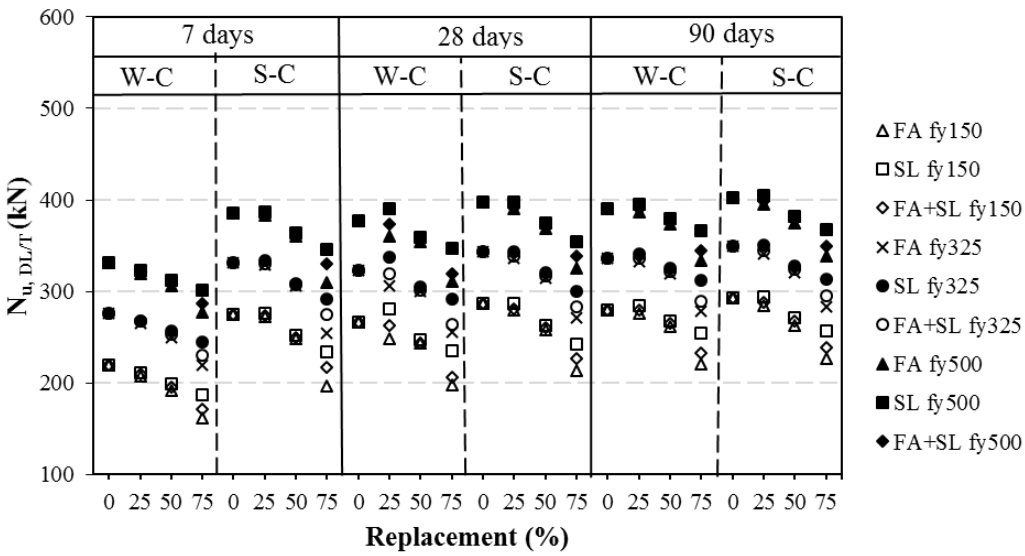

(a)

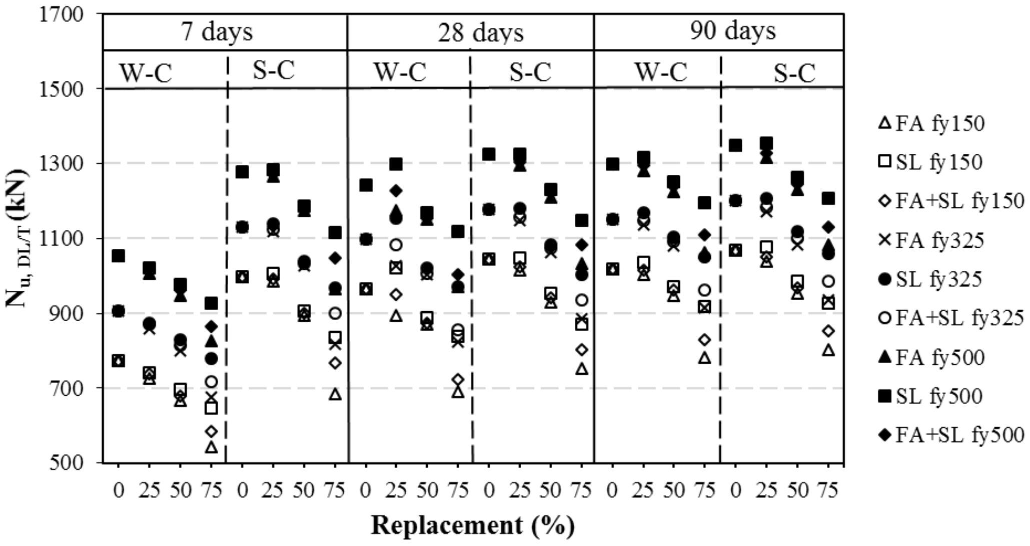
7 days
28 days
90 days
W-C
S-C
$N_{u, DL/T}$ (kN)
Replacement (%)
FA fy150
SL fy150
FA+SL fy150
FA fy325
SL fy325
FA+SL fy325
FA fy500
SL fy500
FA+SL fy500

(b)

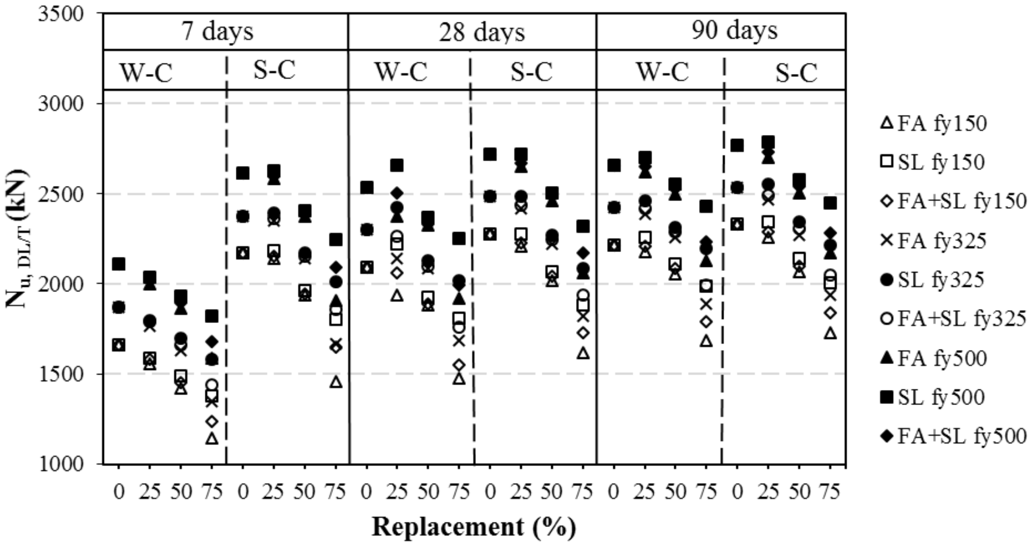
7 days
28 days
90 days
W-C
S-C
$N_{u, DL/T}$ (kN)
Replacement (%)
FA fy150
SL fy150
FA+SL fy150
FA fy325
SL fy325
FA+SL fy325
FA fy500
SL fy500
FA+SL fy500

(c)

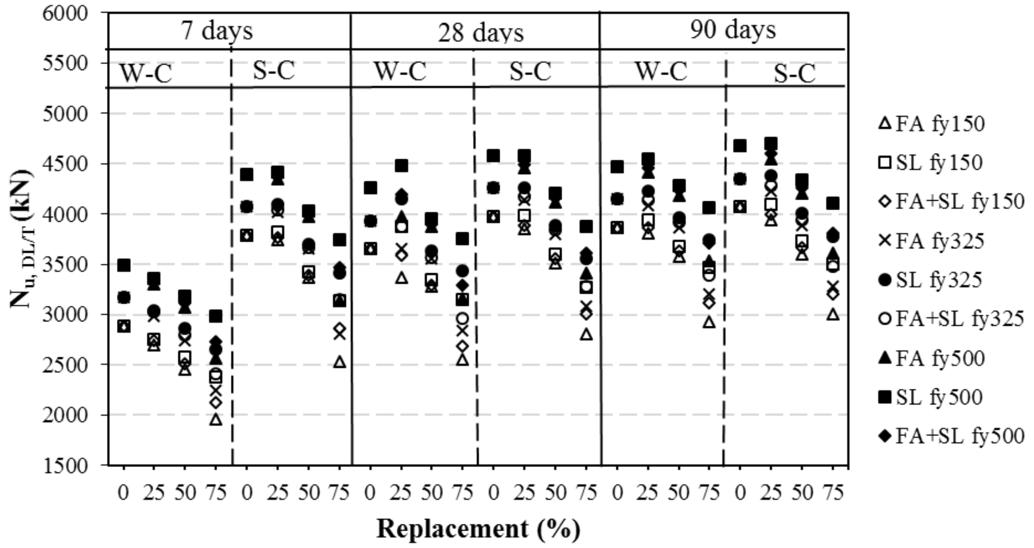

(d)

Figure 5.3 Axial capacity of UHPC filled steel tubular columns based on DL/T code for D/t ratios of a) 25, b) 50, c) 75 and d) 100

5.2.2 Effect of curing period and regime on UHPC columns

The effect of age of curing on the axial capacity of UHPC filled steel tubular columns were estimated as the axial load carrying capacity at 7 and 90 days divided by the axial load carrying capacity at 28 days. The effect of age of curing of 7/28 days axial load showed in Figures 5.4 (a-c), 5.5 (a-c), and 5.6 (a-c), while the 90/28 days axial load showed in Figures 5.7 (a-c), 5.8 (a-c), and 5.9 (a-c) computed by Eurocode 4 (2004), ACI-318R (2005) and Chinese code DL/T (1999), respectively. These figures indicated that the steam curing gives higher ratios of axial load carrying capacity at 7/28 days compared with corresponding water curing. For example in Eurocode 4 (2004) when the yield strength of steel equal to 150 MPa, the ratios of axial load carrying capacity at 7/28 days reached to 0.85, 0.82, 0.81 and 0.81% for water curing and 0.98, 0.97, 0.97 and 0.97% for steam curing with D/t 25, 50, 75 and 100, respectively. Whereas the water curing gives higher ratios of axial load carrying capacity at 90/28 than the corresponding steam curing and the ratios reached to 1.1, 1.1, 1.2 and 1.2% for water curing and 1.05, 1.06, 1.07 and 1.07% for steam curing with D/t 25, 50, 75 and 100, respectively. This is because of the steam curing accelerates the reactions of the concrete compounds at early ages compared with water curing. The same trend was observed in ACI-318R (2005) and Chinese code DL/T (1999).

It can also observed that the steam curing mix gives higher axial load capacity compared with corresponding water cured mix at all ages up to 90 days as presented in Figures 5.10 (a-c), 5.11 (a-c) and 5.12 (a-c) for Eurocode 4 (2004), ACI-318R (2005) and DL/T (1999) codes, respectively. The increasing for D/t=25 and f_y=150 reached to 27.8, 11.0 and 4.1% for Eurocode 4 (2004), 30.6, 11.9 and 4.0% for ACI-318R (2005) and 31.3, 12.9 and 4.5% for Chinese code DL/T (1999) at 7, 28 and 90 days, respectively.

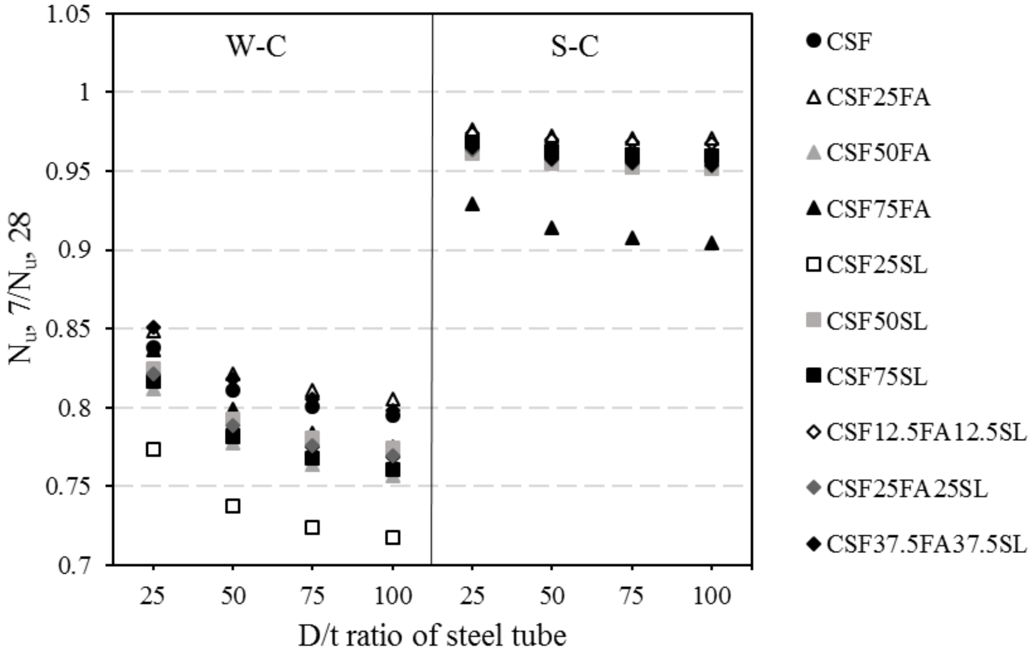

(a)

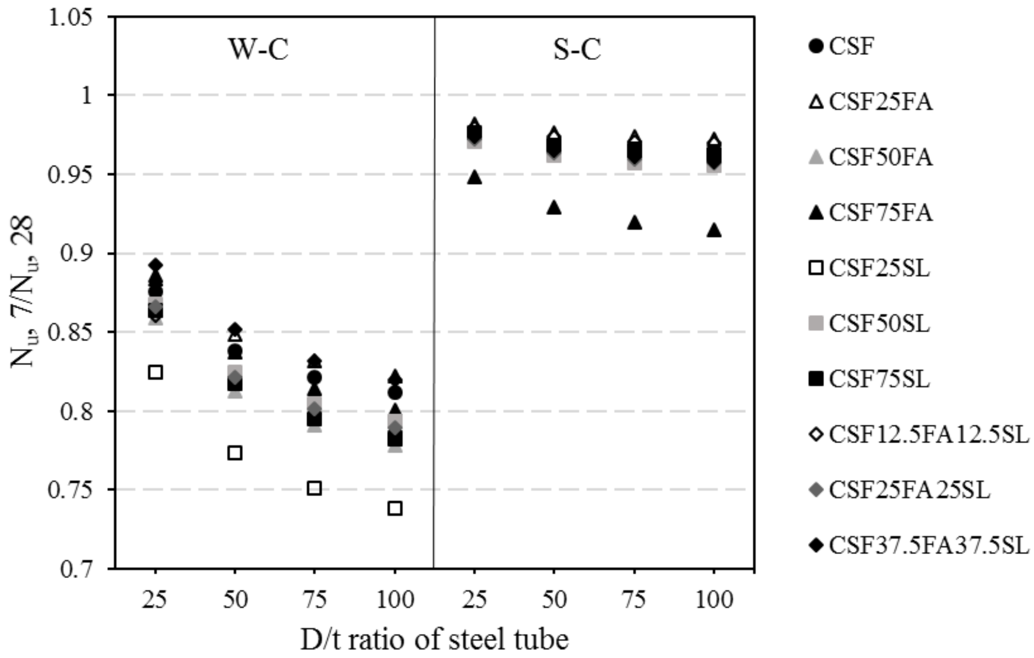

(b)

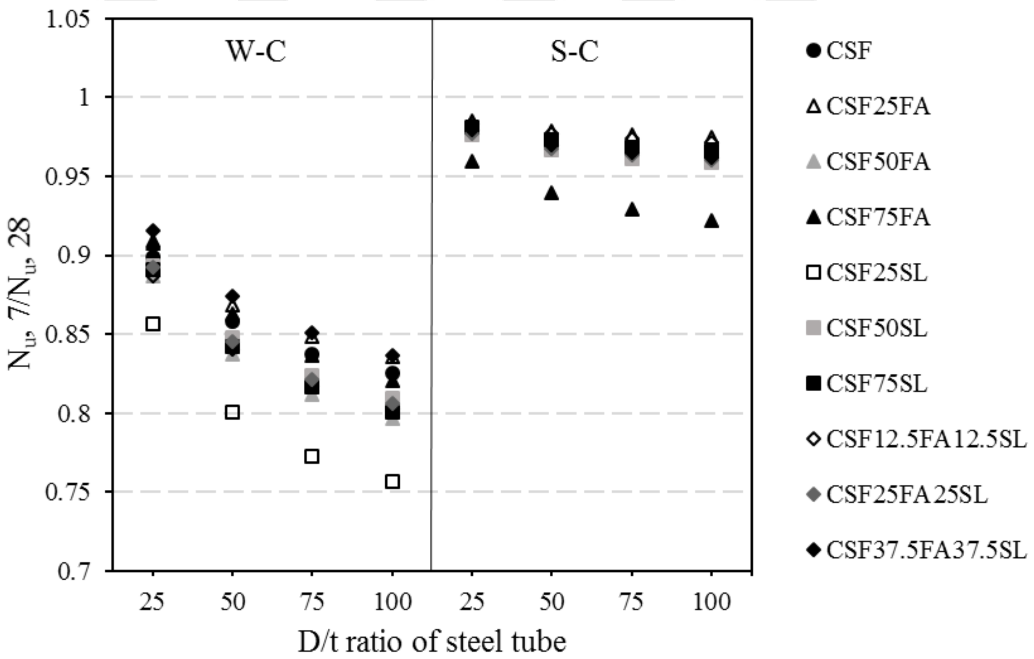

(c)

Figure 5.4 Effect of D/t ratio of steel tube on 7/28 day predicted capacity of the column with UHPC by Eurocode 4 at steel yield strength of a) 150, b) 325 and c) 500 MPa

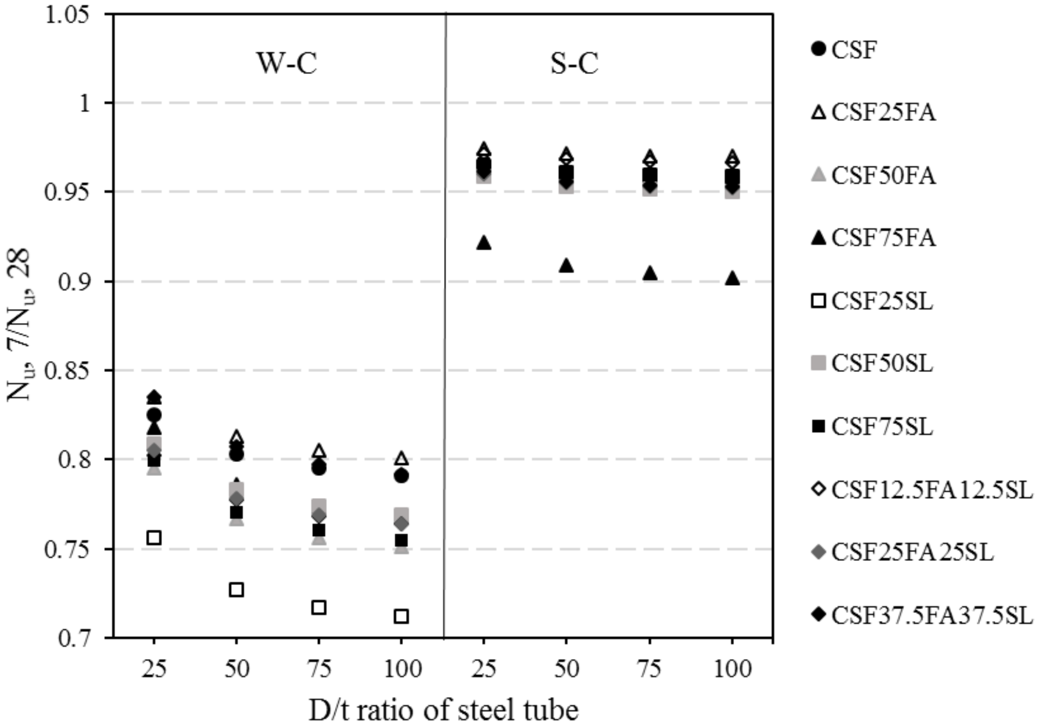
W-C
S-C
1.05
1
0.95
0.9
0.85
0.8
0.75
0.7
N_u, $7/N_u$, 28
25
50
75
100
25
50
75
100
D/t ratio of steel tube
CSF
CSF25FA
CSF50FA
CSF75FA
CSF25SL
CSF50SL
CSF75SL
CSF12.5FA12.5SL
CSF25FA25SL
CSF37.5FA37.5SL

(a)

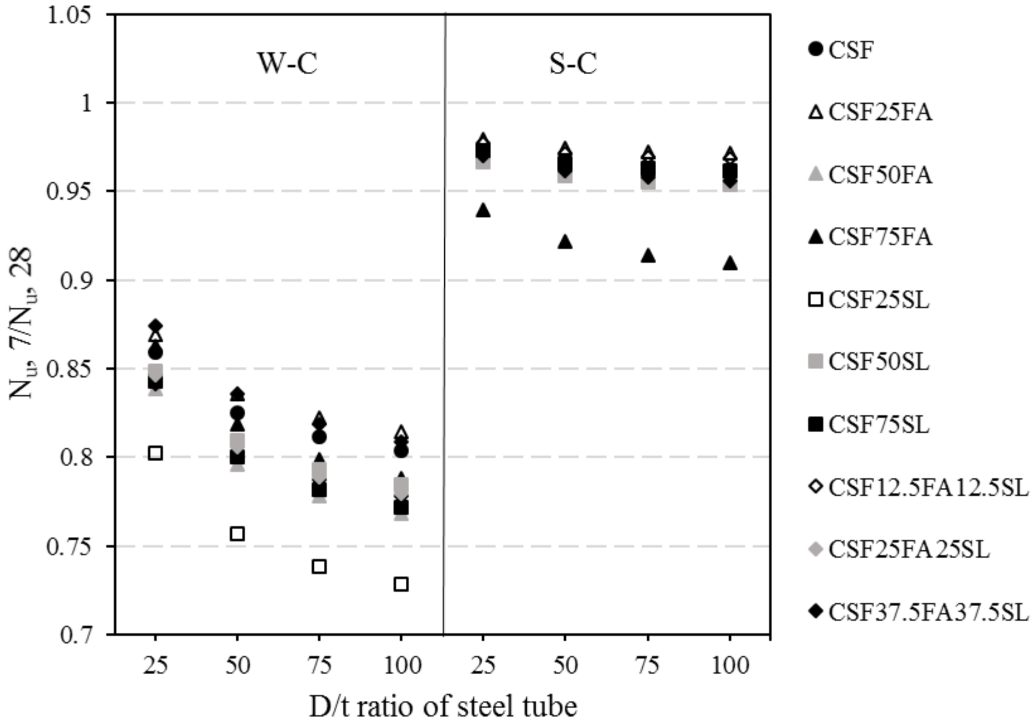
W-C
S-C
1.05
1
0.95
0.9
0.85
0.8
0.75
0.7
N_u, $7/N_u$, 28
25
50
75
100
25
50
75
100
D/t ratio of steel tube
CSF
CSF25FA
CSF50FA
CSF75FA
CSF25SL
CSF50SL
CSF75SL
CSF12.5FA12.5SL
CSF25FA25SL
CSF37.5FA37.5SL

(b)

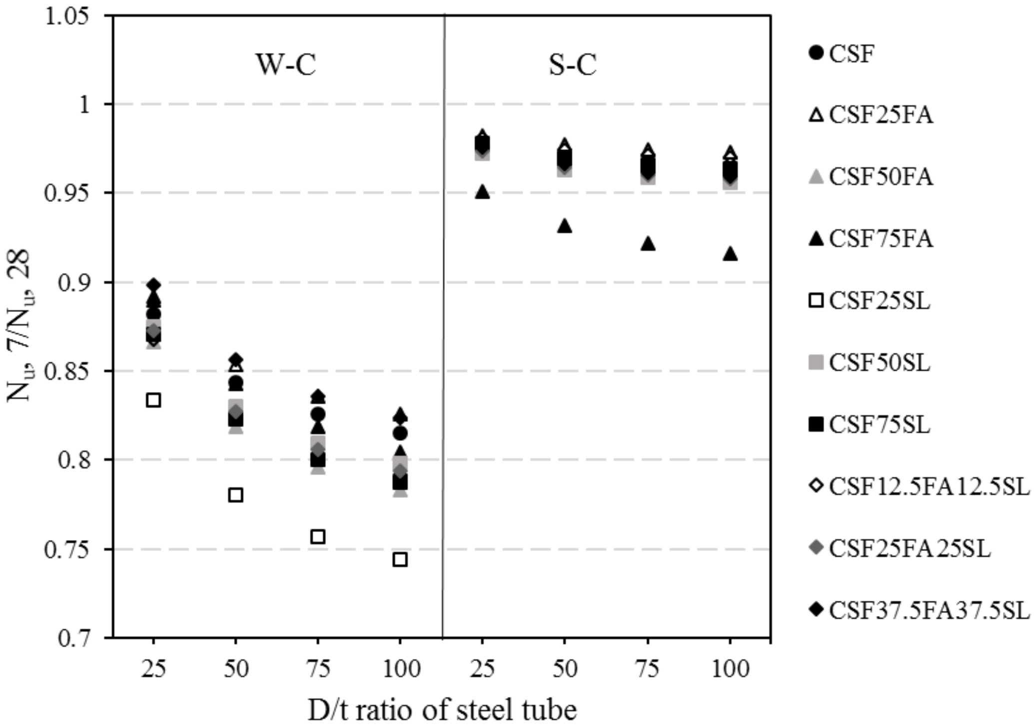

(c)

Figure 5.5 Effect of D/t ratio of steel tube on 7/28 day predicted capacity of the column with UHPC by ACI 318 at steel yield strength of a) 150, b) 325 and c) 500 MPa

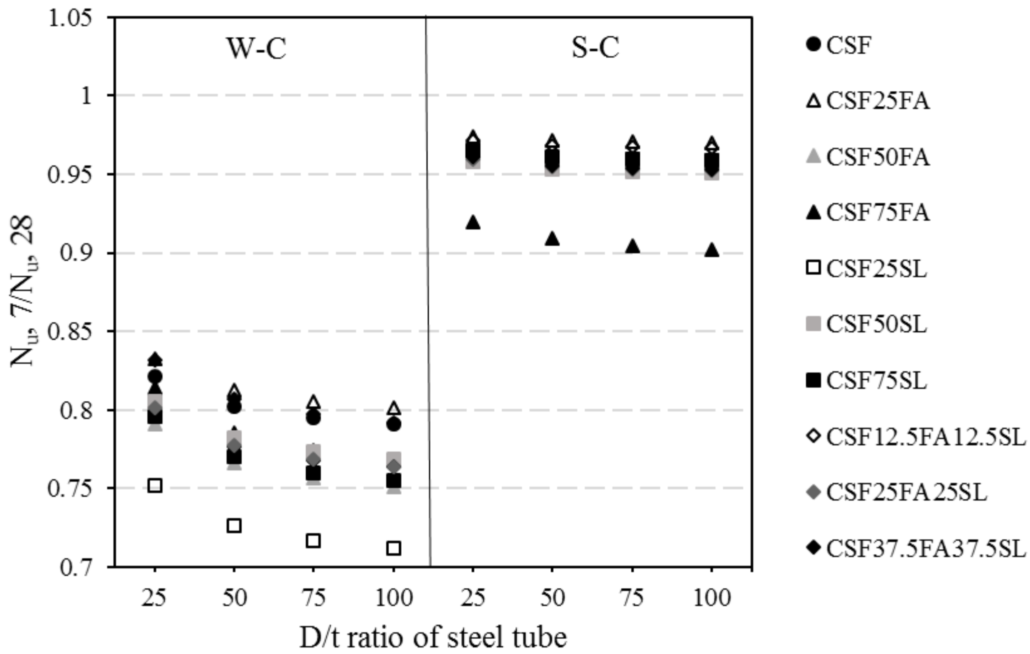

(a)

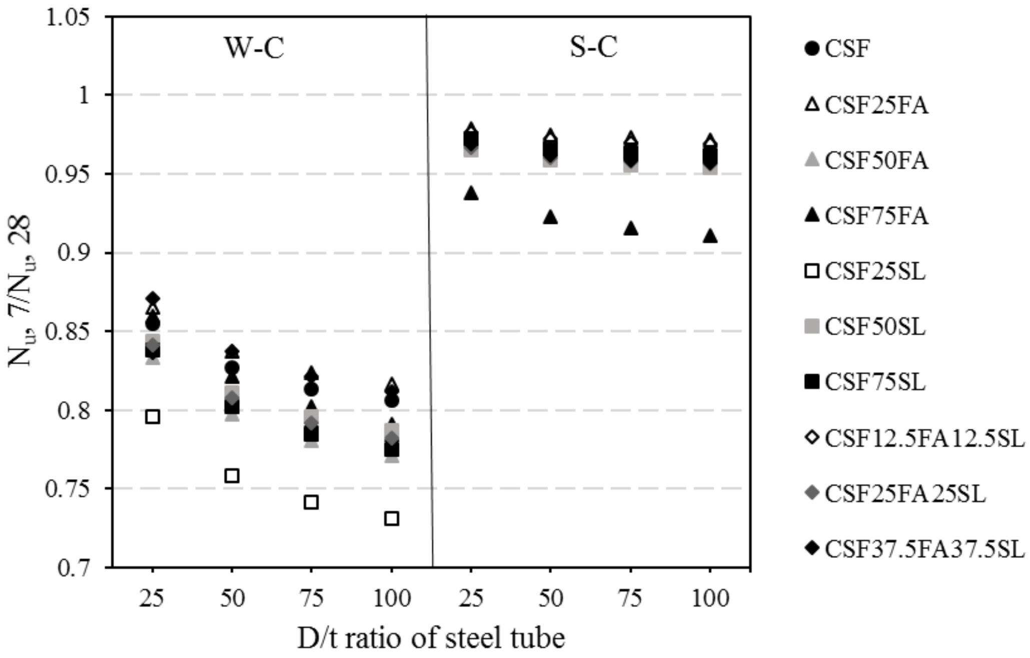

(b)

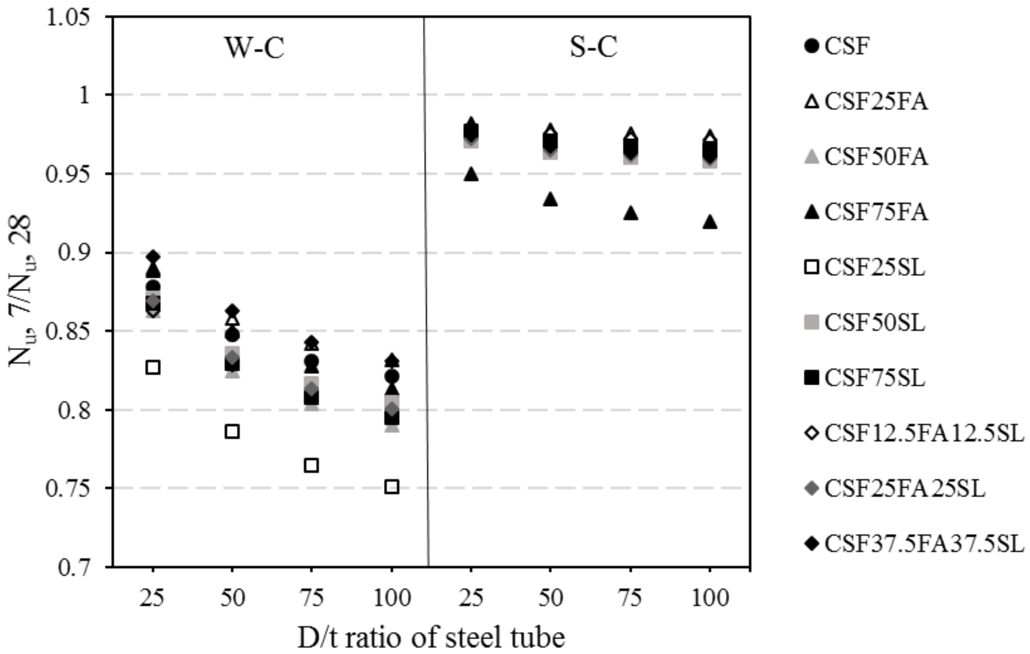

(c)

Figure 5.6 Effect of D/t ratio of steel tube on 7/28 day predicted capacity of the column with UHPC by DL/T code at steel yield strength of a) 150, b) 325 and c) 500 MPa

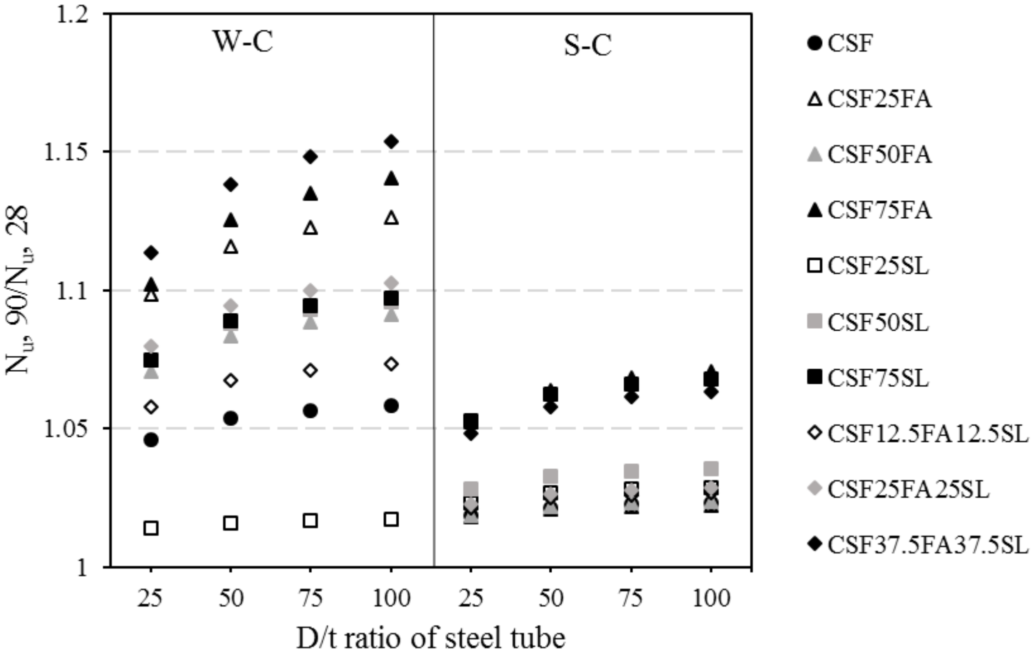

W-C
S-C
Nu, 90/Nu, 28
D/t ratio of steel tube
1.2
1.15
1.1
1.05
1
25
50
75
100
CSF
CSF25FA
CSF50FA
CSF75FA
CSF25SL
CSF50SL
CSF75SL
CSF12.5FA12.5SL
CSF25FA25SL
CSF37.5FA37.5SL

(a)

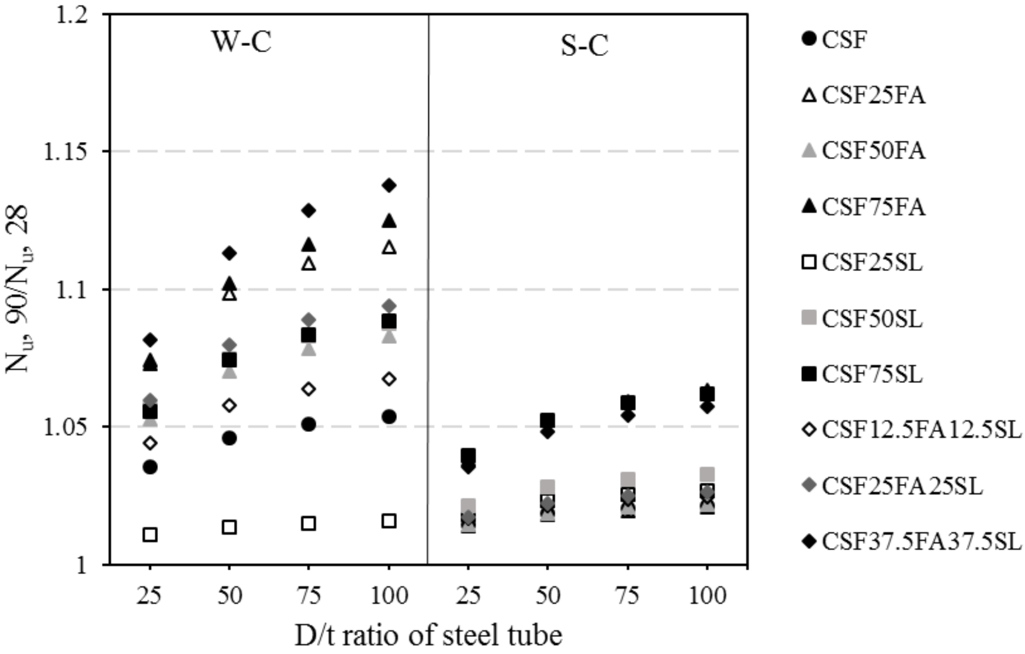

W-C
S-C
Nu, 90/Nu, 28
D/t ratio of steel tube
1.2
1.15
1.1
1.05
1
25
50
75
100
CSF
CSF25FA
CSF50FA
CSF75FA
CSF25SL
CSF50SL
CSF75SL
CSF12.5FA12.5SL
CSF25FA25SL
CSF37.5FA37.5SL

(b)

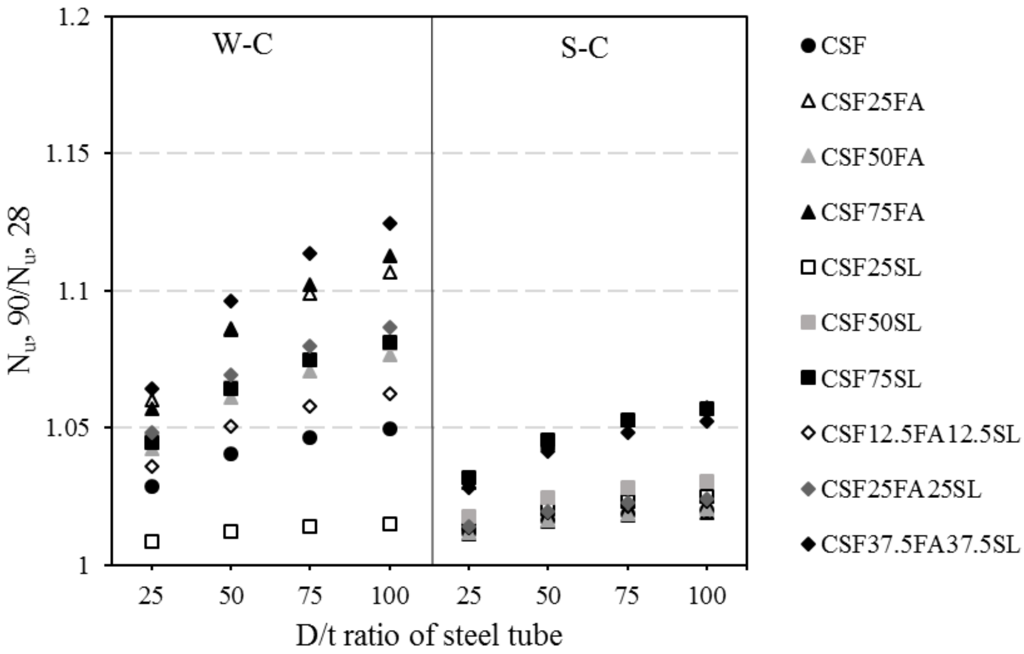

(c)

Figure 5.7 Effect of D/t ratio of steel tube on 90/28 day predicted capacity of the column with UHPC by Eurocode 4 at steel yield strength of a) 150, b) 325 and c) 500 MPa

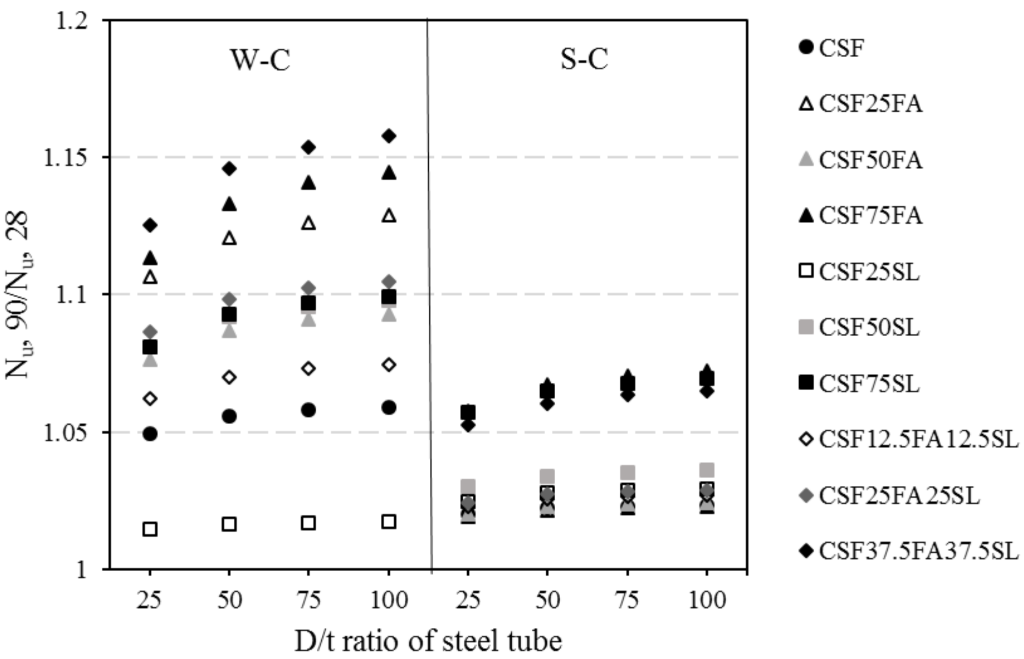

(a)

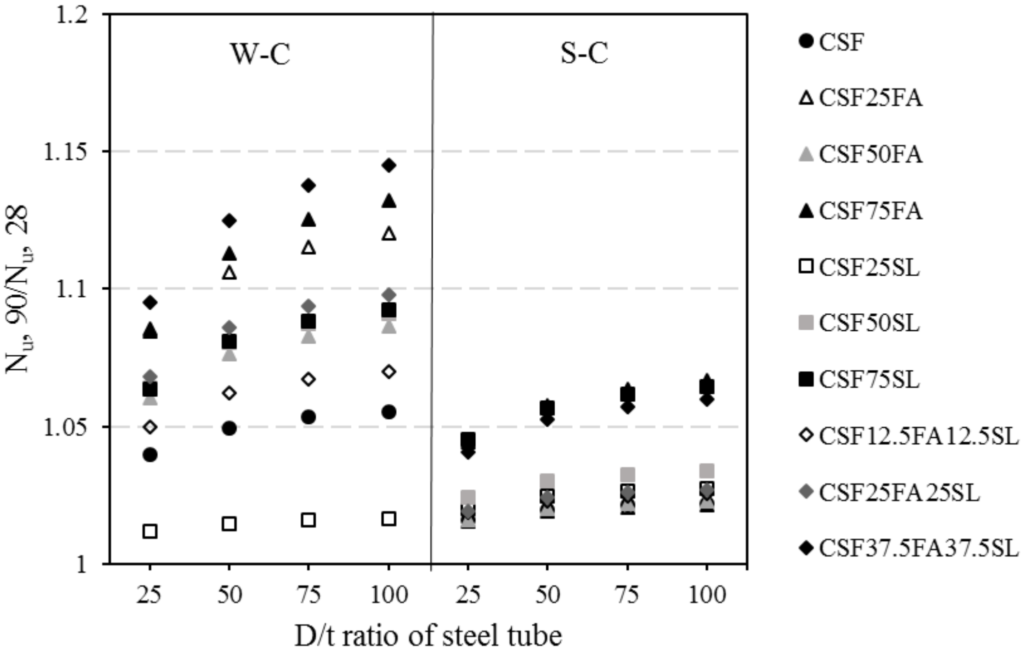

(b)

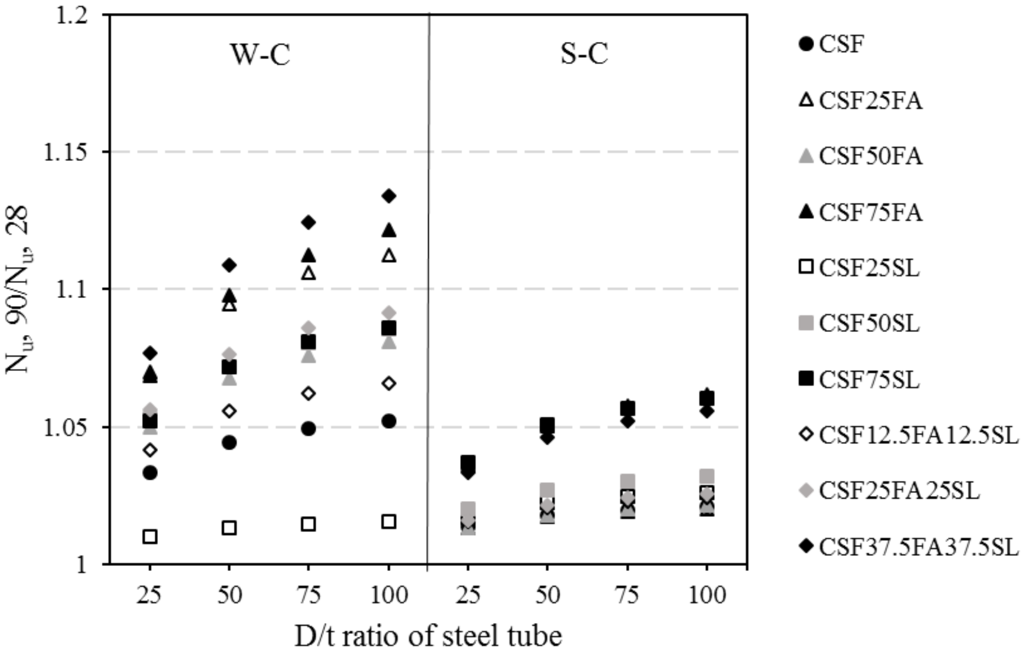

(c)

Figure 5.8 Effect of D/t ratio of steel tube on 90/28 day predicted capacity of the column with UHPC by ACI 318 at steel yield strength of a) 150, b) 325 and c) 500 MPa

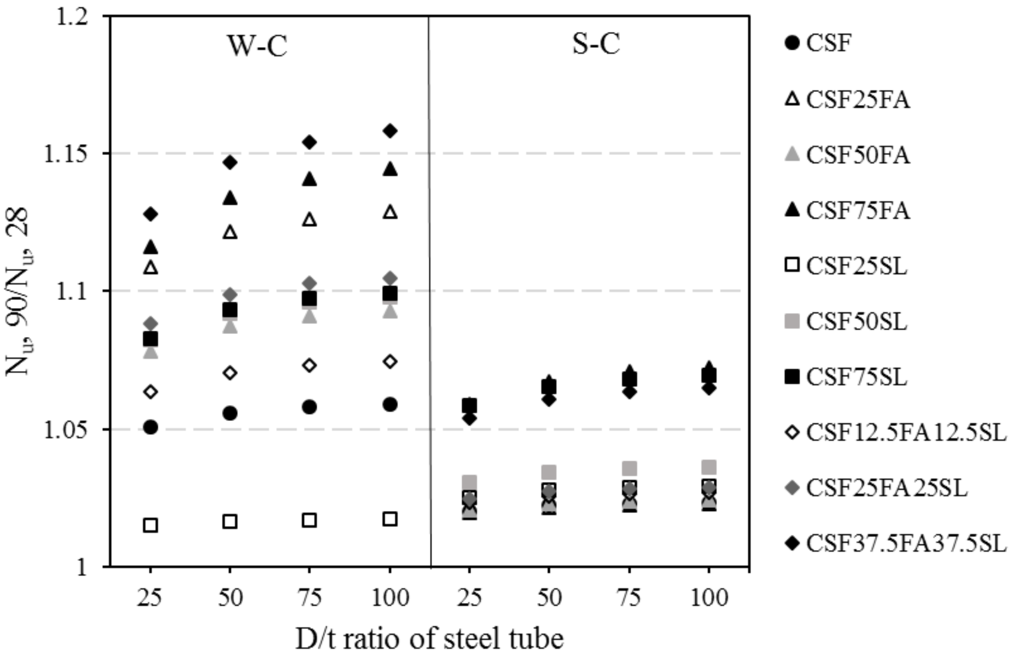
1.2
1.15
1.1
1.05
1
W-C
S-C
25
50
75
100
25
50
75
100
N_u, 90/N_u, 28
D/t ratio of steel tube
CSF
CSF25FA
CSF50FA
CSF75FA
CSF25SL
CSF50SL
CSF75SL
CSF12.5FA12.5SL
CSF25FA25SL
CSF37.5FA37.5SL

(a)

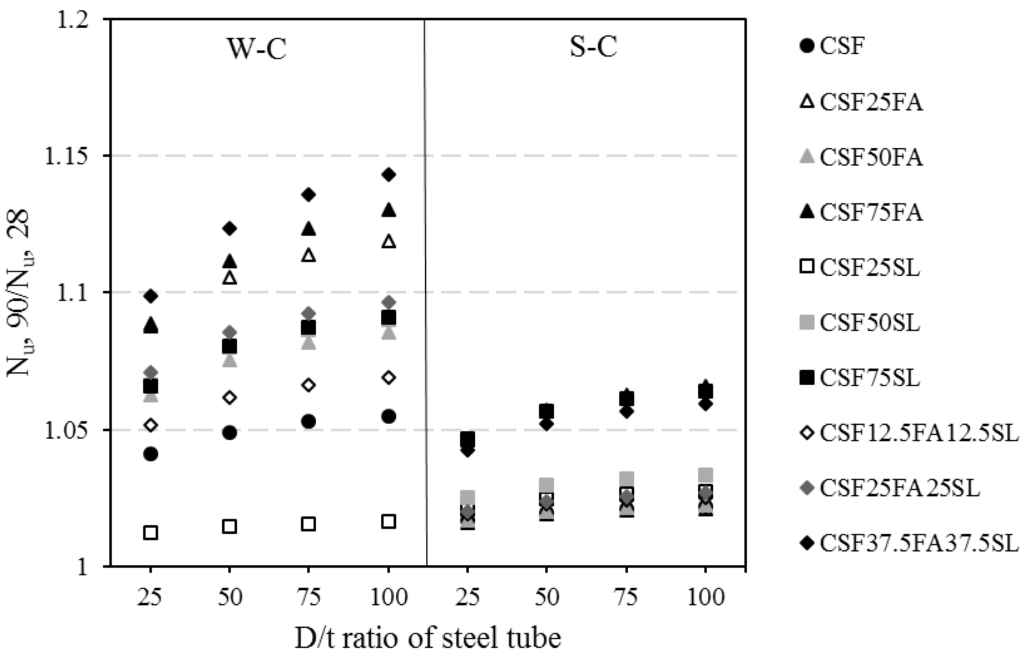
1.2
1.15
1.1
1.05
1
W-C
S-C
25
50
75
100
25
50
75
100
N_u, 90/N_u, 28
D/t ratio of steel tube
CSF
CSF25FA
CSF50FA
CSF75FA
CSF25SL
CSF50SL
CSF75SL
CSF12.5FA12.5SL
CSF25FA25SL
CSF37.5FA37.5SL

(b)

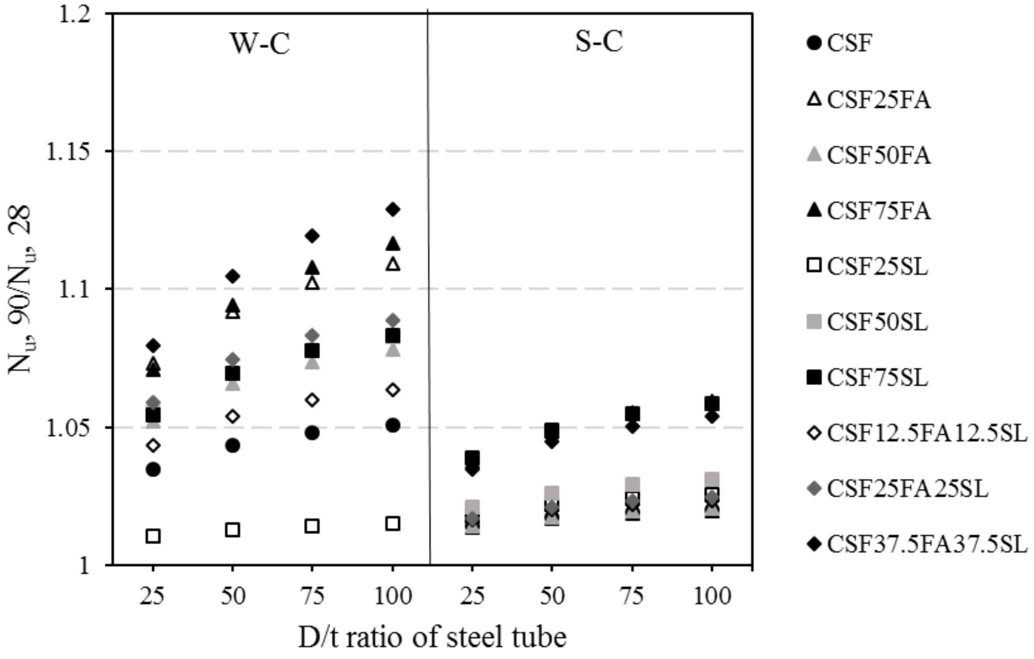

(c)

Figure 5.9 Effect of D/t ratio of steel tube on 90/28 day predicted capacity of the column with UHPC by DL/T code at steel yield strength of a) 150, b) 325 and c) 500 MPa

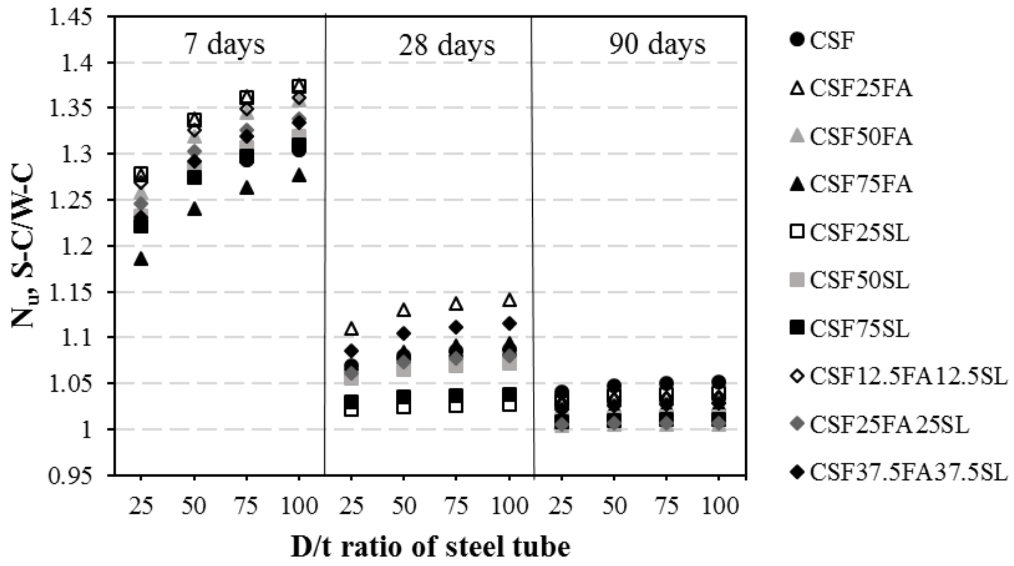

(a)

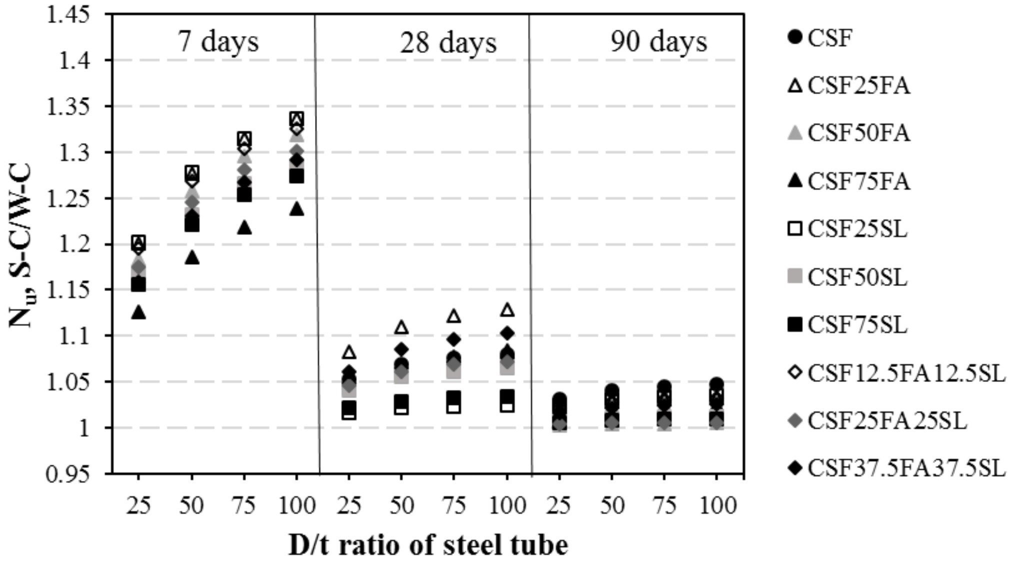

(b)

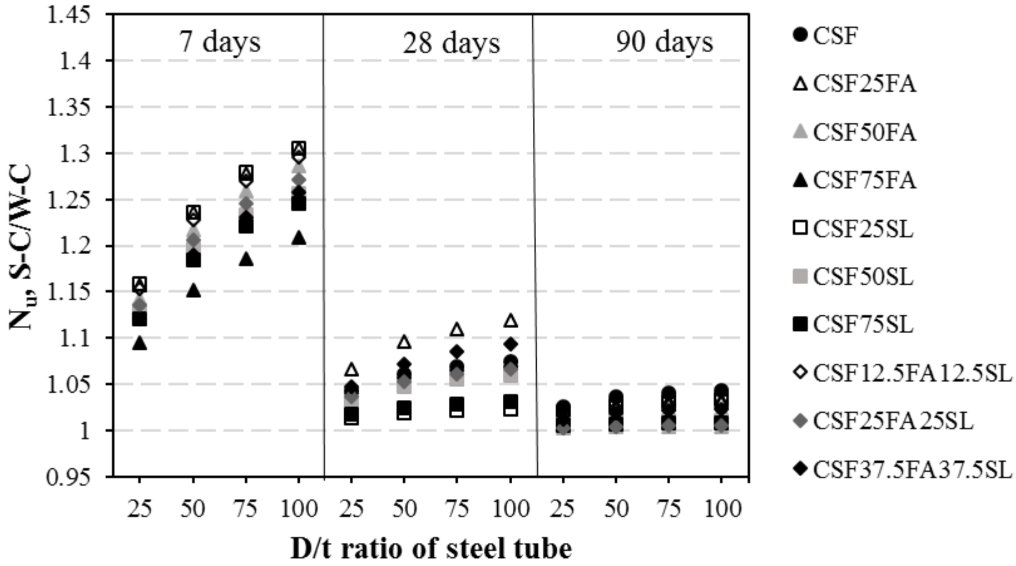

(c)

Figure 5.10 Effect of curing regime on the capacity of the column with UHPC according to Eurocode 4 at steel yield strength of a) 150, b) 325 and c) 500 MPa

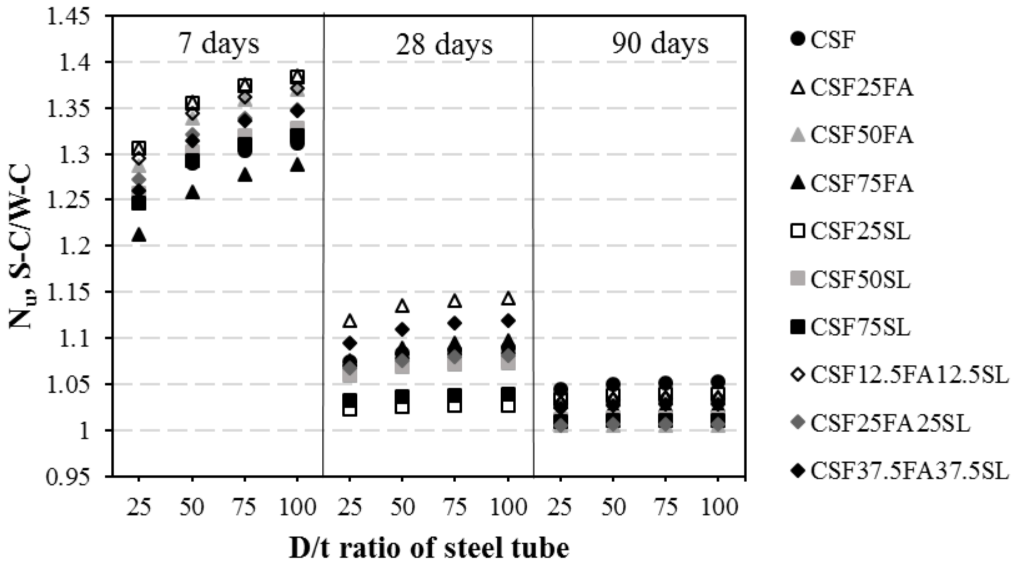
7 days
28 days
90 days
N_u, S-C/W-C
D/t ratio of steel tube
CSF
CSF25FA
CSF50FA
CSF75FA
CSF25SL
CSF50SL
CSF75SL
CSF12.5FA12.5SL
CSF25FA25SL
CSF37.5FA37.5SL

(a)

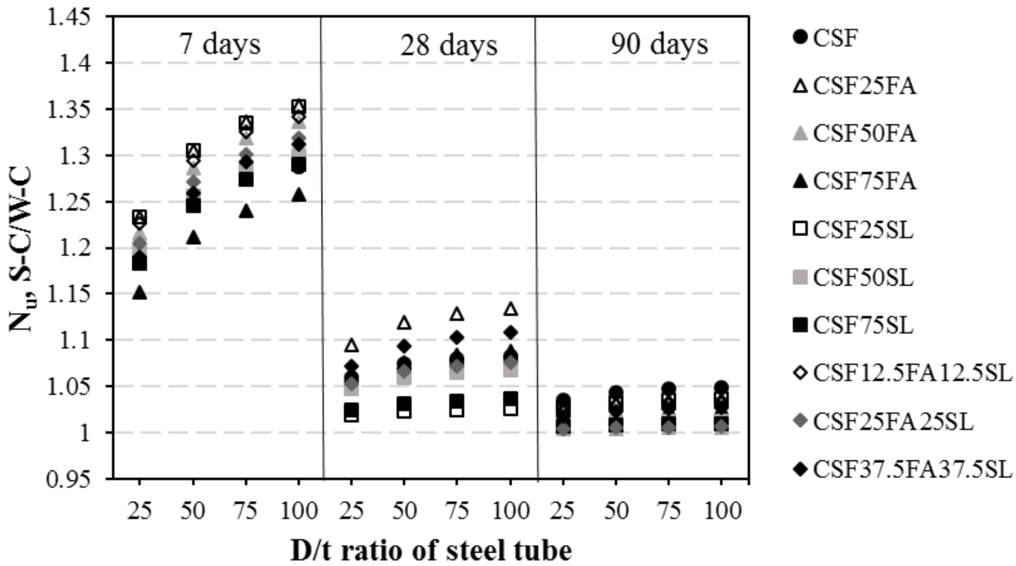
7 days
28 days
90 days
N_u, S-C/W-C
D/t ratio of steel tube
CSF
CSF25FA
CSF50FA
CSF75FA
CSF25SL
CSF50SL
CSF75SL
CSF12.5FA12.5SL
CSF25FA25SL
CSF37.5FA37.5SL

(b)

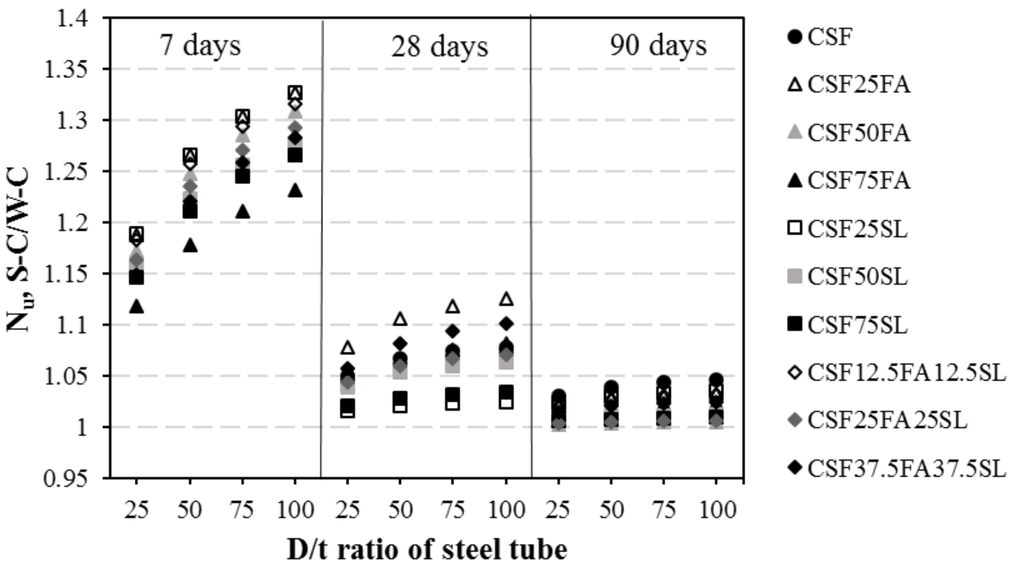

(c)

Figure 5.11 Effect of curing regime on the capacity of the column with UHPC according to ACI 318 at steel yield strength of a) 150, b) 325 and c) 500 MPa

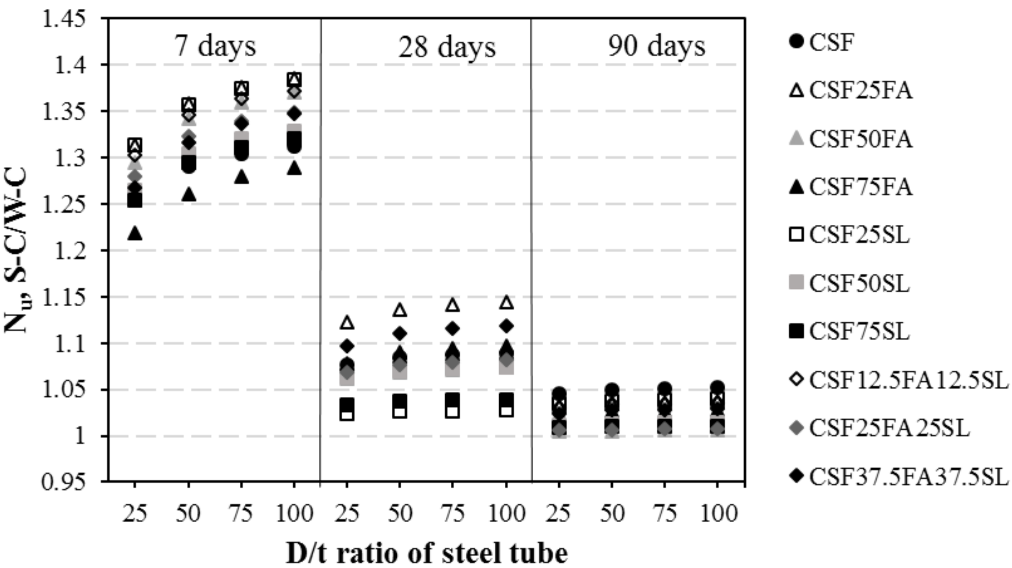

(a)

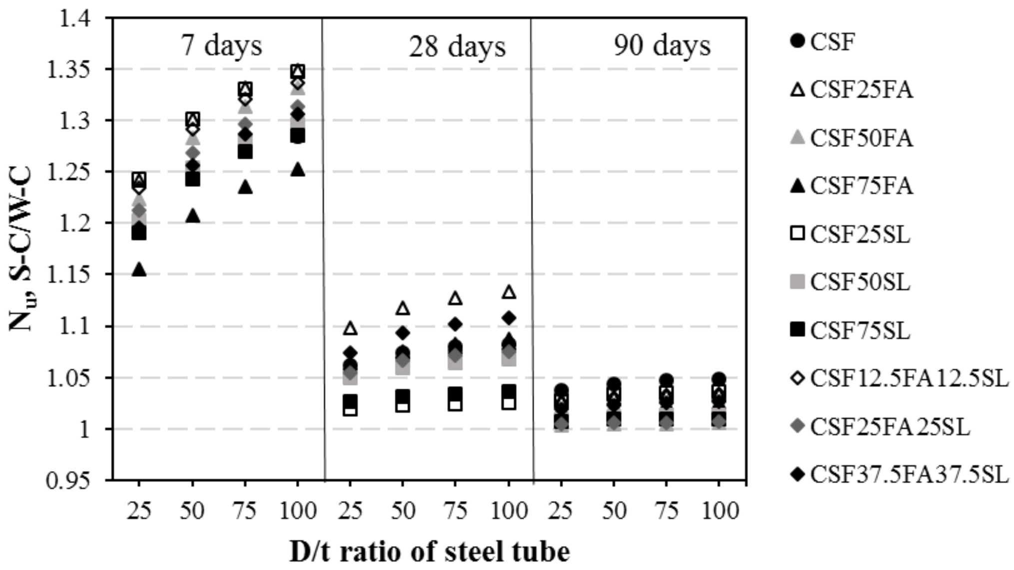

(b)

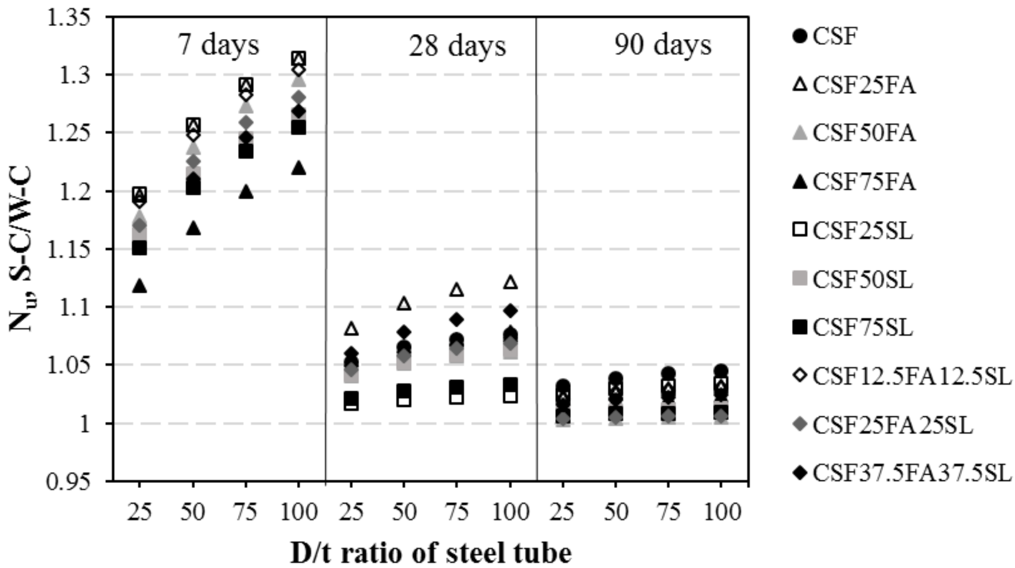

(c)

Figure 5.12 Effect of curing regime on the capacity of the column with UHPC according to DL/T code at steel yield strength of a) 150, b) 325 and c) 500 MPa

5.3 UHPGC filled steel tubular columns

5.3.1 Axial capacity variations

The axial load carrying capacity of UHPGC at 7, 28 and 90 days are shown in Figures 5.13 (a-d), 5.14 (a-d) and 5.15 (a-d) for Eurocode 4 (2004), ACI-318R (2005) and Chinese code DL/T (1999), respectively. These figures indicated that, irrespective to the variation in D/t and yield strength of steel tube, the axial load carrying capacity growth with age.

The results indicated that, in the mixes containing (FA + SF), the heat curing gives higher load carrying capacity than the corresponding steam curing. For example in ACI-318R (2005) when D/t=25 and f_y =150 MPa the increasing when the silica fume (SF) added to the geopolymer were 7.6, 6.0 and 6.1% at 7, 28 and 90 days, respectively, and the corresponding increasing when the SF inclusion in the geopolymer concrete were 6.3, 5.5 and 5.0% at the 7, 28 and 90 days, respectively, while the mixes containing (SL + SF) and (SL + FA + SF) gives higher load carrying capacity in steam curing comparing with corresponding heat curing mixes at all ages. Similar trend was observed in Eurocode 4 (2004), and Chinese code DL/T (1999).

The results showed that irrespective to the curing regime the axial load carrying capacity of UHPG increased with increasing the slag (SL) percent at all ages. This is because of the addition of SL contributed to increase the rate of hardening and the calcium that dissolves from SL considerably affected both early and late age properties (Puligilla and Mondal, 2013). The increasing in load carrying due to use SL in ACI-318R (2005) when D/t=25 and f_y =150 MPa at 7 days reached to 64.3 and 117.4%, in Eurocode 4 (2004) reached to 55.0 and 99.0% and the corresponding increasing in Chinese code DL/T (1999) was 66.2 and 121.3% for heat and steam curing, respectively.

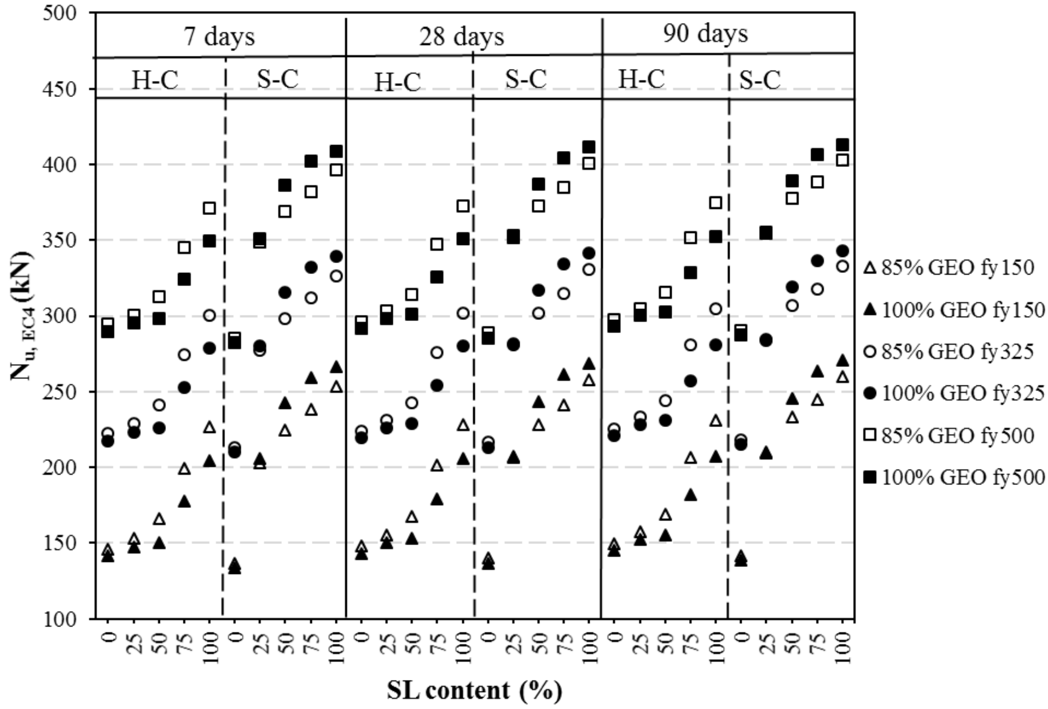

7 days
28 days
90 days
H-C
S-C
$N_{u, EC4}$ (kN)
SL content (%)
85% GEO fy150
100% GEO fy150
85% GEO fy325
100% GEO fy325
85% GEO fy500
100% GEO fy500

(a)

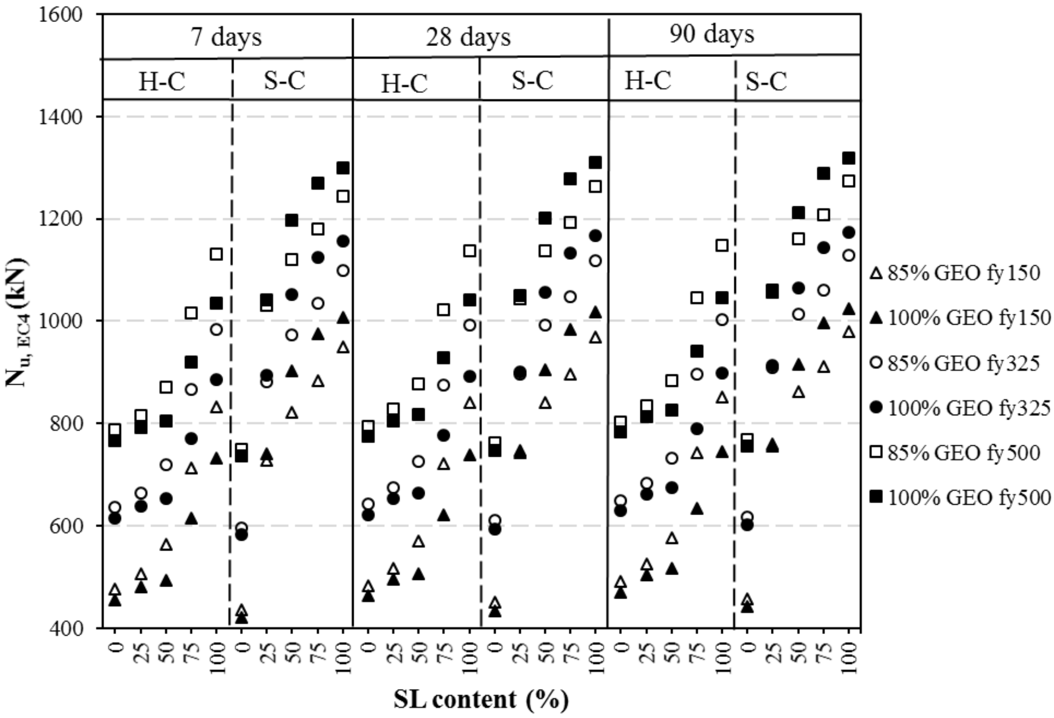

7 days
28 days
90 days
H-C
S-C
$N_{u, EC4}$ (kN)
SL content (%)
85% GEO fy150
100% GEO fy150
85% GEO fy325
100% GEO fy325
85% GEO fy500
100% GEO fy500

(b)

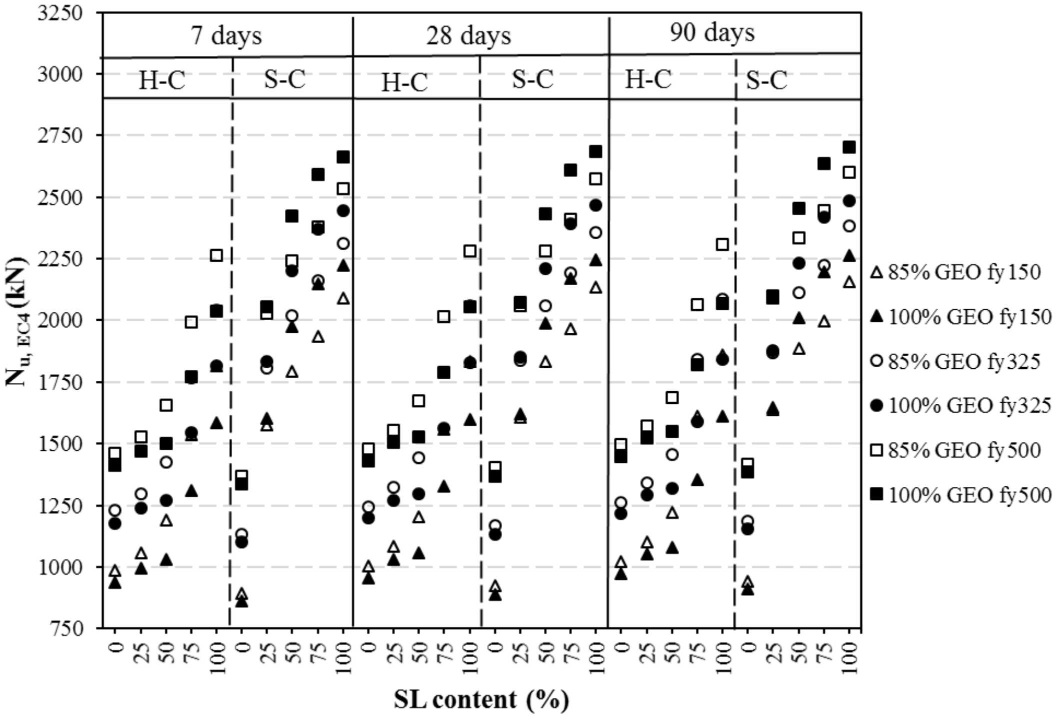

(c)

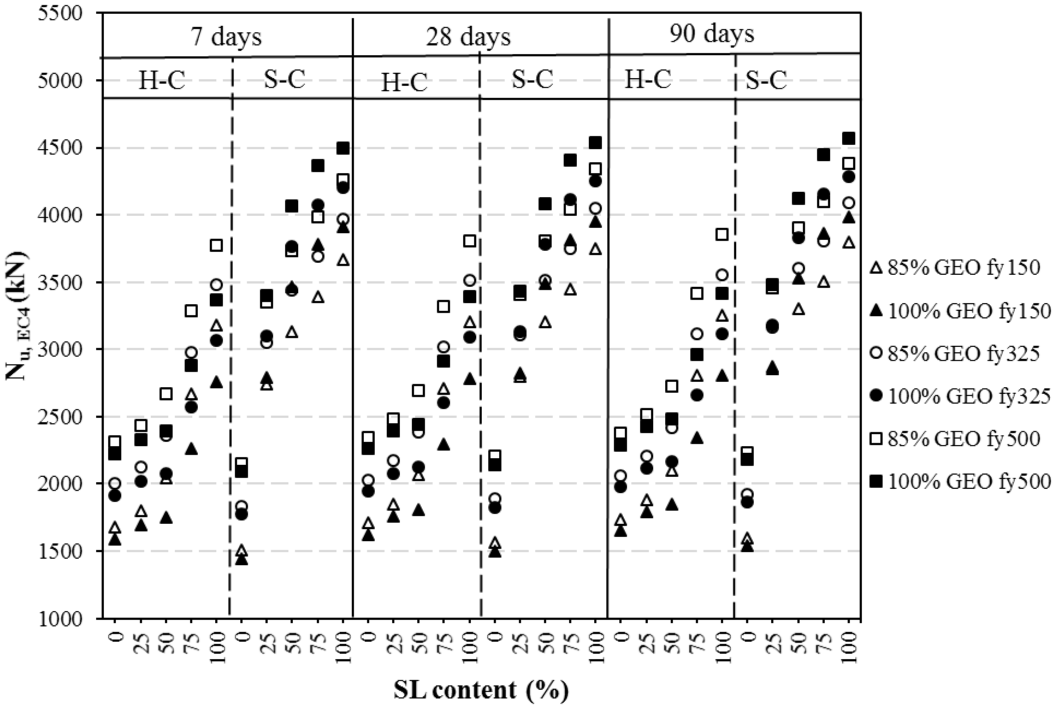

(d)

Figure 5.13 Axial capacity of UHPGC filled steel tubular columns based on Eurocode 4 for D/t ratios of a) 25, b) 50, c) 75 and d) 100

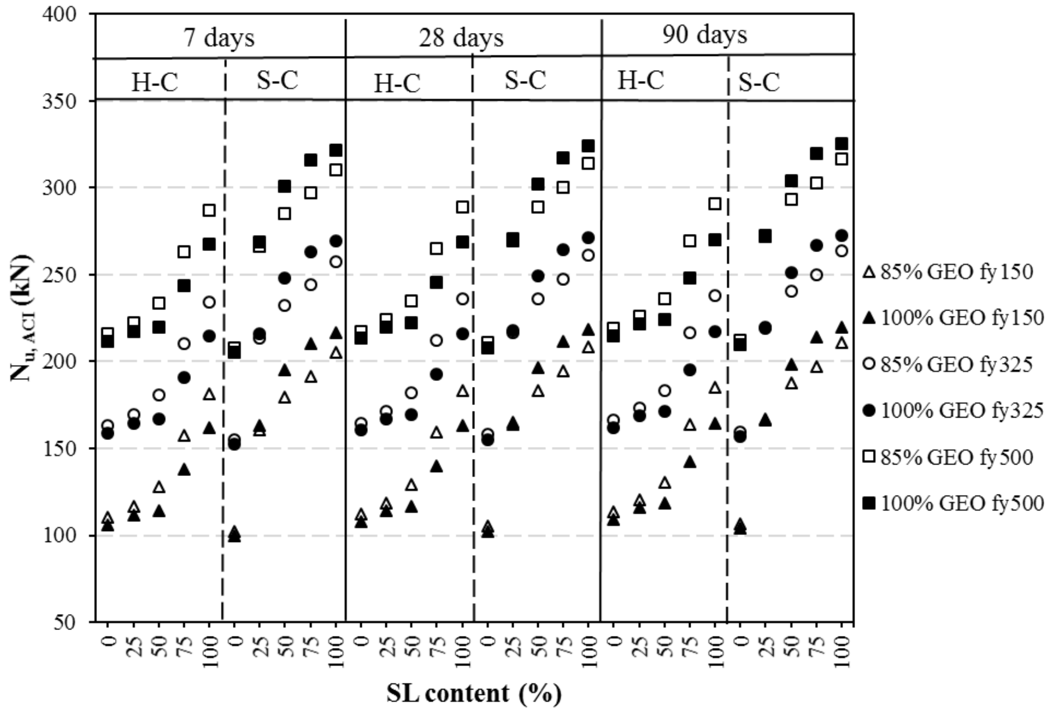

7 days
28 days
90 days
H-C
S-C
$N_{u, ACI}$ (kN)
SL content (%)
85% GEO fy150
100% GEO fy150
85% GEO fy325
100% GEO fy325
85% GEO fy500
100% GEO fy500

(a)

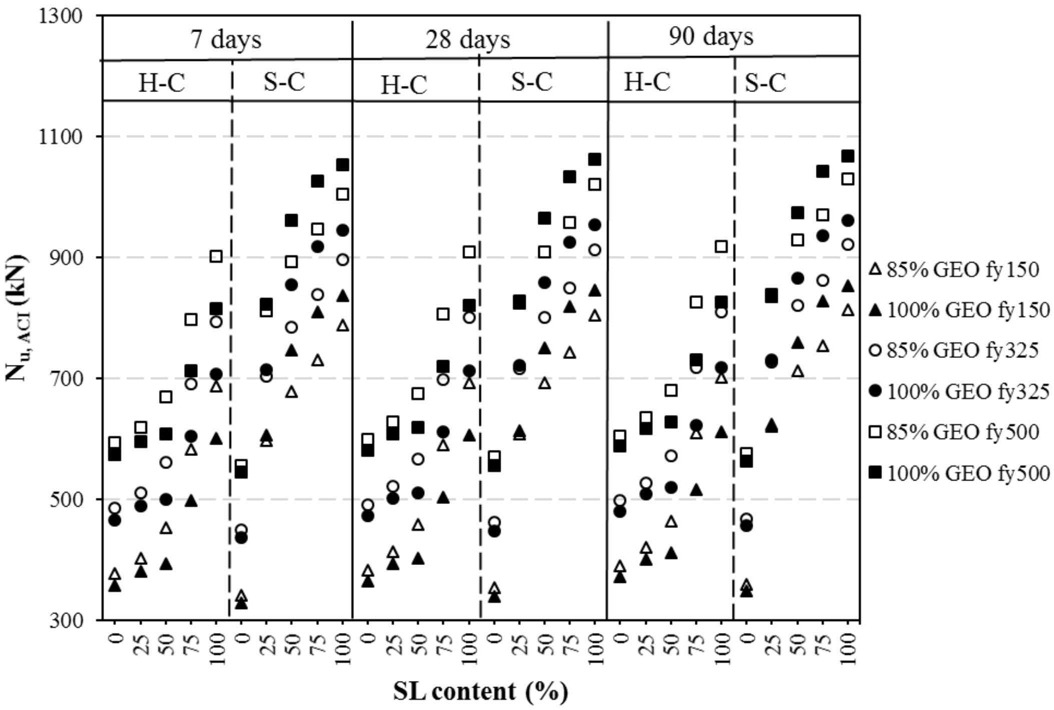

7 days
28 days
90 days
H-C
S-C
$N_{u, ACI}$ (kN)
SL content (%)
85% GEO fy150
100% GEO fy150
85% GEO fy325
100% GEO fy325
85% GEO fy500
100% GEO fy500

(b)

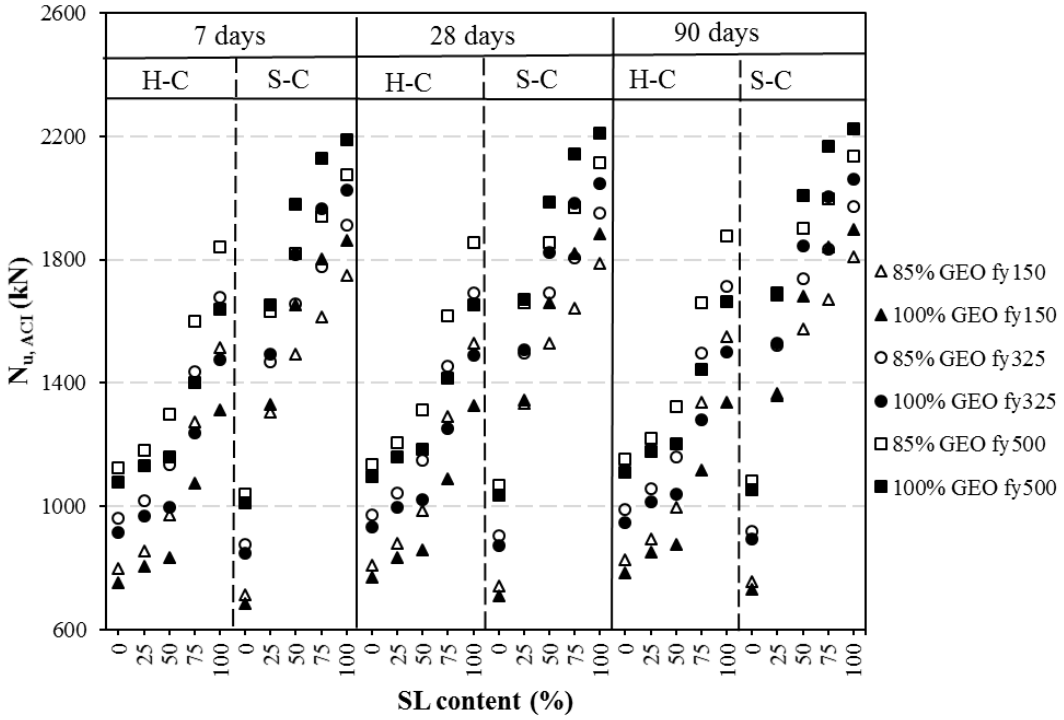

(c)

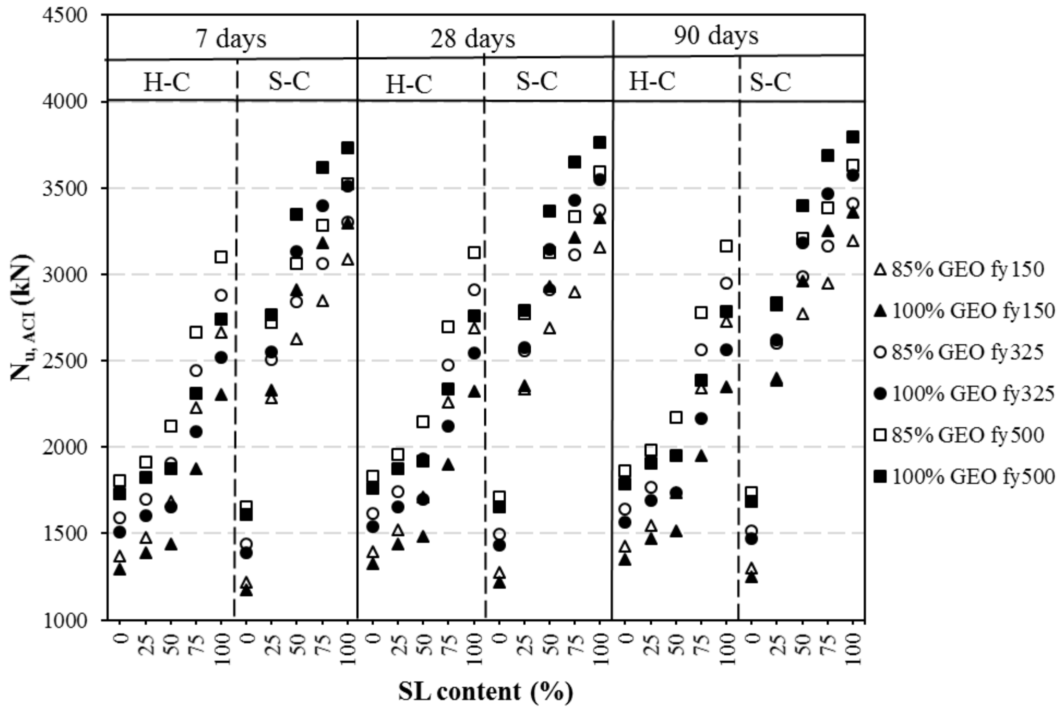

(d)

Figure 5.14 Axial capacity of UHPGC filled steel tubular columns based on ACI 318 code for D/t ratios of a) 25, b) 50, c) 75 and d) 100

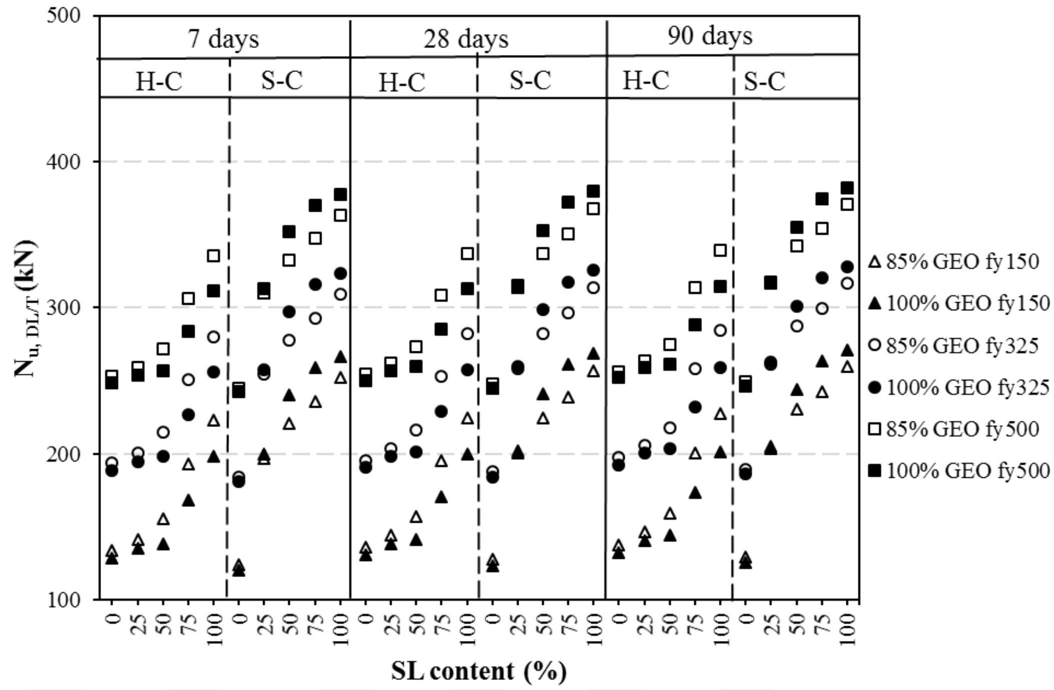
7 days
28 days
90 days
H-C
S-C
$N_{u, DL/T}$ (kN)
SL content (%)
85% GEO fy150
100% GEO fy150
85% GEO fy325
100% GEO fy325
85% GEO fy500
100% GEO fy500

(a)

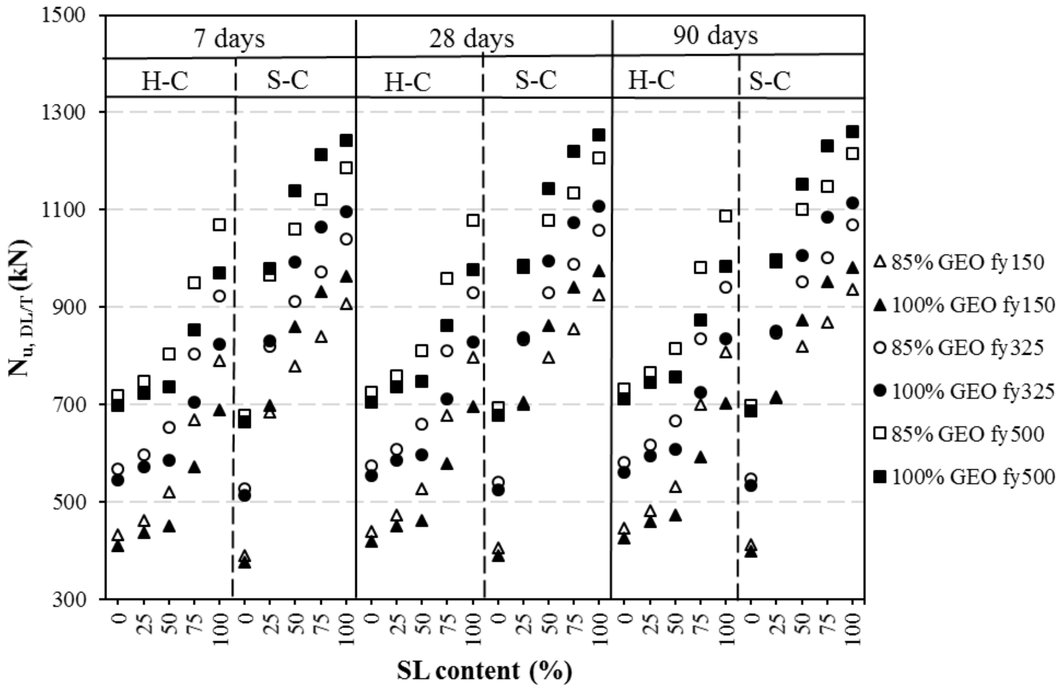
7 days
28 days
90 days
H-C
S-C
$N_{u, DL/T}$ (kN)
SL content (%)
85% GEO fy150
100% GEO fy150
85% GEO fy325
100% GEO fy325
85% GEO fy500
100% GEO fy500

(b)

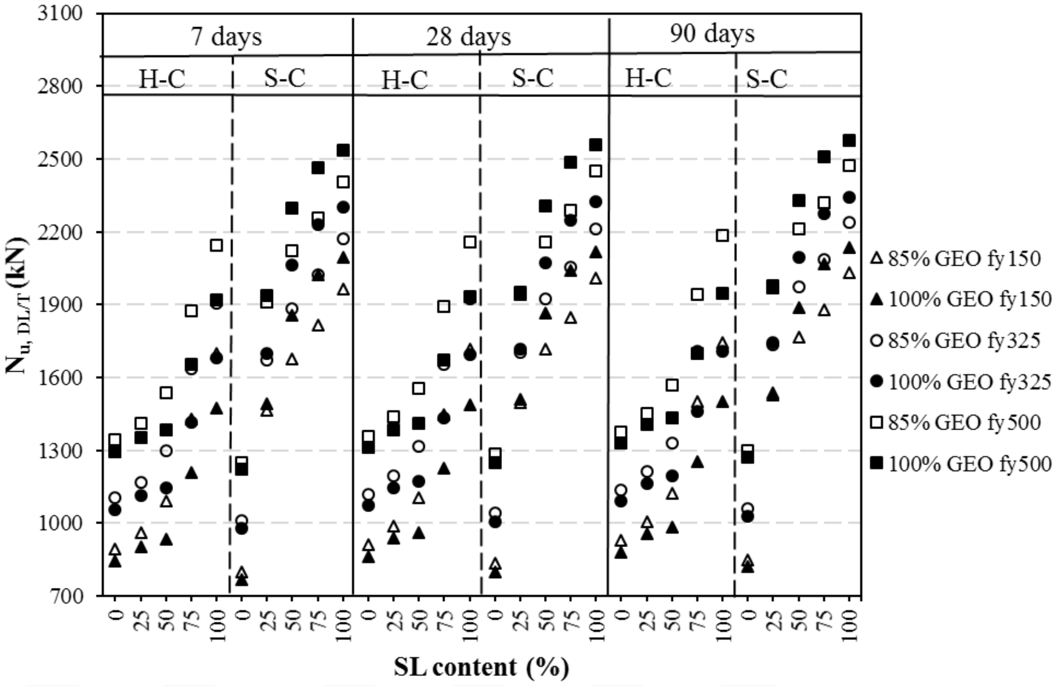

(c)

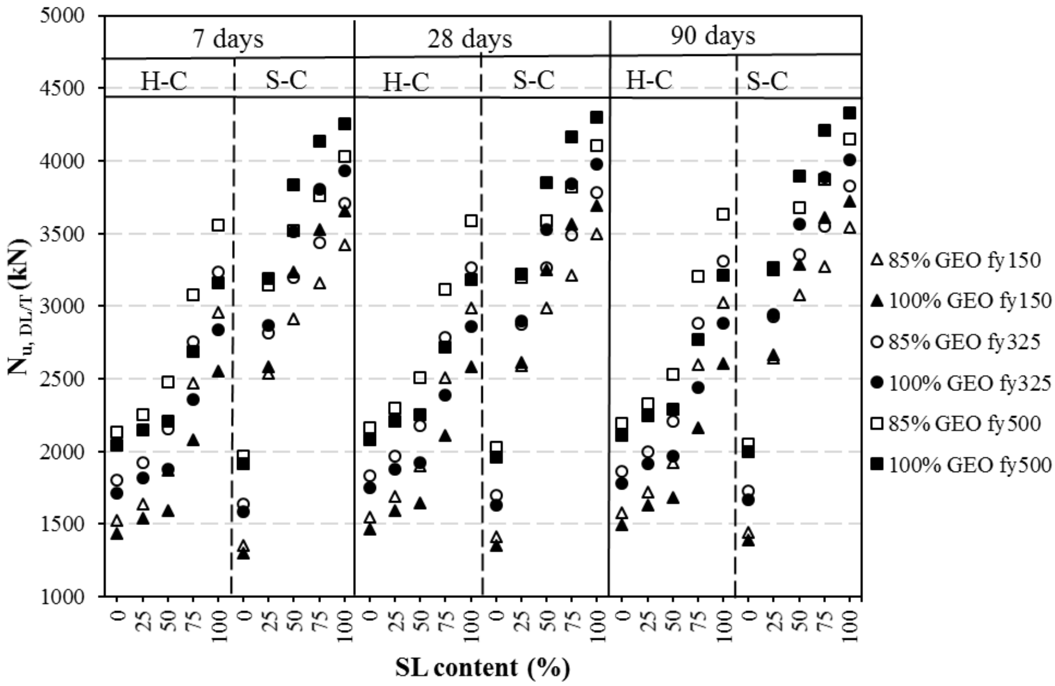

(d)

Figure 5.15 Axial capacity of UHPGC filled steel tubular columns based on DL/T code for D/t ratios of a) 25, b) 50, c) 75 and d) 100

5.3.2 Effect of curing period and regime on UHPGC columns

The effect of age of curing on the axial capacity of UHPGC filled steel tubular columns were estimated as the axial load carrying capacity at 7 and 90 days divided by the axial load carrying capacity at 28 days. The effect of age of curing of 7/28 days axial load showed in Figures 5.16 (a-c), 5.17 (a-c), and 5.18 (a-c), while the 90/28 days axial load showed in Figures 5.19 (a-c), 5.20 (a-c), and 5.21 (a-c) computed by Eurocode 4 (2004), ACI-318R (2005) and Chinese code DL/T (1999), respectively. These figures indicated that the development of the load carrying capacity of UHPGC is very low. For example in Eurocode 4 (2004) when the yield strength of steel equal to 150 MPa, the ratios of axial load carrying capacity at 7/28 days reached to 0.993, 0.991, 0.99 and 0.99% for heat curing and 0.996, 0.995, 0.995 and 0.995% for steam curing with D/t 25, 50, 75 and 100, respectively. Whereas at 90/28 the corresponding ratios reached to 1.03, 1.03 , 1.034 and 1.035 % for heat curing and 1.02, 1.03 , 1.03 and 1.03% for steam curing with D/t 25, 50, 75 and 100, respectively. The same trend was observed in ACI-318R (2005) and Chinese code DL/T (1999). It can be detected from the above ratios that the development of axial load carrying capacity in UHPGC is very low. This is resulting from higher curing temperature which is attributed to substantially fast polymerisation process through the chemical reaction of the geopolymer gel (Hardjito et al., 2004).

The effect of curing regime (SC/HC) presented in Figures 5.22 (a-c), 5.23 (a-c) and 5.24 (a-c) for Eurocode 4 (2004), ACI-318R (2005) and DL/T (1999) codes, respectively. It can be observed from these figures that, in SC, the mixes containing (SL + SF) and (SL + FA + SF) gives higher axial load capacity than the corresponding HC mixes, while opposite behavior can be seen in the mixes containing (FA + SF). The SC/HC ratio for D/t=25 and f_y=150 at 7 days ranged between (0.94 to 1.61), (0.92 to 1.71) and (0.92 to 1.73) for Eurocode 4 (2004), ACI-318R (2005) and DL/T (1999) codes, respectively.

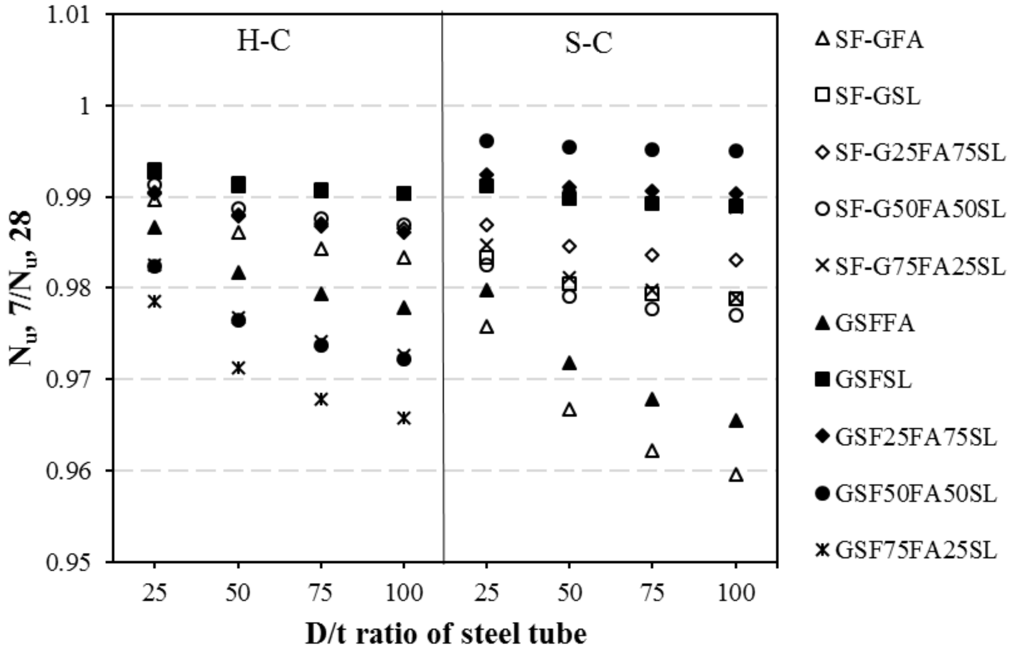
H-C
S-C
SF-GFA
SF-GSL
SF-G25FA75SL
SF-G50FA50SL
SF-G75FA25SL
GSFFA
GSFSL
GSF25FA75SL
GSF50FA50SL
GSF75FA25SL
N_u, 7/N_u, 28
D/t ratio of steel tube

(a)

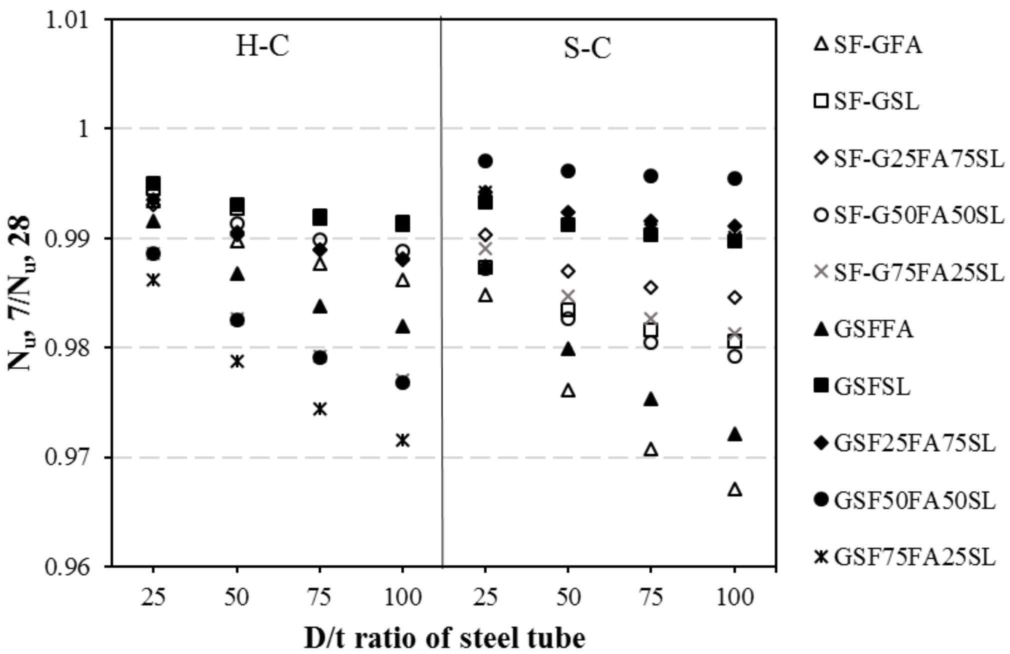
H-C
S-C
SF-GFA
SF-GSL
SF-G25FA75SL
SF-G50FA50SL
SF-G75FA25SL
GSFFA
GSFSL
GSF25FA75SL
GSF50FA50SL
GSF75FA25SL
N_u, 7/N_u, 28
D/t ratio of steel tube

(b)

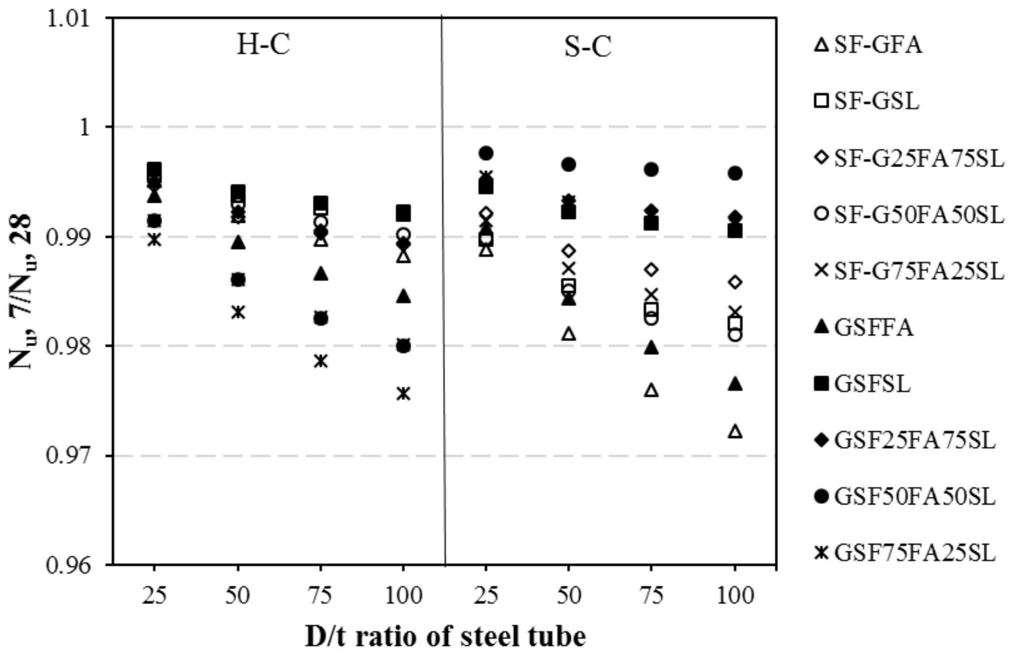

(c)

Figure 5.16 Effect of D/t ratio of steel tube on 7/28 day predicted capacity of the column with UHPGC by Eurocode 4 at steel yield strength of a) 150, b) 325 and c) 500 MPa

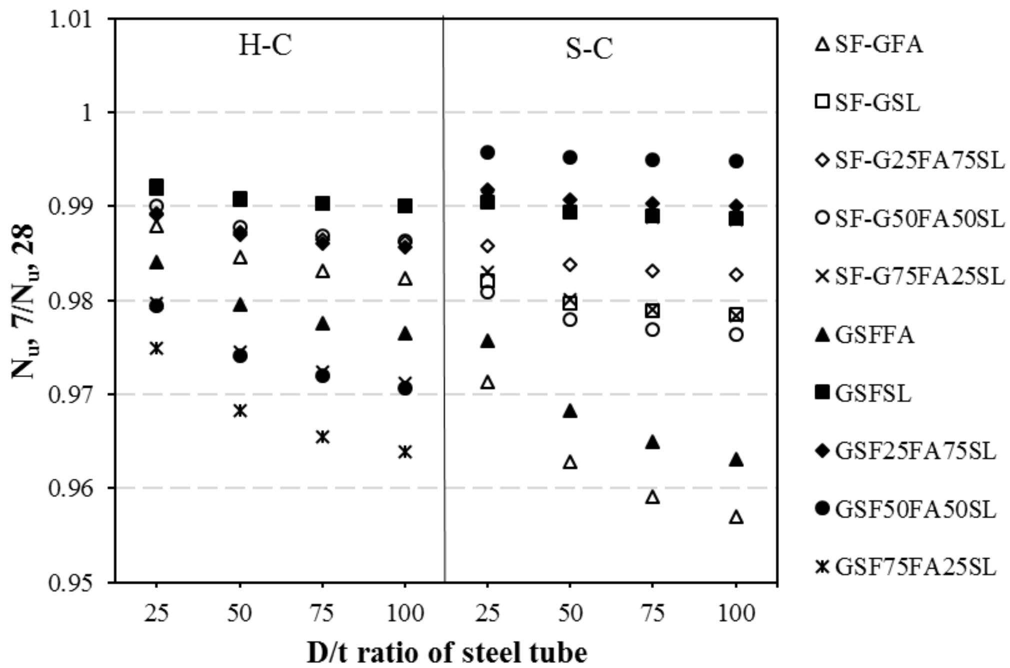

(a)

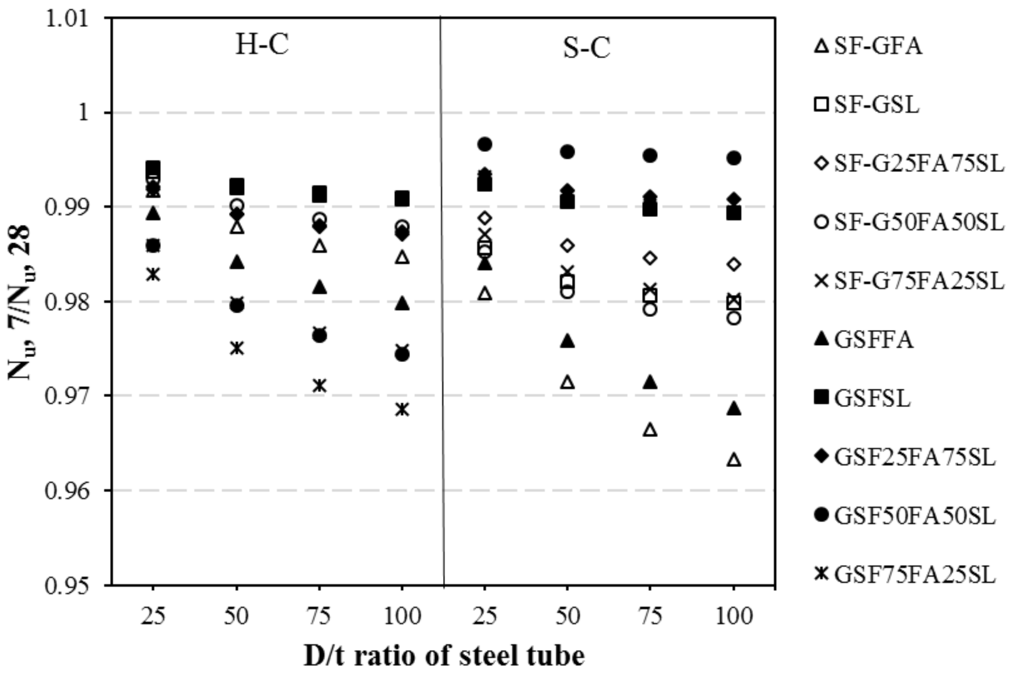

(b)

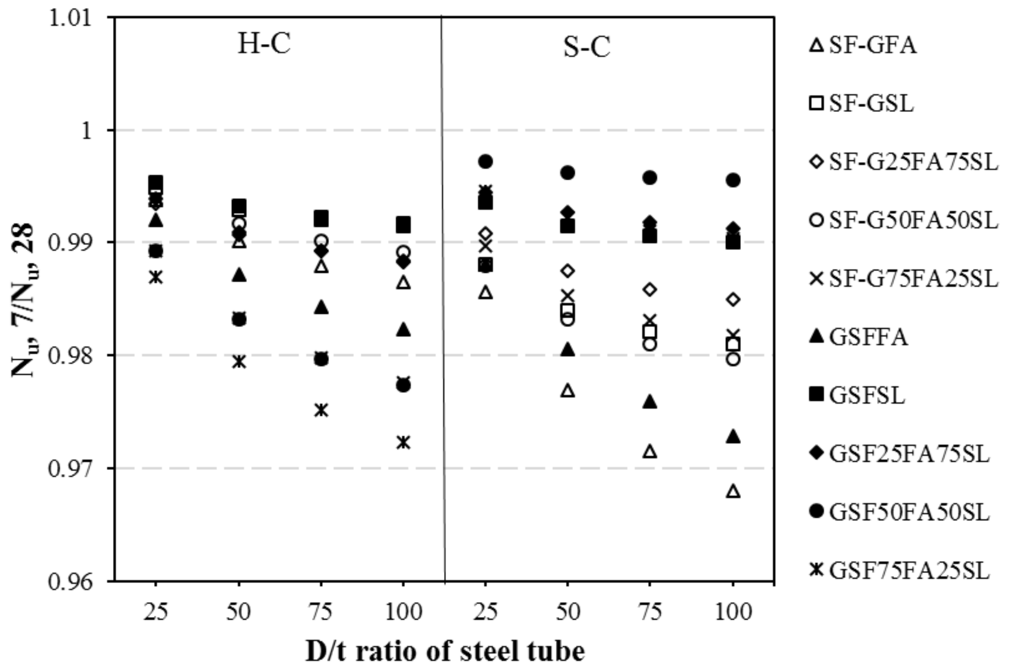

(c)

Figure 5.17 Effect of D/t ratio of steel tube on 7/28 day predicted capacity of the column with UHPGC by ACI 318 at steel yield strength of a) 150, b) 325 and c) 500 MPa

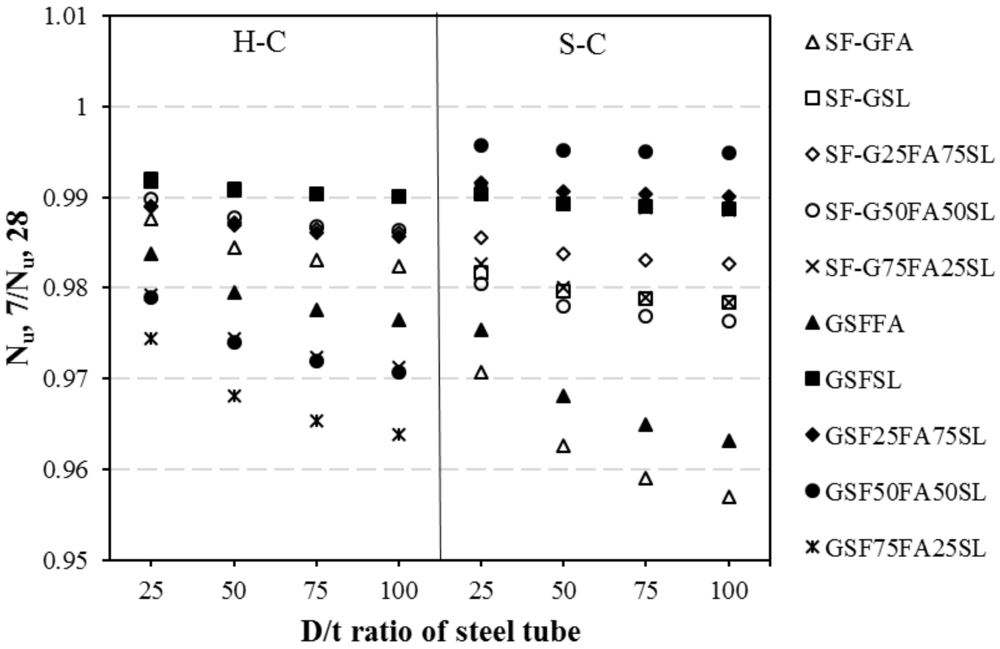
H-C
S-C
1.01
1
0.99
0.98
0.97
0.96
0.95
25
50
75
100
N_u, $7/N_u$, 28
D/t ratio of steel tube
SF-GFA
SF-GSL
SF-G25FA75SL
SF-G50FA50SL
SF-G75FA25SL
GSFFA
GSFSL
GSF25FA75SL
GSF50FA50SL
GSF75FA25SL

(a)

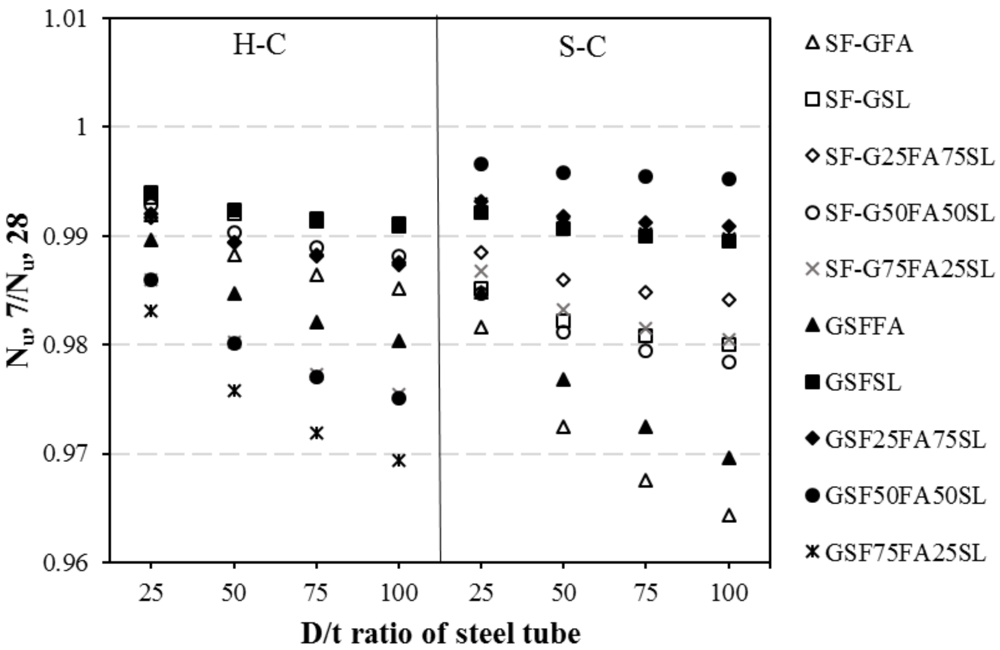
H-C
S-C
1.01
1
0.99
0.98
0.97
0.96
25
50
75
100
N_u, $7/N_u$, 28
D/t ratio of steel tube
SF-GFA
SF-GSL
SF-G25FA75SL
SF-G50FA50SL
SF-G75FA25SL
GSFFA
GSFSL
GSF25FA75SL
GSF50FA50SL
GSF75FA25SL

(b)

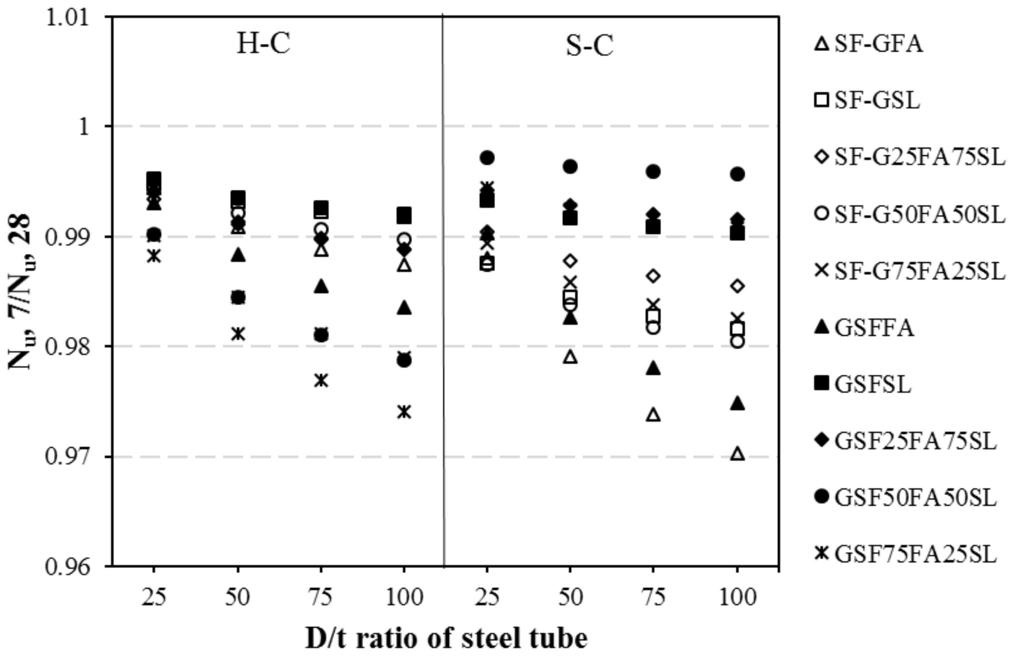

(c)

Figure 5.18 Effect of D/t ratio of steel tube on 90/28 day predicted capacity of the column with UHPGC by DL/T code at steel yield strength of a) 150, b) 325 and c) 500 MPa

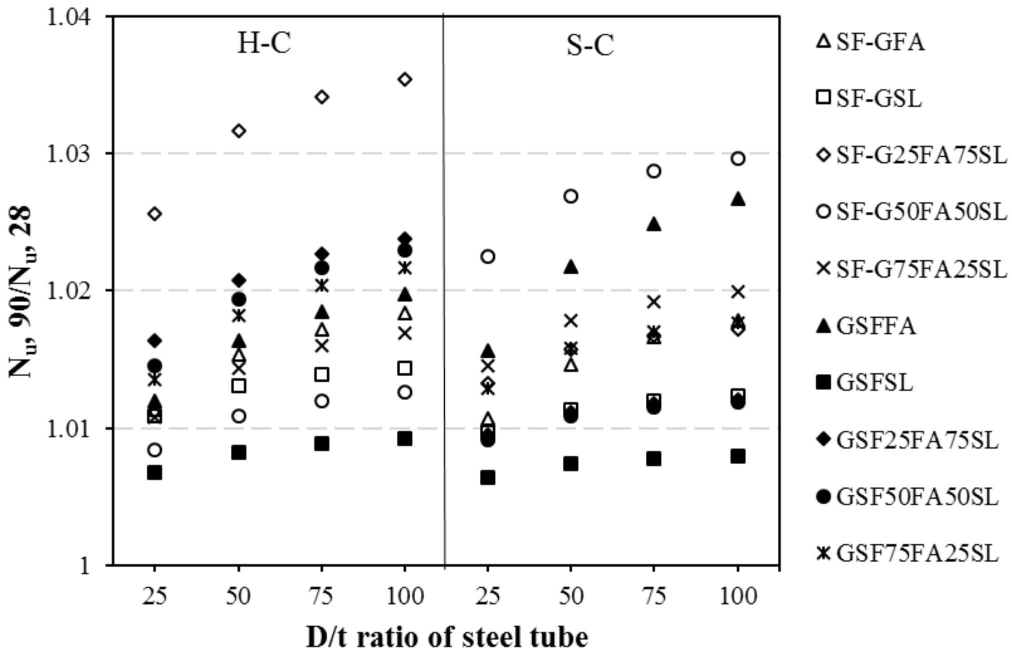

(a)

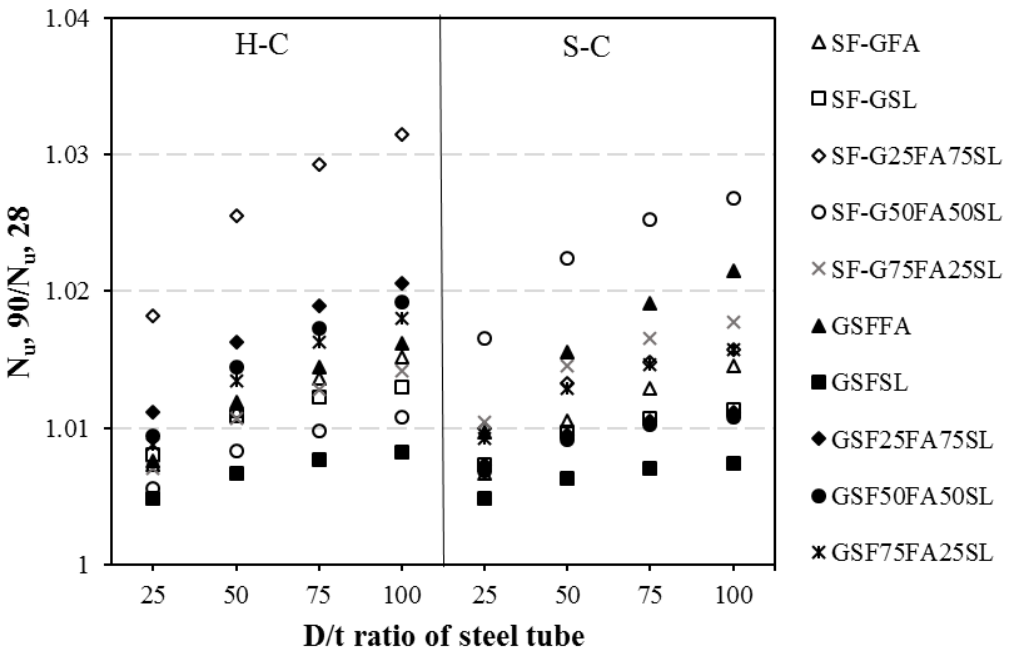

(b)

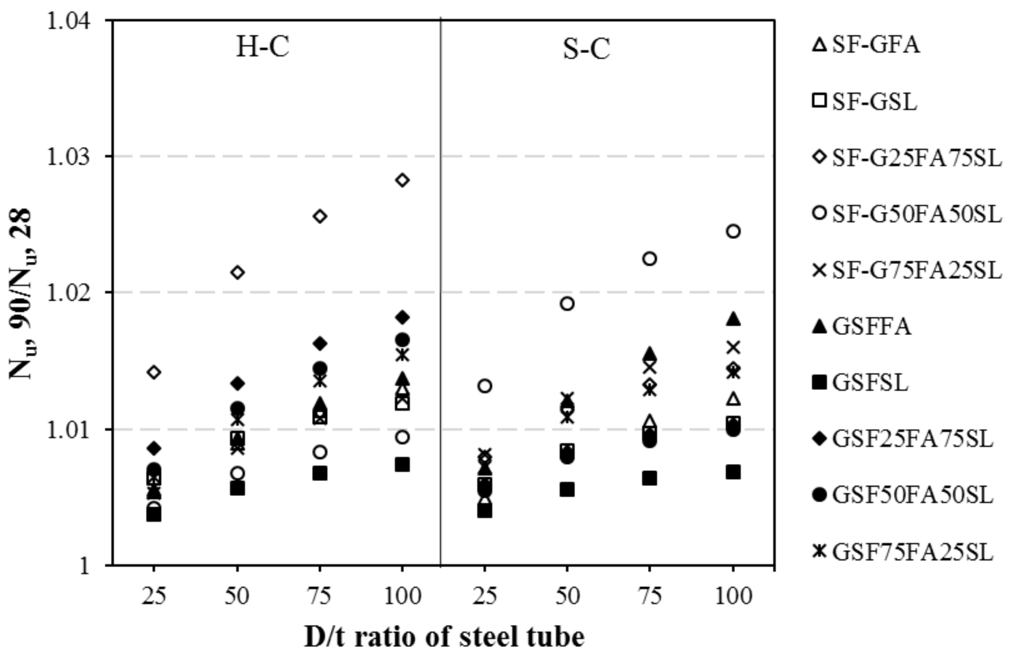

(c)

Figure 5.19 Effect of D/t ratio of steel tube on 90/28 day predicted capacity of the column with UHPGC by Eurocode 4 at steel yield strength of a) 150, b) 325 and c) 500 MPa

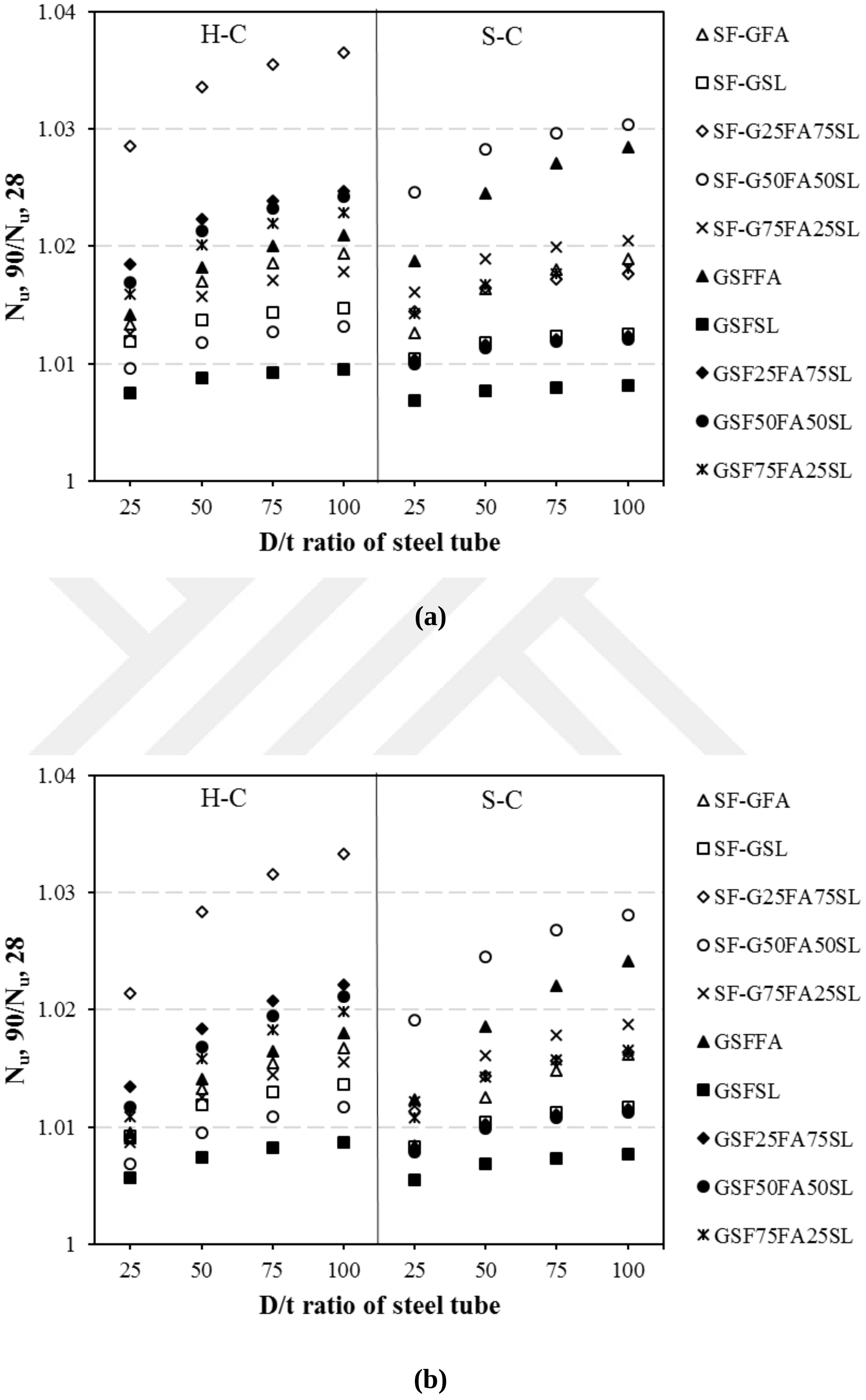
1.04
1.03
1.02
1.01
1
H-C
S-C
25
50
75
100
N_u, 90/N_u, 28
D/t ratio of steel tube
SF-GFA
SF-GSL
SF-G25FA75SL
SF-G50FA50SL
SF-G75FA25SL
GSFFA
GSFSL
GSF25FA75SL
GSF50FA50SL
GSF75FA25SL

(a)

(b)

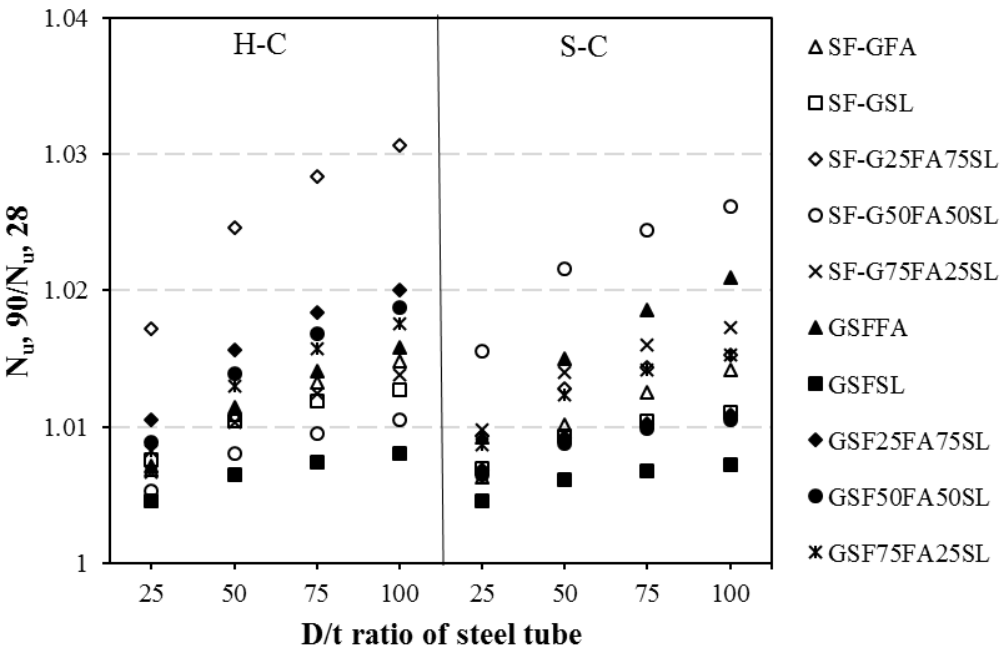

(c)

Figure 5.20 Effect of D/t ratio of steel tube on 90/28 day predicted capacity of the column with UHPGC by ACI 318 at steel yield strength of a) 150, b) 325 and c) 500 MPa

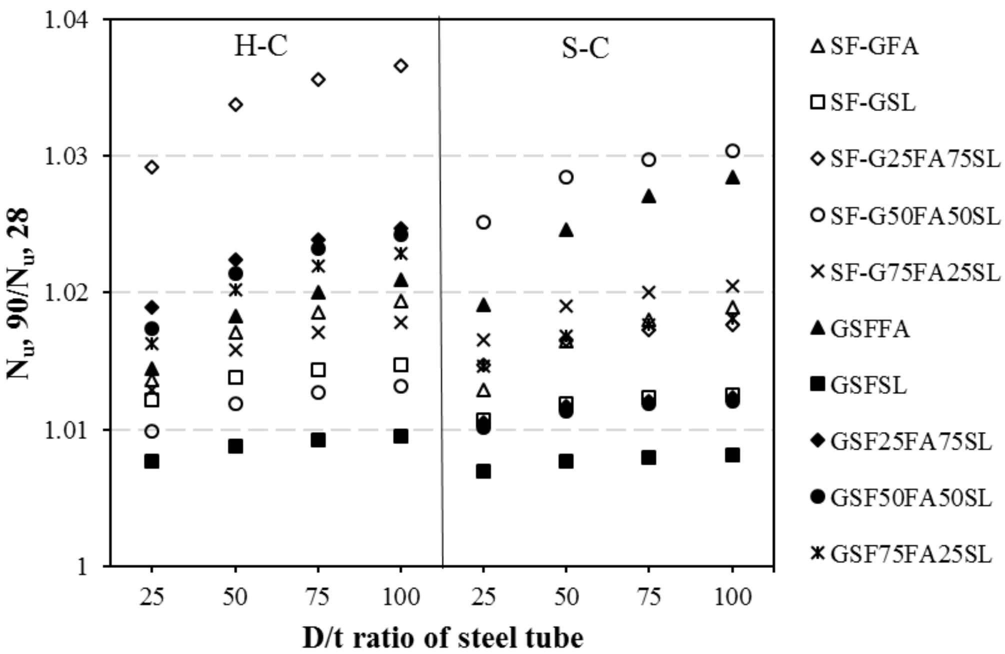

(a)

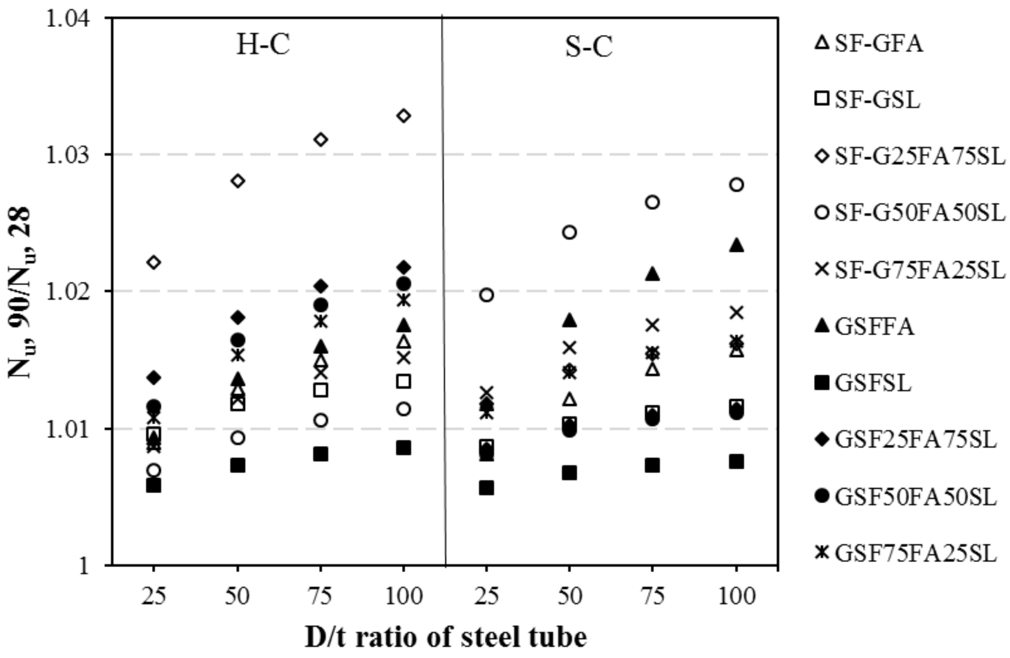

(b)

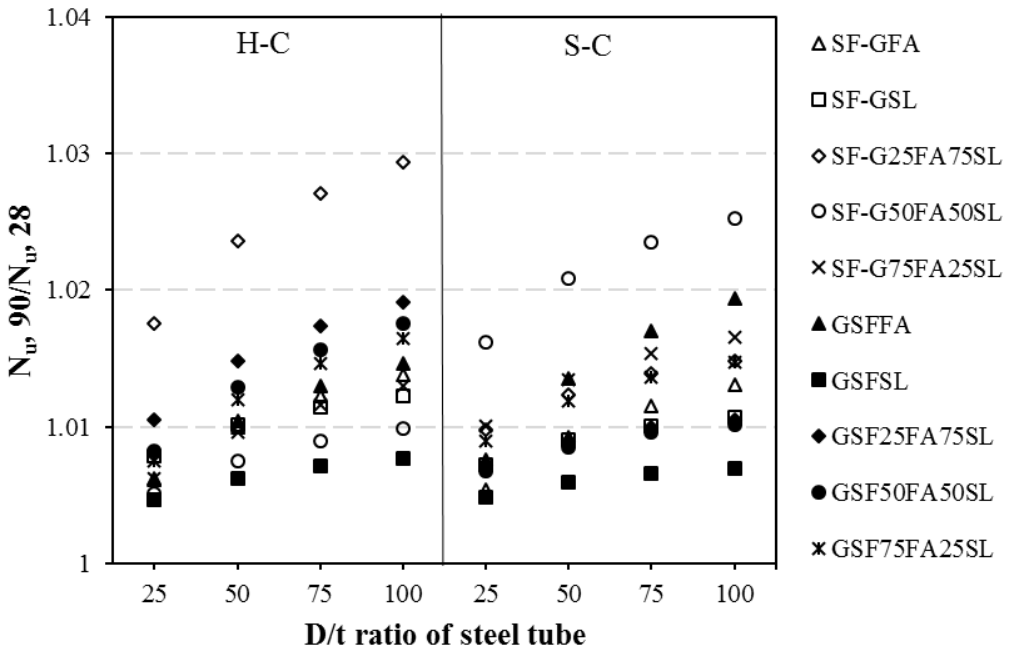

(c)

Figure 5.21 Effect of D/t ratio of steel tube on 90/28 day predicted capacity of the column with UHPGC by DL/T code at steel yield strength of a) 150, b) 325 and c) 500 MPa

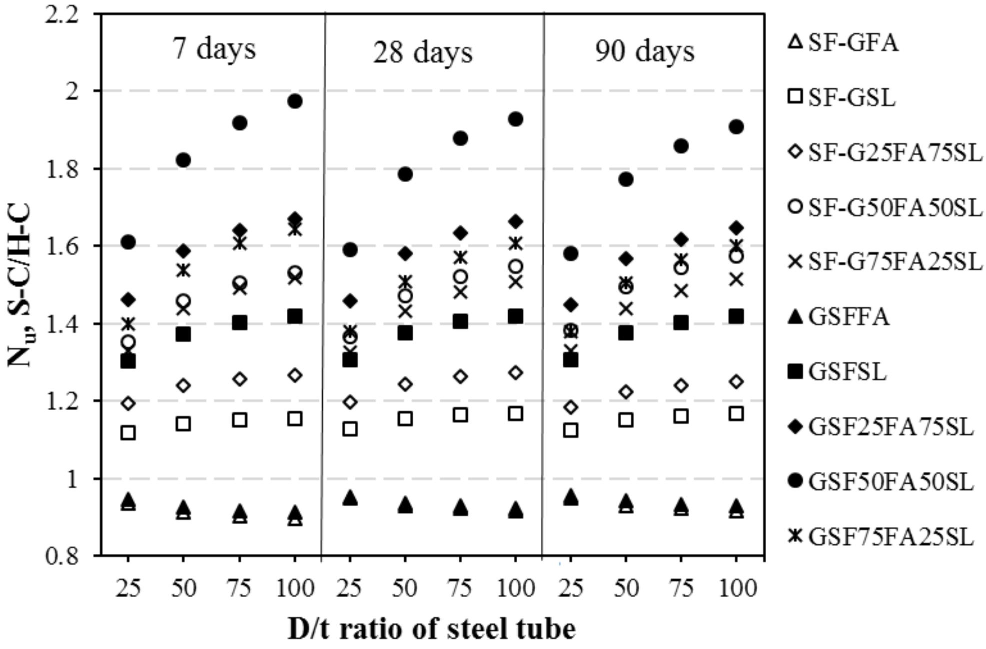
7 days
28 days
90 days
Nu, S-C/H-C
D/t ratio of steel tube
SF-GFA
SF-GSL
SF-G25FA75SL
SF-G50FA50SL
SF-G75FA25SL
GSFFA
GSFSL
GSF25FA75SL
GSF50FA50SL
GSF75FA25SL

(a)

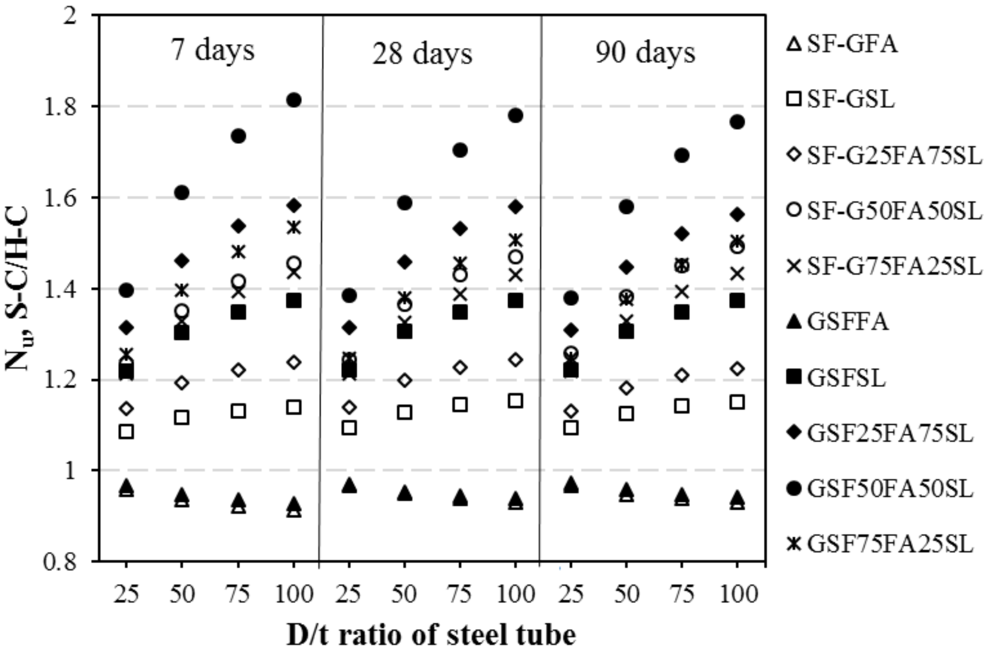
7 days
28 days
90 days
Nu, S-C/H-C
D/t ratio of steel tube
SF-GFA
SF-GSL
SF-G25FA75SL
SF-G50FA50SL
SF-G75FA25SL
GSFFA
GSFSL
GSF25FA75SL
GSF50FA50SL
GSF75FA25SL

(b)

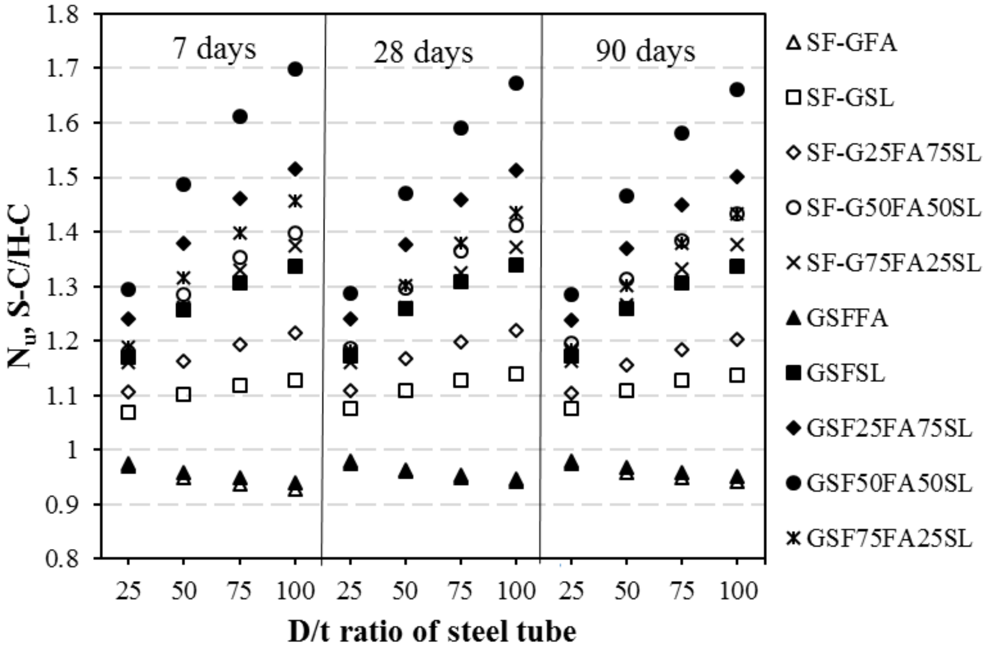

(c)

Figure 5.22 Effect of curing regime on the capacity of the column with UHPGC according to Eurocode 4 at steel yield strength of a) 150, b) 325 and c) 500 MPa

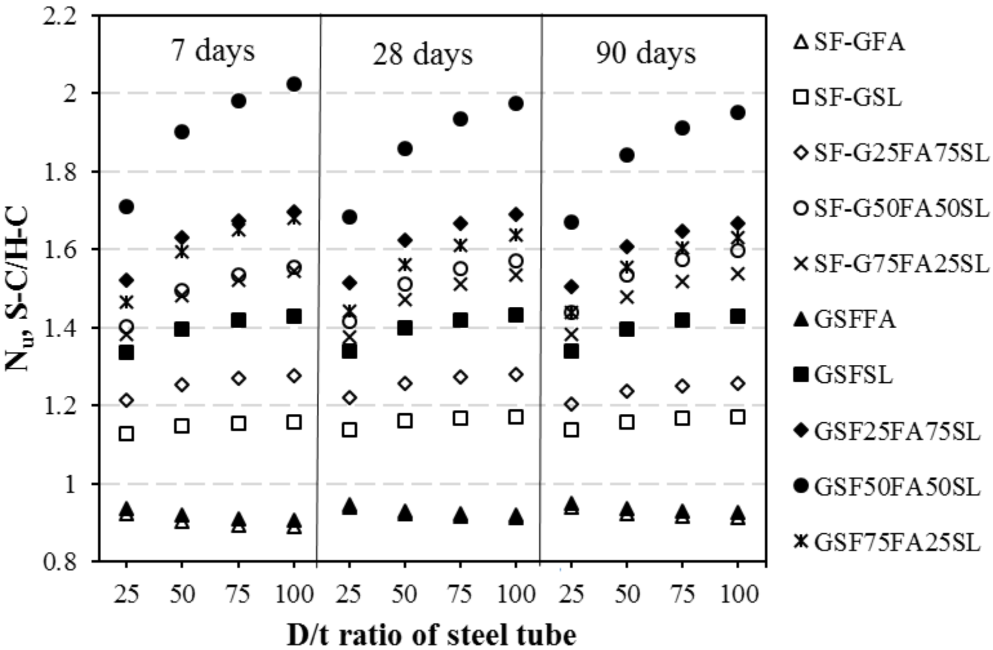

(a)

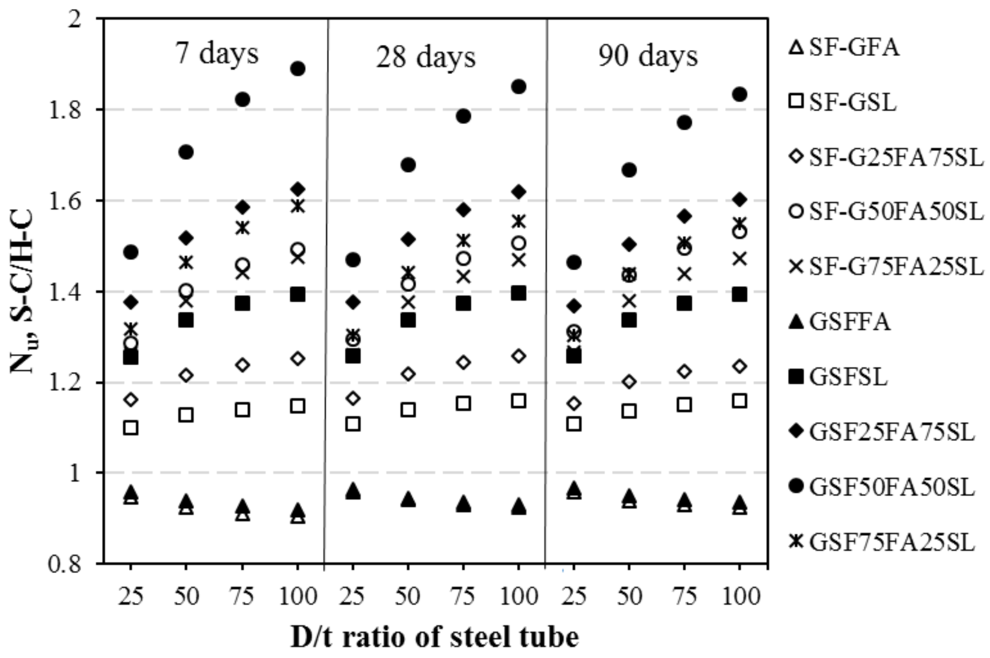

(b)

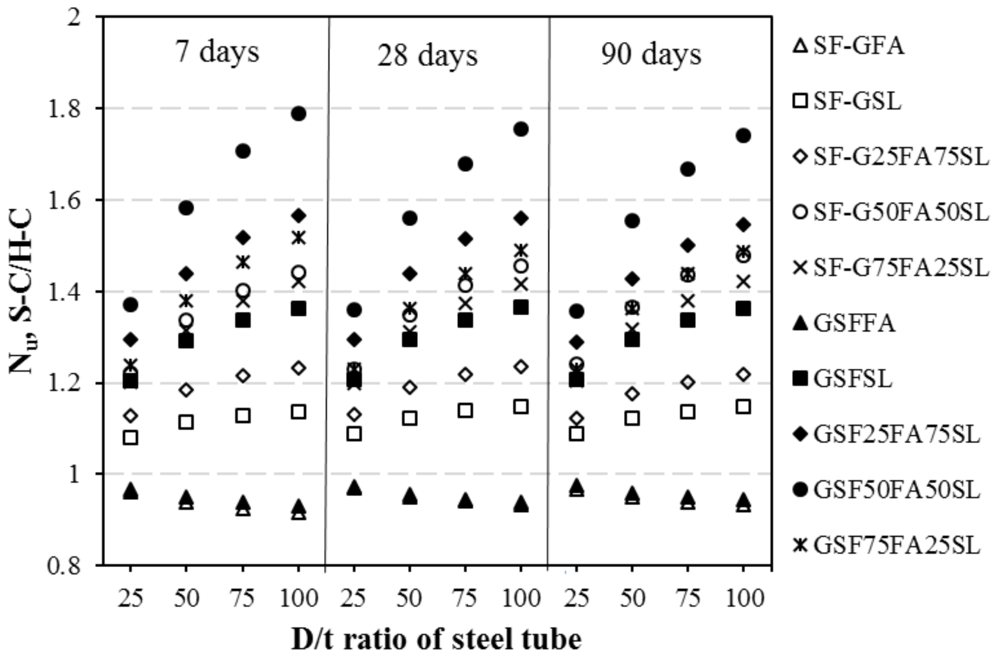

(c)

Figure 5.23 Effect of curing regime on the capacity of the column with UHPGC according to ACI 318 at steel yield strength of a) 150, b) 325 and c) 500 MPa

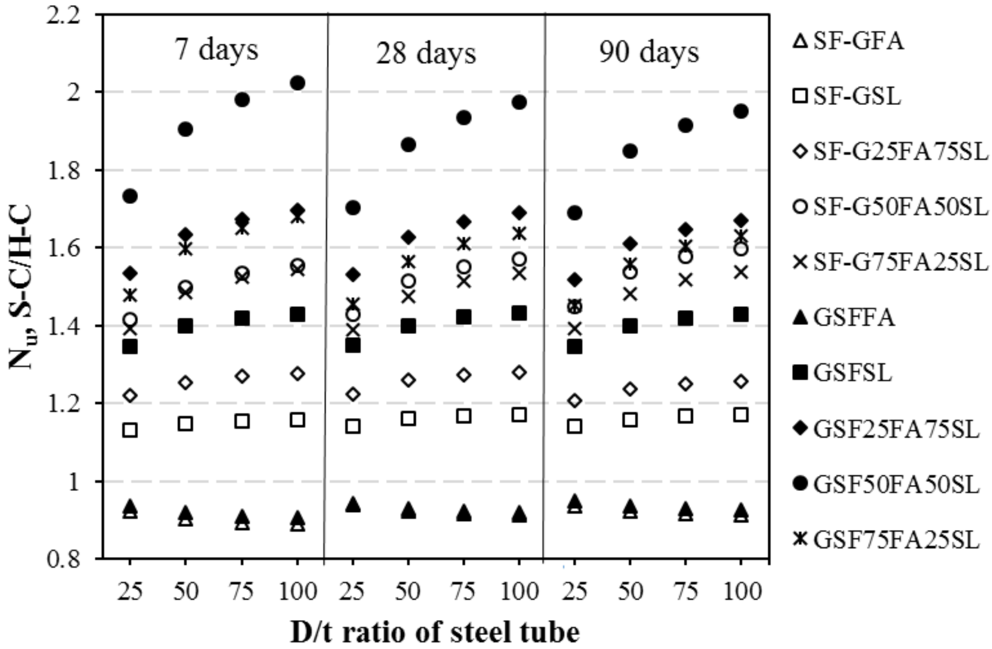
7 days
28 days
90 days
N_u, S-C/H-C
D/t ratio of steel tube
SF-GFA
SF-GSL
SF-G25FA75SL
SF-G50FA50SL
SF-G75FA25SL
GSFFA
GSFSL
GSF25FA75SL
GSF50FA50SL
GSF75FA25SL

(a)

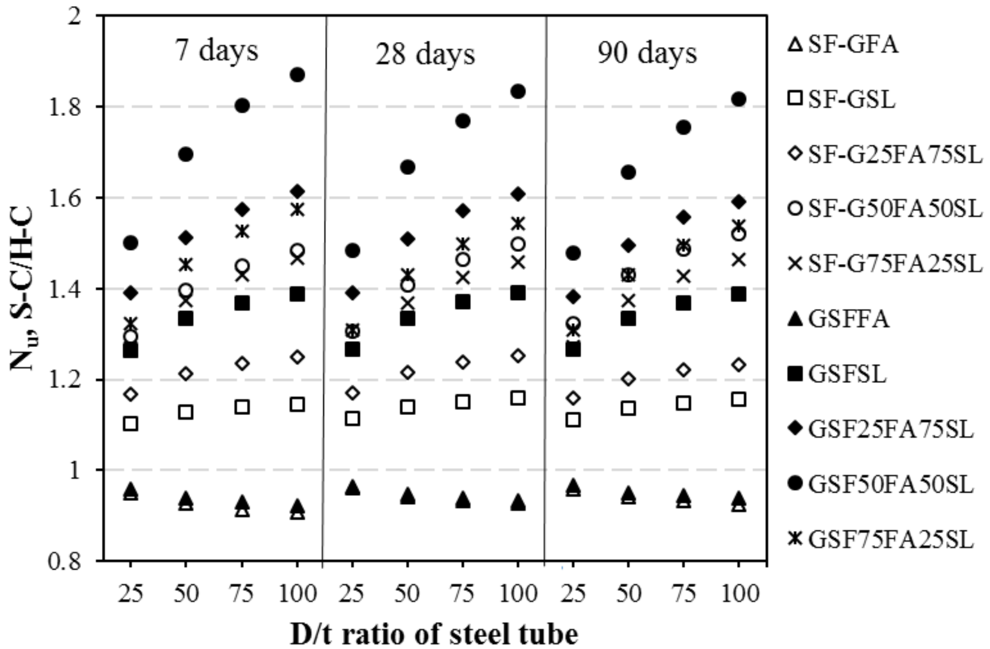
7 days
28 days
90 days
N_u, S-C/H-C
D/t ratio of steel tube
SF-GFA
SF-GSL
SF-G25FA75SL
SF-G50FA50SL
SF-G75FA25SL
GSFFA
GSFSL
GSF25FA75SL
GSF50FA50SL
GSF75FA25SL

(b)

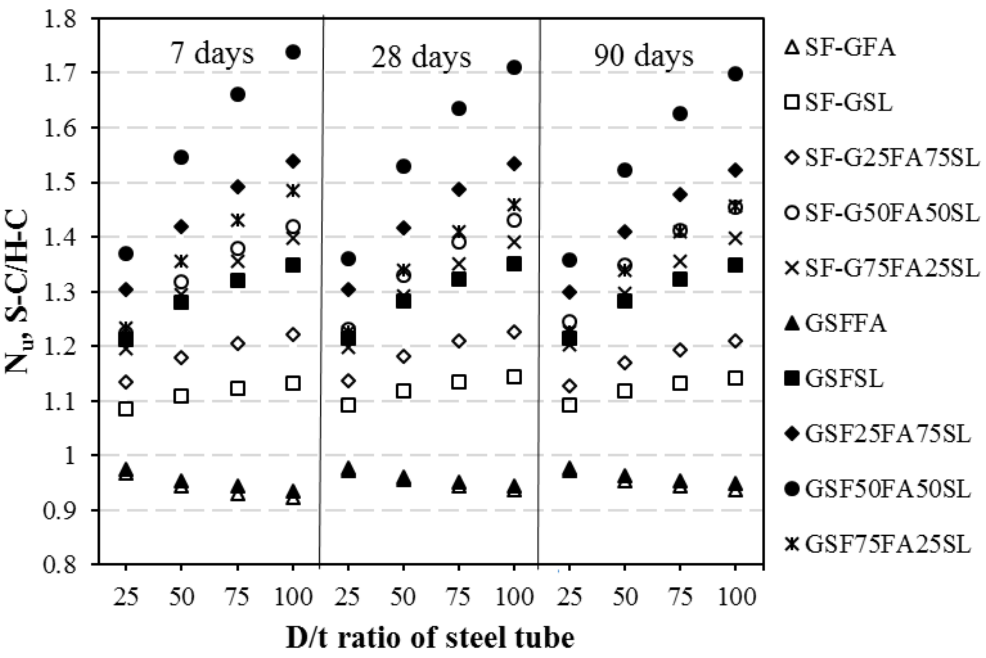

(c)

Figure 5.24 Effect of curing regime on the capacity of the column with UHPGC according to DL/T code at steel yield strength of a) 150, b) 325 and c) 500 MPa

5.4 Comparison of the performance of the design codes

A comparative study of predictions data was conducted to recognize the behavior of the ultimate axial strength of circular CFST columns by applying ACI-318R (2005), Eurocode 4 (2004) and Chinese code DL/T (1999) provisions. Three comparison were performed to attain the objective of this section as follows:

1. The relations of $N_{u, EC4}$/ $N_{u, ACI}$ and $N_{u, EC4}$/ $N_{u, DL/T}$ vs. the compressive strength at 7, 28 and 90 days for UHPC and UHPGC are shown in Figures 5.25 (a-c), 5.26 (a-c), 5.27 (a-c) and 5.28 (a-c), respectively.
2. The ratios of $N_{u, EC4}$/ $N_{u, ACI}$ and $N_{u, EC4}$/ $N_{u, DL/T}$ vs. the total number of specimens at 7, 28 and 90 days for UHPC and UHPGC are shown in Figures 5.29 (a-c), 5.30 (a-c), 5.31 (a-c) and 5.32 (a-c), respectively.
3. Regression analysis of $N_{u, EC4}$ versus $N_{u, ACI}$ and $N_{u, EC4}$ versus $N_{u, DL/T}$ for UHPC and UHPG at 7, 28 and 90 days are shown in Figures 5.33 (a-c), 5.34 (a-c), 5.35 (a-c) and 5.36 (a-c), respectively.

From section 1, it can be seen that for UHPC the $N_{u, EC4}$/ $N_{u, ACI}$ ratio decreased with increasing the compressive strength at all ages, for example when the D/t= 25 and f_y=

150 MPa, the ratio ranged between (1.2 to 1.3) at 7 days. The same trend was observed in $N_{u, EC4}/ N_{u, DL/T}$ ratio, which is ranged between (0.99 to 1.1) for the same above conditions. The same behavior were observed in UHPGC, for example when the D/t= 25 and f_y= 150 MPa, the ratio ranged between (1.2 to 1.3) and (0.99 to 1.1) at 7 days for $N_{u, EC4}/ N_{u, ACI}$ and $N_{u, EC4}/ N_{u, DL/T}$ ratios, respectively. It can be also observed that the $N_{u, EC4}/ N_{u, DL/T}$ ratio are closer to 1 than the $N_{u, EC4}/ N_{u, ACI}$ ratio.

From section 2, it can be seen that the $N_{u, EC4}/ N_{u, ACI}$ ratio for UHPC at 7 days ranged between (1.19 to 1.34) and between (1.19 to 1.31) for water and steam curing, respectively. The corresponding range at 28 days were (1.19 to 1.31) and (1.19 to 1.3) and at 90 days were (1.12 to 1.3) and (1.186 to 1.29) water and steam curing, respectively. The ratio of $N_{u, EC4}/ N_{u, ACI}$ for UHPGC at 7 days were (1.2 to 1.37) and (1.2 to 1.4) and at 28 days the ratio were (1.2 to 1.37) and (1.2 to 1.38) and at 90 days were (1.2 to 1.36) and (1.2 to 1.4) for heat and steam curing, respectively. It can be revealed that the axial capacity of UHPC and UHPG filled CFST columns prediction from Eurocode 4 (2004) are generally higher than the predicted values obtained from ACI-318R (2005). This is principally owing to the fact that the composite action between the steel tube and the concrete core was not deemed in ACI-318R (2005) (Lu and Zhao 2010).

The $N_{u, EC4}/ N_{u, DL/T}$ ratio for UHPC at 7 days ranged between (1.019 to 1.147) and between (0.996 to 1.12) for water and steam curing, respectively. The corresponding range at 28 days were (0.995 to 1.12) and (0.993 to 1.11) and at 90 days were (0.994 to 1.11) and (0.991 to 1.11) water and steam curing, respectively. The ratio of $N_{u, EC4}/ N_{u, DL/T}$ for UHPGC at 7 days were (1.02 to 1.17) and (0.999 to 1.17) and at 28 days the ratio were (1.02 to 1.16) and (0.999 to 1.17) and at 90 days were (1.02 to 1.16) and (0.998 to 1.17) for heat and steam curing, respectively. From these results it can be seen that the Eurocode 4 (2004) and Chinese code DL/T (1999) are closer each other than the ACI-318R (2005).

Regarding to section 3 described previously, it can be seen that there were considerably high relationship between the predicted values of ACI-318R (2005) and Eurocode 4 (2004) and between Chinese code DL/T (1999) and Eurocode 4 (2004). The regression analysis provided correlation coefficient (R^2) of 0.999 for all codes and ages. Within the predicted axial capacity results by using the different provisions of this study, all models appeared to be well close to each other and provided higher prediction in terms of the regression analysis.

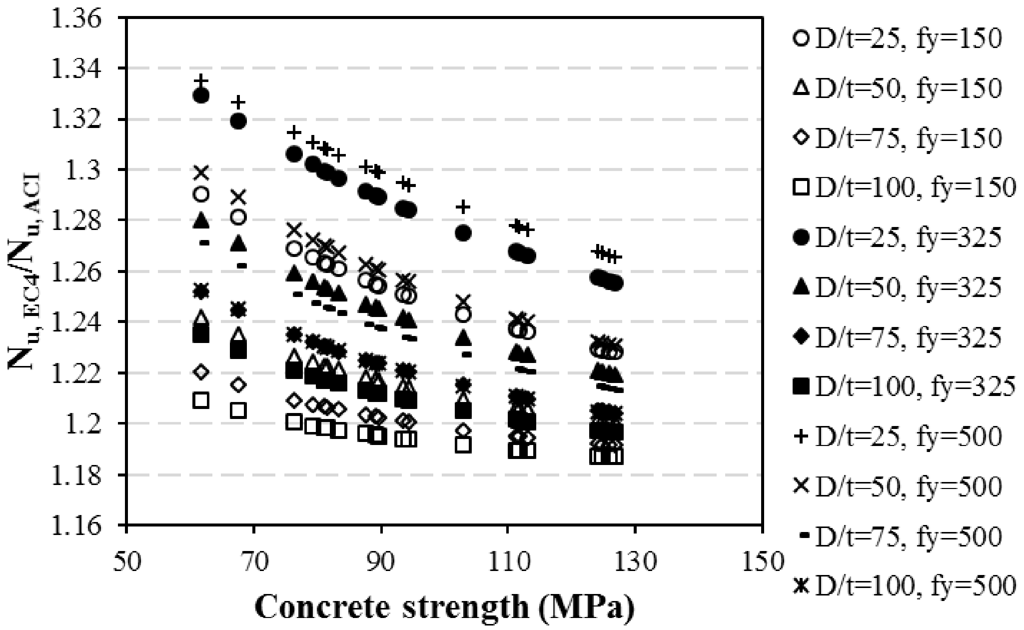

(a)

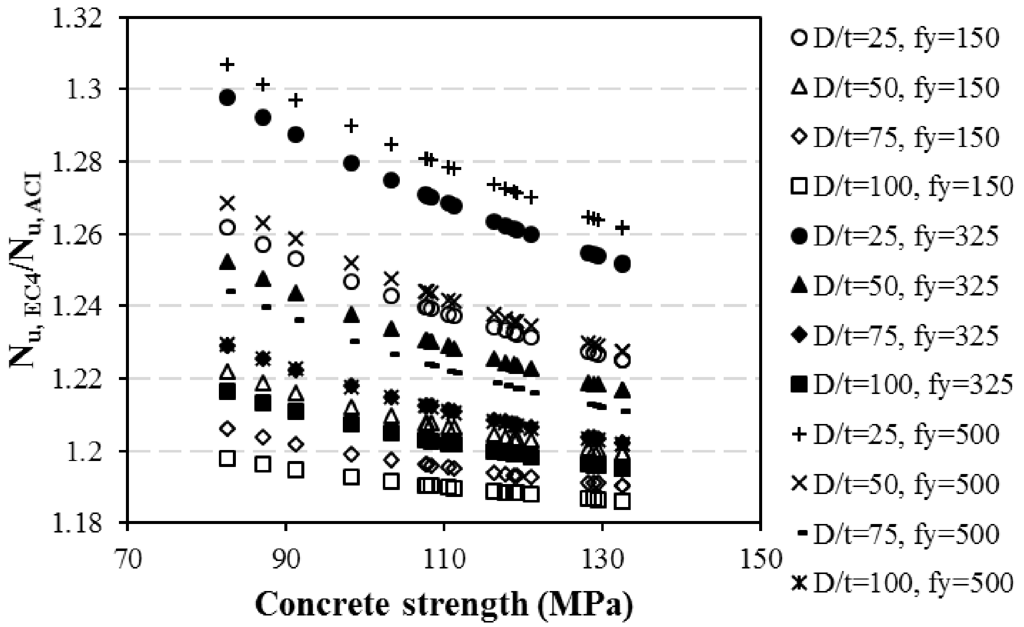

(b)

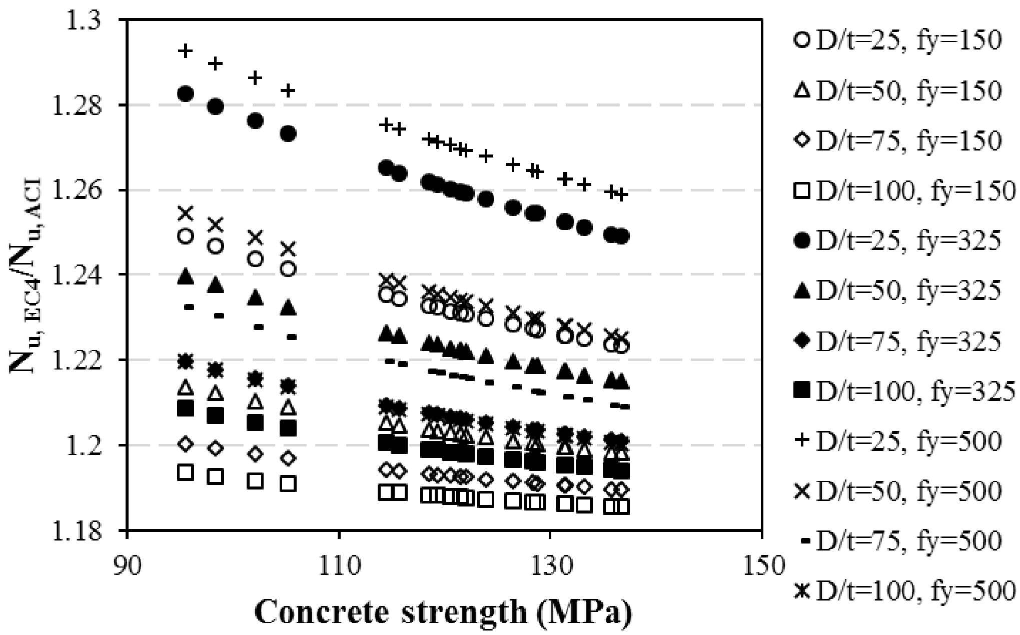

(c)

Figure 5.25 Relation between EC4/ACI 318 vs. concrete strength of the column with UHPC at a) 7, b) 28 and c) 90 days

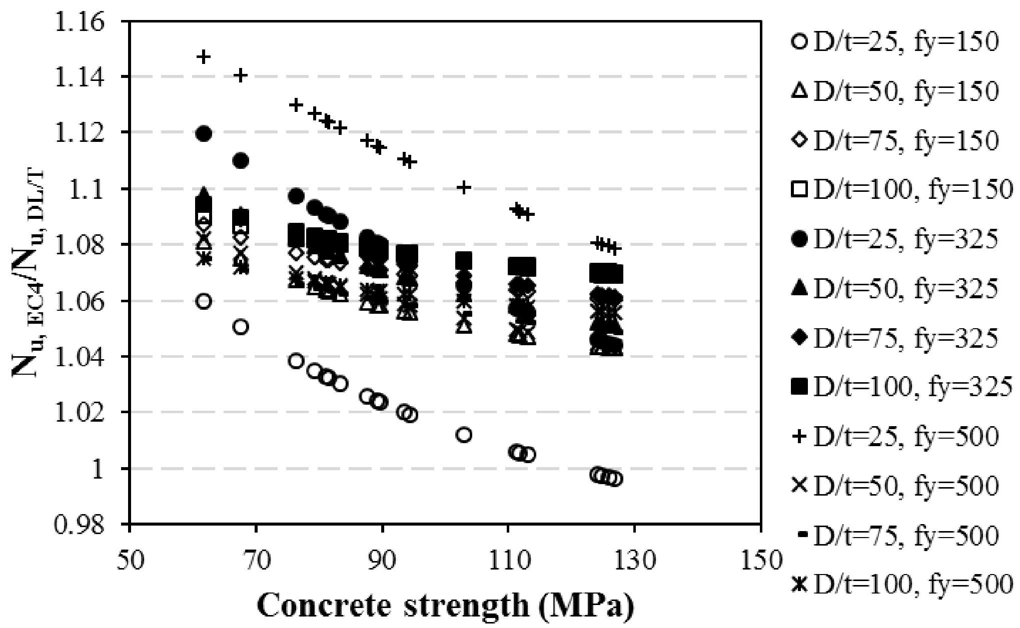

(a)

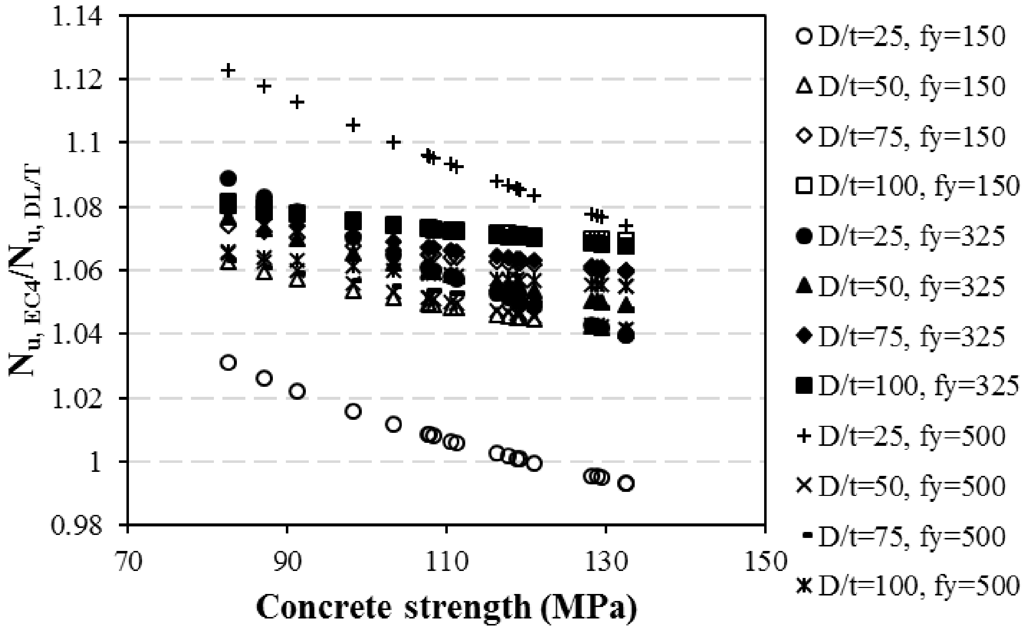

(b)

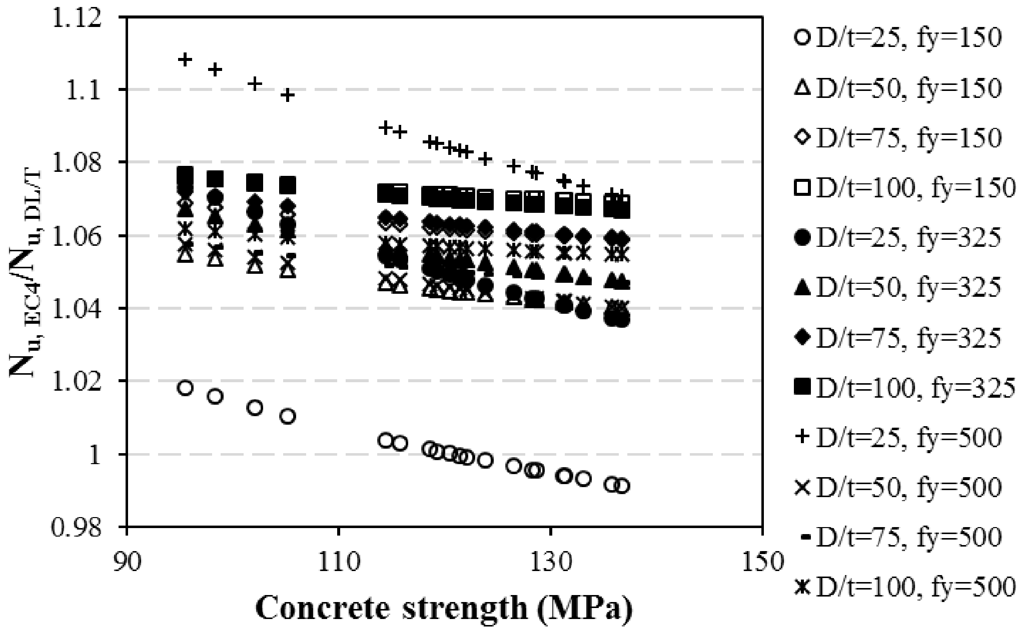

(c)

Figure 5.26 Relation between EC4/(DL/T) vs. concrete strength of the column with UHPC at a) 7, b) 28 and c) 90 days

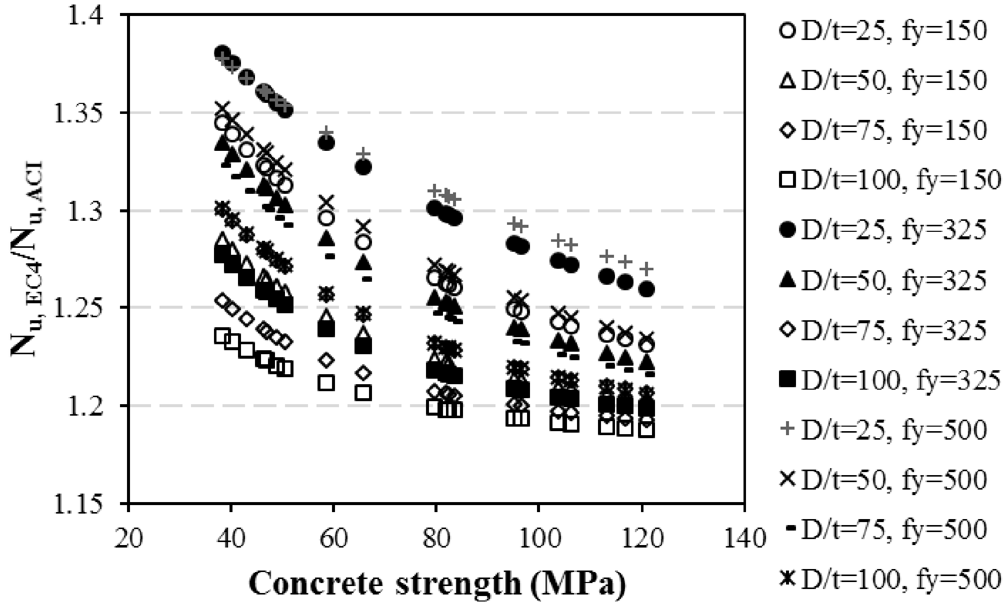

1.4
1.35
1.3
1.25
1.2
1.15
$N_{u, EC4}/N_{u, ACI}$
20
40
60
80
100
120
140
Concrete strength (MPa)
D/t=25, fy=150
D/t=50, fy=150
D/t=75, fy=150
D/t=100, fy=150
D/t=25, fy=325
D/t=50, fy=325
D/t=75, fy=325
D/t=100, fy=325
D/t=25, fy=500
D/t=50, fy=500
D/t=75, fy=500
D/t=100, fy=500

(a)

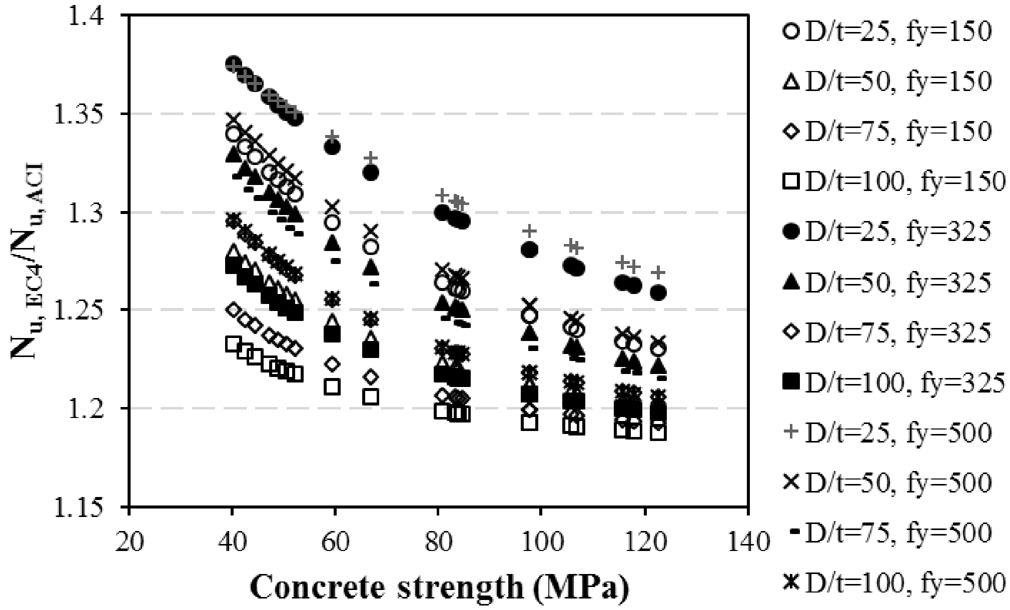

1.4
1.35
1.3
1.25
1.2
1.15
$N_{u, EC4}/N_{u, ACI}$
20
40
60
80
100
120
140
Concrete strength (MPa)
D/t=25, fy=150
D/t=50, fy=150
D/t=75, fy=150
D/t=100, fy=150
D/t=25, fy=325
D/t=50, fy=325
D/t=75, fy=325
D/t=100, fy=325
D/t=25, fy=500
D/t=50, fy=500
D/t=75, fy=500
D/t=100, fy=500

(b)

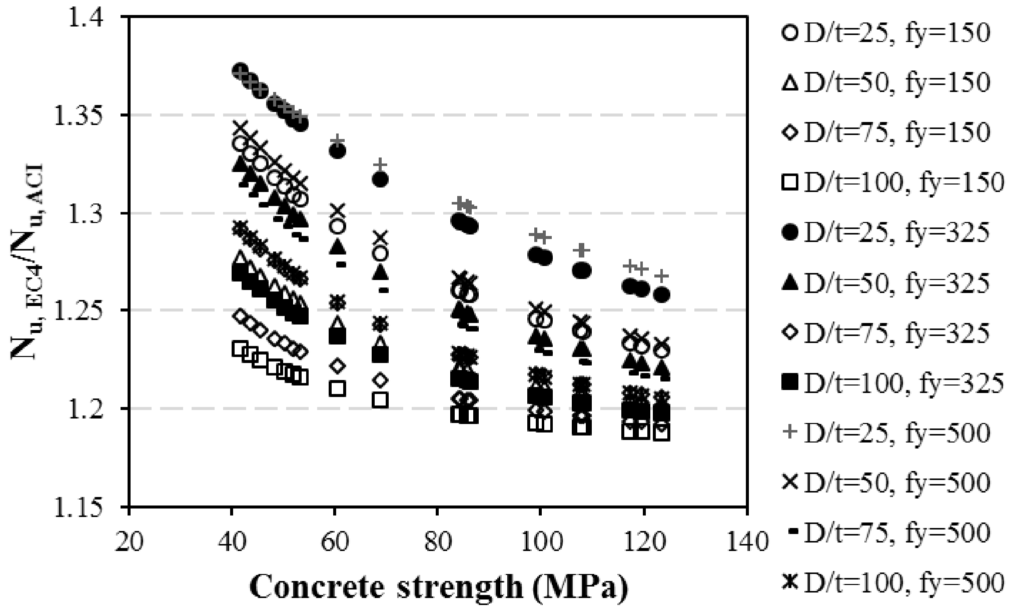

(c)

Figure 5.27 Relation between EC4/ACI 318 vs. concrete strength of the column with UHPGC at a) 7, b) 28 and c) 90 days

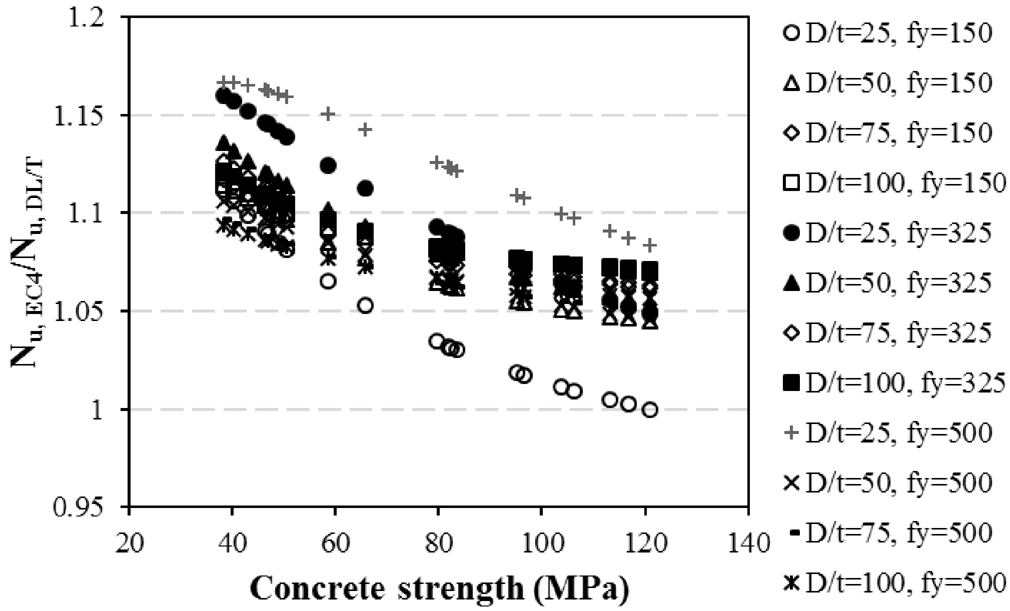

(a)

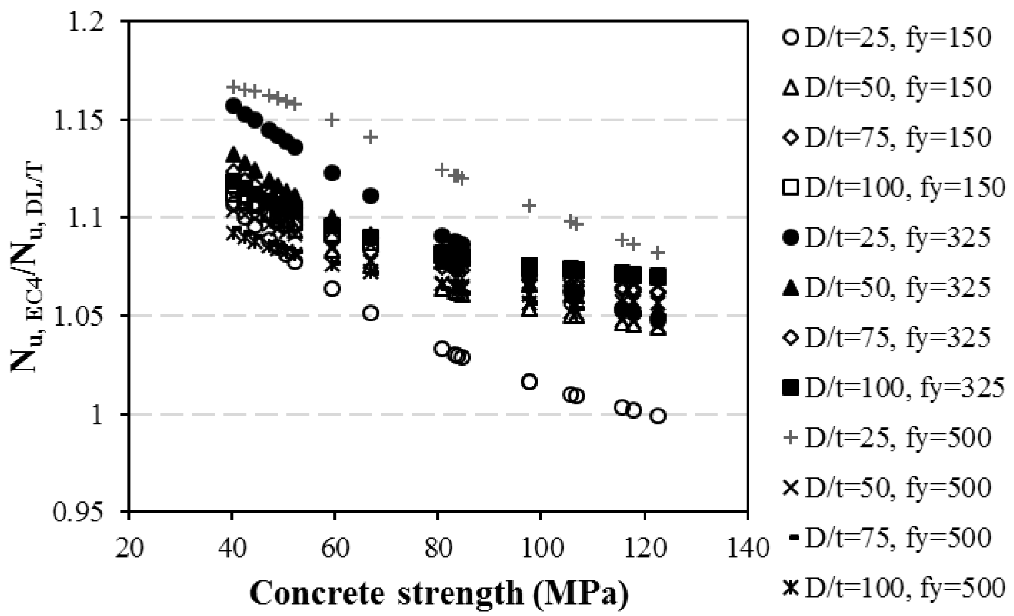

(b)

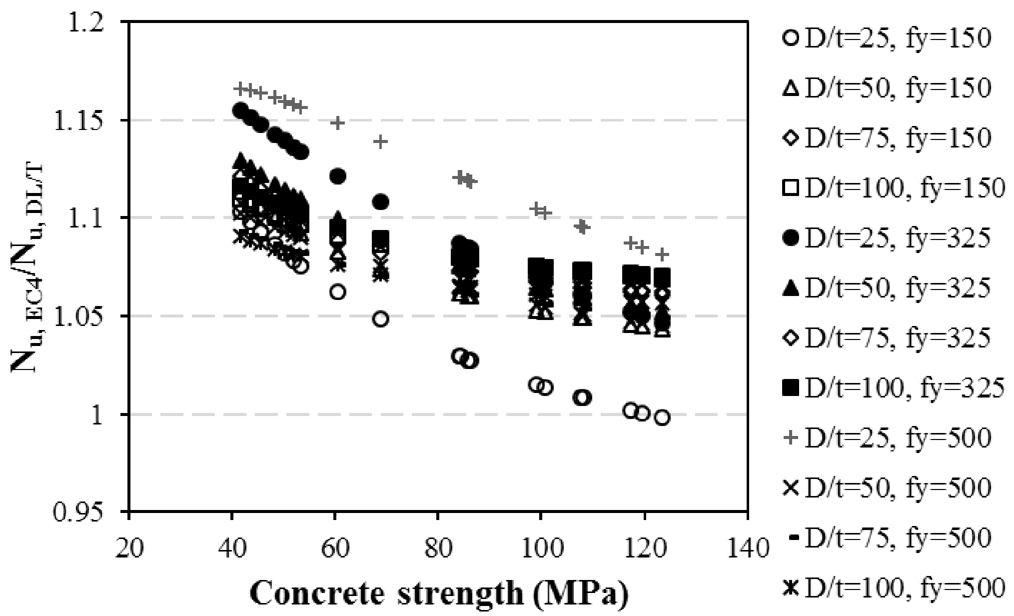

(c)

Figure 5.28 Relation between EC4/(DL/T) vs. concrete strength of the column with UHPGC at a) 7, b) 28 and c) 90 days

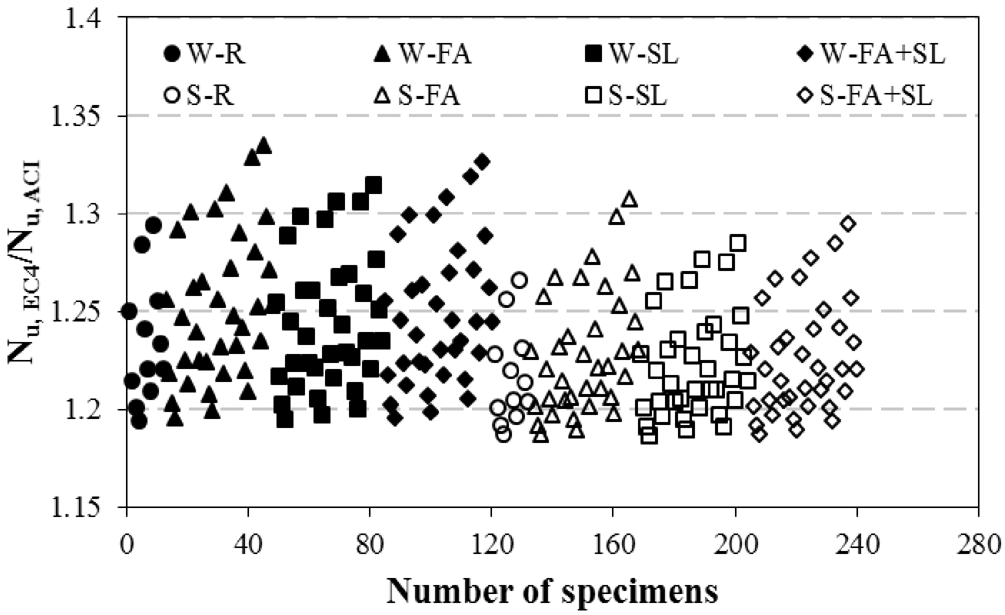

1.4
1.35
1.3
1.25
1.2
1.15
0
40
80
120
160
200
240
280
W-R
W-FA
W-SL
W-FA+SL
S-R
S-FA
S-SL
S-FA+SL
$N_{u,EC4}/N_{u,ACI}$
Number of specimens

(a)

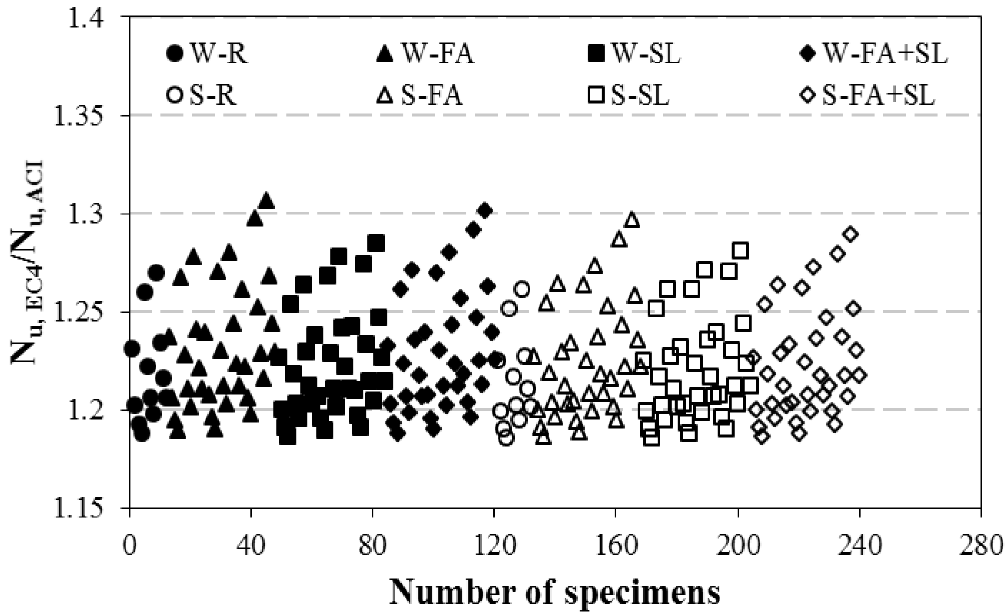

1.4
1.35
1.3
1.25
1.2
1.15
0
40
80
120
160
200
240
280
W-R
W-FA
W-SL
W-FA+SL
S-R
S-FA
S-SL
S-FA+SL
$N_{u,EC4}/N_{u,ACI}$
Number of specimens

(b)

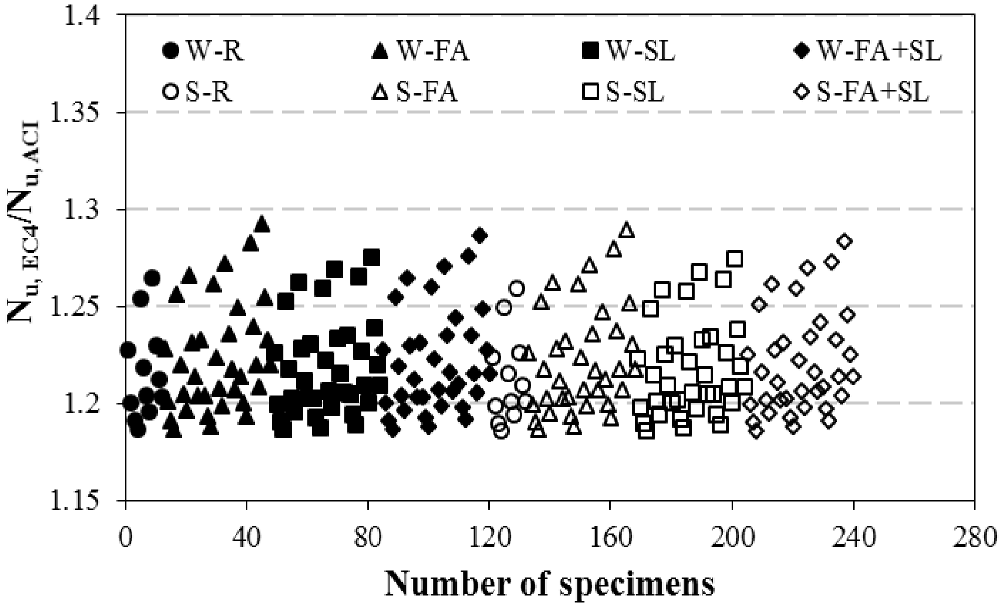

(c)

Figure 5.29 Ratio of predicted axial capacity results of UHPC by using the Eurocode 4 and ACI 318 at a) 7, b) 28 and c) 90 days

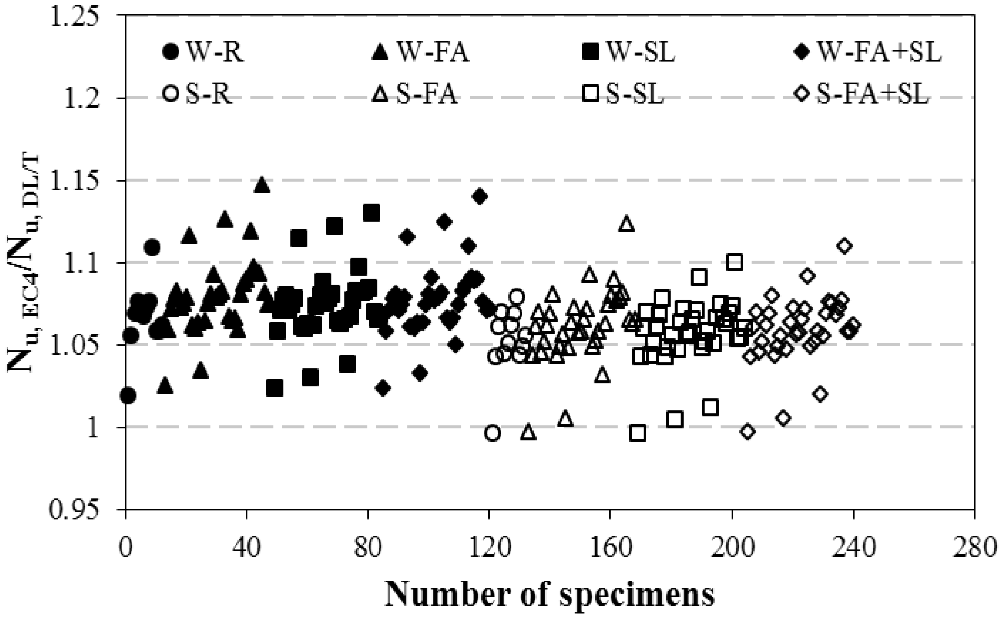

(a)

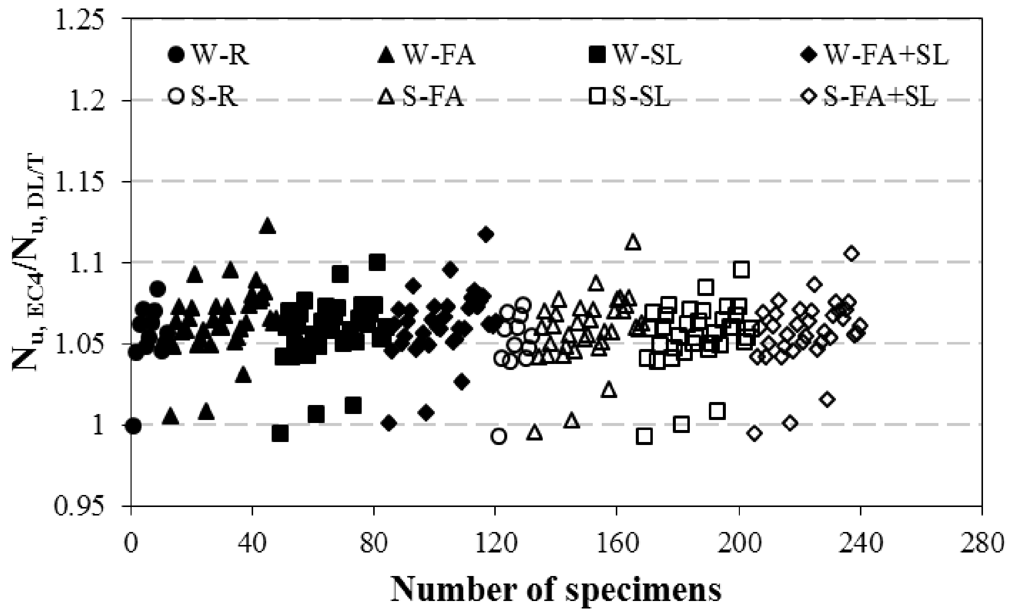

(b)

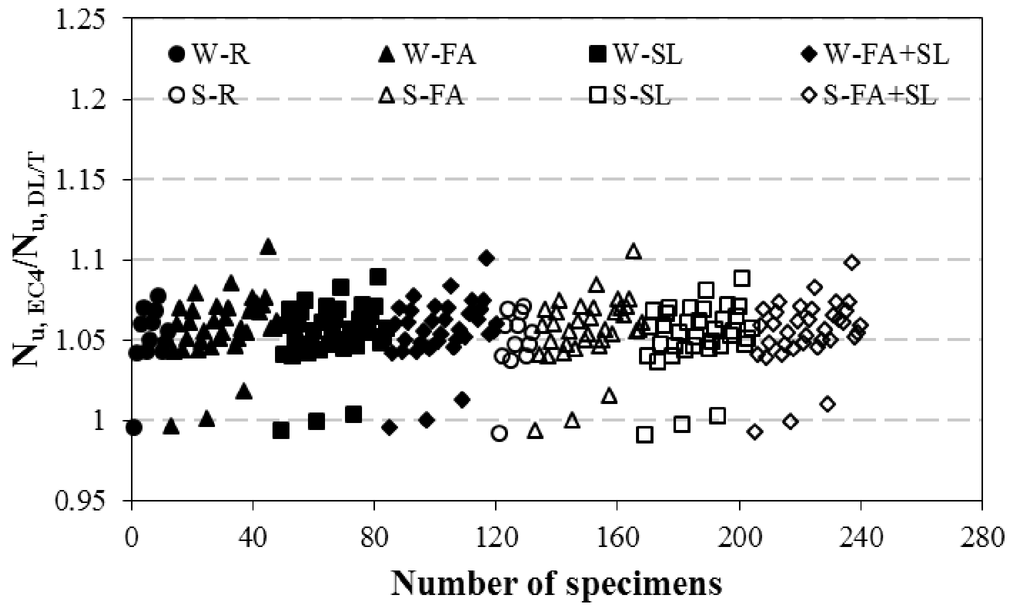

(c)

Figure 5.30 Ratio of predicted axial capacity results of UHPC by using the Eurocode 4 and DL/T code at a) 7, b) 28 and c) 90 days

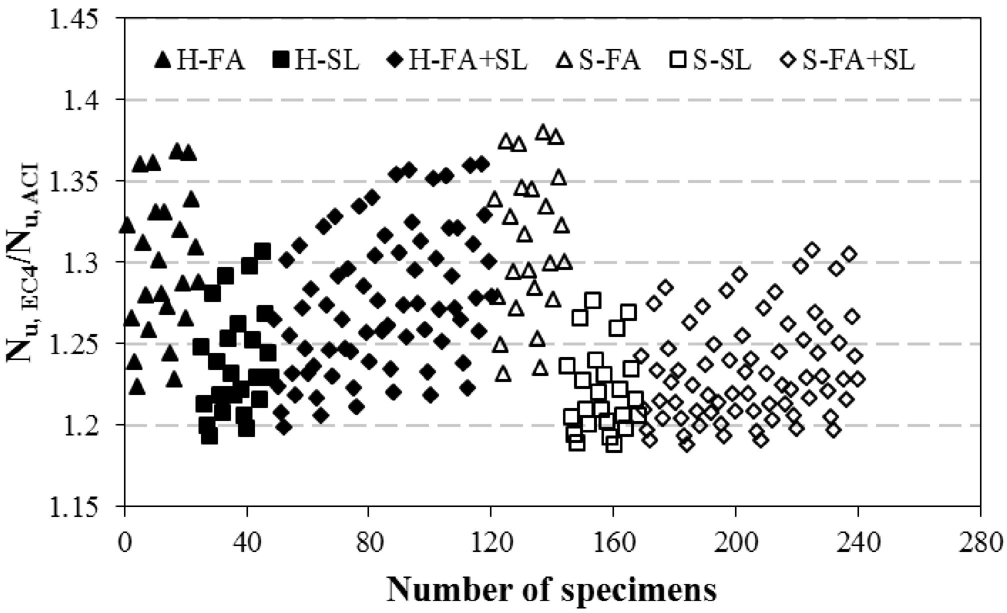
H-FA
H-SL
H-FA+SL
S-FA
S-SL
S-FA+SL
N u, EC4/N u, ACI
Number of specimens

(a)

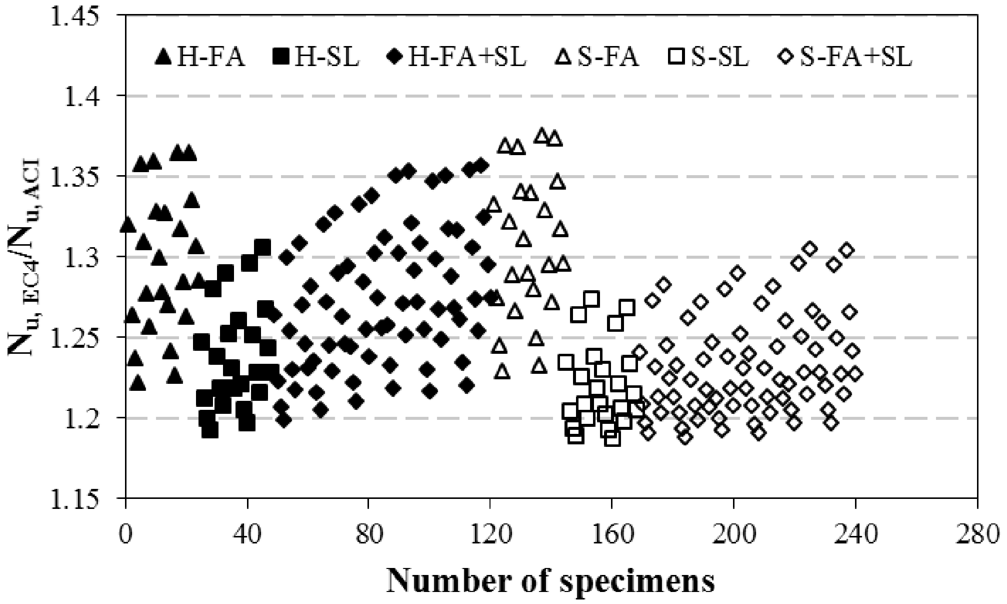
H-FA
H-SL
H-FA+SL
S-FA
S-SL
S-FA+SL
N u, EC4/N u, ACI
Number of specimens

(b)

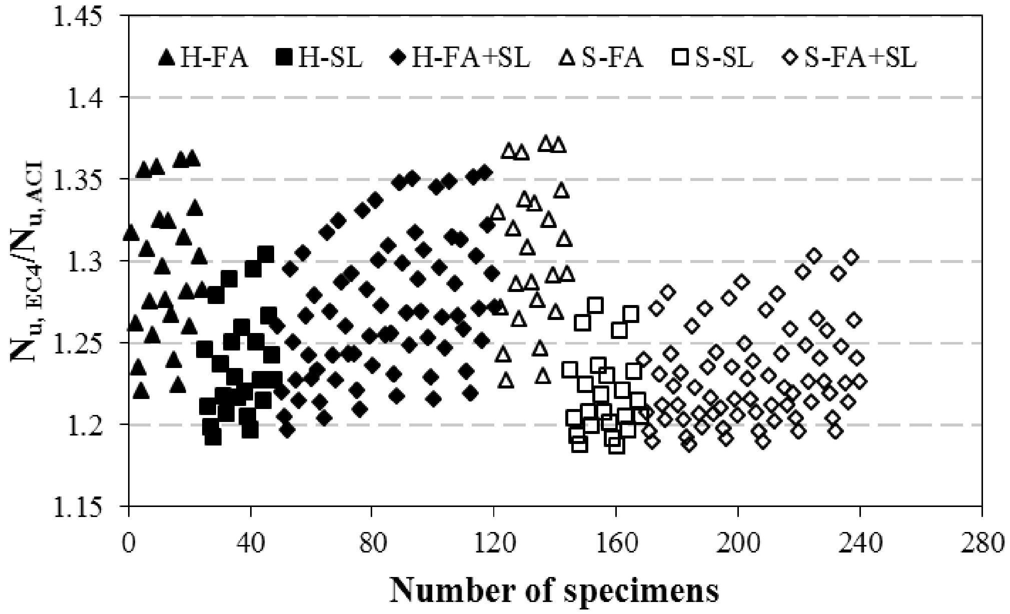

(c)

Figure 5.31 Ratio of predicted axial capacity results of UHPGC filled steel tubular columns by using the Eurocode 4 and ACI 318 at a) 7, b) 28 and c) 90 days

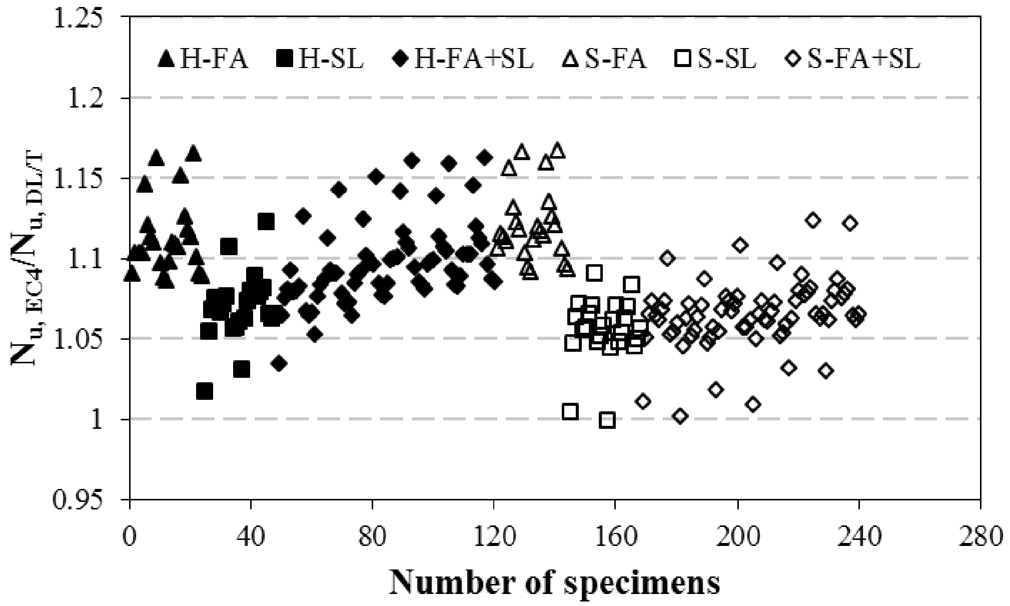

(a)

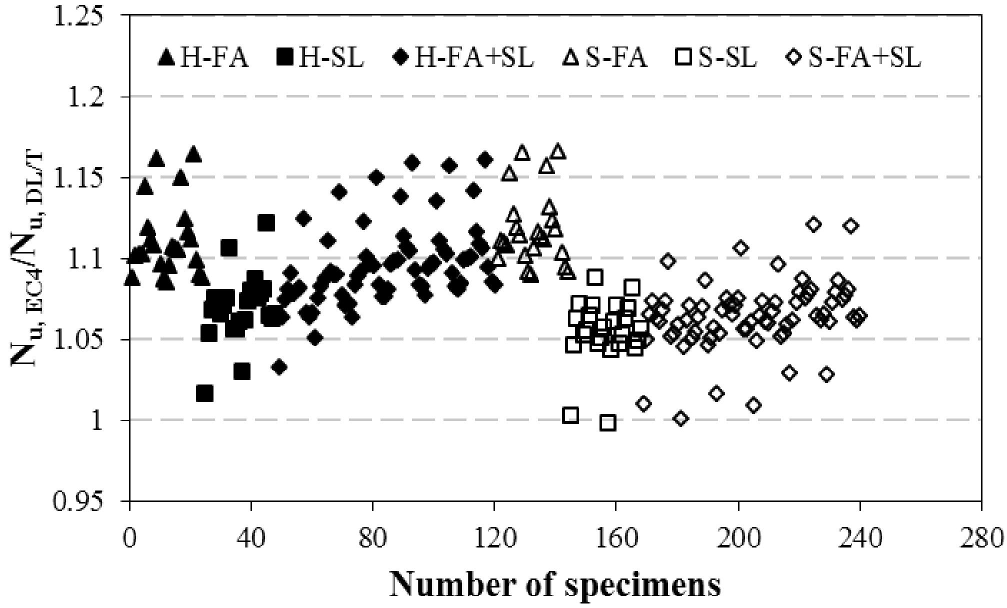

(b)

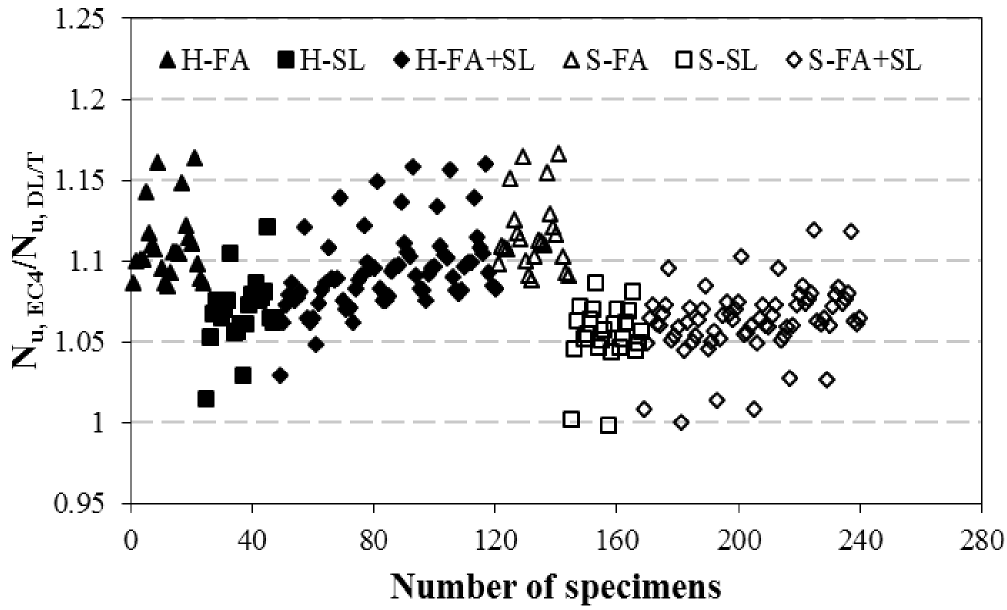

(c)

Figure 5.32 Ratio of predicted axial capacity results of UHPGC filled steel tubular columns by using the Eurocode 4 and DL/T code at a) 7, b) 28 and c) 90 days

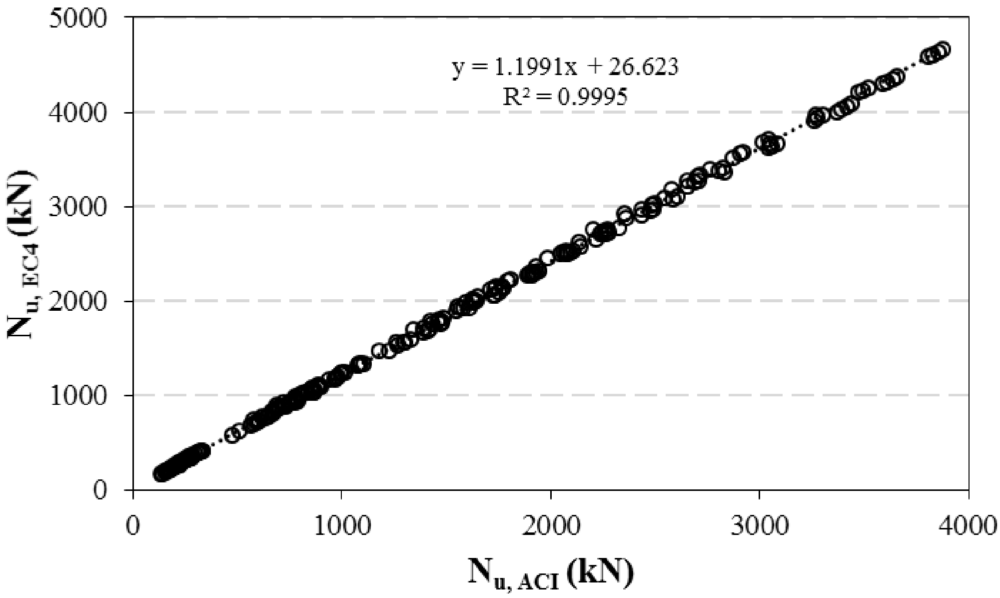
y = 1.1991x + 26.623
R² = 0.9995
5000
4000
3000
2000
1000
0
0
1000
2000
3000
4000
Nu, EC4 (kN)
Nu, ACI (kN)

(a)

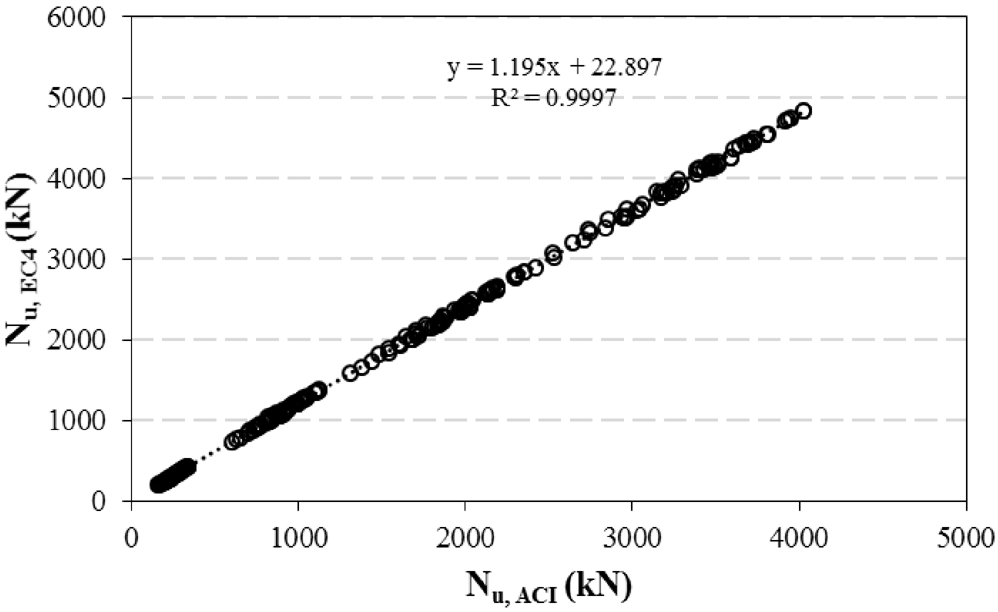
y = 1.195x + 22.897
R² = 0.9997
6000
5000
4000
3000
2000
1000
0
0
1000
2000
3000
4000
5000
Nu, EC4 (kN)
Nu, ACI (kN)

(b)

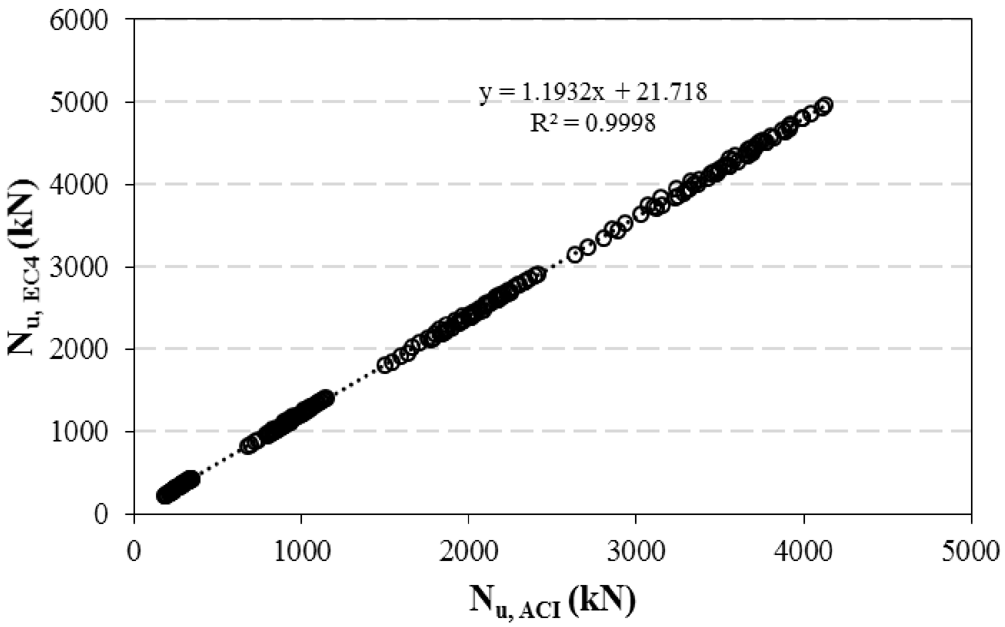

(c)

Figure 5.33 Regression model of predicted axial capacities of UHPC filled steel tubular columns between Eurocode 4 and ACI 318 code at a) 7, b) 28 and c) 90 days

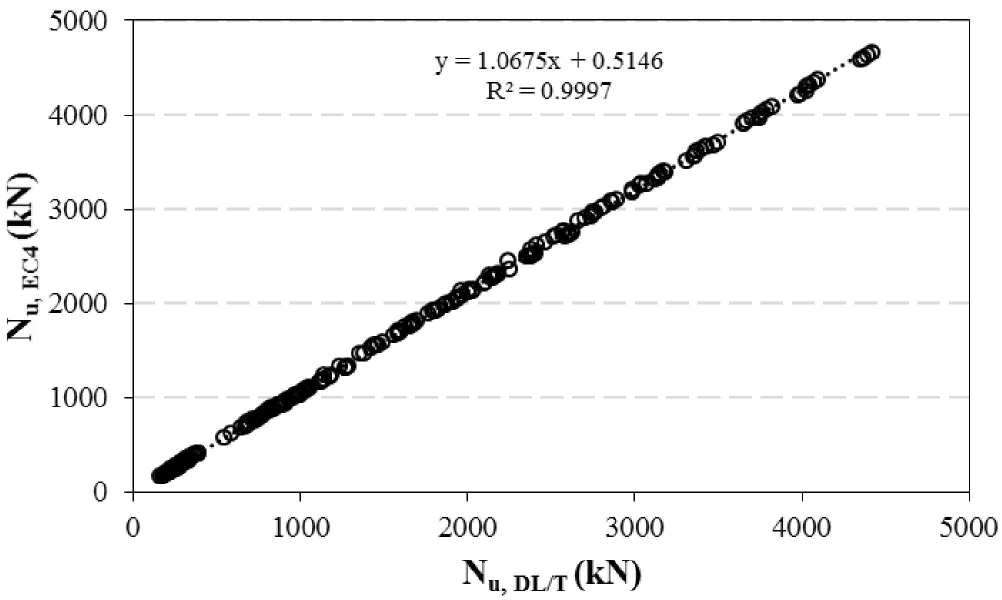

(a)

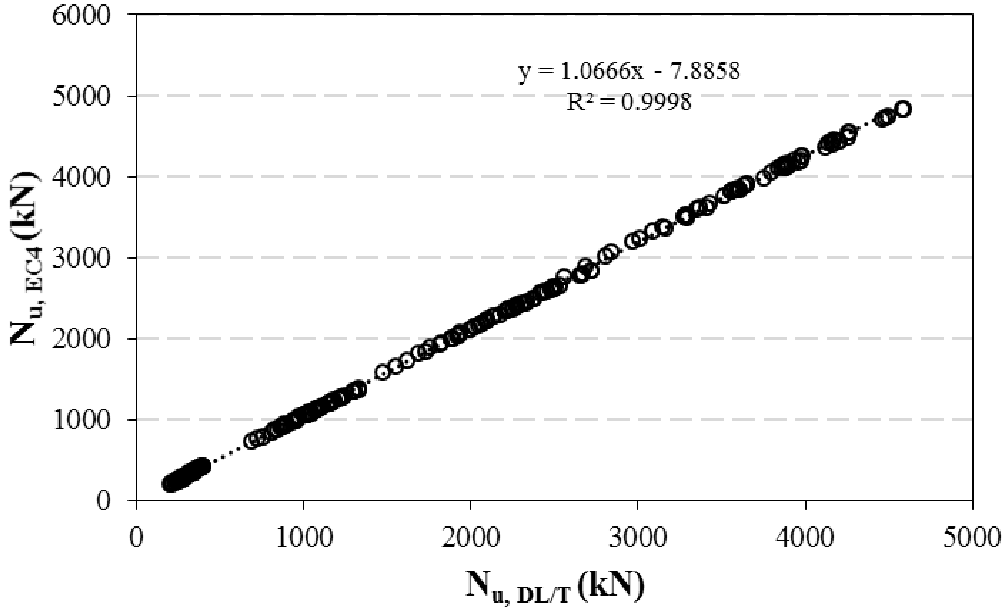

(b)

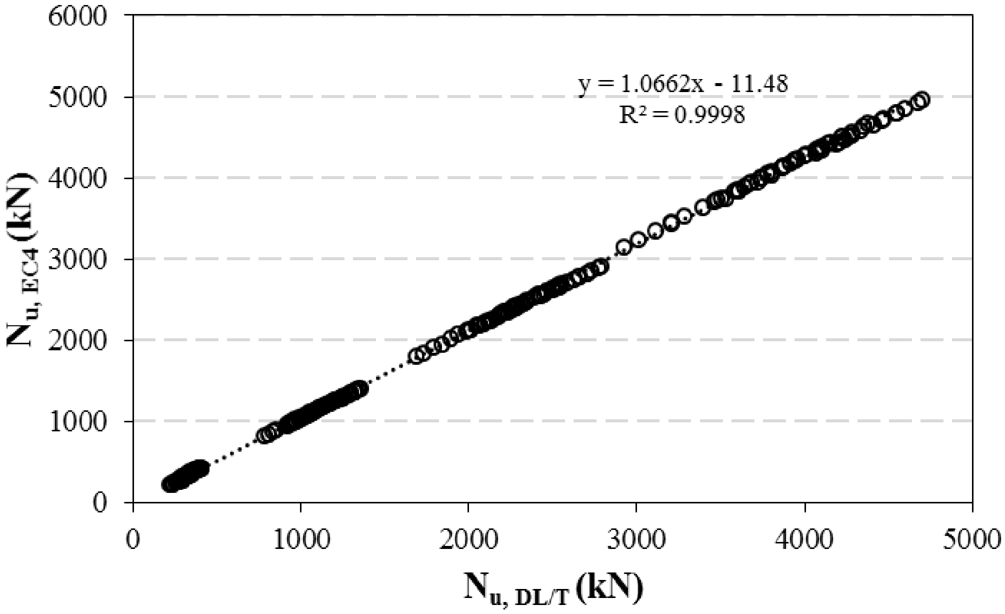

(c)

Figure 5.34 Regression model of predicted axial capacities of UHPC filled steel tubular columns between Eurocode 4 and DL/T code at a) 7, b) 28 and c) 90 days

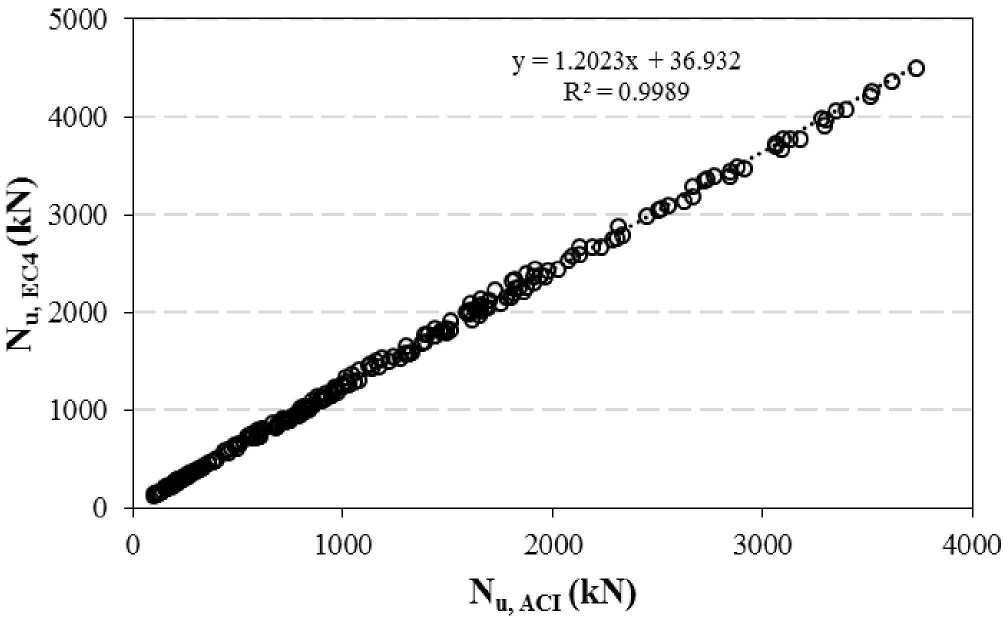
y = 1.2023x + 36.932
R² = 0.9989
0
1000
2000
3000
4000
5000
0
1000
2000
3000
4000
N u, EC4 (kN)
N u, ACI (kN)

(a)

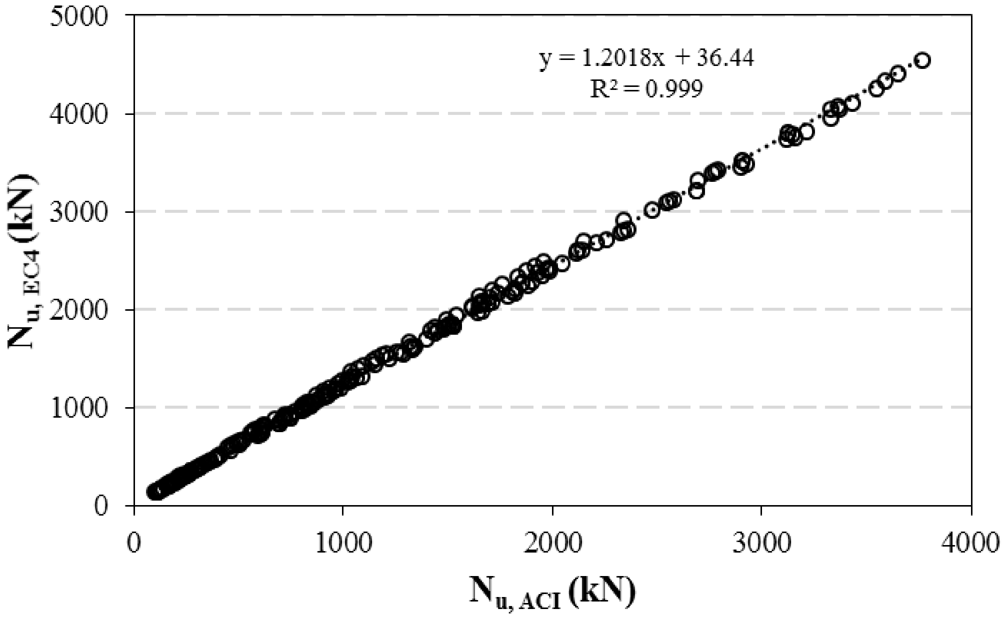
y = 1.2018x + 36.44
R² = 0.999
0
1000
2000
3000
4000
5000
0
1000
2000
3000
4000
N u, EC4 (kN)
N u, ACI (kN)

(b)

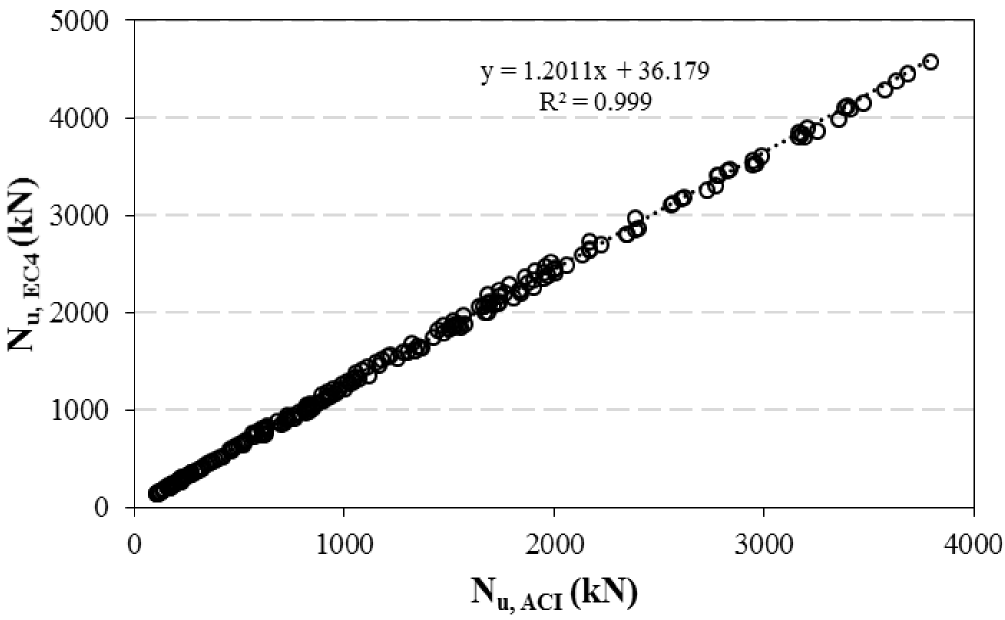

(c)

Figure 5.35 Regression model of predicted axial capacities of UHPGC filled steel tubular columns between Eurocode 4 and ACI 318 code at a) 7, b) 28 and c) 90 days

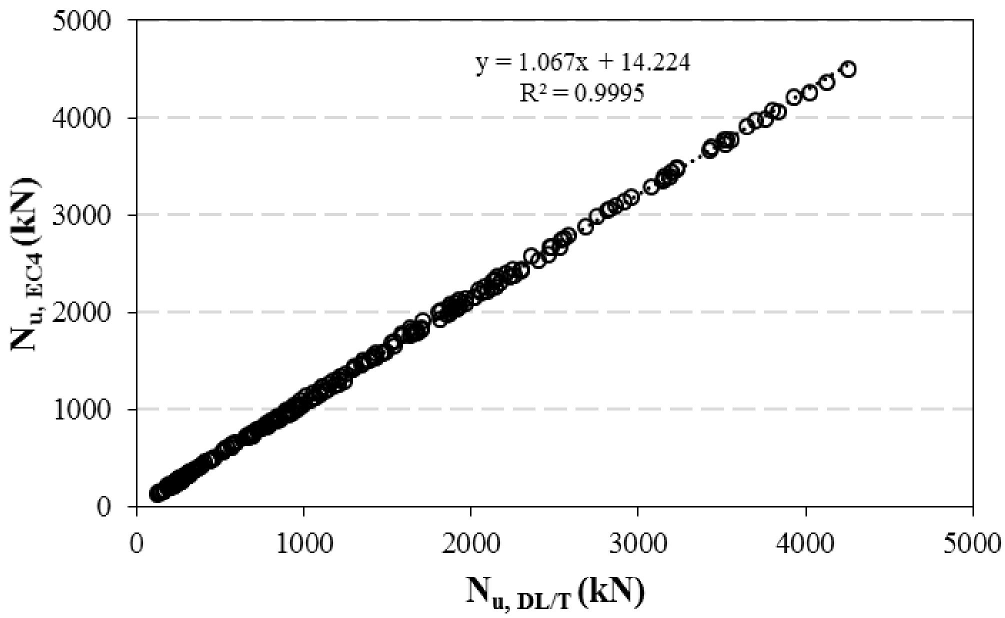

(a)

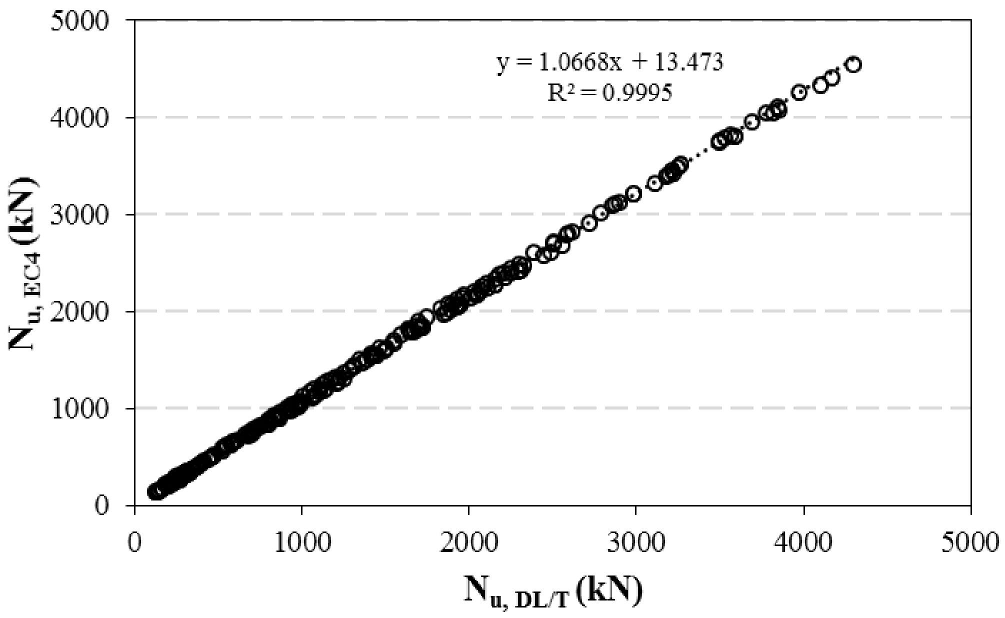

(b)

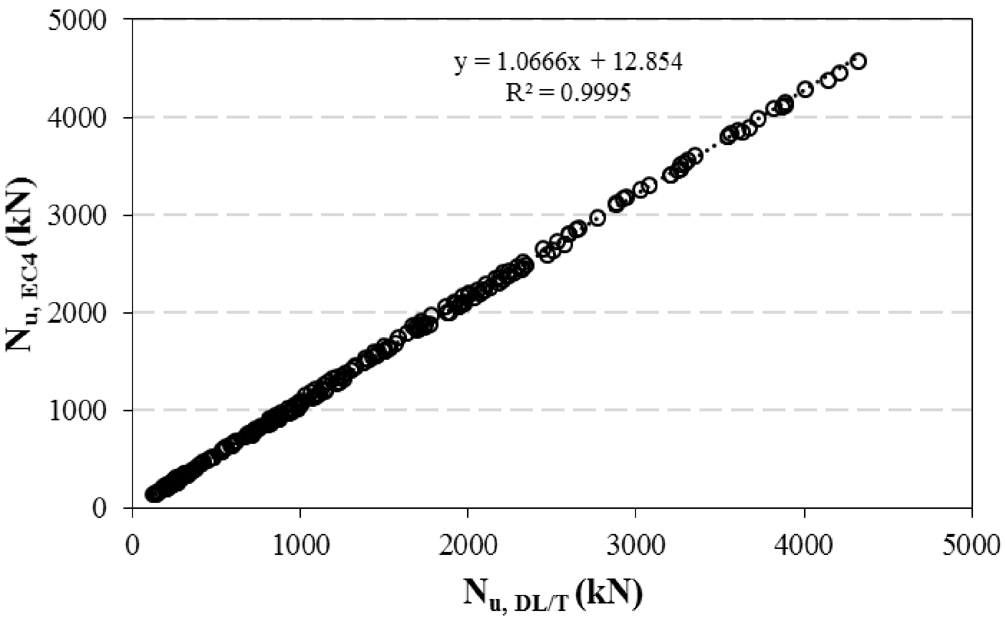

(c)

Figure 5.36 Regression model of predicted axial capacities of UHPGC filled steel tubular columns between Eurocode 4 and DL/T code at a) 7, b) 28 and c) 90 days

CHAPTER 6
CONCLUSIONS

Based on the results of the experimental and numerical analysis on the behavior of UHPC/UHPGC and those filled steel tubular columns manifested in this thesis, the following conclusions were drawn:

- Replacing of cement by 15% SF improved the flowability of UHPC. The mixes containing FA required less amount of SP than the corresponding the mixes containing SL and FA + SL at all replacement levels.
- The test results indicated that for the same mix proportions the steam cured samples performed better mechanical and fracture performance compared to corresponding standard water cured samples at all testing ages.
- Replacing of cement by 15% SF lead to improve the compressive strength compared with control mix up to 90 days. The increasing was 14.7, 29.5 and 28.7% for water curing compared with 31.9, 25.1 and 21.7% for steam curing at 7, 28 and 90 days, respectively. The same trend was observed in splitting tensile strength, modulus of elasticity, fracture energy, flexural strength, characteristic length and load carrying capacity.
- It was noticed that the compressive strength decreased with increasing the replacement of FA and/or SL beyond 25% for all ages, but the decreasing in the strength of the mixes comprising FA was higher than the mixes containing SL and (SL+FA). The decreasing at 28 days were 10.9, 8.7 and 10.5% at 50% replacement level for water curing for the mixes containing FA, SL and FA+SL and 12.2, 10.0 and 11.1% for the steam cured mixes, respectively. The corresponding decreasing at the same age for 75% replacement level were 31.8, 14.6 and 28.0% for water curing and 31.2, 18.7 and 25.8% for steam curing. The same behavior was observed in splitting tensile strength, modulus of elasticity, fracture energy, flexural strength, characteristic length and load carrying capacity.

- The mix containing (15% SF+ 25% SL) showed higher compressive strength compared to other mixes. This mix gave 163.3 and 166.3 MPa for water curing at 28 and 90 days with corresponding 168.0 and 173.2 MPa for steam curing at the same ages, respectively.
- The results indicated that the geopolymer mixes containing (FA + SF), the heat curing gave higher compressive strength than the corresponding steam curing. The increasing when the SF added to the geopolymer under the heat curing were up to 14.7%, depending on the testing age, and the corresponding increasing when the SF inclusion in the geopolymer concrete were up to 12.2%.
- The geopolymer concrete mixes containing (SL + SF) and (SL + FA + SF) yielded higher compressive strength in steam curing comparing with corresponding heat curing mixes at all ages. For example, the increasing in compressive strength of S-SF-GSL mix compared with corresponding heat curing mix (H-SF-GSL) was up to 18.5%, depending on the testing age. The same behavior was noticed in splitting tensile strength, modulus of elasticity, fracture energy, flexural strength, characteristic length and load carrying capacity.
- The results showed that irrespective to the curing regime of UHPGC, the compressive strength increased with increasing the SL percent. The increasing in compressive strength due to use SL reached to 109, 107 and 105% in heat curing regime at 7, 28 and 90 days, respectively, whereas the corresponding increasing in steam curing regime reached to 215, 205 and 198%.
- The results also showed that when adding SF to the geopolymer concrete provided higher compressive strength than when it is included in the geopolymer concrete in heat curing mixes and in S-SF-GFA mix, while it gave higher compressive strength when it is included in the geopolymer concrete in other steam curing mixes. This is also observed in the other testing results.
- The S-GSFSL mix had the highest compressive strength of 153.4, 155.2 and 156.6 MPa at 7, 28 and 90 days, respectively. This mix also gave the highest splitting tensile strength, modulus of elasticity, fracture energy, flexural strength, characteristic length and load carrying capacity at 90 days.
- Generally, UHPC showed higher compressive strength than UHPGC. The compressive strength reached to 160.7, 168 and 173.2 MPa for conventional concrete compared with 153.4, 155.2 and 156.6 MPa for geopolymer concrete at

7, 28 and 90 days, respectively. The conventional concrete also gave higher splitting tensile strength, modulus of elasticity and fracture energy than the geopolymer concrete.

- The results revealed that the strength gain of UHPGC was lower than UHPC even in the steam curing regime of conventional concrete. The strength development at 28 days compared with 7 days in UHPC reached to 43.8 and 11.8% for water and steam curing, respectively, while the corresponding development in UHPGC reached to 4.3 and 5.3% for heat and steam curing, respectively.
- The results of peak load of UHPGC specimen was in general higher than that of UHPC specimen of the similar compressive strength. The same trend was observed with the fracture energy, flexural strength and characteristic length. Whereas the results of modulus of elasticity was comparable between two types of concrete.
- The axial compressive load capacities of CFST columns infilled with UHPC/UHPGC were sensitive to D/t ratio and steel yield strength. It clearly appears that the axial capacity increased with increasing the D/t ratio and f_y. The higher the concrete diameter used, the higher the concrete cross section area, consequently, the ultimate axial capacity value enhanced with increasing of D/t ratio as the increase of cross section area of concrete core in all the three codes contribute to the ultimate axial capacity. CFST columns with high strength steel obtained higher axial capacity in UHPC and UHPGC.
- Regardless to D/t, f_y and age the axial load capacity decreased with increasing the replacement of FA and/or SL beyond 25% for all ages, but the decreasing in axial load capacity of the mixes containing FA was higher than the corresponding mixes containing SL and (SL+FA). The decreasing in for D/t=25 and f_y =150 MPa in ACI-318R (2005) at 28 days were 9.4, 7.4 and 9.1% at 50% replacement level for water curing for the mixes containing FA, SL and FA+SL and 10.9, 8.7 and 9.8% for the corresponding steam curing mixes, respectively. The corresponding decreasing at the same age for 75% replacement level were 33.7, 13.0 and 28.5% for water curing and 33.5, 17.7 and 26.2% for steam curing for the mixes comprising FA, SL and FA+SL, respectively.
- In UHPC, steam curing gave higher ratios of axial load carrying capacity at 7/28 days compared with corresponding water curing. For example, in Eurocode 4

(2004) when the yield strength of steel equal to 150 MPa, the ratios of axial load carrying capacity at 7/28 days reached up to 0.81 for water curing and up to 0.97 for steam curing, depending on ratio. Whereas the water curing yielded higher ratios of axial load carrying capacity at 90/28 than the corresponding steam curing and the ratios reached up to 1.2 for water curing and up to 1.07 for steam curing.

- In UHPC, steam curing gave higher axial load capacity compared with corresponding water cured at all ages.
- The axial load carrying capacity of UHPG increased with increasing SL percent at all ages. The increasing in load carrying due to use of SL in ACI-318R (2005) when D/t=25 and f_y =150 MPa at 7 days reached to 64.3 and 117.4%, in Eurocode 4 (2004) reached to 55.0 and 99.0% and the corresponding increasing in Chinese code DL/T (1999) was 66.2 and 121.3% for heat and steam curing, respectively.
- The development of the load carrying capacity of the column with UHPGC was very low. For example in Eurocode 4 (2004) when the yield strength of steel equal to 150 MPa, the ratios of axial load carrying capacity at 7/28 days was about 0.99 for steam curing. Whereas at 90/28, the corresponding ratios was about 1.03 for steam curing, irrespective of D/t ratio used.
- In the case of the column with UHPGC, the mixes containing (SL + SF) and (SL + FA + SF) resulted in higher axial load capacity in steam curing condition than the corresponding heat curing one, while opposite behavior can be seen in the mixes containing (FA + SF). The ratio of capacity of the column under steam curing to those under heat curing for D/t=25 and f_y=150 at 7 days ranged between (0.94 to 1.61), (0.92 to 1.71) and (0.92 to 1.73) for Eurocode 4 (2004), ACI-318R (2005) and DL/T (1999) codes, respectively.
- In the case of the column with UHPC, the $N_{u,\ EC4}$/ $N_{u,\ ACI}$ ratio decreased with increasing the compressive strength at all ages, for example when the D/t= 25 and f_y= 150 MPa, the ratio ranged between (1.2 to 1.3) at 7 days. The same trend was observed in $N_{u,\ EC4}$/ $N_{u,\ DL/T}$ ratio, which is ranged between (0.99 to 1.1) for the same above conditions. The same behavior were observed for the column with UHPGC, for example when the D/t= 25 and f_y= 150 MPa, the ratio ranged between (1.2 to 1.35) and (0.99 to 1.1) at 7 days for $N_{u,\ EC4}$/ $N_{u,\ ACI}$ and $N_{u,\ EC4}$/ $N_{u,\ DL/T}$ ratios, respectively. Moreover, it was noted that for UHPC/UHPGC the $N_{u,\ EC4}$/ $N_{u,\ DL/T}$ ratio were very closer to 1 than the $N_{u,\ EC4}$/ $N_{u,\ ACI}$ ratio.

- The $N_{u, EC4}$/ $N_{u, ACI}$ ratio for UHPC filled steel tubular column at 7 days ranged between (1.19 to 1.34) and between (1.19 to 1.31) for water and steam curing, respectively. The corresponding range at 28 days were (1.19 to 1.31) and (1.19 to 1.3) and at 90 days were (1.12 to 1.3) and (1.186 to 1.29) water and steam curing, respectively. The ratio of $N_{u, EC4}$/ $N_{u, ACI}$ for UHPGC filled steel tubular column at 7 days were (1.2 to 1.37) and (1.2 to 1.4) and at 28 days the ratio were (1.2 to 1.37) and (1.2 to 1.38) and at 90 days were (1.2 to 1.36) and (1.2 to 1.4) for heat and steam curing, respectively.
- The $N_{u, EC4}$/ $N_{u, DL/T}$ ratio for UHPC column at 7 days ranged between (1.019 to 1.147) and between (0.996 to 1.12) for water and steam curing, respectively. The corresponding range at 28 days were (0.995 to 1.12) and (0.993 to 1.11) and at 90 days were (0.994 to 1.11) and (0.991 to 1.11) water and steam curing, respectively. The ratio of $N_{u, EC4}$/ $N_{u, DL/T}$ for UHPGC column at 7 days were (1.02 to 1.17) and (0.999 to 1.17) and at 28 days the ratio were (1.02 to 1.16) and (0.999 to 1.17) and at 90 days were (1.02 to 1.16) and (0.998 to 1.17) for heat and steam curing, respectively.
- It can be noticed that there were considerably high relationship between the predicted values of ACI-318R (2005) and Eurocode 4 (2004) and between Chinese code DL/T (1999) and Eurocode 4 (2004). The regression analysis provided correlation coefficient (R^2) of 0.99 for all codes and ages.

REFERENCES

Abbas, S., Nehdi, M. L., Saleem, M. A. (2016). Ultra-High Performance Concrete: Mechanical Performance, Durability, Sustainability and Implementation Challenges. *International Journal of Concrete Structures and Materials*, **10(3)**, 271–295.

ACI-318R. (2005). Building Code Requirements for Structural Concrete (ACI 318-05) and Commentary. *Farmington Hills (MI, USA): American Concrete Institute;*

Adak, D., Sarkar, M., Mandal, S. (2014). Effect of nano-silica on strength and durability of fly ash based geopolymer mortar. *Construction and Building Materials*, **70**, 453–459.

AFGC / SETRA WORKING GROUP. (2002). Ultra High Performance Fibre-Reinforced Concrete – Interim Recommendations. *Report, Association Française de Génie Civil, Paris, France*.

Ahlborn, T. M., Misson, D. L., Peuse, E. J., Gilbertson, C. G. (2008). Durability and Strength Characterization of Ultra-High Performance Concrete under Variable Curing Regimes. In *2nd International Symposium on Ultra High Performance Concrete*, 197–204.

Ahmad, S., Hakeem, I., Maslehuddin, M. (2014). Development of UHPC mixtures utilizing natural and industrial waste materials as partial replacements of silica fume and sand. *Scientific World Journal*, **2014**, 1–8.

Akcay, B., Agar-Ozbek, Safak, A., Bayramov, F., Atahan, H. N., Sengul, C., Tasdemir, M. A. (2012). Interpretation of aggregate volume fraction effects on fracture behavior of concrete. *Construction and Building Materials*, **28(1)**, 437–443.

Alaee, F. J. (2002). Retrofitting of concrete structures using high performance fibre reinforced cementitious composite (HPFRCC). *Doctoral dissertation, Cardiff University, Cardiff University.*

Albitar, M., Mohamed Ali, M. S., Visintin, P., Drechsler, M. (2015). Effect of granulated lead smelter slag on strength of fly ash-based geopolymer concrete. *Construction and Building Materials*, **83(MAY)**, 128–135.

Albitar, M., Visintin, P., Mohamed Ali, M. S., Drechsler, M. (2014). Assessing behaviour of fresh and hardened geopolymer concrete mixed with Class-F fly ash. *KSCE Journal of Civil Engineering*, 1–11.

Alonso, S., Palomo, A. (2001). Calorimetric study of alkaline activation of calcium hydroxide–metakaolin solid mixtures. *Cement and Concrete Research*, **31(1)**, 25–30.

Alsalman, A., Dang, C. N., & Micah Hale, W. (2017). Development of ultra-high performance concrete with locally available materials. *Construction and Building Materials*, **133**, 135–145.

Ambily, P. S. (2014). Development of ultra-high- performance geopolymer concrete. *Magazine of Concrete Research*, **66(2)**, 82–89.

Anand, S., Vrat, P., Dahiya, R. P. (2006). Application of a system dynamics approach for assessment and mitigation of CO 2 emissions from the cement industry, **79**, 383–398.

Andini, S., Cioffi, R., Colangelo, F., Grieco, T., Montagnaro, F., Santoro, L. (2008). Coal fly ash as raw material for the manufacture of geopolymer-based products. *Waste Management*, **28(2)**, 416–423.

Assi, L. N., Deaver, E., Elbatanouny, M. K., Ziehl, P. (2016). Investigation of early compressive strength of fly ash-based geopolymer concrete. *Construction and Building Materials*, **112(April)**, 807–815.

Assi, L., Ghahari, S. A., Deaver, E. E., Leaphart, D., Ziehl, P. (2016). Improvement of the early and final compressive strength of fly ash-based geopolymer concrete at ambient conditions. *Construction and Building Materials*, **123**, 806–813.

ASTM C109/C109M. American Society for Testing and Materials. (2016). Standard Test Method for Compressive Strength of Hydraulic Cement Mortars (Using 2-in . or [50-mm] Cube Specimens). *Annual book of ASTM standards*, **vol. 04.02.** West Conshohocken, PA: ASTM.

ASTM C469. American Society for Testing and Materials. (2014). Standard Test Method for Static Modulus of Elasticity and Poisson's Ratio of Concrete in Compression. *Annual book of ASTM standards,* **vol. 04.02.** West Conshohocken, PA: ASTM.

ASTM C494. American Society for Testing and Materials. (2013). Standard Specification for Chemical Admixtures for Concrete. *Annual book of ASTM standards,* **vol. 04.02.** West Conshohocken, PA: ASTM.

ASTM C1437. American Society for Testing and Materials. (2015). Standard Test Method for Flow of Hydraulic Cement Mortar. *Annual book of ASTM standards,* **vol. 04.02.** West Conshohocken, PA: ASTM.

Banthia, N. (1994). Fiber Reinforced Concrete. *ACI SP-142ACI, Detroit, MI*, 1–29.

Barbosa, V. F. F., MacKenzie, K. J. D. (2003). Thermal behaviour of inorganic geopolymers and composites derived from sodium polysialate. *Materials Research Bulletin*, **38(2)**, 319–331.

Bijen, J. (1996). Benefits of slag and fly ash. *Construction and Building Materials*, **10(5)**, 309–314.

Bradford, M. A., Loh, H. Y., Uy, B. (2002). Slenderness limits for filled circular steel tubes. *Journal of Constructional Steel Research*, **58(2)**, 243–252.

BS 1881: Part 117 (1983). Method for determination of tensile splitting strength. *British Standard Institutions, UK.*

CEB/FIP, S. C. (2009). *Structural Concrete: Textbook on Behaviour, Design and Performance: Updated Knowledge of the CEB/FIP Model Code 1990*.

Chen, C., Habert, G., Bouzidi, Y., Jullien, A. (2010). Environmental impact of cement production: detail of the different processes and cement plant variability evaluation. *Journal of Cleaner Production*, **18(5)**, 478–485.

Chu, K. (2014). Axial load behaviour of steel tube columns in-filled with various high-performance concretes. *M.Sc. Thesis Ryerson University, Toronto, Ontario,* 1–114.

Cornelia Magureanu, Ioan Sosa, Camelia Negrutiu, Bogdan Heghes (2012). Mechanical Properties and Durability of Ultra-High-Performance Concrete. *ACI Materials Journal*, **109(2)**, 177–183.

Davidovits, J. (1991). Geopolymers Inorganic polymerie new materials. *Journal of Thermal Analysis*, **37(8)**, 1633–1656.

Davidovits, J. (1994). High-Alkali Cements for 21st Century Concretes. *American Concrete Institute*, **144**, 383–398.

Davidovits, J. (1999). Chemistry of Geopolymeric Systems, Terminology. *Geopolymer ’99 International Conference,Universite and Technologie. Compiegne, France*, 9–40.

De Oliveira, W. L. A., De Nardin, S., El Debs, A. L. H. de C., El Debs, M. K. (2010). Evaluation of passive confinement in CFT columns. *Journal of Constructional Steel Research*, **66(4)**, 487–495.

De Vargas, A. S., Dal Molin, D. C. C., Vilela, A. C. F., Silva, F. J. Da, Pavão, B., Veit, H. (2011). The effects of Na2O/SiO2 molar ratio, curing temperature and age on compressive strength, morphology and microstructure of alkali-activated fly ash-based geopolymers. *Cement and Concrete Composites*, **33(6)**, 653–660.

Deb, P. S., Nath, P., Sarker, P. K. (2014). The effects of ground granulated blast-furnace slag blending with fly ash and activator content on the workability and strength properties of geopolymer concrete cured at ambient temperature. *Materials and Design*, **62**, 32–39.

Dejaa, J., Uliasz-Bochenczykb, A., Eugeniusz Mokrzyckib. (2010). CO2 emissions from Polish cement industry. *International Journal of Greenhouse Gas Control*, **4(4)**, 583–588.

Demie, S., Nuruddin, M. F., Ahmed, M. F., Shafiq, N. (2011). Effects of curing temperature and superplasticizer on workability and compressive strength of self-compacting geopolymer concrete. *2011 National Postgraduate Conference - Energy and Sustainability: Exploring the Innovative Minds, NPC 2011*.

Derangula Padmaroja, Sri Chandana. (2015). Experimental Study on Strength and Sorptivity Properties of Geopolymer Mortar. *International Journal & Magazine of Engineering, Technology, Management and Research*, **2(4)**, 48–52.

DL/T. (1999). Chinese design code for steel-concrete composite structures. In: DL/T 5085-1999. *Chinese Electricity Press, Beijing, China (in Chinese).*

Dombrowski, K., Buchwald, A., Weil, M. (2007). The influence of calcium content on the structure and thermal performance of fly ash based geopolymers. *Journal of Materials Science*, **42(9)**, 3033–3043.

Dong, J. F., Wang, Q. Y., Guan, Z. W. (2013). Structural behaviour of recycled aggregate concrete filled steel tube columns strengthened by CFRP. *Engineering Structures*, **48**, 532–542.

Duan, P., Yan, C., Zhou, W., Luo, W., Shen, C. (2015). An investigation of the microstructure and durability of a fluidized bed fly ash-metakaolin geopolymer after heat and acid exposure. *Materials and Design*, **74**, 125–137.

Dundu, M. (2012). Compressive strength of circular concrete filled steel tube columns. *Thin Walled Structures*, **56**, 62–70.

Duxson, P., Fernández-Jiménez, A. M., Provis, J. L., Lukey, G. C., Palomo, A., Deventer, J. S. J. van. (2007). Geopolymer technology: The current state of the art. *Journal of Materials Science*, **42(9)**, 2917–2933.

Duxson, P., Provis, J. L., Lukey, G. C., van Deventer, J. S. J. (2007). The role of inorganic polymer technology in the development of "green concrete." *Cement and Concrete Research*, **37(12)**, 1590–1597.

Elremaily, A., & Azizinamini, A. (2002). Behavior and strength of circular concrete-filled tube columns. *Journal of Constructional Steel Research*, **58(12)**, 1567–1591.

EN, 197-1 TS. (2002). Cement- Part 1: Composition, specifications and conformity criteria for common cements. *Turkish Standards*.

Eurocode 4. (2004). Design of composite steel and concrete structures. Part 1.1, General rules and rules for buildings. EN 1994-1-1. *European Committee for Standardization: British Standards Institution*.

Fam, A., Qie, F. S., Rizkalla, S. (2004). Concrete-Filled Steel Tubes Subjected to Axial Compression and Lateral Cyclic Loads. *Journal of Structural Engineering*, **130(4)**, 631–640.

Fernández-jiménez, A. M., Palomo, A., López-hombrados, C. (2006). Engineering Properties of Alkali-Activated Fly Ash Concrete. *ACI Materials Journal*, **103(2)**, 106–112.

Fernández-Jiménez, A., Palomo, A. (2003). Characterisation of fly ashes. Potential reactivity as alkaline cements. *Fuel*, **82(18)**, 2259–2265.

Ferretti, E. (2004). On poisson's ratio and volumetric strain in concrete. *International Journal of Fracture*, **126(3)**, L49–L55.

Flower, D. J. M., Sanjayan, J. G. (2007). Green house gas emissions due to concrete manufacture. *The International Journal of Life Cycle Assessment*, **12(5)**, 282–288.

Gardner, N. J., Jacobson, E. R. (1967). Structural Behavior of Concrete Filled Steel Tubes. *ACI Journal Proceedings*, **64(7)**, 404–412.

Gartner, E. (2004). Industrially interesting approaches to "low-CO2" cements. *Cement and Concrete Research*, **34(9)**, 1489–1498.

Gautam, L., Sheethal, K. T., Prema Kumar, W. P., Prathap Kumar, M. T. (2015). Development of High Strength Geopolymer Concrete using Low Molarity Naoh. *International Journal of Engineering Research & Technology (IJERT)*, **4(7)**, 194–200.

Gesoglu, M., Güneyisi, E., Asaad, D. S., Muhyaddin, G. F. (2016). Properties of low binder ultra-high performance cementitious composites: Comparison of nanosilica and microsilica. *Construction and Building Materials*, **102**, 706–713.

Ghasemian, M., & Schmidt, L. C. (1999). Curved Circular Hollow Section (CHS) Steel Struts Infilled with Higher-Strength Concrete. *ACI Structural Journal*, **96(2)**.

Giakoumelis, G., Lam, D. (2004). Axial capacity of circular concrete-filled tube columns. *Journal of Constructional Steel Research*, **60(7)**, 1049–1068.

Gokulram, H., Anuradha, R. (2013). Strength Studies on Polypropylene Fibre Reinforced Geopolymer Concrete using M-Sand. *International Journal of Emerging Trends in Engineering and Development*, **2(3)**, 242–250.

Gopalaratnam, V. S., Shah, S. P., John, R. (1984). A modified instrumented charpy test for cement-based composites. *Experimental Mechanics*, **24(2)**, 102–111.

Görhan, G., Kürklü, G. (2014). The influence of the NaOH solution on the properties of the fly ash-based geopolymer mortar cured at different temperatures. *Composites Part B: Engineering*, **58**, 371–377.

Graybeal, B. a. (2005). Characterizacion of the behavior of UHPC, (mild), 1–377.

Graybeal, B. A. (2007). Compressive Behavior of Ultra-High-Performance Fiber-Reinforced Concrete. *ACI Materials Journal*, **104(2)**, 146–152.

Greenberg, S. A. (1961). Reaction between silica and calcium hydroxide solutions. I. kinetics in the temperature range 30 to 85°C. *The Journal of Physical Chemistry*, **65(1)**, 12–16.

Gunasekara, M. P. C. M., Law, D. W., Setunge, S. (2015). A comparative study of durability characteristics and microstructure of five different fly ash based geopolymer concretes. *14th International Congress on the Chemistry of Cement*, 1–12.

Güneyisi, E. M., Gültekin, A., Mermerdaş, K. (2016). Ultimate capacity prediction of axially loaded CFST short columns. *International Journal of Steel Structures*, **16(1)**, 99–114.

Gupta, P. K., Sarda, S. M., Kumar, M. S. (2007). Experimental and computational study of concrete filled steel tubular columns under axial loads. *Journal of Constructional Steel Research*, **63(2)**, 182–193.

Habert, G., D'Espinose De Lacaillerie, J. B., Lanta, E., Roussel, N. (2010). Environmental evaluation for cement substitution with geopolymers. *2nd International Conference on Sustainable Construction Materials and Technologies*, 1607–1615.

Habert, G., D'Espinose De Lacaillerie, J. B., Roussel, N. (2011). An environmental evaluation of geopolymer based concrete production: Reviewing current research trends. *Journal of Cleaner Production*, **19(11)**, 1229–1238.

Han, L. H., Li, W., Bjorhovde, R. (2014). Developments and advanced applications of concrete-filled steel tubular (CFST) structures: Members. *Journal of Constructional Steel Research*, ***100***, 211–228.

Han, L. H., Wang, W. Da, Tao, Z. (2011). Performance of circular CFST column to steel beam frames under lateral cyclic loading. *Journal of Constructional Steel Research*, **67(5)**, 876–890.

Han, L.-H. (2002). Tests on stub columns of concrete-filled RHS sections. *Journal of Constructional Steel Research*, **58(3)**, 353–372.

Han, L.-H., Yao, G.-H., Zhao, X.-L. (2005). Tests and calculations for hollow structural steel (HSS) stub columns filled with self-consolidating concrete (SCC). *Journal of Constructional Steel Research*, **61(9)**, 1241–1269.

Han, L.-H., Zhao, X.-L., Tao, Z. (2001). Tests and mechanics model for concrete-filled SHS stub columns, columns and beam-columns. *Steel and Composite Structures*, **1(1)**, 51–74.

Hardjito, D., Cheak, C. C., Ho, C., Ing, L., Ing, C. H. L. (2008). Strength and Setting Times of Low Calcium Fly Ash-based Geopolymer Mortar. *Modern Applied Science*, **2**, 3–11.

Hardjito, D., Rangan, B. V. (2005). Development and properties of low-calcium fly ash-based geopolymer concrete. *Research Report GC*, 94.

Hardjito, D., Wallah, S. E., Dody M.J. Sumajouw, Rangan, B.V. (2004). Factors Influencing the Compressive Strength of Fly Ash-Based Geopolymer Concrete. *Civil Engineering Dimension*, **6(2)**, 88–93.

Hardjito, D., Wallah, S. E., Sumajouw, D. M. J., Rangan, B. V. (2004). On the development of fly ash-based geopolymer concrete. *ACI Materials Journal*, **101(6)**, 467–472.

Hillerborg, A. (1985). The theoretical basis of a method to determine the fracture energy GF of concrete. *Materials and Structures*, **18(4)**, 291–296.

Hillerborg, A., Modéer, M., Petersson, P.-E. (1976). Analysis of crack formation and crack growth in concrete by means of fracture mechanics and finite elements. *Cement and Concrete Research*, **6(6)**, 773–781.

Hoenig, V., Hoppe, H., Emberger, B. (2007). Carbon Capture Technology-Options and Potentials for the Cement Industry. *PCA R&D Serial No. 3022*, **(3022)**, 98.

Hu, Y. M., Yu, T., Teng, J. G. (2011). FRP-Confined Circular Concrete-Filled Thin Steel Tubes under Axial Compression. *Journal of Composites for Construction*, **15(5)**, 850–860.

Huntzinger, D. N., Eatmon, T. D. (2009). A life-cycle assessment of Portland cement manufacturing: comparing the traditional process with alternative technologies. *Journal of Cleaner Production*, **17(7)**, 668–675.

Johansson, M. (2002). The efficiency of passive confinement in CFT columns. *Steel and Composite Structures*, **2(5)**, 379–396.

Johansson, M., Gylltoft, K. (2002). Mechanical Behavior of Circular Steel–Concrete Composite Stub Columns. *Journal of Structural Engineering*, **128(8)**, 1073–1081.

JSCE Guide Line. (2010). Recommendations for Design and Construction of Ultra-High Strength Fiber- Reinforced Concrete Structures. *JSCE Draft Version-Appendix* **5**, 1–5.

Jun, Y., Oh, J. E. (2015). Microstructural characterization of alkali-activation of six korean class F fly ashes with different geopolymeric reactivity and their zeolitic precursors with various mixture designs. *KSCE Journal of Civil Engineering*, **19(0)**, 1775–1786.

JX, P., L, H., YB, Z., P, C., L., Z. (2012). Modeling of carbon dioxide measurement on cement plants. *InAdvanced Materials Research*, **610**, 2120–2128.

Kadri, E.-H., Duval, R., Aggoun, S., Kenai, S. (2009). Silica Fume Effect on Hydration Heat and Compressive Strength of High Performance Concrete. *ACI Materials Journal*, **(106)**, 107–113.

Kamen, A., Denarié, E., Brühwiler, E. (2007). Thermal effects on physico-mechanical properties of ultra-high-performance fiber-reinforced concrete. *ACI Materials Journal*, **104(4)**, 415–423.

Kazemi, S., Lubell, A. S. (2012). Influence of Specimen Size and Fiber Content on Mechanical Properties of Ultra-High-Performance Fiber-Reinforced Concrete. *ACI Materials Journal*, **109(109)**, 675–684.

Kilpatrick, A. E., Rangan, B. V. (1999). Tests on High-Strength Concrete-Filled Steel Tubular Columns. *ACI Structural Journal*, **96(2)**, 268–274.

Kim, H., Koh, T., Pyo, S. (2016). Enhancing flowability and sustainability of ultra high performance concrete incorporating high replacement levels of industrial slags. *Construction and Building Materials*, **123**, 153–160.

Komljenović, M., Baščarević, Z., Bradić, V. (2010). Mechanical and microstructural properties of alkali-activated fly ash geopolymers. *Journal of Hazardous Materials,* **181**, 35–42.

Korpa, A., Kowald, T., Trettin, R. (2008). Hydration behaviour, structure and morphology of hydration phases in advanced cement-based systems containing micro and nanoscale pozzolanic additives. *Cement and Concrete Research*, **38(7)**, 955–962.

Krishan, A. L., Troshkina, E. A., Chernyshova, E. P. (2016). Efficient Design of Concrete Filled Steel Tube Columns. *Procedia Engineering*, **150**, 1709–1714.

Kuranovas, A., Kvedaras, A. K. (2007). Behaviour of hollow concrete-filled steel tubular composite elements. *Journal of Civil Engineering and Management*, **13(2)**, 131–141.

L.Krishnan, S.Karthikeyan, S.Nathiya, K. Suganya. (2014). Geopolymer Concrete an Eco-Friendly Construction Material. *International Journal of Research in Engineering and Technology*, **3(11)**, 164–167.

Lavanya, G., Jegan, J. (2015). Durability Study on High Calcium Fly Ash Based Geopolymer Concrete. *Advances in Materials Science and Engineering*, **2015(April)**.

Lee, N. K., An, G. H., Koh, K. T., Ryu, G. S. (2016). Improved Reactivity of Fly Ash-Slag Geopolymer by the Addition of Silica Fume. *Advances in Materials Science and Engineering*, 1–11.

Li C, G. X., SP, C., ZH, W., Y, Z., BC., C. (2011). CO2 emissions due to cement manufacture. *InMaterials Science Forum*, **685**, 181–187.

Liao, F.-Y., Han, L.-H., He, S.-H. (2011). Behavior of CFST short column and beam with initial concrete imperfection: Experiments. *Journal of Constructional Steel Research*, **67(12)**, 1922–1935.

Liew, J. Y. R., Xiong, M. (2015). Design Guide for Concrete Filled Tubular Members with High Strength Materials to Eurocode 4,146.

Liew, J. Y. R., Xiong, M. X., Xiong, D. X. (2014). Design of High Strength Concrete Filled Tubular Columns for Tall Design of High Strength Concrete Filled Tubular Columns for Tall Buildings. *International Journal of High-Rise Buildings*, **3(3)**, 215-221.

Liew, J., Xiong, D. (2012). Ultra-High Strength Concrete Filled Composite Columns for Multi-Storey Building Construction. *Advances in Structural Engineering*, **15(9)**, 1487–1504.

Lothenbach, B., Scrivener, K., Hooton, R. D. (2011). Supplementary cementitious materials. *Cement and Concrete Research*, **41(12)**, 1244–1256.

Lu, X., Hsu, C.-T. T. (2007). Tangent Poisson's ratio of high-strength concrete in triaxial compression. *Magazine of Concrete Research*, **59(1)**, 69–77.

Lu, Z. H., Zhao, Y. G. (2010). Suggested empirical models for the axial capacity of circular CFT stub columns. *Journal of Constructional Steel Research*, **66(6)**, 850–862.

Luksha, L. K., Nesterovich, A. P. (1991). Strength testing of larger-diameter concrete filled steel tubular members. In *Paper presented at the Proceeding of the 3rd internaltional conference on steel-concrete composite structures.*

Madhava, N., Rao, M. D., Divya, N. (2016). An experimental study on geo-polymer concrete. *INTERNATIONAL JOURNAL OF ENGINEERING SCIENCES & RESEARCH TECHNOLOGY*, **5(8)**, 545–553.

Markowski, J., Lohaus, L. (2017). UHPC Sandwich Structures with Composite Coating under Compressive Load. *Acta Polytechnica CTU Proceedings*, **7**, 38–42.

Masse, S., Zanni, H., Lecourtier, J., Roussel, J. C., Rivereau, A. (1993). 29Si solid state NMR study of tricalcium silicate and cement hydration at high temperature. *Cement and Concrete Research*, **23(5)**, 1169–1177.

Mclellan, B. C., Williams, R. P., Lay, J., Riessen, A. Van, Glen, D. (2011). Costs and carbon emissions for geopolymer pastes in comparison to ordinary portland cement》.pdf. *J Cleaner Prod*, **19**, 1080–1090.

Memon, F. A., Nuruddin, M. F., Shafiq, N. (2013). Effect of silica fume on the fresh and hardened properties of fly ash-based self-compacting geopolymer concrete. *International Journal of Minerals, Metallurgy and Materials*, **20(2)**, 205–213.

Meyer, C. (2009). The greening of the concrete industry. *Cement and Concrete Composites*, **31(8)**, 601–605.

Motorwala, A., Shah, V., Kammula, R., Nannapaneni, P., Raijiwala, P. D. B. (2013). ALKALI Activated FLY-ASH Based Geopolymer Concrete. *Journal Article*, **3(1)**, 159–166.

Mustafa Al Bakri, A. M., Kamarudin, H., Bnhussain, M., Rafiza, A. R., Zarina, Y. (2012). Effect of Na2SiO3/NaOH ratios and NaOH molarities on compressive strength of fly-ash-based geopolymer. *ACI Materials Journal,* **109(5)**, 503–508.

Naaman, A. E., K.Wille. (2012). The path to ultra-high performance fiber reinforced concrete (UHP-FRC): five decades of progress, in: M. Schmidt, E. Fehling, C. Glotzbach, et al., (Eds.),Proceedings of 3rd Hipermat: International Symposiumon UHPC and Nano- technology for High Performanc, Kassel University Press, Kassel, 3–16.

Naidu, G., Prasad, A. S. S. N., Adiseshu, S., Satayanarayana, P. V. V. (2012). A Study on Strength Properties of Geopolymer Concrete with Addition of G.G.B.S. *International Journal of Engineering Research and Development*, **2(4)**, 19–28.

Naik, T. R. (2008). Sustainability of Concrete Construction. *Practice Periodical on Structural Design and Construction*, **13(2)**, 98–103.

Nath, P., Sarker, P. K. (2014). Effect of GGBFS on setting, workability and early strength properties of fly ash geopolymer concrete cured in ambient condition. *Construction and Building Materials*, **66**, 163–171.

Nath, P., Sarker, P. K., Rangan, V. B. (2015). Early age properties of low-calcium fly ash geopolymer concrete suitable for ambient curing. *The 5th International Conference of Euro Asia Civil Engineering Forum (EACEF-5) Surabaya, Indonesia*, 601–607.

Ng, T. S., Foster, S. J. (2013). Development of a mix design methodology for high-performance geopolymer mortars. *Structural Concrete*, **14(2)**, 148–156.

Nicholson, C., Fletcher, R., Miller, N., Stirling, C., Morris, J., Hodges, S., Schmücker, M. (2005). Building Innovation through Geopolymer Technology. *Chemistry in New Zealand*, **(September)**, 10–12.

Noushini, A., Castel, A. (2016). The effect of heat-curing on transport properties of low-calcium fly ash-based geopolymer concrete. *Construction and Building Materials*, **112(April)**, 464–477.

O'Shea, M. D., Bridge, R. Q. (1998). Tests on circular thin-walled steel tubes filled with medium and high strength concrete. *Australian Civil Engineering Transactions*, **(40)**, 15.

O'Shea, M. D., Bridge, R. Q. (2000). Design of Circular Thin-Walled Concrete Filled Steel Tubes. *Journal of Structural Engineering*, **126(11)**, 1295–1303.

Oertel, T., Helbig, U., Hutter, F., Kletti, H., Sextl, G. (2014). Influence of amorphous silica on the hydration in ultra-high performance concrete. *Cement and Concrete Research*, **58**, 121–130.

Oertel, T., Hutter, F., Helbig, U., Sextl, G. (2014). Amorphous silica in ultra-high performance concrete: First hour of hydration. *Cement and Concrete Research*, **58**, 131–142.

Ozbakkaloglu, T., Xie, T. (2016). Geopolymer concrete-filled FRP tubes: Behavior of circular and square columns under axial compression. *Composites Part B: Engineering*, **96**, 215–230.

Pacheco-Torgal, F., Castro-Gomes, J., Jalali, S. (2008). Alkali-activated binders: A review. Part 2. About materials and binders manufacture. *Construction and Building Materials*, **22(7)**, 1315–1322.

Palomo, A., Grutzeck, M. W., Blanco, M. T. (1999). Alkali-activated fly ashes: A cement for the future. *Cement and Concrete Research*, **29(8)**, 1323–1329.

Partha, S. D., Pradip, N., Prabir, K. S. (2013). Strength and Permeation Properties of Slag Blended Fly Ash Based Geopolymer Concrete. *Advanced Materials Research*, **651**, 168–173.

Peng, J. X., Huang, L., Zhao, Y. B., Chen, P., Zeng, L., Zheng, W. (2013). Modeling of Carbon Dioxide Measurement on Cement Plants. *Advanced Materials Research*, **610**, 2120–2128.

Peng, L. (2014). Form Follows Function - The Composite Construction and Mixed Structures in Modern Tall Buildings. *International Journal of High-Rise Buildings*, **3(3)**, 191-198.

Persson, B. (1999). Poisson's ratio of high-performance concrete. *Cement and Concrete Research*, **29(10)**, 1647–1653.

Popa, M., Corbu, O., Kiss, Z., Zagon, R. (2013). Achieving Mixtures of Ultra-High Performance Concrete. *Constructii*, **1(1)**, 40–46.

Prem, P. R., Bharatkumar, B. H., Iyer, N. R. (2013). Influence of curing regimes on compressive strength of ultra high performance concrete. *Sadhana - Academy Proceedings in Engineering Sciences*, **38(6)**, 1421–1431.

Puligilla, S., Mondal, P. (2013). Role of slag in microstructural development and hardening of fly ash-slag geopolymer. *Cement and Concrete Research*, **43(1)**, 70–80.

Pyo, S., Kim, H. K. (2017). Fresh and hardened properties of ultra-high performance concrete incorporating coal bottom ash and slag powder. *Construction and Building Materials,* **131**, 459–466.

Qing, Y., Zenan, Z., Deyu, K., Rongshen, C. (2007). Influence of nano-SiO2 addition on properties of hardened cement paste as compared with silica fume. *Construction and Building Materials*, **21(3)**, 539–545.

Raijiwala, D. B., Patil, H. S. (2011). Geopolymer Concrete : a Concrete of Next Decade. *Journal of Engineering Research and Studies*, **2(1)**, 19–25.

Ramujee, K. (2014). Development of Low Calcium Flyash Based Geopolymer Concrete. *International Journal of Engineering and Technology*, **6(1)**, 1–4.

Rangan, B. V. (2008). Low-Calcium Fly Ash-based Geopolymer Concrete. *Chapter 26 in Concrete Construction Engineering Handbook, Editor-in Chief: E.G. Nawy, 2nd ed., New York: CRC Press*, 1–20.

Rashid, M. A., Mansur, M. A., Paramasivam, P. (2002). Correlations between Mechanical Properties of High-Strength Concrete. *Journal of Materials in Civil Engineering*, **14(3)**, 230–238.

Ravindra, K.D., Henderson, N. A. (1999). Specialist Techniques and Materials for Concrete Production. *Thomas Telford Publishing, Thomas Telford Ltd*.

Reda, M. M., Shrive, N. G., Gillott, J. E. (1999). Microstructural investigation of innovative UHPC. *Cement and Concrete Research*, **29(3)**, 323–329.

Ren, Q.-X., Han, L.-H., Lam, D., Hou, C. (2014). Experiments on special-shaped CFST stub columns under axial compression. *Journal of Constructional Steel Research*, **98**, 123–133.

Ren, X. Q., Chen, Y. J., Yan, W. M., Gu, D. P., Wang, J. J. (2013). Experimental Research of Uniaxial Compression Bearing Capacity on Large Diameter CFST Columns. *Key Engineering Materials*, **540**, 107–118.

RILEM 50-FMC. Committee of fracture mechanics of concrete. (1985). Determination of the Fracture Energy of Mortar and Concrete by Means of Three-Point Bend Tests on Notched Beames. *Materials and Structures*, **18(106)**, 285–290.

Sakino, K., Hayashi, H. (1991). Behavior of concrete filled steel tubular stub columns under concentric loading. In *Paper presented at the The Third International Conference on Steel-Concrete Composite Structures, Fukoka, Japan.*

Sakino, K., Nakahara, H., Morino, S., Nishiyama, I. (2004). Behavior of Centrally Loaded Concrete-Filled Steel-Tube Short Columns. *Journal of Structural Engineering*, **130(2)**, 180–188.

Sanni, S. H., Khadiranaikar, R. B. (2012). Performance of geopolymer concrete under severe environmental conditions. *Journal, International Civil of Engineering, Structural*, **3(2)**, 396–407.

Santos, R. A. dos. (2012). Structural behaviour of short concrete filled steel tube columns. *Técnico, Lisboa*, 1–11.

Sarker, P. K. (2011). Bond strength of reinforcing steel embedded in fly ash-based geopolymer concrete. *Materials and Structures*, **44(5)**, 1021–1030.

Sarker, P. K., Haque, R., Ramgolam, K. V. (2013). Fracture behaviour of heat cured fly ash based geopolymer concrete. *Materials and Design*, **44(February)**, 580–586.

Schmidt, M., Fehling, E., Bunje, K., Tue, N. V. (2004). Ultra High Performance Composite Bridge across the River Fulda in Kassel. In *Proceedings of the International Symposium on Ultra High Performance Concrete* (pp. 819–825).

Schneider, S. P. (1998). Axially Loaded Concrete-Filled Steel Tubes. *Journal of Structural Engineering*, **124(10)**, 1125–1138.

Schneider, S. P., Kramer, D. R., Sarkkinen, D. L. (2004). The design and construction of concrete-filled steel tube column frames. In *13th World Conference on Earthquake Engineering Vancouver, B.C., Canada*, 1–12.

Scholle, N., Lohaus, L. (2012). Numerical analyses of filigree steel-wrapped UHPC tubes. In *Proceedings of XIII th Bilateral Czech / German Symposium Experimental Methods and Numerical Simulation in Engineering Sciences*, 47–50.

Senff, L., Hotza, D., Repette, W. L., Ferreira, V. M., Labrincha, J. A. (2010). Mortars with nano-SiO2 and micro-SiO2 investigated by experimental design. *Construction and Building Materials*, **24(8)**, 1432–1437.

Shi, X.-S., Wang, Q.-Y., Zhao, X.-L., Collins, F. G. (2015). Structural behaviour of geopolymeric recycled concrete filled steel tubular columns under axial loading. *Construction and Building Materials*, **81(April)**, 187–197.

Singh, B., Rahman, M. R., Paswan, R., Bhattacharyya, S. K. (2016). Effect of activator concentration on the strength, ITZ and drying shrinkage of fly ash/slag geopolymer concrete. *Construction and Building Materials*, **118**, 171–179.

Smith, J., Cusatis, G., Pelessone, D., Landis, E., O'Daniel, J., Baylot, J. (2014). Discrete modeling of ultra-high-performance concrete with application to projectile penetration. *International Journal of Impact Engineering*, **65**, 13–32.

Sobuz, H. R., Visintin, P., Mohamed Ali, M. S., Singh, M., Griffith, M. C., Sheikh, A. H. (2016). Manufacturing ultra-high performance concrete utilising conventional materials and production methods. *Construction and Building Materials*, **111**, 251–261.

Sofi, M., van Deventer, J. S. J., Mendis, P. A., Lukey, G. C. (2007). Bond performance of reinforcing bars in inorganic polymer concrete (IPC). *Journal of Materials Science*, **42(9)**, 3107–3116.

Soutsos, M., Boyle, A. P., Vinai, R., Hadjierakleous, A., Barnett, S. J. (2016). Factors influencing the compressive strength of fly ash based geopolymers. *Construction and Building Materials*, **110**, 355–368.

Srinivasan.K, Ganesh, D. G. M., Santhi. A.S. (2015). Prediction of Compressive Strength of the Fibre Reinforced Slag Geopolymer Concrete. *International Journal of Applied Engineering Research*, **10(11)**, 28561–28574.

Sumajouw, D. M. J., Hardjito, D., Wallah, S. E., Rangan, B. V. (2007). Fly ash-based geopolymer concrete: Study of slender reinforced columns. *Journal of Materials Science*, **42(9)**, 3124–3130.

Teng, J. G., Hu, Y. M., Yu, T. (2013). Stress–strain model for concrete in FRP-confined steel tubular columns. *Engineering Structures*, **49**, 156–167.

Thomas, J. J., Jennings, H. M., Chen, J. J. (2009). Influence of Nucleation Seeding on the Hydration Mechanisms of Tricalcium Silicate and Cement. *The Journal of Physical Chemistry C*, **113(11)**, 4327–4334.

Tue, N. V, Ma, J., Orgass, M., Fehling, E. (2008). Influence of addition method of superplasticizer on the properties of fresh UHPC. In *2nd International Symposium on Ultra High Performance Concrete*, 93–104.

Tue, N. V., Küchler, M., Schenck, G., Reinhardt, J. (2004). Application of UHPC filled Tubes in Buildings and Bridges. In *Proceedings of the International Symposium on Ultra High Performance Concrete*, 807–809.

Turner, L. K., Collins, F. G. (2013). Carbon dioxide equivalent (CO2-e) emissions: A comparison between geopolymer and OPC cement concrete. *Construction and Building Materials*, **43**. 125–130.

Uy, B., Tao, Z., Han, L.-H. (2011). Behaviour of short and slender concrete-filled stainless steel tubular columns. *Journal of Constructional Steel Research*, **67(3)**, 360–378.

Van Deventer, J. S. J., Provis, J. L., Duxson, P., Brice, D. G. (2010). Chemical research and climate change as drivers in the commercial adoption of alkali activated materials. *Waste and Biomass Valorization*, **1(1)**, 145–155.

Van Tuan, N., Ye, G., Van Breugel, K., Copuroglu, O. (2011). Hydration and microstructure of ultra high performance concrete incorporating rice husk ash. *Cement and Concrete Research*, **41(11)**, 1104–1111.

Vijai, K., Kumutha, R., Vishnuram, B. G. (2010). Effect of types of curing on strength of geopolymer concrete. *International Journal of the Physical Sciences*, **5(9)**, 1419–1423.

Weil, M., Dombrowski, K., A. Buchawald. (2009). Life-cycle analysis of geopolymers. *Geopolymers, Structure, Processing, Properties and Applications. Cambridge: Woodhead Publishing Limited Abington Hall*, 194–210.

Wille, K., Naaman, A. E., El-Tawil, S. (2011). Optimizing Ultra-High- Performance Fiber- Reinforced Concrete Mixtures with twisted fibers exhibit record performance under tensile loading, **(september)**, 35–42.

Wille, K., Naman, A. E., Parra-Montesinos, G. J. (2011). Ultra - High Performance Concrete with Compressive Strength Exceeding 150 MPa (22ksi) : A Simpler Way. *ACI Materials Journal*, **108(1)**, 46–53.

Witherspoon, R., Wang, H., Aravinthan, T., & Omar, T. (2009). Energy and emissions analysis of fly ash based geopolymers. *SSEE 2009: Solutions for a Sustainable Planet*, 311.

WSDOT. (2016). Concrete-filled Steel Tubes, **(360)**, 1–2.

Xu, H., Van Deventer, J. S. J. (2000). The geopolymerisation of alumino-silicate minerals. *International Journal of Mineral Processing*, **59(3)**, 247–266.

Xue, J.-Q., Briseghella, B., Chen, B.-C. (2012). Effects of debonding on circular CFST stub columns. *Journal of Constructional Steel Research*, **69(1)**, 64–76.

Yang, K. H., Song, J. K., Song, K. I. (2013). Assessment of CO 2 reduction of alkali-activated concrete. *Journal of Cleaner Production*, **39**, 265–272.

Yazıcı, H. (2007). The effect of curing conditions on compressive strength of ultra high strength concrete with high volume mineral admixtures. *Building and Environment*, **42(5)**, 2083–2089. Retrieved from

Yazıcı, H., Yardimci, M. Y., Aydin, S., Karabulut, A. Ş (2009). Mechanical properties of reactive powder concrete containing mineral admixtures under different curing regimes. *Construction and Building Materials*, **23(3)**, 1223–1231.

Yazıcı, H., Yardimci, M. Y., Yiğiter, H., Aydin, S., Türkel, S. (2010). Mechanical properties of reactive powder concrete containing high volumes of ground granulated blast furnace slag. *Cement and Concrete Composites*, **32(8)**, 639–648.

Yazıcı, H., Yiğiter, H., Karabulut, A. Ş., Baradan, B. (2008). Utilization of fly ash and ground granulated blast furnace slag as an alternative silica source in reactive powder concrete. *Fuel*, **87(12)**, 2401–2407.

Yigiter, H., Aydin, S., Yazıcı, H., Yardimci, M. Y. (2012). Mechanical performance of low cement reactive powder concrete (LCRPC). *Composites Part B: Engineering*, **43(8)**, 2907–2914.

Yip, C. K., van Deventer, J. S. J. (2003). Microanalysis of calcium silicate hydrate gel formed within a geopolymeric binder. *Journal of Materials Science*, **38(18)**, 3851–3860.

Yip, C. K., Lukey, G. C., Van Deventer, J. S. J. (2005). The coexistence of geopolymeric gel and calcium silicate hydrate at the early stage of alkaline activation. *Cement and Concrete Research*, **35(9)**, 1688–1697.

Yip, C. K., Lukey, G. C., Provis, J. L., van Deventer, J. S. J. (2008). Effect of calcium silicate sources on geopolymerisation. *Cement and Concrete Research*, **38(4)**, 554–564.

Yu, R., Spiesz, P., Brouwers, H. J. H. (2014). Mix design and properties assessment of Ultra-High Performance Fibre Reinforced Concrete (UHPFRC). *Cement and Concrete Research*, **56**, 29–39.

Yu, Z., Ding, F., Cai, C. S. (2007). Experimental behavior of circular concrete-filled steel tube stub columns. *Journal of Constructional Steel Research*, **63(2)**, 165–174.

Yunsheng, Z., Wei, S., Sifeng, L., Chujie, J., Jianzhong, L. (2008). Preparation of C200 green reactive powder concrete and its static–dynamic behaviors. *Cement and Concrete Composites*, **30(9)**, 831–838.

Yuvaraj, P., Murthy, A. R., Iyer, N. R., Sekar, S. K. (2014). ANN Model to Predict Fracture Characteristics of High Strength and Ultra High Strength Concrete Beams, **41(3)**, 193–213.

Zeghiche, J. (1988). Concrete-filled composite columns. In *MSc Thesis*, *University of Manchester*.

Zeghiche, J., Chaoui, K. (2005). An experimental behaviour of concrete-filled steel tubular columns. *Journal of Constructional Steel Research*, **61(1)**, 53–66.

Zhang, B., Bicanic, N., Pearce, C., Balabanic, G. (2000). Residual fracture properties of normal-and high-strength concrete subject to elevated temperatures. *Magazine of Concrete Research*, **52(2)**, 123–136.

Zhang, F., & Wu, C. (2015). Numerical simulation of UHPC filled tube columns against blast. In *International Conference on Performance-based and Life-cycle Structural Engineering. School of Civil Engineering, The University of Queensland*, 386–393.

PERSONAL INFORMATION

Full name: Ali Kadhim AL-KARAGHOLI

Nationality: Iraqi

Birth place and date: Baghdad, 1979

Marital status: Married, 3 children

Phone number: 05398490244

Email: ali.alkaragholi@mail2.gantep.edu.tr

ali_kadhum79@yahoo.com

alikadhim1979@gmail.com

EDUCATION

Degree	Graduate school	Year
Master	Building & Construction Engineering Dep., University of Technology, Baghdad, Iraq	2005
Bachelor	Building & Construction Engineering Dep., University of Technology, Baghdad, Iraq	2001
High school	Abu Graib for boys	1997

WORK EXPERIENCE

2006-2013	Assistant lecturer	Highway and Transportation Engineering Dep., College of Engineering, Almustansiriyah University, Iraq
2013-Present	Lecturer	Highway and Transportation Engineering Dep., College of Engineering, Almustansiriyah University, Iraq

PUBLICATIONS

[1] Ali Kadhim Ibrahim, (2011). Activation of Red Kaolin Clay as a Pozzolanic Material. *Al-Qadisiya Journal for Engineering Sciences*, **4(3)**, 353-363.

[2] Ali Kadhim Ibrahim, (2013). Effect of Partial Replacement of Cement by Hydrated Cement on Properties of Cement Paste and Cement Mortar. *Iraqi Journal of Civil Engineering*, **9(1)**, 110-119.

FOREIGN LANGUAGE

Arabic (Mother language), English and Turkish

HOBBIES

Reading, Traveling, Football